ERCB/AGS Bulletin 65

Northern Alberta Kimberlite Province: The First 20 Years

Energy Resources Conservation Board

AGS Alberta Geological Survey

ERCB/AGS Bulletin 65

Northern Alberta Kimberlite Province: The First 20 Years

D.R. Eccles[1]

[1]Apex Geoscience
(formerly of Alberta Geological Survey)

Energy Resources Conservation Board
Alberta Geological Survey

November 2011

ISBN 978-0-7785-8643-2

External author address:
APEX Geoscience
Suite 200, 9797 – 45th Avenue
Edmonton Alberta T6E 5V8

Published November 2011 by:
Energy Resources Conservation Board
Alberta Geological Survey
4th Floor, Twin Atria Building
4999 – 98th Avenue
Edmonton, Alberta
T6B 2X3
Canada

Tel: 780.422.1927
Fax: 780.422.1918
E-mail: AGS-Info@ercb.ca
Website: www.ags.gov.ab.ca

Cover photo: This spectacular 0.76 carat yellow diamond, recovered from the K6 kimberlite in the Buffalo Head Hills, illustrates the potential for high-quality stones in the northern Alberta kimberlite province. Photo compliments of Ashton Mining of Canada Inc.

Contents

Tables

Figures

Author's Preface and Acknowledgments

In the early 1990s, I remember sitting on an outcrop of Shaftesbury Formation shale with colleagues from industry (M. Dufresne of APEX Geoscience Ltd.) and the Geological Survey of Canada (D. Leckie). We debated how discontinuous horizons of bentonite and marine kill zones (fish scales and bone beds) in northern Alberta could possibly relate to major volcanic episodes sourced in southeastern British Columbia and northern Montana (at the time, the most 'proximal' and 'acceptable' chronostratigraphic volcanic sources). Our preferred, but contentious, consensus was to link Cretaceous ash- and organic-rich strata to geological processes that occurred within northern Alberta. In one solution, we proposed that the small but powerful volcanic eruptions were caused by the rapid ascent of kimberlite—a type of intrusive igneous rock originating in the asthenosphere and penetrating upward to the surface of the Earth. It appeared we were not alone in our thinking, as kimberlite and related rock discoveries from 1990 to 2010 resulted in the most exciting decades of mineral exploration Alberta has ever known.

Alas, how did 20 years go by so fast? A long-term diamond strategy by the Alberta government, periodic collaborative initiatives between provincial and federal geological surveys and universities, and continual discoveries and assessment reporting by industry created a wealth of data and research that simply made 20 years fly by. And so, the timing and level of confidence are now right to produce a fundamental report documenting the first 20 years (1990–2010) of ultramafic discovery and examination in northern Alberta.

Much of the work in this report was accomplished in a collaborative spirit, and it is to these co-conspirators that I am forever grateful. I have always said scientific partnerships are ultimately responsible for much of our current knowledge about the geological processes that were prevalent in northern Alberta tens to hundreds of millions of years ago. Here, I attempt to acknowledge the partners (collaborators, colleagues and advisors) who contributed in some substantive way to advancing our knowledge of Alberta's diamond-related geology.

I would be remiss not to start by thanking the companies responsible for kimberlite and related rock discoveries and advancement in Alberta, including Monopros Limited, Ashton Mining of Canada Inc. (in a joint venture with Alberta Energy Company Ltd. and Pure Gold Minerals Inc.), Kennecott Canada Exploration Inc. (in a joint venture with Montello Resources Ltd. and Redwood Resources Ltd.), New Blue Ribbon Resources Ltd., Stornoway Diamond Corporation, APEX Geoscience Ltd. and Grizzly Discoveries Inc.

Of course, it's the people who make these companies excel, and I acknowledge B. Wood, W. Hillier, S. Carlson, D. Skelton, B. Clements, T. McCandless, J. Ward, A. Berry, R. Pryde, B. Doyle, K. Kivi, L. Kryska, J. Armstrong, M. Dufresne and B. Testo. My thanks also go to the 'new kids on the block,' including G. Read, S. Harvey and T. French of Shore Gold Inc.; and R. Turner of Canterra Minerals Corporation. I wish you continued success.

The University of Alberta played a particularly important role, not only in generating high-quality data but, of equal importance, ensuring that the following faculty and staff were available for, and genuinely interested and knowledgeable in, kimberlite-related tête-à-tête: L. Heaman, R. Luth, R. Creaser, T. Stachel, D. Caird, S. Matveev, J-P. Zonneveld, K. Muehlenbachs, A. Simonetti, S. Simonetti and G. Chen. Kimberlite-based collaborative initiatives with the Geological Survey of Canada, in particular D. Leckie, A. Sweet, B. Kjarsgaard and J. Mwenifumbo, provided the interest and knowledge to better understand and model Alberta's diamond potential. My thanks go to K. Hoal, formerly with the Colorado School of Mines, for co-ordinating QEMSCAN® mineralogical determinations, and to L. Boyer for kindly granting permission to reproduce her schematic thesis representation of a proposed kimberlite eruption in the Buffalo Head Hills area of northern Alberta. Special thanks go

to D. Magee of the Alberta Geological Survey for meticulous and timely figure preparation.

Finally, I was very fortunate to have external reviewers who are well versed in worldwide kimberlite exploration and modelling. I am immensely grateful to T. McCandless of MCC Geoscience Inc. and J. Armstrong of Stornoway Diamond Corporation for their thoughtful and thorough reviews of the report.

Abstract

This report integrates documentation of the first 20 years (1990–2010) of kimberlite and related rock discovery and examination in the northern Alberta kimberlite province. Comprehensively summarized are the events that led to the discovery of kimberlitic rocks in Alberta, the geological setting in which they were discovered, geochronology, physical and chemical volcanological characteristics, rock classification, emplacement setting, and diamond content.

At present, 51 Late Cretaceous to Paleocene (~88–60 Ma), serpentine- to carbonate-bearing kimberlite and related alkaline bodies have been discovered in three separate areas of northern Alberta: Mountain Lake, Buffalo Head Hills and Birch Mountains. These bodies occur as pyroclastic, resedimented volcaniclastic, and intrusive dikes or sills in complex volcanic fields whose geological history comprises short intervals of violent volcanism punctuated by longer, volcanically quiescent intervals. The regions are generally distinguished from one another by their non-archetypal kimberlite signature (Mountain Lake) or, in the case of kimberlite fields, primitive (Buffalo Head Hills) to evolved (Birch Mountains) magmatic signatures. Recognition of these different rock types in both inter- and intra-field settings is important because rock classification correlates with diamond content. Primitive kimberlite magma with elevated diamond content is associated with ~88–81 Ma intrusives in the Buffalo Head Hills field. In contrast, more evolved kimberlite in some of the Birch Mountains bodies (e.g., Legend and Phoenix) and alkaline rock types at Mountain Lake, Birch Mountains (e.g., Xena and Kendu) and the ~60 Ma Buffalo Head Hills bodies have mostly low diamond content or are barren of diamond.

Northern Alberta is underlain by a heterogeneous mantle, which implies selective sampling by individual intrusions and/or significant local variability in the mantle due to depletion or re-enrichment of the protolith. In general, the mantle is characterized by a shallow (<135 km), low-temperature zone of fertile lherzolite and wehrlite, followed by depleted and depleted/metasomatized lherzolite that dominates from 160 to 190 km, followed by a dominant melt metasomatized lherzolitic mantle component below 190 km. Depleted lherzolite with low Ti, Y and Zr, which underlies the Buffalo Head Hills field at 160–180 km and 1000°–1130°C, is consistent with an Archean subcontinental lithospheric mantle that was strongly modified in Proterozoic time.

Geochronological determinations on diamondiferous kimberlites define a Buffalo Head Hills diamond window at ~88–81 Ma, with an emphasis at ~81 Ma. The presence of a dominant lherzolitic (±wehrlitic) garnet xenocryst assemblage, and lherzolitic and wehrlitic diamond inclusions, suggests the diamond populations recovered from the Buffalo Head Hills include a significant population from a peridotitic, albeit not harzburgitic, source. In addition, the presence of group 3D (Na_2O >0.7 wt. %) eclogitic garnet suggests the Buffalo Head Hills mantle also includes an eclogite/websterite component with diamond-facies compositional characteristics. In contrast, the Mountain Lake and Birch Mountains fields exhibit diamond-poor scenarios, in which individual bodies appear to have sampled metasomatized mantle with an extremely high temperature of last equilibration or from significantly shallower depths in the lower crust/upper mantle.

The northern Alberta kimberlite province represents a unique opportunity to study some of the best preserved, near-surface kimberlite edifices in the world, and intrusives that were emplaced through strongly modified and controversial tectonic domains of western Laurentia. The integration and discussion of information in this report will therefore enable explorers to evaluate present and future diamondiferous kimberlite discoveries in northern Alberta and the Western Canada Sedimentary Basin. Consequently, a primary function of the report is to encourage continued diamond exploration in Alberta that may one day lead to an economic deposit. In addition, it provides the background necessary to update the bedrock geological map of Alberta and enable governments to better manage and sustain

this potentially new provincial resource. Lastly, the report will provide a summary for Albertans about the diamond potential of their province and communities.

1 Introduction

The first clue to the presence of possible diamond-bearing source rocks in northern Alberta was the 1958 discovery of a perfect 0.83 carat octahedral alluvial diamond by E. Opdahl in a farm field near Evansburg in west-central Alberta (Figure 1). Despite the Ophdal diamond discovery, noteworthy Alberta diamond exploration did not commence until the early 1990s, coincident with Canada's emergence as a globally recognized diamond producer following the 1991 discovery of the Ekati deposit at Lac de Gras, Northwest Territories.

Alberta entered Canada's modern era of diamond exploration in 1989–1990 after Monopros Limited (the then-Canadian exploration subsidiary of De Beers) discovered the Mountain Lake alkaline intrusion in the Peace River–Grande Prairie region of northwestern Alberta. Although the Mountain Lake intrusion was uneconomic, it represented the first ultramafic occurrence discovered in northern Alberta and serves as an excellent case history of volcanic emplacement in the Western Canada Sedimentary Basin (WCSB) because of its road accessibility and the fact that it remains an isolated, multi-erupted body.

In 1996, the Alberta Geological Survey released Bulletin 63, *The Diamond Potential of Alberta* (Dufresne et al., 1996). At the time of its release, the Mountain Lake intrusion remained the only ultramafic rock discovery in northern Alberta. Hence, the primary objective of that report was to identify geological anomalies and target areas for future diamond exploration in the province. It was successful in that it made industry aware of Alberta's kimberlite potential, and kimberlite discoveries were subsequently made in two other regions of northern Alberta.

To date, 51 occurrences of kimberlite and non-archetypal kimberlite (alkaline) rocks have been found in three separate areas of northern Alberta: Mountain Lake, and the Buffalo Head Hills and Birch Mountains fields (Figure 1). A summary of the location, geochronology and diamond content of the individual bodies is presented in Appendix 1.

Because the ultramafic bodies in northern Alberta are removed spatially and tectonically from other North American kimberlite-bearing cratons, the northern Alberta fields are collectively referred to as the northern Alberta kimberlite province (Eccles et al., 2004). More than 90 km separate the three areas of kimberlitic rocks in northern Alberta, so the three areas may be referred to as separate clusters or fields within the northern Alberta kimberlite province. The diamondiferous Buffalo Head Hills kimberlite field in north-central Alberta has received the most exploration attention because of the large, near-surface dimensions of its kimberlite bodies, their potentially economic grades and the high ratio of diamondiferous to barren kimberlite. However, it is fair to say that all kimberlitic bodies in northern Alberta are of interest due to the preservation of intra- and extra-crater facies of kimberlite, which allows researchers to study the uppermost portion of kimberlite bodies that is commonly sheared off or eroded in many other parts of the world. In addition, the kimberlite sample tract, which includes material sequestered from the deep mantle (150–450 km) through to the Earth's surface, provides a unique opportunity to study otherwise inaccessible geological environments.

The intent of this report is not to act as a sequel to Bulletin 63 by placing emphasis on prospective target areas. Rather, its main goal is to document the first 20 years (1990–2010) of ultramafic discovery and examination in the northern Alberta kimberlite province. The comprehensive summary comprises publicly available kimberlite and related rock information from industry, academia and government. Industry assessment reports and peer-reviewed publications include contributions detailing exploration, discovery, history, geology and estimated diamond content of northern Alberta ultramafic discoveries (e.g., Wood and Williams, 1994; Wood et al., 1998; Skelton and Bursey, 1998, 1999; Aravanis, 1999; Carlson et al., 1999; Skelton and Willis, 2002; Skelton et al., 2003; Hood and McCandless, 2004; French, 2010).

Academic theses and research studies have provided some of the first glimpses of northern

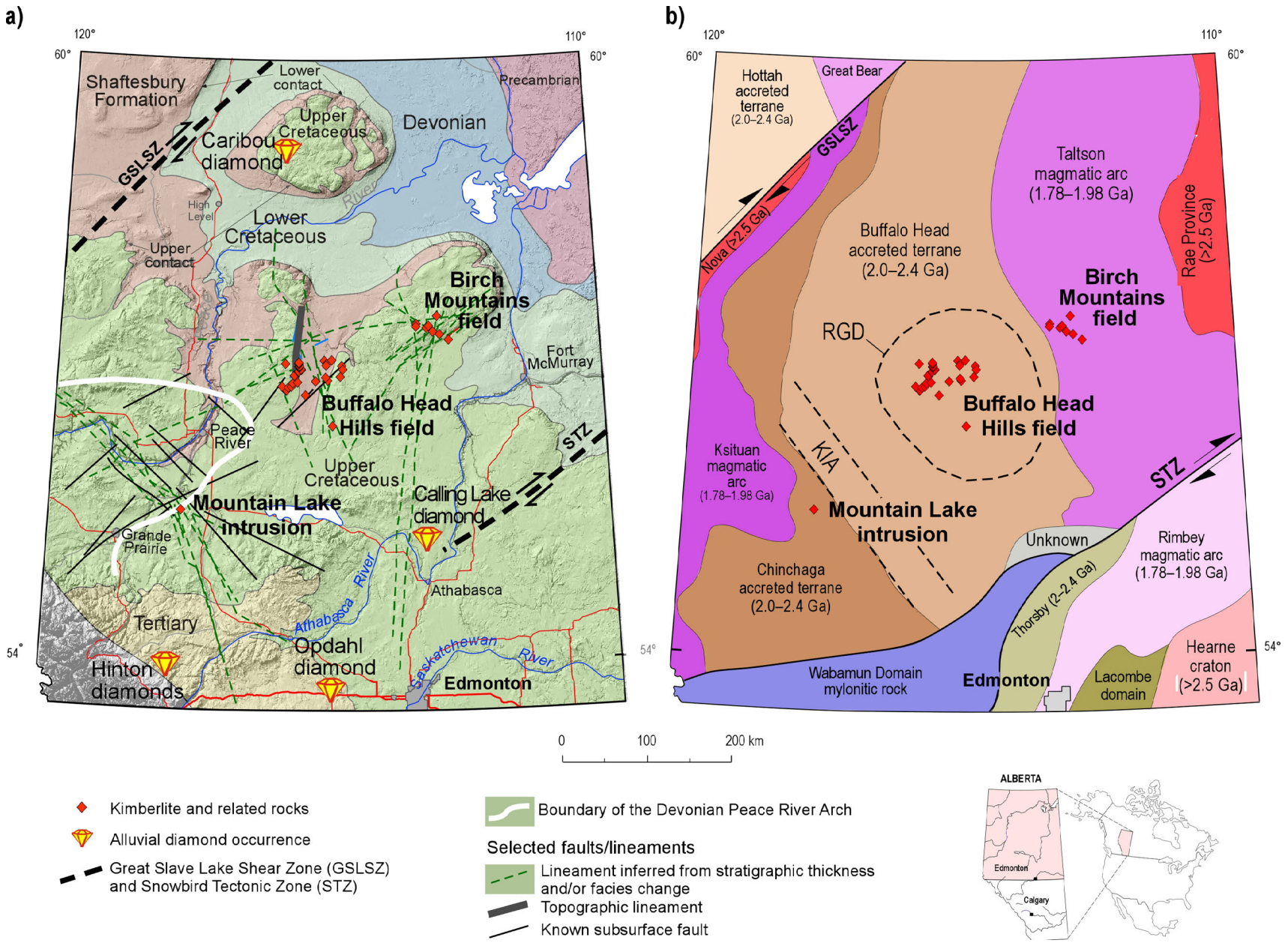
a)
120°
110°
60°
54°
Shaftesbury Formation
Lower contact
Upper Cretaceous
Caribou diamond
Devonian
Precambrian
GSLSZ
High Level
Lower Cretaceous
Upper contact
Birch Mountains field
Fort McMurray
Buffalo Head Hills field
Peace River
STZ
Upper Cretaceous
Calling Lake diamond
Mountain Lake intrusion
Grande Prairie
Athabasca River
Athabasca
Tertiary
Opdahl diamond
Hinton diamonds
Saskatchewan River
Edmonton
b)
Hottah accreted terrane (2.0–2.4 Ga)
Great Bear
GSLSZ
Nova (>2.5 Ga)
Taltson magmatic arc (1.78–1.98 Ga)
Rae Province (>2.5 Ga)
Buffalo Head accreted terrane (2.0–2.4 Ga)
Birch Mountains field
RGD
Buffalo Head Hills field
KIA
Ksituan magmatic arc (1.78–1.98 Ga)
STZ
Mountain Lake intrusion
Unknown
Rimbey magmatic arc (1.78–1.98 Ga)
Chinchaga accreted terrane (2.0–2.4 Ga)
Thorsby (2–2.4 Ga)
Hearne craton (>2.5 Ga)
Wabamun Domain mylonitic rock
Edmonton
Lacombe domain
0
100
200 km
Kimberlite and related rocks
Alluvial diamond occurrence
Great Slave Lake Shear Zone (GSLSZ) and Snowbird Tectonic Zone (STZ)
Boundary of the Devonian Peace River Arch
Selected faults/lineaments
Lineament inferred from stratigraphic thickness and/or facies change
Topographic lineament
Known subsurface fault
ALBERTA
Edmonton
Calgary

Alberta diamond-inclusion data, mantle mineralogy and kimberlite petrography, as well as mechanisms of emplacement (e.g., Aulbach et al., 2004; Davies et al., 2004; Griffin et al., 2004; Boyer, 2005; Banas et al., 2007; Stachel et al., 2010). Government studies are also considered in this synthesis, particularly those that compare and contrast the physical and chemical characteristics of the northern Alberta kimberlite province with worldwide kimberlite and related rock types, and contemplate inter- and intra-field relationships within the northern Alberta kimberlite province. A detailed list of selected kimberlite-related government publications is presented in Appendix 2.

Lower crust and mantle xenocryst data created by Alberta Geological Survey (Eccles et al., 2002; Dufresne and Eccles, 2005; Eccles, 2007a), together with mineral assessment report data (e.g., Aravanis, 1999), form an inclusive discussion of mantle characteristics. In addition to publicly available information, this report presents previously unreleased kimberlite and related rock data, including new geochronological, QEMSCAN® mineralogy, and whole-rock and mineral-separate geochemical/isotopic data.

The report provides a field-by-field description of the three fields that make up the northern Alberta kimberlite province, in chronological order of discovery: Mountain Lake, Buffalo Head Hills and Birch Mountains. This field-by-field approach is used—as opposed to an amalgamated story that combines all three fields—to present an assortment of geological idiosyncrasies for each of the fields. Summarized are the events that led to the discovery of the kimberlitic rocks, the geological setting in which they were discovered, geochronology, physical and chemical volcanological characteristics, rock classification, emplacement characteristics, and diamond content. The compilation and interpretations will enable

- explorers to evaluate present and future diamondiferous kimberlite discoveries that may one day lead to an economic diamond deposit in Alberta;
- government to better manage this potentially new provincial resource; and
- Albertans to be better informed about diamondiferous kimberlite in their province and communities.

Figure 1. (see page 2) Distribution of kimberlite and related rocks, and alluvial diamond occurrences in the **northern Alberta kimberlite province: a) general bedrock geology on a hill-shaded digital elevation model (from Hamilton et al., 1999), showing the inferred boundary of the Devonian Peace River Arch (O'Connell et al., 1990) and lineaments from stratigraphic isopach thickness and/or facies changes (Pană et al., 2001); b) inferred basement terrane (from Ross et al., 1994), with dashed outlines of the Kimiwan isotopic anomaly (KIA; Burwash et al., 1993) and the Red Earth granulite domain (RGD; Burwash et al., 2000).**

2 Mountain Lake Intrusion

2.1 Discovery and Exploration History

The Mountain Lake ultramafic intrusion is approximately 75 km northeast of the city of Grande Prairie in northwestern Alberta (Figure 1). Monopros Limited, the then-Canadian exploration subsidiary of De Beers, initially targeted the area in 1988 and 1989 because of positive stream-sediment, heavy-mineral sampling results in Mountain Lake Creek, where it crosses Highway 676 (Figure 2). Monopros recovered northern Alberta's first ultramafic volcaniclastic rocks in 1990 after a group of geologists shovelled into the crown of a topographic high adjacent to Mountain Lake creek. In 1991, follow-up ground geophysics outlined two separate positive magnetic anomalies (Wood and Williams, 1994). Monopros drilled nine holes (totalling about 1750 m) and identified two adjacent bodies that coincided with the ground geophysical anomalies: Mountain Lake South and Mountain Lake North (Wood et al., 1998).

In 1995, the Geological Survey of Canada and the Alberta Geological Survey conducted a collaborative two-drillhole scientific program to study the petrology, indicator-mineral geochemistry, aeromagnetic signature, age,

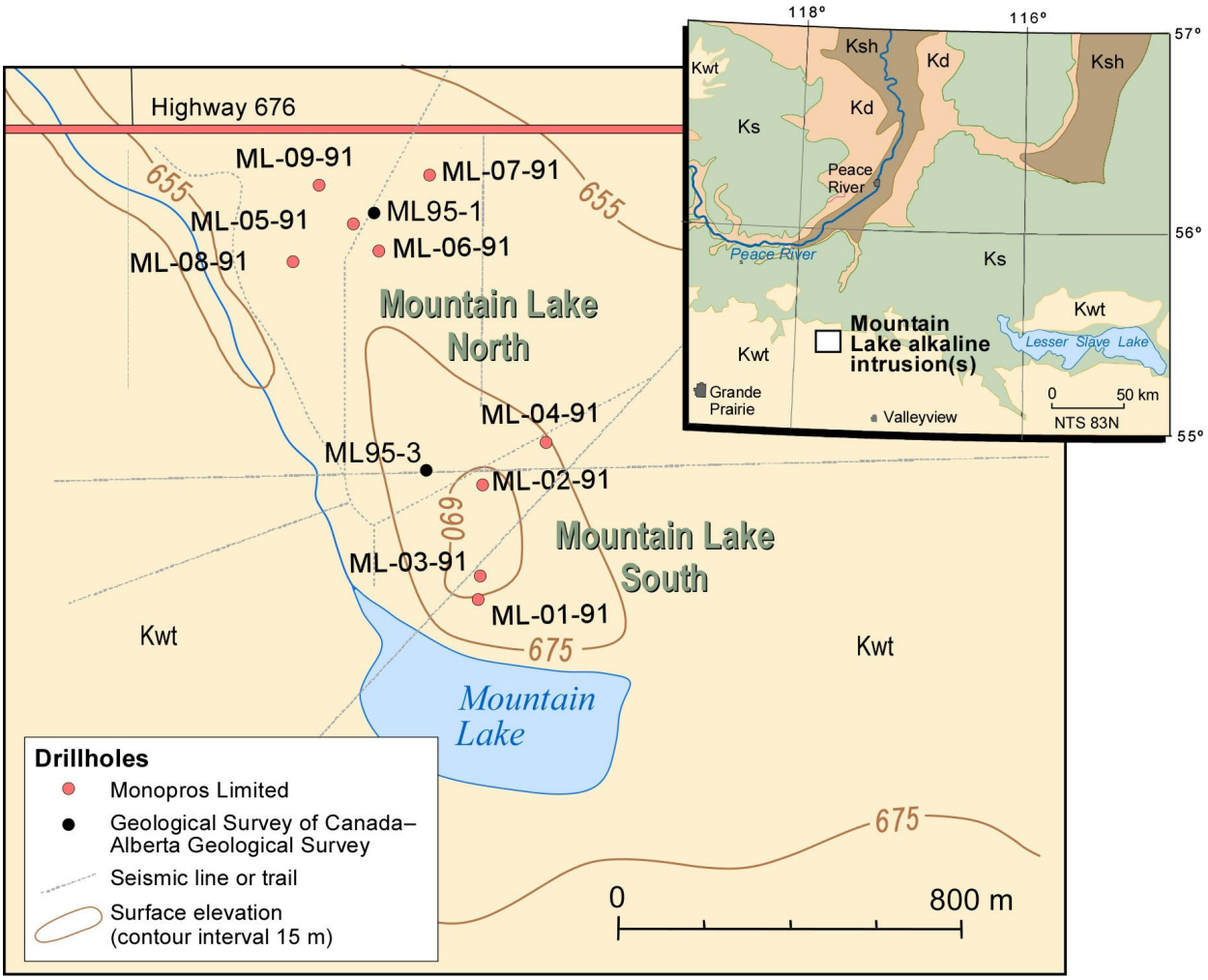

Figure 2. General bedrock geology and drillhole locations for the Mountain Lake South and North alkaline ultrabasic bodies in northwestern Alberta. Late Cretaceous bedrock geology abbreviations: Ksh, Shaftesbury Formation; Kd, Dunvegan Formation; Ks, Smoky Group; Kwt, Wapiti Formation.

stratigraphic position and emplacement setting of the Mountain Lake intrusion (Figure 2, drillholes ML95-1 and -3; Leckie et al., 1997). In 2000, Monopros allowed the Mountain Lake mineral permit to lapse and the property was re-staked by New Claymore Resources Ltd. New Claymore completed airborne and ground geophysical surveys, and drilled the Pearl anomaly directly west of Mountain Lake in an attempt to locate other kimberlitic intrusions, but none was encountered (Rich, 2003). To date, no other intrusions have been reported in the Mountain Lake area.

2.2 Geological Setting

The Mountain Lake intrusion is situated within a prominent, curvilinear aeromagnetic low known as the Chinchaga Terrane (Figure 1b). These Precambrian basement rocks are covered by approximately 2500–2900 m of Phanerozoic sedimentary rocks. The few drillholes to penetrate the Phanerozoic and extend into the Chinchaga basement recovered metasedimentary and metaplutonic rocks, with one occurrence of massive porphyritic granitic rock (Ross et al., 1994). The metaplutonic rocks crystallized ca. 2.19–2.08 Ga, and ε_{Nd} data suggest the presence of an Archean component but with a greater proportion of juvenile material relative to the Taltson and Buffalo Head domains to the east (Thériault and Ross, 1991).

The Phanerozoic sequence, from base to surface, comprises

- Cambrian Granite Wash siliciclastics;
- Devonian carbonate, evaporite and shale; Mississippian carbonate and shale;
- Permian mixed carbonate and sandstone;
- Triassic dolomite, siltstone and shale;
- Jurassic shale and limestone; and
- a thick (1100–1180 m) sequence of Cretaceous siliciclastic sedimentary rocks.

The Mountain Lake bodies subcrop or outcrop within the early Late Campanian to Maastrichtian Wapiti Formation of the Western Canada Sedimentary Basin (Figure 3; Leckie et al., 1997).

The Wapiti Formation consists of light grey, fine- to medium-grained, argillaceous, carbonaceous sandstone with interbedded siltstone, silty shale and thin layers of bentonite and coal, and is locally conglomeratic (Dawson et al., 1989). Leckie et al. (1997) estimated the thickness of the Wapiti Formation to be 150–200 m at Mountain Lake.

Surficial deposits in the Mountain Lake area are associated with ice-advance, stagnation, deglaciation and postglacial processes, and include diamict (till) and glaciolacustrine silt and clay. Sediments of glaciofluvial, eolian, colluvial, alluvial and organic origin are widespread but of limited areal extent. Balzer (2000) completed a regional surficial geology interpretation in the Winagami region, which encompasses Mountain Lake, and interpreted the Quaternary geology of the region as being consistent with at least one Late Wisconsinan advance of the Laurentide Ice Sheet. Glacial sediments of possible earlier advances are present, but their chronostratigraphic relationship is speculative. The dominant ice-flow direction was south to southwest (Balzer, 2000) and corresponds with the main advance of the ice sheet (i.e., when ice thickness was at its maximum). Topographically controlled ice-flow directions correspond to thinner ice lobes marginal to the ice sheet, during the initial stages of ice advance and deglaciation.

Drift thickness in the Winagami region varies from a veneer on topographic highs to more than 150 m within at least six infilled paleochannels of variable depth, although their exact geometry

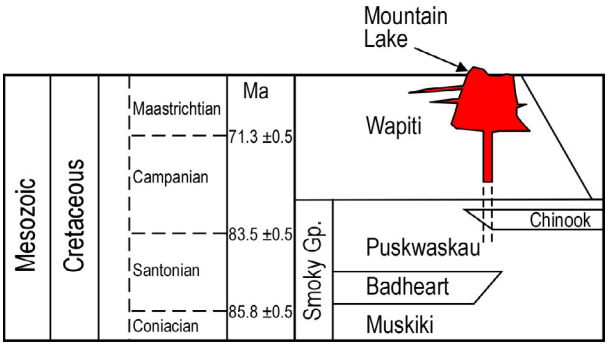

Figure 3. Stratigraphic setting of the northwestern Great Plains region and inferred emplacement position of the Mountain Lake intrusion. Isotopic age references from Okulitch (2002).

remains unknown (Balzer, 2000). Rotary drilling by Pawlowicz et al. (1995) showed there is about 1.5 m of till on the top and about 1.5 m of clay on the northern flank of the Mountain Lake South intrusion. The surface till is olive-brown silty clay and contains abundant clasts of the local bedrock, primarily sandstone and shale. Pawlowicz et al. (1995) reported that the till thickens to about 22 m in an augerhole located about 2 km southwest of Mountain Lake. The till in this core is composed of olive-brown silty clay in the upper 10 m, changing gradually at depth to a dark grey clayey till.

Structurally, the Mountain Lake intrusion occurs on the southern flank of the Peace River Arch, which protruded during the Devonian before forming an embayment during the Campanian (Figure 1a; O'Connell et al., 1990). Ross et al. (1991) noted that a sharp aeromagnetic boundary separates the Chinchaga Terrane from the Buffalo Head Terrane on the east and the Ksituan Terrane on the west, possibly suggesting a faulted contact on both sides of the Chinchaga Terrane. This aeromagnetic boundary also coincides with a zone of significantly depleted $\delta^{18}O_{SMOW}$[1] values that led Muehlenbachs et al. (1993) and Burwash et al. (2000) to suggest that the anomaly, known as the Kimiwan isotopic anomaly (KIA on Figure 1b), formed by surface-derived fluids interacting with basement rocks in a northwest-trending zone of crustal extension. A LITHOPROBE Peace River Arch Industry Seismic Experiment (PRAISE) seismic survey across the Kimiwan isotopic anomaly showed pre–1.8 Ga extensional faults penetrating to depths of at least 35 km (and probably to the Moho; Hope and Eaton, 2002). On a local scale, Leckie et al. (1997) inferred, from high-resolution aeromagnetic data (HRAM), that three north-trending faults occur east of the Mountain Lake bodies. However, there does not appear to be any correlation between these faults and the orientation and position of the bodies, so it is unknown whether regional faulting played a role in controlling the location of the intrusion.

Lastly, a west–east LITHOPROBE seismic reflection survey in northwestern Alberta identified a series of subhorizontal reflections, known as the Winagami reflection sequence, that are interpreted as discordant, tabular, mafic intrusions covering an inferred area of 120 000 km^2 at depths of 10–20 km (Ross and Eaton 2002). The limited extent of this survey and the perception that only the thickest sheets (>60 m) would fall above seismic resolution suggest that the true volumetric significance of this magmatic pulse is understated. Ross and Eaton (1997) tentatively constrained the age of the sequence to between 1880 and 1760 Ma. Importantly, they noted that seismic evidence, such as crosscutting fabrics, demonstrates post-tectonic emplacement. Ross and Eaton (2002) suggested that the 'centre' of the Winagami reflection sequence magmatic emplacement was not imaged and may lie north-northeast of the reflection survey, a proposal based on the presence of a 10–12 km thick, intermediate velocity (7.0–7.4 km/s) interval of lower crust at the north end of the section.

2.3 Palynology and Geochronology

Palynology of nonmarine sedimentary clasts within the intrusion was used by Wood et al. (1998) to infer a maximum emplacement age of mid-Maastrichtian, probably ca. 68 Ma (Figure 3). Leckie et al. (1997) reported that laminated sediments, which they interpreted to be interbedded with volcaniclastic deposits, and mudstone clasts have a palynological assemblage similar to the Dinosaur Park Formation and are latest Campanian (between ca. 76 and 75 Ma). Three samples of sandstone from Mountain Lake North (drillhole ML95-1) were processed for apatite fission-track (AFT) dating. The central AFT ages range from 78 ±9 to 72 ±7 Ma (Leckie et al., 1997). To summarize, the existing sedimentary data indicate the emplacement age for the Mountain Lake intrusion is late Late Cretaceous, or between ca. 76 and 68 Ma.

Isotopically datable minerals in the Mountain Lake intrusive are either rare (perovskite) or pervasively altered (phlogopite). Relatively fresh perovskite was identified in Mountain Lake North drillhole ML95-1 at a depth of 63.5–65.1 m. A single fraction of fresh, cubic, brownish-black perovskite yielded a robust U-Pb isotopic age of 90.6

[1] see Table 1

Table 1. Abbreviations and calculations used in this report.

cpht	carats per hundred tonnes
HREE	heavy rare-earth element (Ho, Er, Tm, Yb and Lu)
LA-ICP-MS	laser-ablation inductively coupled plasma–mass spectrometry
LREE	light rare-earth element (La, Ce and Nd)
m asl	metres above sea level
Ma	million years
MREE	medium rare-earth element (Sm, Eu, Gd, Tb and Dy)
P	pressure
REE	rare-earth element
REEN	chondrite-normalized rare-earth element
T	temperature (°C)
Pyroxene End-Member Compositions	
Ae	aegirine
En	enstatite
Fs	ferrosilite
Jd	jadeite
Wo	wollastonite
Garnet End-Member Compositions	
Alm	almandine
Gr	grossular
Py	pyrope
Sp	spessartine
Uv	uvarovite
G1, G2…G12	Group 1, Group 2…Group 12 garnet classification following the nomenclature of Dawson and Stephens (1975)
Magnesium-Rich Olivine End-Member Compositions	
Fo	forsterite
Calculations	
CI	Contamination index of Clement (1982) = $(SiO_2 + Al_2O_3 + Na_2O) / (MgO + 2K_2O)$; used to measure the proportion of clay minerals and tectosilicates relative to olivine and phlogopite
Ca intercept	If $CaO \leq 3.375 + (0.25 \times Cr_2O_3)$, then Ca intercept = $(13.5 \times CaO) / (Cr_2O_3 + 13.5)$; otherwise, Ca intercept = $CaO - (0.25 \times Cr_2O_3)$ (Grütter et al., 2004)
Ca#	100 x atomic Ca / (Ca + Mg)
Cr#	100 x atomic Cr / (Cr + Al)
Mg#	100 x atomic Mg / (Mg + total Fe)
SMOW	Oxygen isotope value ($\delta^{18}O$) normalized to standard mean ocean water
T_{Mn} (°C)	For garnet with $Cr_2O_3 > 1$ wt. % and $TiO_2 < 0.4$ wt. % = $1000 / [0.268 + 0.374 \times \ln(MnO_{gt} / MnO_{ol})]$, where $MnO_{ol} = 0.104$ (Grütter et al., 1999)
T_{Ni} (°C)	= $8772 / (2.53 - \ln(D_{Ni}^{gt/ol}))$ (Canil, 1999)

±3.0 Ma (2σ; L. Heaman, pers. comm., 2010). This age is significantly older (by ~15–23 million years) than the palynological and apatite fission-track ages. Perhaps the best explanation for this age discrepancy is that the Mountain Lake intrusion experienced multiple eruptive episodes. The ~91 Ma age is then representative of an older eruption, such that the seemingly isolated perovskite-laden material is autolithic and was transported to the present-day surface by the palynologically determined, younger (ca. 76–68 Ma) eruptive event. The autolithic theory could explain why perovskite is present in this particular section of the intrusion but not observed in the majority of the Mountain Lake core and trench material. Regardless, the discrepancies between

the radiometric dating and the various independent methods mean that further examination and analyses are needed to resolve the Mountain Lake intrusion's absolute emplacement age.

2.4 Inferred Morphology

Because the Mountain Lake intrusion remains isolated and is road accessible, Kellett et al. (2005) compiled several orientation geophysical studies completed over the intrusion. The Mountain Lake intrusion has a distinct topographic, magnetic, resistivity and gravity response compared to its Late Cretaceous host rocks. It produces a 10 nT magnetic anomaly and a 0.3 mGal Bouguer gravity anomaly, and has a 50 m thick conductive core (<10 ohm•m). The Mountain Lake intrusion forms a positive-relief, ovoid feature approximately 0.5 km wide by 1.5 km long (Figure 2). The Mountain Lake South body forms a pronounced topographic high (about 30 m high) and measures 400 by 650 m (26 ha), whereas Mountain Lake North has little topographic expression and measures about 250 by 350 m (9 ha) as defined by the boundary of a weakly positive ground-magnetic signature. It is presumed that Mountain Lake South is topographically elevated because the regional country rock of the Wapiti Formation is less resistant to erosion than the volcanogenic rocks.

The actual geometry of the Mountain Lake intrusion at depth is unknown. Because of the shallow depth and volume of natural gas in northern Alberta, regulatory conditions are imposed on drilling, such that protective equipment (e.g., blow-out protectors) is generally required for holes being drilled to depths greater than approximately 200 m. Hence, drillholes to test Mountain Lake have not penetrated beyond this depth. Models of magnetic and resistivity data show deeper parts of the intrusion (250–400 m) to have subtly elevated magnetic susceptibility (0.01 [SI]) and elevated resistivity values (30 ohm•m). The intrusive body can be recognized by the presence of strong seismic diffractions, which extend to depth in the seismic section and have apices coinciding with the topographic and other geophysical expressions of the intrusion.

Three-dimensional (3-D) analyses of high-resolution aeromagnetic data show the Mountain Lake intrusion (at depth) is characterized by a single isolated body with two overlapping centres. In addition, the intrusion has widths of 500–750 m at a depth of ~200 m, and then narrows vertically to depth (Leckie et al., 1997).

2.5 Volcanogenic Observations

In hand specimen, Mountain Lake core comprises dark greenish-grey to black ash and juvenile lapilli tuff. The material is altered, such that the predominant feature is olivine phenocrysts and macrocrysts pseudomorphed to buff-coloured clay. The majority of the juvenile lapilli and single-grain olivine pseudomorphs are matrix supported and highly altered. The magmatic material is variably contaminated by clasts of sandstone (possibly Wapiti Formation) and shale (possibly Kaskapau Formation). Some core contains variable amounts of country-rock contamination by quartz, presumably from the Wapiti Formation. Mantle xenoliths are extremely rare. When potential mantle xenoliths are observed, they are small (<1 cm) and highly altered, making recognition and subsequent analysis extremely difficult. Basement xenoliths are rare and small (<4 cm), and typically comprise feldspathic gneiss. In general, there is a lack of visible 'kimberlite' indicator minerals; when present, they are typically peridotitic assemblages <1 mm in diameter. Petrographic descriptions by Leckie et al. (1997), Wood et al. (1998), Skupinski and Langenberg (2002) and Eccles (2004) are summarized below. Pyroclastic material is best observed in the Mountain Lake South part of the intrusion. The high volume of juvenile magmatic material, with only a minor component of xenocrystic quartz, in Mountain Lake South has led several authors (e.g., Leckie et al., 1997; Field and Scott Smith, 1999) to suggest that Mountain Lake South be defined as a pyroclastic deposit. In contrast, Mountain Lake North, although similar in petrographic character to Mountain Lake South, has matrices that are variably contaminated by quartz, plagioclase, alkali feldspar, hornblende and biotite, suggestive of resedimented volcaniclastic rather than pyroclastic material.

Mountain Lake South consists mainly of olivine pseudomorph–rich, juvenile lapilli tuff (>2 mm clast size) and coarse ash tuff (<2 mm) that may be described simply as crystal tuff (Figure 4a). Single-crystal olivine phenocrysts and macrocrysts, which occur within the matrix and in juvenile lapilli, are euhedral to anhedral, up to 5 mm in size and completely pseudomorphed to Mg-Fe–silicate clay, carbonate and/or serpentine (Figure 4b). The juvenile lapilli have rounded to curvilinear boundaries (Figure 4c) and comprise altered olivine, serpentine, mica (phlogopite-biotite), spinel, rutile, perovskite, apatite, calcite, clay and occasionally fresh, euhedral clinopyroxene. Skupinski and Langenberg (2002) reported that some lapilli have cores of feldspar or other fragments (potentially from the wallrock), which may have acted as nucleating centres.

The olivine pseudomorphs and lapilli are set in a fine-grained matrix that has been extensively altered to clay materials, thus making the original mineralogy and textures difficult to describe optically. Mineralogical determinations using QEMSCAN® show that the matrix comprises an abundance of Mg-Fe±Ca–silicate clay with fine-grained micas (phlogopite?) and traces (<1%) of illite, Ti-minerals, K-feldspar, pyrite, chlorite, calcite and spinel (Figure 5). Alteration minerals were analyzed using a portable infrared mineral

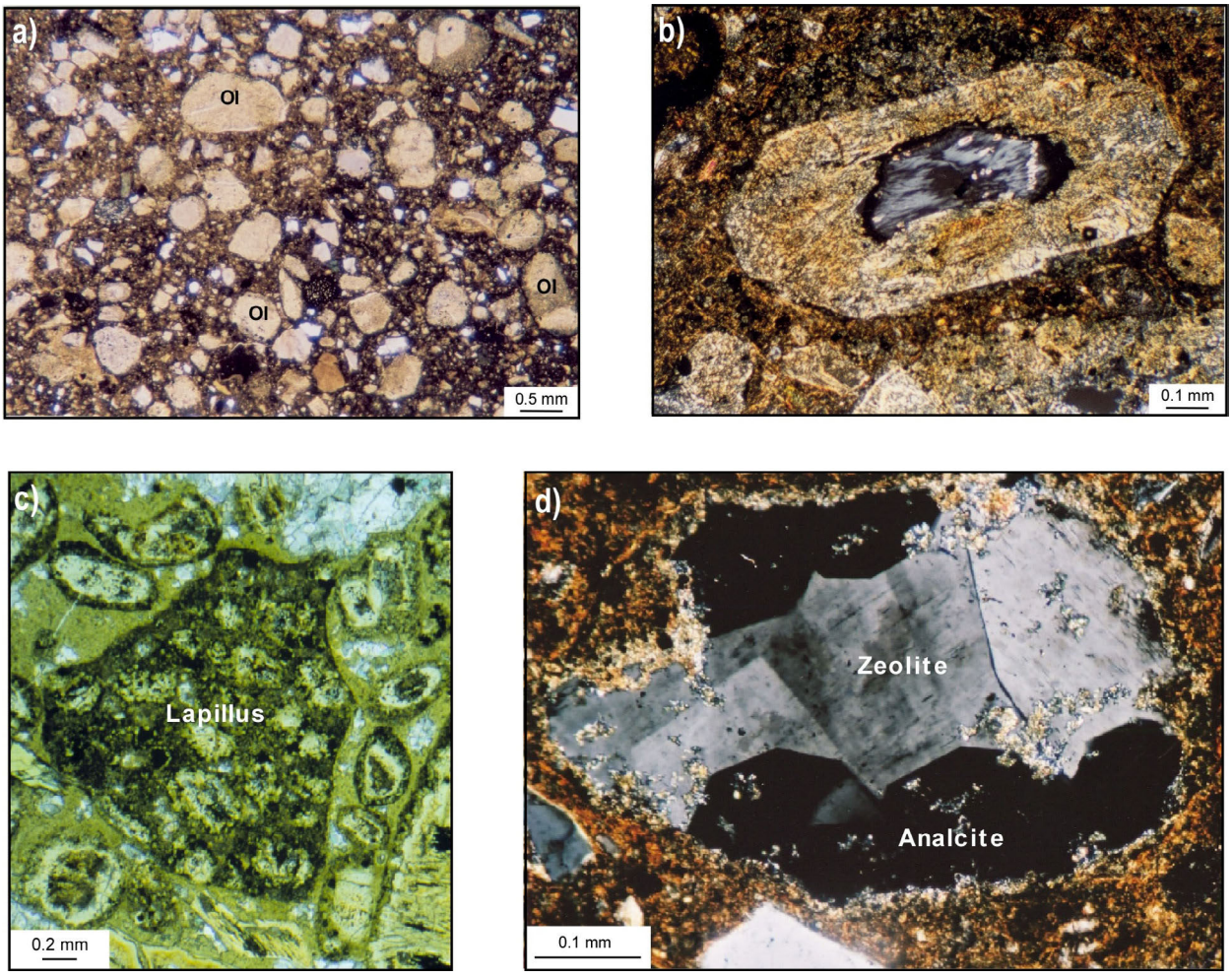

Figure 4. Selected photomicrographs from the Mountain Lake intrusion: a) crystal tuff texture (drillhole ML95-1, 161.9 m; partly crossed polars; Skupinski and Langenberg, 2002); b) euhedral olivine crystal pseudomorphed by clay and serpentine (ML95-3, 117.9 m; crossed polars; Skupinski and Langenberg, 2002); c) juvenile lapillus with curvilinear margins (ML95-3, 29.8 m; plane polars); d) black euhedral analcite and grey zeolite (ML95-1, 7.22 m; crossed polars; Skupinski and Langenberg, 2002). Abbreviation: Ol, olivine.

analyzer (PIMA™). The mineral suite within the shortwave infrared spectrum from a single Mountain Lake core sample comprises Mg-silicate and apophyllite phases, the latter implying a zeolitic phase (Hauff et al., 2001).

Skupinski and Langenberg (2002) reported that minerals atypical of *sensu stricto* kimberlite are common and include amphibole, spessartine and analcite (e.g., Figure 4d). In addition, they noted that secondary analcite and apophyllite are similar in appearance to those of some alnoitic ultramafic rocks from the Missouri River Breaks in Montana (Hearn, 1986).

2.6 Whole-Rock Geochemistry

Kimberlites sample crustal material as they penetrate from depths of >150 km to the Earth's surface. Tests proposed by Clement (1982) and Kjarsgaard et al. (2009) are used to determine the extent of contamination. Clement (1982) used the contamination index (CI = [SiO_2 + Al_2O_3 + Na_2O] / [MgO + 2K_2O]) to measure the proportion of clay minerals and tectosilicates relative to olivine and phlogopite. Clement (1982) found that uncontaminated Group I kimberlite has a CI near 1.0. Kjarsgaard et al. (2009) suggested that the natural logarithm (log_e) of Si/Al is a sensitive parameter for dividing high-Al crustal rocks from kimberlite and should be used in combination with the CI. Whole-rock geochemical data from Mountain Lake have low to moderate Al influx (log_e(Si/Al) <2.5), with two distinct high CI groups (Figure 6). Mountain Lake South has a lower CI (2.7–3.2) than Mountain Lake North (3.5–8.8). Correlating with petrographic observations, Mountain Lake North has higher CI values due to resedimentation and mixing of magmatic rocks with the Wapiti Formation, compared to Mountain

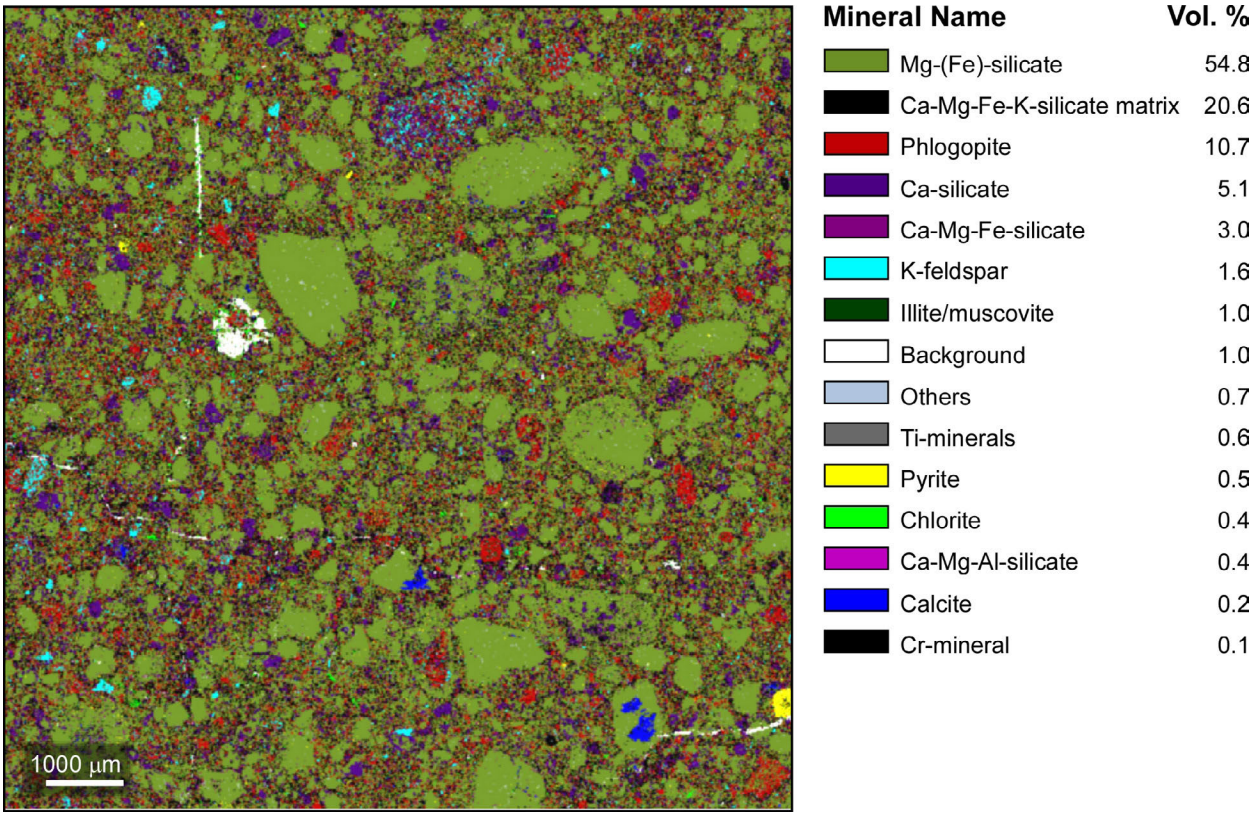

Figure 5. Mineralogical determination of the Mountain Lake South intrusion using QEMSCAN® **analysis at 10 µm resolution (drillhole ML-95-3, 88.6 m). Olivine macrocrysts are pseudomorphed to a Mg-(Fe)–silicate that may be an intermediate alteration phase between serpentine and saponite with minor alteration to calcite. There is an abundance of phlogopite in the matrix, together with an unidentified Ca-silicate (apophyllite?). A few K-feldspar grains are present, some of which have been altered to illite.**

Lake South, which comprises mainly juvenile-rich pyroclastic rocks.

The freshest, least contaminated samples from Mountain Lake South are characterized by 47.6 wt. % SiO_2, 8.4 wt. % Al_2O_3, 15.4 wt. % MgO with Mg# of 82, 2.1 wt. % K_2O, 1.5 wt. % Na_2O, peralkalinity index (molar $[K_2O + Na_2O] / Al_2O_3$) of 0.56, Niggli *k* (molar $K_2O / [K_2O + Na_2O]$) of 0.48 and Niggli *mg* (molar MgO / [MgO + FeO + Fe_2O_3 + MnO]) of 0.75. This major-element chemistry is not consistent with either kimberlite (25–35 wt. % SiO_2, <5 wt. % Al_2O_3 and Na_2O/K_2O ratio <0.5) or lamproite (peralkaline index <0.7, Niggli *k* >0.8 and Niggli *mg* >0.8). Rather, the diagram of $CaO + Na_2O + K_2O$ versus $SiO_2 + Al_2O_3$ of Le Maitre (1989) clearly discriminates between worldwide kimberlite and other ultramafic rock types, with the Mountain Lake South samples being more comparable to basanitic alkaline rocks (Figure 7).

The chondrite-normalized rare-earth element (REE_N) abundances from the Mountain Lake samples ($\Sigma_{Y, La–Lu} = 273$) are also lower than average kimberlite and lamproite ($\Sigma_{Y, La–Lu} = 508$ and 929, respectively) and have a flatter chondrite-normalized REE profile relative to kimberlite (Figure 8). Light REE (LREE; 90 to 210 times chondrite abundance for La) and the average La/Yb ratio (44) are lower in the Mountain Lake samples compared to those for average kimberlite. Some of the Mountain Lake samples display a slightly negative chondrite-normalized Eu anomaly similar to Roman Province–type lava and basanite in central Italy. In general, however, the overall Mountain Lake REE_N profile does not mimic these rock types. Rather, in REE_N space, the profile from Mountain Lake more closely resembles those of the southern Alberta Sweet Grass olivine minette and the Montana alnoite than kimberlite (Figure 8).

2.7 Mantle Characteristics

There are no known data available for mantle xenoliths from Mountain Lake due to their rarity and/or pervasive alteration. A representative

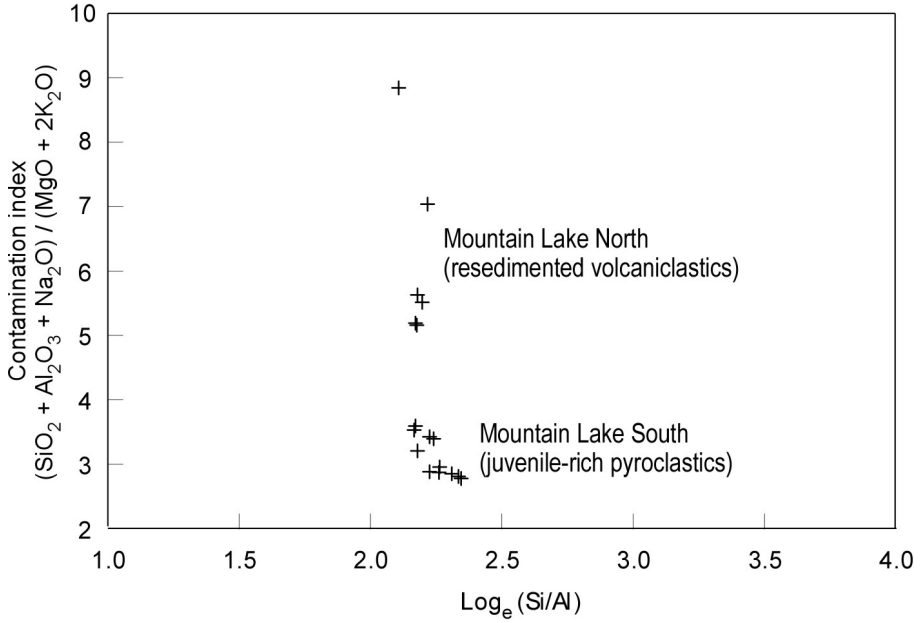

Figure 6. Plot of the contamination index (CI = [$SiO_2 + Al_2O_3 + Na_2O$] / [$MgO + 2K_2O$]) of Clement (1982) versus log_e(Si/Al) for whole-rock samples from the Mountain Lake intrusion. The Mountain Lake alkaline rocks have a wide CI range (between 2.7 and 8.8). In comparison, Clement (1982) found that uncontaminated Group I kimberlite has a CI near 1.0. The Mountain Lake South juvenile-rich pyroclastics are significantly less contaminated (2.7–3.6) than the Mountain Lake North resedimented volcaniclastics (5.2–8.8).

xenocryst assemblage was recovered by standard indicator-mineral processing and grain-picking from whole-rock samples of drillcore and surface-trench bulk samples (up to 10 kg). Recovered grains included peridotitic (and crustal) garnet, clinopyroxene, spinel and orthopyroxene. No eclogitic garnet or fresh olivine was recovered. Electron microprobe analysis on xenocrysts has been reported by Leckie et al. (1997), Skupinski and Langenberg (2002), and Eccles and Simonetti (2008), along with the new clinopyroxene and chromite data included in this report. Laser-ablation inductively coupled plasma–mass spectrometry (LA-ICP-MS) analysis on lherzolitic garnet was reported by Eccles and Simonetti (2008).

Using the garnet classification scheme of Grütter et al. (2004), which builds upon multivariate statistical analysis (e.g., Dawson and Stephens, 1975) and diamond-inclusion data (e.g., Gurney, 1984), peridotitic garnet (n = 62) from the Mountain Lake intrusion classifies as G9 lherzolitic garnet, with G11 high-TiO_2

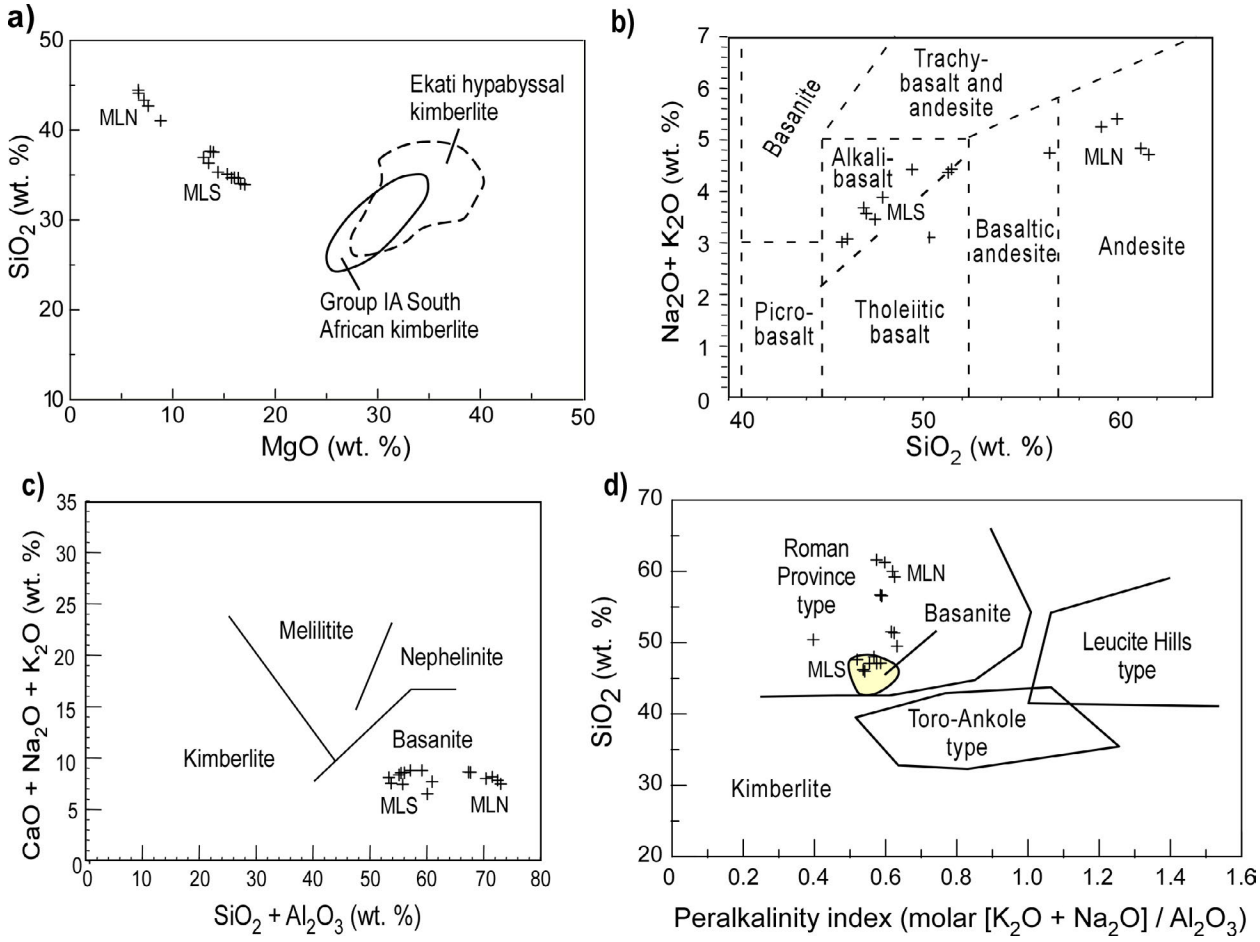

Figure 7. Alkali classification plots for whole-rock compositions from the Mountain Lake intrusion: a) SiO_2 versus MgO, with compositions of South African kimberlites (solid polygons) from le Roex et al. (2003), Harris et al. (2004) and Becker and le Roex (2006), and hypabyssal kimberlite from Ekati, Northwest Territories (dashed polygons) from Kjarsgaard et al. (2009) for comparison; b) total alkalis versus SiO_2 on the modified classification scheme of Le Maitre (1989); c) CaO + Na_2O + K_2O versus SiO_2 + Al_2O_3, with basanite, melilitite and nephelinite fields from Le Bas (1989) and kimberlite field from kimberlite in the northern Alberta kimberlite province; d) SiO_2 versus peralkalinity index (molar [K_2O + Na_2O] / Al_2O_3) for northern Alberta kimberlitic whole-rock compositions, with solid vectors and polygons representing the three groups of potassic lavas recognized by Barton (1979), specifically Roman Province–type (RPT) lavas, Leucite Hills–type (LHT) lavas and Toro-Ankole–type (TAT) lavas. Worldwide basanite fields in (c) and (d) from Le Maitre (1976) and Le Bas (1989). Abbreviations: MLS, Mountain Lake South; MLN, Mountain Lake North.

peridotitic and, less commonly, G12 wehrlitic types (Figure 9a, b). The peridotitic garnet has moderate to high Cr_2O_3 (averaging 8.3 wt. % and up to 12.8 wt. %); Mg# ranging from 78 to 86; and TiO_2 between 0.04 and 0.84 wt. %, averaging near the high-TiO_2 peridotitic (G11) cutoff of 0.3 wt. % TiO_2. The peridotitic garnet has a Ca-intercept distribution of between 4.2 and 5.3 (mode at 4.9). The high Ca-intercept could be due to an alkaline source and/or highly metasomatized mantle with elevated Ti and Ca (Figure 9c). In addition to peridotitic garnet, approximately 35% of the garnets analyzed (n = 33; not shown) were classified as crustal garnet, with end-member compositions of $Gr_{64–79}$ and $Alm_{20–32}$.

Temperatures of last equilibration were calculated using the Mn in peridotitic garnet temperature regression at 50°C (T_{Mn}; Grütter et al., 1999) and Ni-in-garnet geothermometer (T_{Ni}; Canil, 1999). Cores of lherzolitic garnet xenocrysts from the Mountain Lake intrusion are generally characterized by high T_{Mn} (>1100°C) and high T_{Ni} (>1130ºC; Figure 9b, d; Eccles and Simonetti 2008). The chondrite-normalized REE profiles and trace-element data for garnet show that two garnet types are evident: a high-Ti melt metasomatized lherzolite and a moderately fertile lherzolite (Figure 9e). Thus, the Mountain Lake lherzolitic garnet reflects entrainment of either two different protoliths or a single protolith that has undergone localized processes. The high-Ti melt metasomatized lherzolite has high Zr/Y ratios that correspond to high-T melt metasomatism and low Sc/Y_N, suggestive of re-enriched garnet (Figure 9f).

In contrast, the moderately fertile lherzolite, which trends toward a regime characterized by a high geothermal gradient, is less re-enriched (higher Nd/Y_N and Sc/Y_N) and has a negative Eu anomaly (Eu/Eu^*_N, where $Eu^*_N = [Sm_N + Gd_N] / 2$, of between 0.45 and 0.89). Thus, the moderately fertile lherzolitic garnet could represent a shallow level of subcontinental lithospheric mantle, an interpretation consistent with the Mountain Lake intrusion being classified as non-kimberlite, but not with the high T_{Ni} associated with these garnets. A deeper origin is therefore favoured for Mountain Lake peridotite.

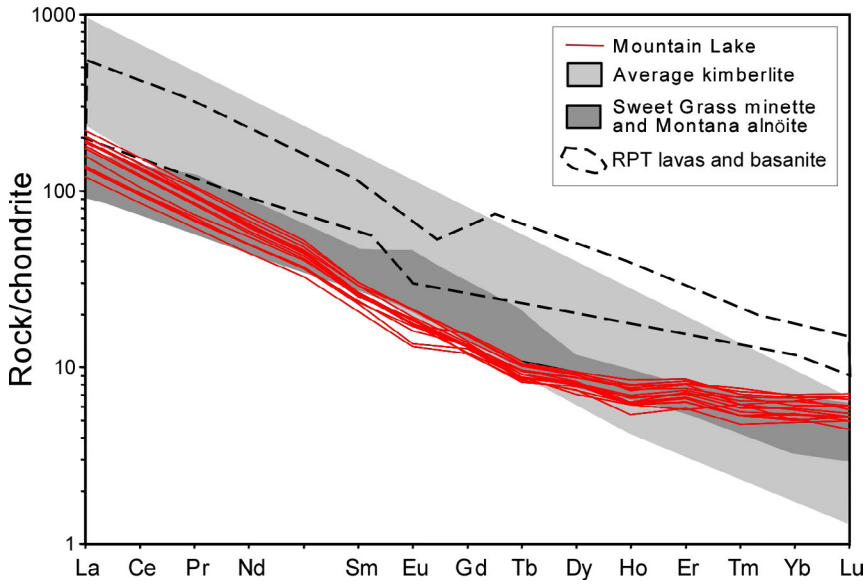

Figure 8. Chondrite-normalized (from Sun and McDonough, 1989) REE patterns for whole-rock compositions from the Mountain Lake intrusion. Provided for comparison are worldwide kimberlite from Mitchell (1986), Roman Province–type (RPT) lavas and basanite from Civetta et al. (1981) and Mitchell and Bergman (1991), and Sweet Grass minette and Montana alnoite from Hearn (1986), Kjarsgaard (1994) and Buhlmann et al. (2000).

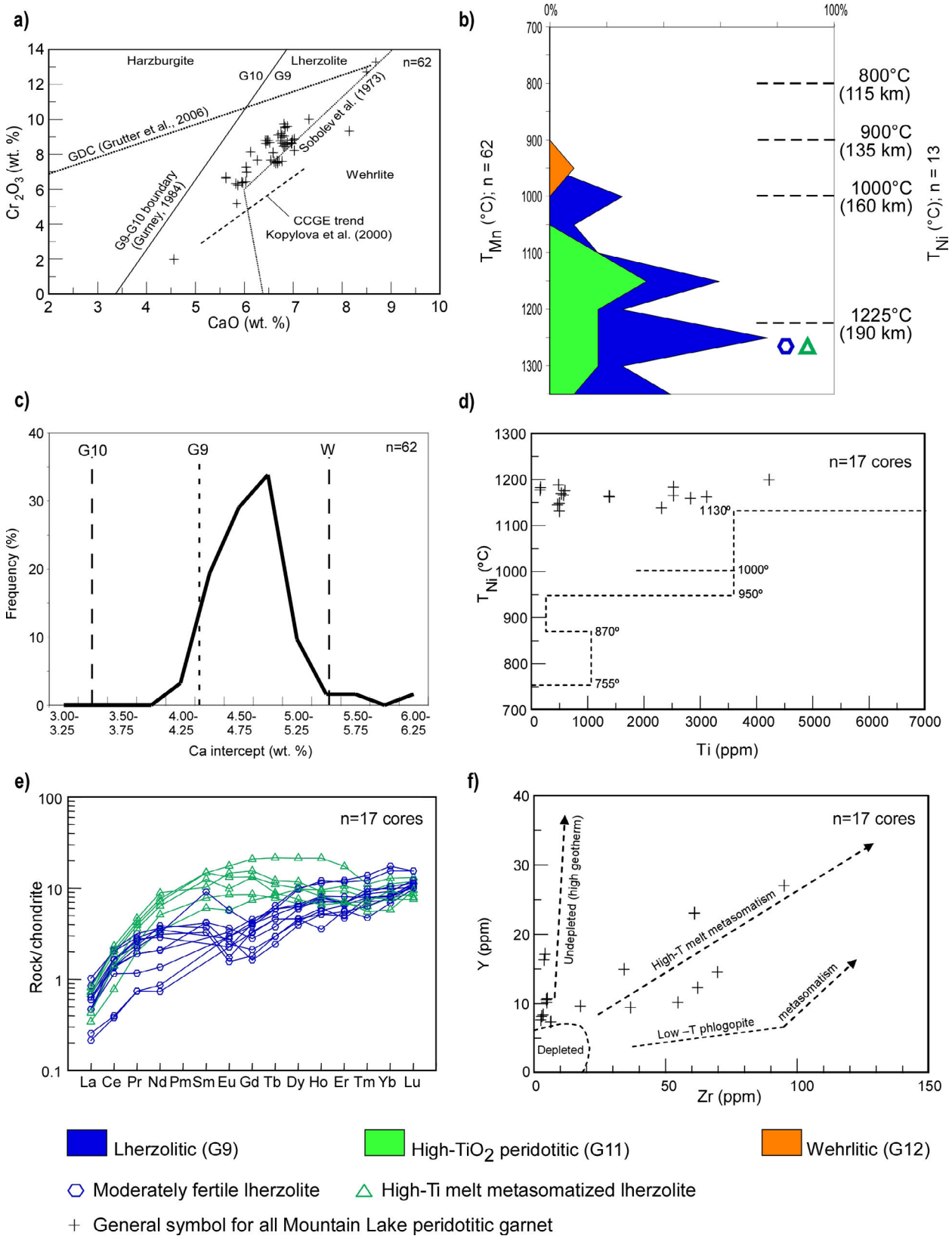
a)
Harzburgite
Lherzolite
G10
G9
n=62
GDC (Grutter et al., 2006)
Sobolev et al. (1973)
Wehrlite
G9-G10 boundary (Gurney, 1984)
CCGE trend Kopylova et al. (2000)
Cr2O3 (wt. %)
CaO (wt. %)
b)
0%
100%
800°C (115 km)
900°C (135 km)
1000°C (160 km)
1225°C (190 km)
TMn (°C); n = 62
TNi (°C); n = 13
c)
G10
G9
W
n=62
Frequency (%)
Ca intercept (wt. %)
d)
n=17 cores
1130°
1000°
950°
870°
755°
TNi (°C)
Ti (ppm)
e)
n=17 cores
Rock/chondrite
La Ce Pr Nd Pm Sm Eu Gd Tb Dy Ho Er Tm Yb Lu
f)
n=17 cores
Undepleted (high geotherm)
High-T melt metasomatism
Low –T phlogopite metasomatism
Depleted
Y (ppm)
Zr (ppm)
Lherzolitic (G9)
High-TiO2 peridotitic (G11)
Wehrlitic (G12)
Moderately fertile lherzolite
High-Ti melt metasomatized lherzolite
General symbol for all Mountain Lake peridotitic garnet

The co-existence of high-Cr garnet with Cr-spinel at Mountain Lake implies that garnet Cr content can be correlated with depth (Grütter et al., 1999). In addition, Skupinski and Langenberg (2002) reported the presence of rod-like β-ilmenite inclusions in olivine from Mountain Lake, a phenomenon that has been related to exsolution from the ultra high pressure Ti-bearing polymorph of olivine, wadsleyite, at depths of between 300 and 450 km (metamorphic peridotite from Alpe Arami, central Alps; Dobrzhinetskaya et al., 1996). Therefore, more suitable explanations for the negative Eu anomaly observed in the Mountain Lake fertile lherzolite garnet must involve a deeper source. Two possibilities for the negative Eu anomalies are 1) high-pressure, low-volume melts (e.g., majoritic garnet; Moore et al., 1991), or 2) a subducted oceanic lithosphere with enrichment in garnet-incompatible trace elements caused by dehydration and/or melt release from subducted slabs (Stachel et al., 2000).

The pyroxene data are calculated using the PX-NOM program of Sturm (2002), employing the Droop (1987) equation for estimating Fe^{3+}. Mountain Lake clinopyroxene (n = 77) generally plots within the quadrilateral diopside field on the ternary Wo-En-Fs system, with some grains falling within the augite and wollastonite fields (Figure 10a). End-member compositions have the following ranges: $Wo_{34–51}En_{40–56}Fs_{2–15}Ae_{0.2–10}$.

The diopside has variable Mg# (75–96), Ca# (38–56), low Na_2O (averaging 1.1 wt. %) and generally high Al_2O_3 (up to 6.3 wt. % and averaging 2.7 wt. %). Consequently, the majority of the Mountain Lake diopside grains do not plot in the mantle-equilibrated field between the jadeite and kosmochlor molecules on the Al-Cr-Na ternary diagram of Morris et al. (2002; Figure 10b). Rather, the high-Al diopside is better classified as either clinopyroxene from non-kimberlite sources or clinopyroxene that has equilibrated under crustal conditions. Leckie et al. (1997) tested the chemical composition of primary clinopyroxene from within juvenile lapilli. They also concluded that they do not fall in the field of clinopyroxene from kimberlite or from mantle lherzolite.

All clinopyroxene data are plotted on the Nimis and Taylor (2000) P-T diagram (Figure 10c). The majority of the data cluster near the graphite-diamond boundary or in an area of low-T and low-P clinopyroxene. The low-T and low-P data are likely invalid using this calculation due to their non-mantle source or the absence of garnet, in which case this clinopyroxene is attributable to spinel facies–type clinopyroxene, such that only the temperature calculation is valid. Mountain Lake orthopyroxene is bronzite, bordering on enstatite composition. It contains such wide variations in Mg# (81–94) and Al_2O_3 (0.6–3.6 wt. %) that it is not reliable for empirical thermobarometer estimates.

Mountain Lake Cr-spinel varies in composition from 30 to 59 wt. % Cr_2O_3, from 0.0 to 4.5 wt. % TiO_2 and from 8 to 17 wt. % MgO. No grains plot within the Cr_2O_3-MgO diamond-inclusion field defined by Gurney et al. (1993; Figure 11a). Chromite with >45 wt. % Cr_2O_3 and <5.5 wt. % TiO_2 can occur in a variety of high-pressure melts (e.g., Grütter and Apter, 1998; Barnes and Roeder, 2001). Using the empirical chromite classification

Figure 9. (see page 14) Variation diagrams for peridotitic garnet from the Mountain Lake intrusion: a) Cr_2O_3 versus CaO diagram; b) relative garnet species proportion and pressure-temperature distribution of peridotitic garnet cores; left Y-axis and solid polygon shading represent general peridotitic garnet paragenesis (i.e., G9, G11 and G12), together with the Grütter et al. (1999) Mn in peridotitic garnet temperature regression at 50°C (T_{Mn}) intervals; right Y-axis and symbols represent a significantly smaller subset of peridotitic garnet data to provide a detailed garnet nomenclature based on correlations between garnet Ni thermometry (Canil, 1999) and trace-element concentrations (Eccles and Simonetti, 2008); c) Ca-intercept method of representing garnet Cr/Ca content by a single number; Grütter et al. (2004) suggested that Ca-intercept values of <4.3 may be useful to discriminate diamond-stable from graphite-stable conditions in cratonic upper-mantle lithospheres (abbreviations: G9, Group 9 lherzolitic garnet; G10, Group 10 harzburgitic garnet; W, wehrlitic garnet); d) distribution of T_{Ni} versus Ti, where T_{Ni} is calculated using the Ni-in-garnet geothermometer of Canil (1999); e) chondrite-normalized REE diagram using chondrite values from Sun and McDonough (1989), with the two garnet groupings from Eccles and Simonetti (2008); f) Y versus Zr on the fields and metasomatic trends of Griffin et al. (1999).

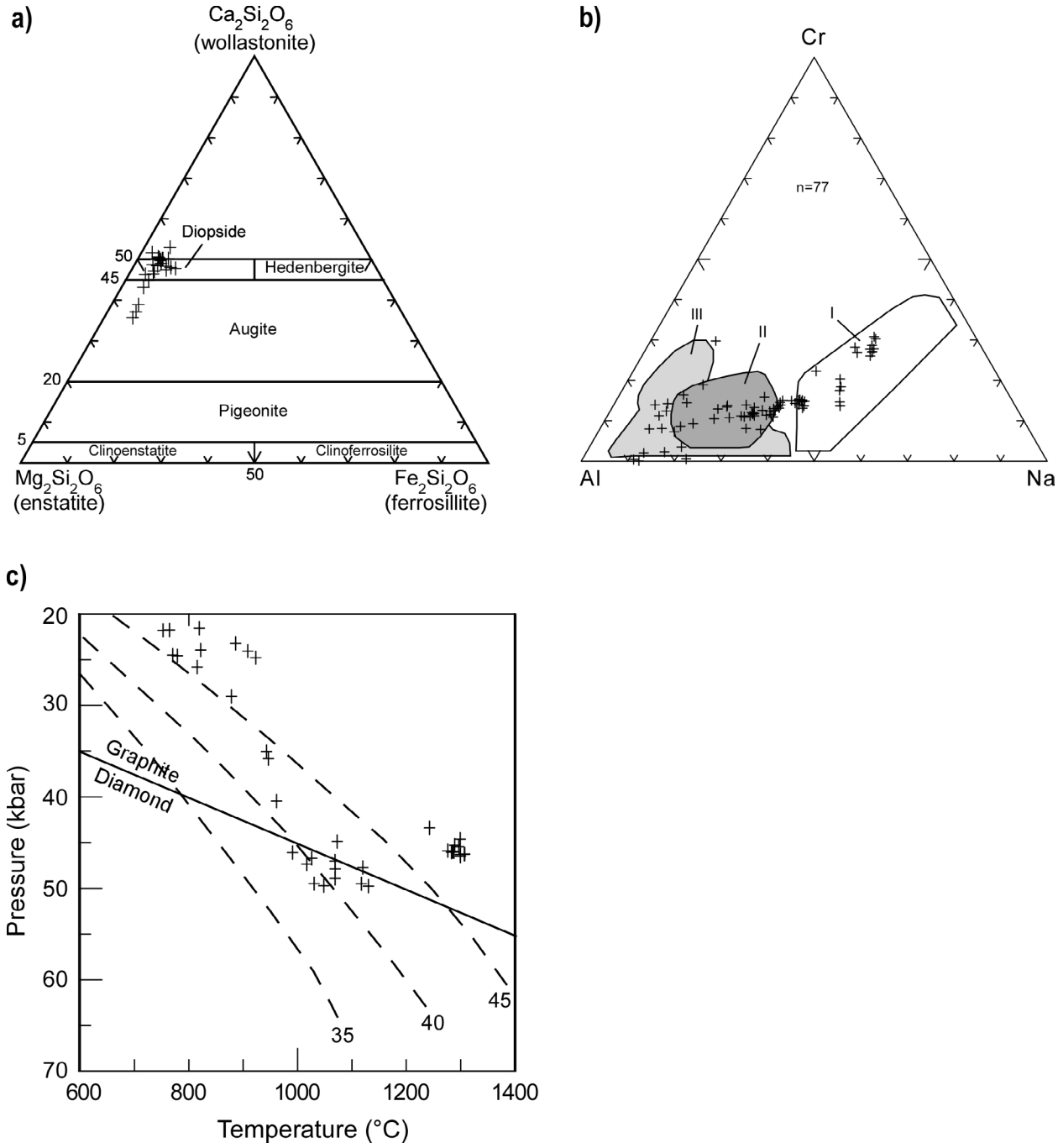

Figure 10. Variation diagrams for cores of clinopyroxene xenocrysts from the Mountain Lake intrusion: a) Ca-Mg-Fe quadrilateral pyroxene classification based on the scheme of Morimoto et al. (1988); b) Al-Cr-Na diagram, with classification fields modified after Morris et al. (2002), including mantle-equilibrated clinopyroxene derived from kimberlite (I), clinopyroxene from non-kimberlitic sources (II), and clinopyroxene equilibrated under crustal conditions (III); c) pressure-temperature diagram for clinopyroxene based on the thermobarometer of Nimis and Taylor (2000); garnet lherzolite–type clinopyroxene filters used cut-offs of <23 wt. % CaO, and >0.5 wt. % Cr_2O_3 with <4.0 wt. % Al_2O_3 (<4.5 wt. % Al_2O_3 for Cr_2O_3 >2.25 wt. %); geotherms (in mW/m^2, dashed lines) from Pollack and Chapman (1977); diamond-graphite equilibrium (solid dark line) from Kennedy and Kennedy (1976).

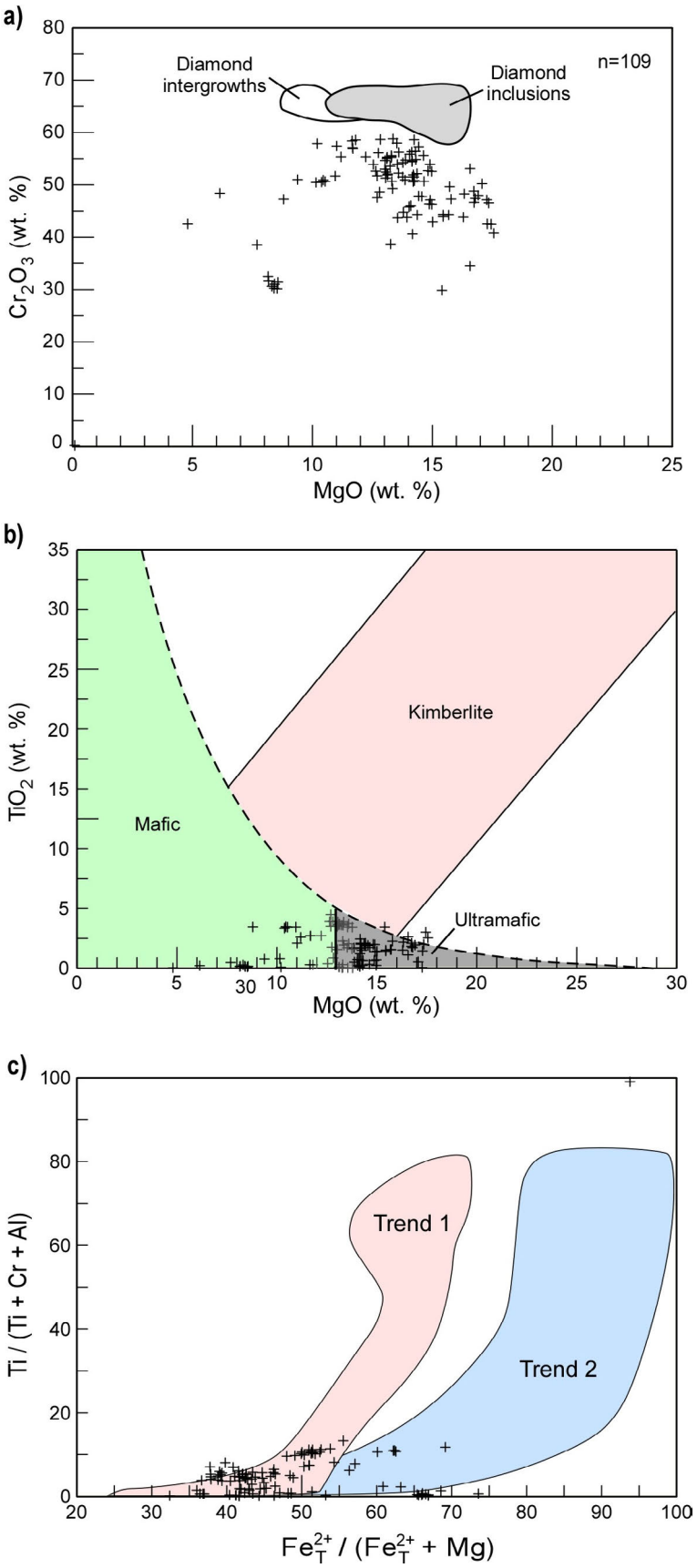

Figure 11. Variation diagrams for cores of **spinel xenocrysts from the Mountain Lake intrusion: a) Cr_2O_3 versus MgO diagram, with** diamond-inclusion and diamond-intergrowth **fields from Fipke et al. (1995); b) TiO_2** versus **MgO diagram, with fields from Creighton and Stachel (2008); c) Ti / (Ti + Cr + Al) versus** Fe^{2+} **/ (Fe^{2+} + Mg), with magmatic trend 1 and 2 fields from Mitchell (1986).**

scheme of Creighton and Stachel (2008), Mountain Lake chromite plots predominantly in the field of ultramafic rocks (Figure 11b). Wood et al. (1998) reported that the compositions of groundmass spinel exhibit a compositional 'magmatic trend 1,' which Mitchell (1995) associated with Group I kimberlite. However, Figure 11c shows that a chromite trend 1 is equivocal and the data could just as easily resemble a magmatic trend 2 signature.

2.8 Classification

The Mountain Lake rocks were initially described as "known kimberlite" (Wood and Williams, 1994). However, as various volcanologists examined rocks from the Mountain Lake intrusion, it became apparent that these rocks are not archetypal kimberlite. For example, Kjarsgaard (1997) reported that the Mountain Lake body may be of ultramafic lamprophyre affinity, based on results from whole-rock geochemistry, petrography and mineralogy. Ensuing petrographic and geochemical reports now seem to have established a basis for the classification of Mountain Lake. Conclusions from several workers include the following:

> *"Although previously suggested to be ultramafic lamprophyres (Kjarsgaard, 1997), results of new geochemical and petrographic studies indicate this is not a suitable term. The rocks do not have a lamprophyric texture, and are not ultramafic in composition. At present the most suitable classification for the Mountain Lake body [is] that they are alkaline ultrabasic volcanics."* (Leckie et al., 1997)

> *"Insufficient evidence could be obtained to apply a strict petrological classification. The observed features are similar to, but not totally characteristic of, kimberlites and there are no features indicating any alternative rock type. These rocks could represent a marginal or more extreme type of kimberlite and, are therefore, referred to as kimberlitic."* (Wood et al., 1998)

> *"Based on whole-rock geochemical analysis, the Mountain Lake volcaniclastic rocks do not exhibit an archetypal kimberlite geochemical signature, but rather a hybrid with geochemical affinities similar to basanite (olivine potassic basalt), Sweet Grass minette and Montana alnöite."* (Eccles and Luth, 2001)

> *"Rocks of the Mountain Lake Pipe show a mixed origin and have been tentatively classified as hybrid alkaline ultramafic rocks, with some petrologic affinities to alnöitic magmas."* (Skupinski and Langenberg, 2002)

In summary, the lack of major- and trace-element overlap between worldwide kimberlite and the Mountain Lake rocks must reflect major mineralogical differences between their magmatic sources. The presence of amphibole, spessartine and analcite is atypical of *sensu stricto* kimberlite. The unequivocal conclusion is that the Mountain Lake intrusion is not archetypal kimberlite. Proposed classifications are somewhat equivocal, probably because of the pervasive clay alteration, but general consensus is an alkaline ultrabasic rock. Geochemical similarities between Mountain Lake and potassic alkaline Roman Province rock types make a case for an alkali olivine basalt or basanite classification.

2.9 Emplacement Style and Kimberlite–Host-Rock Relationships

The volcanics are interpreted to represent pyroclastic airfall and debris-flow deposits (Leckie et al., 1997) that erupted coeval with deposition of the Wapiti Formation in a coastal-plain depositional setting. The Mountain Lake South body comprises mainly juvenile-rich volcaniclastic rocks. In contrast, the Mountain Lake North body is characterized by resedimented volcaniclastic rocks. Quartz and feldspar are common in the matrix, and the volcaniclastic pile contains interbedded sandstone and siltstone, which likely represent storm events, levee/floodplains and/or fluvial point-bars. It is possible, therefore, that Mountain Lake South is the main body formed predominantly by effusive volcanism at surface,

whereas Mountain Lake North represents reworked material that has been displaced from the main feeder.

2.10 Diamond Content

The exact sample weight or analytical methodology is not known, but Wood et al. (1998) reported that "insignificant quantities of diamonds" were recovered from trench and drillcore material at Mountain Lake, and that the Mountain Lake South and North bodies were deemed uneconomic. Geochemical and petrographic classification of Mountain Lake as an alkaline ultrabasic rock and the general lack of diamond-favourable xenocrystic chemistry are consistent with poor diamond results.

3 Buffalo Head Hills

3.1 Discovery and Exploration History

The Buffalo Head Hills–Peerless Lake area is typical of much of northern Alberta, in that exploration has focused predominantly on energy resources. After all, the primary established reserves in the Peerless Lake area contain upwards of 47 x 10^6 m^3 of oil in 12 conventional fields and 800 x 10^6 m^3 gas in 3 fields (Eccles et al., 2000). Diamondiferous kimberlite discoveries generated a new natural-resource interest for the area in early 1997 after Ashton Mining of Canada Inc. announced the discovery of kimberlitic intrusions on the southeastern flanks of the Buffalo Head Hills, which are located approximately 350 km north-northwest of Edmonton in north-central Alberta. This section provides a summary of the discovery.

In September 1995, the Alberta Geological Survey recovered 152 possible pyrope garnets from a single 25 kg sample of dark greyish-brown, silty clay till; the sample was collected northwest of Red Earth Creek (lat. 56°50.834'N, long. 115°45.237'W; Fenton and Pawlowicz, 1997). Thirty-five garnet grains were analyzed by a scanning electron microprobe, of which 27 were classified as G9 lherzolitic garnet. The same site was resampled in August 1996, and 176 possible pyrope grains were recovered, thus duplicating the high number of peridotitic garnets initially recovered from this site.

Alberta Energy Company Ltd. (now EnCana Corporation) conducted a fixed-wing aeromagnetic survey over the Buffalo Head Hills in 1995. The survey identified dominant features defined by several shallow, long-wavelength, high-frequency anomalies that also corresponded to strong diffractions in the seismic profiles. An astute geologist with Alberta Energy Company Ltd., R. Pryde, realized that the anomalies may be related to intrusions.

In October 1996, an option agreement was signed by Ashton Mining of Canada Inc., Alberta Energy Company Ltd. and Pure Gold Minerals Inc. to investigate these anomalies. Closer inspection of the total-field profile from the aeromagnetic survey revealed more than 100 shallow targets, and the highest priority anomalies were evaluated by helicopter high-resolution magnetic surveys (Carlson et al., 1999).

In January 1997, Ashton Mining of Canada Inc. announced a drill program to test 10 isolated geophysical anomalies in the Buffalo Head Hills area, approximately 35–45 km northwest of the community of Red Earth Creek. The initial two drillholes, located on anomalies identified as K7B and K7C, penetrated kimberlite (olivine-dominated fragmental and tuffaceous material) underlying glacial overburden at depths of 34 and 37 m, respectively. By March 1997, a total of 11 intrusions within a 100 km^2 area had been discovered, 10 by drilling and 1 by bulldozing a drill pad: kimberlites K2, K4A, K4B, K4C, K5A, K5B, K6, K7A, K7B, K7C and K14 (Figure 12; Appendix 1).

The first microdiamond analyses of samples collected from the K2, K4 and K14 intrusions, released in April 1997, confirmed that the bodies contained diamond; more significantly, 3 samples totalling 152.5 kg from kimberlite K14 yielded significant numbers of diamonds, including 139 microdiamonds and 11 macrodiamonds. These results, and ensuing news headlines such as "Ashton pulls diamonds from property in Alberta" (Northern Miner, 1997a), "Ashton, Pure Gold find more diamonds in Alberta" (Northern Miner, 1997b), "Forget oil, diamonds new lure" (Calgary Herald, 1998) and "Alberta has 'tremendous potential' for diamonds" (Edmonton Journal, 1998), indicated that a new chapter in the history of the resource potential of Alberta was about to be written.

In 2007, Diamondex Resources Ltd. and Shore Gold Inc. purchased the Buffalo Head Hills diamond project from Ashton Mining of Canada Inc. (now Stornoway Diamond Corporation), which had previously defined 38 kimberlite bodies between 1997 and 2007 by spending approximately $30 million. Between 2008 and

2010, Diamondex (now Canterra Minerals Corporation), as operator of the joint-venture, completed a grid-based drill program on five of the more diamondiferous kimberlite bodies (K5, K6, K14, K91 and K252). The program consisted of 54 drillholes totalling 8328 m, the objective being to develop 3-D models and identify different kimberlite phases prior to diamond evaluation. The results of this work are still pending.

In the northeastern part of the Buffalo Head Hills kimberlite field, Grizzly Diamonds Ltd. (now Grizzly Discoveries Inc.) conducted two separate 2008 drill programs and discovered three previously unknown kimberlite bodies (BE-01, -02 and -03; Figure 12). These discoveries represented the first kimberlites discovered in Alberta since 2003 and the first kimberlites discovered in the Buffalo Head Hills field other than those found by

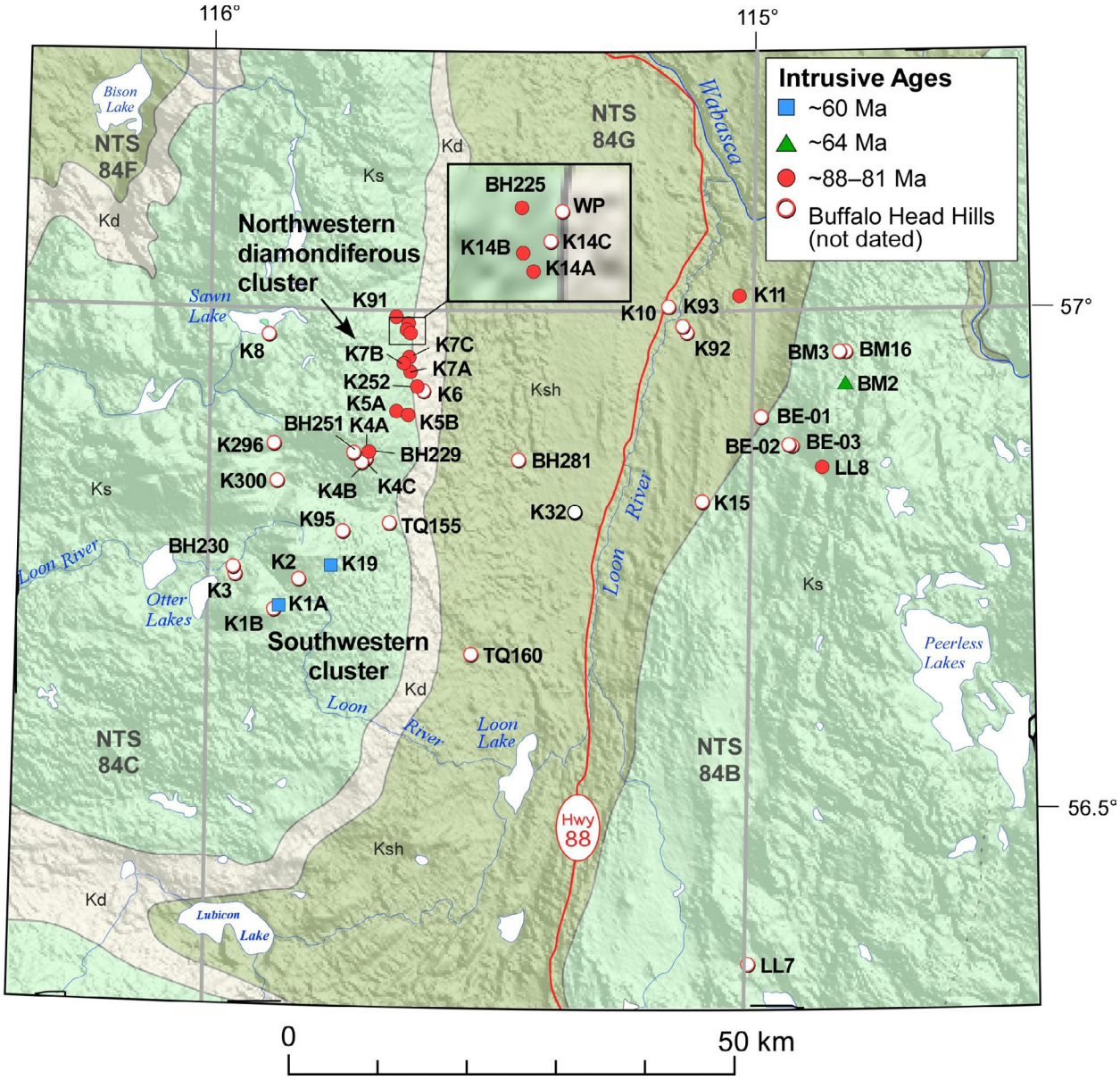

Figure 12. Bedrock geology of the Buffalo Head Hills–Peerless Lake area of north-central Alberta on hill-shaded digital elevation model (from Hamilton et al., 1999), showing kimberlite and related rock occurrences. Solid symbols represent isotopically dated intrusions: ~88–81 Ma, ~64 Ma and ~60 Ma. Late Cretaceous bedrock abbreviations: Ksh, Shaftesbury Formation (shale and silty shale); Kd, Dunvegan Formation (sandstone); and Ks, Smoky Group (shale and silty shale).

Ashton. Grizzly's drill program consisted of 12 holes totalling 2270 m.

To date, 41 kimberlitic intrusions have been discovered in the Buffalo Head Hills field (Figure 12; Appendix 1). All targets and bodies were delineated through geophysical interpretation of magnetic, electromagnetic and gravity data. Of the three ultramafic rock fields in northern Alberta, the Buffalo Head Hills kimberlite field continues to receive the most attention because of large kimberlite dimensions (up to 45 ha), encouraging diamond contents (up to 55 carats per hundred tonnes) and the high ratio of diamondiferous to barren kimberlite (28 of the 41 occurrences are diamondiferous). The Buffalo Head Hills kimberlite field encompasses an area of approximately 2500 km^2, making it the third largest known district of significant diamond-bearing kimberlites in Canada after Lac De Gras in the Northwest Territories and Fort à la Corne in Saskatchewan.

3.2 Geological Setting

The Buffalo Head Hills volcanic bodies intruded upward from the Buffalo Head Terrane through approximately 1600 m of Phanerozoic sedimentary rocks to outcrop or subcrop in bedrock or Quaternary deposits (Figure 1). The outline of the Buffalo Head Terrane has been inferred from aeromagnetic and geochronological data (Ross et al., 1991, 1994). Drillcore samples recovered from the Buffalo Head Terrane are mainly metaplutonic rocks ranging in composition from gabbro to leucogranite, with minor metavolcanic and high-grade gneissic rocks. The U-Pb zircon ages from magmatic rocks range from 2.3 to 2.0 Ga (Thériault and Ross, 1991; Ross et al., 1994).

The Buffalo Head Terrane is interpreted to represent a rifted sliver, or an accretionary terrane, that collided with and amalgamated to the Chinchaga domain to the west and the Churchill Province to the east (Ross and Eaton, 2002). In an alternative basement model, the Buffalo Head Hills kimberlite field occurs within the Red Earth granulite domain of the Athabasca Polymetamorphic Terrane and is representative of Archean crustal material that was reworked during the Paleoproterozoic (Burwash et al., 2000). This latter model, coupled with depleted-mantle Archean Nd ages for the Buffalo Head Terrane (Villeneuve et al., 1993), LITHOPROBE transects west of the Buffalo Head Terrane (Ross and Eaton, 2002) and magnetotelluric studies within the Buffalo Head Terrane (Türkoğlu et al., 2007), contributes to a theory that the lithosphere beneath the Buffalo Head Hills kimberlites had an Archean component that was tectonically reworked during the Proterozoic. However, this theory of reworked Archean epitomizes the controversy pertaining to the mantle underlying this region, because the general lack of sub-calcic G10 peridotitic garnet in the kimberlites and diamonds from the Buffalo Head Hills suggests this is not an Archean lithosphere, reworked or otherwise.

A composite section of the uppermost sedimentary rocks, more than 560 m thick, was assembled from exploratory drillcores to establish chronostratigraphy and the paleoenvironment in the Buffalo Head Hills area (Sweet et al., 2006; Eccles et al., 2008a). The oldest rocks in the composite section are Albian, and the youngest preserved host rocks capping the Buffalo Head Hills belong to the Campanian Wapiti Group (ca. 78 Ma; Pawlowicz et al., 2005b; Sweet et al., 2006; Figure 13). Significantly, palynological examination of the composite bedrock section revealed that an extensive Turonian (in part or in whole) through Early Campanian hiatus, representing approximately 9 million years of missing strata, coincides with Late Cretaceous kimberlite volcanism (Sweet et al., 2006; Eccles et al., 2008a; Figure 13b). Sedimentological interpretation by Hein and Eccles (2008) suggested that the uppermost Late Cretaceous Buffalo Head Hills paleoenvironments ranged from lower shoreface below wave base through tidal flat/channel to fluvial (continental).

Quaternary surficial materials in the Buffalo Head Hills are characterized by low- to high-relief hummocky topography consistent with thick deposits of ablation and melt-out till (ice-stagnation moraine deposits), and nonsorted diamicton (Trommelen et al., 2006). The moraine deposits are occasionally dissected

by glaciofluvial material exhibiting meltwater channels, kettle holes, terraces and minor ice-contact sediments. Eleven auger coreholes drilled by Alberta Geological Survey to obtain Quaternary stratigraphy information revealed that two distinct till units exist on the southern flanks of the Buffalo Head Hills (Pawlowicz et al., 2005a). The upper till is dark grey-brown, strongly calcareous silty clay and contains <5% igneous and metamorphic rocks with minor shale and sandstone. In contrast, the lower till is dark grey and noncalcareous with has a higher proportion of shale clasts.

Structurally, there is no unequivocal association between kimberlite emplacement and readily apparent structures in the Buffalo Head Hills. Eccles et al. (2001) and Paganelli et al. (2002) integrated geological events, RADARSAT-1 images, surface topography and Precambrian-basement digital-elevation models to evaluate structural controls in this area. They found a series of north-, northwest- and northeast-trending lineaments, some of which correspond to major thickness and facies changes in Devonian Duvernay, Woodbend, upper Leduc and Majeau Lake strata, and the western edge of the Grosmont reef complex. The interpreted surface intersections of these conjugate sets of lineaments show first-order spatial correlation with several Buffalo Head Hills kimberlite occurrences. The authors speculated that the regional distribution of the Buffalo Head Hills kimberlite field is controlled by the extension of deep, north-trending basement fault zones, with transcurrent northeast-trending faults having a significant effect on the location and shape of specific kimberlite bodies. However, correlation between Phanerozoic-propagating faults and kimberlite emplacement remains speculative and needs more investigation.

At a regional scale, Early Cretaceous crustal downwarping in the Peace River Arch/Peace River Embayment region (Figure 1a) may have formed a major east-northeast—trending corridor (measuring tens by hundreds of kilometres) of crustal weakness across northern Alberta (Pană and Eccles, 2003). During episodes of Cretaceous extension, reactivation of basement faults intersecting this zone may have created pathways for magma to penetrate upwards through the crust and, in essence, controlled the general location of kimberlite fields within this corridor.

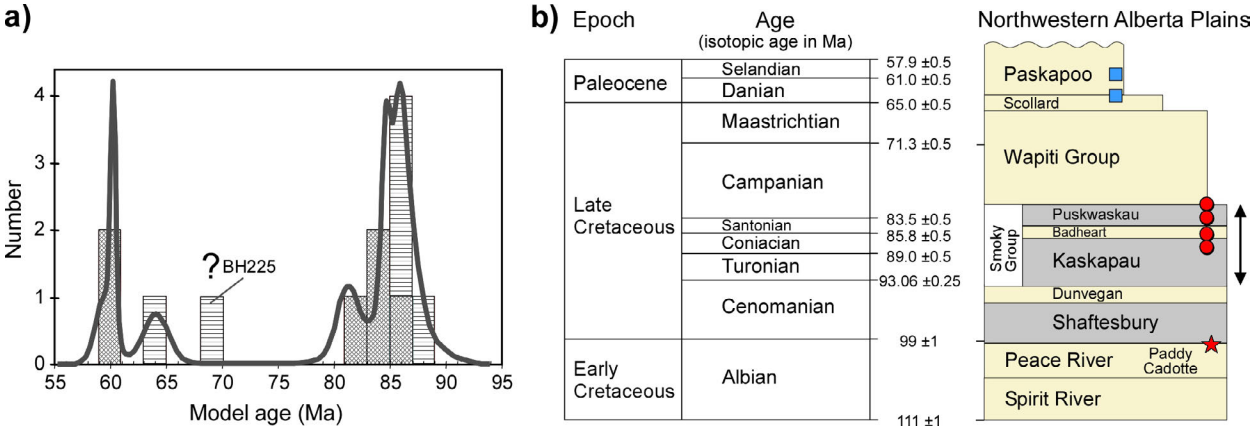

Figure 13. Geochronology of selected bodies from the Buffalo Head Hills kimberlite field: a) cumulative probability diagram of phlogopite Rb-Sr isochron ages (cross-hatched) and perovskite U-Pb model ages (horizontally hatched) for selected ultramafic rocks from the Buffalo Head Hills kimberlite field; a large amount of scatter in the U-Pb perovskite ages for the BH225 body (from ~68 Ma to ~90 Ma) is possibly related to several distinct ages of perovskite (a more robust age for BH225 is presented in a Rb-Sr phlogopite isochron in Figure 14); b) Albian through Selandian chronostratigraphic framework of northwestern Alberta (isotopic age references from Okulitch, 2002), showing the emplacement ages of the ~88–81 Ma, ~64 Ma and ~60 Ma Buffalo Head Hills bodies; red-filled star shows location of ~81 Ma kimberlite intruding Albian and Cenomanian strata in northern Alberta; double black arrow shows extent of Turonian–Early Campanian hiatus in north-central Alberta. Generalized lithology: grey, mudstone; dots, sandstone. Formation nomenclature used in this study correlates with the northwestern Great Plains stratigraphy.

Table 2. Rb-Sr isotopic data for phlogopite from selected diamondiferous kimberlites in the northwestern part of the Buffalo Head Hills kimberlite field.

Phlogopite Sample ID	Kimberlite Body	Surface Trench or Drillhole	Sample Depth (m)	Weight (g)	Rb (ppm)	Sr (ppm)	$^{87}Rb/^{86}Sr$	$^{87}Sr/^{86}Sr$	$^{87}Sr/^{86}Sr$ Uncertainty[1]
K14A-A	K14A	Surface trench	0	0.00239	242.4	22.36	31.49	0.74005	0.00004
K14A-B	K14A	Surface trench	0	0.00503	266.3	25.58	30.21	0.73835	0.00011
K14A-C	K14A	Surface trench	0	0.00711	257.8	24.80	30.17	0.73851	0.00003
K14A-D	K14A	Surface trench	0	0.00722	299.8	24.96	34.88	0.74400	0.00003
K14A-E	K14A	Surface trench	0	0.00816	298.8	29.60	29.30	0.73749	0.00003
K14B-A	K14B	Surface trench	0	0.00427	263.0	34.31	22.23	0.72931	0.00002
~~K14B-B~~[3]	~~K14B~~	~~Surface trench~~	~~0~~	~~0.00549~~	~~230.8~~	~~30.14~~	~~22.22~~	~~0.73015~~	~~0.00005~~
K14B-C	K14B	Surface trench	0	0.00381	155.4	17.22	26.19	0.73414	0.00003
BH225-A	BH225	BH225-07-01	76.8	0.00485	313.8	37.10	24.54	0.73204	0.00003
BH225-B	BH225	BH225-07-01	76.8	0.00433	319.0	53.22	17.38	0.72375	0.00002
252-1[4]	K252	DDH-252-08	118-119	0.00089	270.1	48.19	16.25	0.72234	0.00003
252-3[4]	K252	DDH-252-08	118-119	0.00122	374.2	79.70	13.61	0.71941	0.00004
252-4a[4]	K252	DDH-252-08	118-119	0.00119	382.0	119.4	9.269	0.71429	0.00003
252-4[4]	K252	DDH-252-08	118-119	0.00273	332.9	91.22	10.57	0.71587	0.00003
252-5[4]	K252	DDH-252-08	118-119	0.00363	351.3	79.81	12.75	0.71829	0.00002

[1] Uncertainty in $^{87}Sr/^{86}Sr$ expressed as 2σ

[2] Model age calculated assuming initial $^{87}Sr/^{86}Sr$ value of 0.705

[3] Discarded (strikethrough) analyses: sample K14B-B, slightly chloritized

[4] K252 Rb-Sr phlogopite data from Eccles et al. (2008)

Abbreviation: MSWD, mean square of weighted deviates

3.3 Palynology and Geochronology

Palynological and geochronological determinations have been documented by Carlson et al. (1999), Skelton et al. (2003), Boyer et al. (2003), Eccles (2004) and Eccles et al. (2004, 2008a). The Rb-Sr phlogopite and U-Pb perovskite age determinations for 12 of 41 known ultramafic bodies in the Buffalo Head Hills area of north-central Alberta show that kimberlitic magmatism occurred in at least two separate episodes during the Late Cretaceous and Paleocene (Eccles et al., 2008a; Figure 13; Appendix 3). Nine kimberlites yielded Coniacian to Campanian ages of between 88 ±5 Ma (U-Pb perovskite, K5A) and 81.2 ±2.3 Ma (Rb-Sr phlogopite, K252). A Danian U-Pb perovskite isochron age of 63.5 ±0.7 Ma was obtained for the BM2 kimberlite, and Selandian Rb-Sr ages of 59.6 ±2.8 Ma and 60.3 ±0.8 Ma were determined for the K1A and K19 bodies, respectively. Radiogenic ages of kimberlite emplacement are supported by palynological interpretation (Sweet et al., 2006; Eccles et al., 2008a). Sedimentary clasts incorporated in the ~60 Ma ultramafic bodies include Maastrichtian and Paleocene miospores. Turonian to Santonian host mudstone strata are contemporaneous with the ~88–81 Ma kimberlite suite.

The ~88–81 Ma group generally occurs in the northwestern part of the Buffalo Head Hills kimberlite field and defines the diamond window for the field. Spatially, the ~88–81 Ma kimberlite bodies (K5A, K7A, K11, K14A, K91 and K252) are located in the northwestern part of the Buffalo Head Hills field (Figure 12) and correspond to a northwestern cluster of diamondiferous bodies (e.g., K5A, K6, K11, K14A and K252), as depicted by Hood and McCandless (2004). The ~64 Ma BM2 kimberlite body is in the eastern part of the Buffalo Head Hills kimberlite field. The ~60 Ma occurrences (K1A and K19) are located in a cluster of six to eight intrusive bodies in the southeastern part of the field near Otter Lakes (Figure 12). The ~88–81 Ma kimberlite bodies are bona fide kimberlite, as discussed later in the

Phlogopite Sample ID	$^{87}Sr/^{86}Sr$ Uncertainty[1]	Model Age (Ma)[2]	Individual Age (Ma)	Points, Model, Probability of Fit and MSWD	Recommended Age (Ma)	Points, Model, Probability of Fit and MSWD
K14A-A	0.00004	78.3				
K14A-B	0.00011	77.7		5-point, model 1,		
K14A-C	0.00003	78.2	82.8 ±9.2	fit = 0.93,		
K14A-D	0.00003	78.7		MSWD = 0.15		
K14A-E	0.00003	78.0				
K14B-A	0.00002	77.0				
~~K14B-B~~[3]	~~0.00005~~	~~79.7~~	86 ±11	2-point		14-point (minus K14B-B), model 1, fit = 0.995, MSWD = 0.25
K14B-C	0.00003	78.3			81.51 ±0.78	
BH225-A	0.00003	77.6	81.5 ±5.1	2-point		
BH225-B	0.00002	76.0				
252-1[4]	0.00003	75.1				
252-3[4]	0.00004	74.5		5-point, model 1,		
252-4a[4]	0.00003	70.6	81.3 ±2.8	fit = 0.76,		
252-4[4]	0.00003	72.4		MSWD = 0.39		
252-5[4]	0.00002	73.4				

text. The ~64 Ma BM2 body represents the only known occurrence of hypabyssal-facies kimberlite in this field and is similar in source composition to the ~88–81 Ma kimberlite but has lower diamond content. The ~60 Ma group occurs in the southwestern part of the field, is derived from a weakly diamondiferous/barren, hybrid ultramafic to alkaline source and comprises bodies that are eroded to present-day (ca. 78 Ma) stratigraphic levels.

New isotopic age determinations are included in this report for kimberlites K14A, K14B and BH225 (Table 2), and build upon the geochronological data and interpretations of Eccles et al. (2008a). In conjunction with isotope data from K252, these bodies were targeted for further geochronology because

- their initial diamond contents were significant enough to warrant additional mini–bulk testing;
- K252 and K14 have the highest known diamond content in the Buffalo Head Hills field to date; and
- Eccles et al. (2008a) showed that K252 has the youngest age (~81.3 Ma) within the Late Cretaceous (~88–81 Ma) kimberlite age bracket.

A combined regression using these new Rb-Sr data and the existing K252 Rb-Sr data of Eccles et al. (2008a) yields a 14-point isochron age of 81.5 ±0.8 Ma ($MSWD^2 = 0.25$, Model 1). Thus, the ~81.5 Ma age is interpreted as the best estimate of emplacement for these diamondiferous bodies, emphasizing the economic importance of Campanian volcanism in this region (Figure 14).

It is apparent that specific periods of Buffalo Head Hills kimberlitic magmatism correspond to characteristic intra-field features, such as spatial distribution, diamond content, rock classification and emplacement mechanism. Consequently, the

[2] mean square of weighted deviates

physical and chemical characteristics of the ~88–81 Ma and ~60 Ma episodes of volcanism in the Buffalo Head Hills field are discussed separately in this section.

3.4 Inferred Morphology

The Buffalo Head Hills kimberlite field is distributed over an area of approximately 6000 km^2 (Figure 12). The geophysically inferred near-surface dimensions range from <1 ha up to and possibly much larger than 48 ha. Four Buffalo Head Hills kimberlites are known to crop out (K2, K5, K6 and K14). Approximately 65% of the bodies have <40 m of Cretaceous sediment and/or surficial deposit cover. The uppermost present-day portion of several kimberlite bodies, including those that crop out, has a convex, mound-like appearance.

Skelton et al. (2003) identified two types of intrusion morphology: steep-sided, pipe-like bodies and, in contrast, tabular layers with no known feeder. To date, none of the Buffalo Head Hills bodies has been drill-tested to depths below 250 m, limiting our knowledge of their exact morphologies at depth. Two- and three-dimensional seismic surveys of seven Buffalo Head Hills kimberlites show that the intrusions have widths of 350–600 m at depths of 400–700 m (Atkinson and Pryde, 2006). Despite this apparent continuation at depth, Skelton et al. (2003) reported that a major morphological feature of the Buffalo Head Hills kimberlites is that they are characterized by tabular, volcaniclastic 'layers' that, upon drilling, have no apparent feeder. The physical complexity of the tabular morphology type is illustrated by a drillhole cross-section of K252 (Figure 15; Skelton and Willis, 2002; Boyer, 2005). Not only are several kimberlites interlayered with sedimentary rocks, roughly 60% of the drillholes that have penetrated intrusive kimberlitic rocks in the Buffalo Head Hills terminate in mudstone or sandstone.

Recent (2008–2010) grid-based drilling (>8000 m) on the K5, K6, K14, K91 and K252 kimberlites (Figure 12) may provide additional detail to construct 3-D kimberlite geological models. For example, preliminary modelling from 22 drillholes

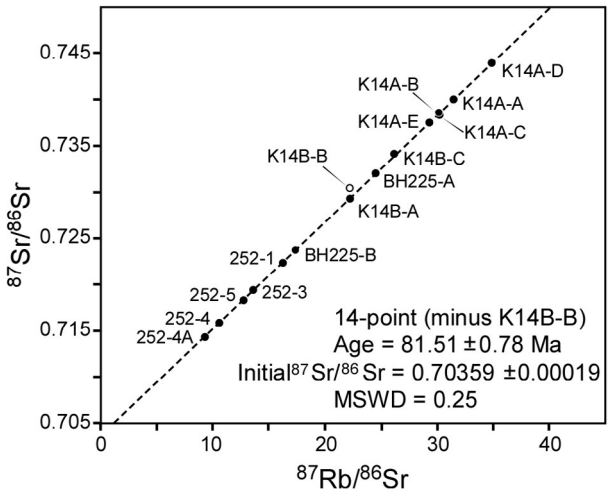

Figure 14. Fourteen-point Rb-Sr phlogopite isochron for selected kimberlites (K14, K225 and K252) from the diamondiferous northwestern part of the Buffalo Head Hills kimberlite field; phlogopite fraction K14B-B (open circle symbol) is not included, as this sample is slightly chloritized.

that tested the K14 body shows an irregularly shaped body about 400 by 450 m in diameter, with six different kimberlite units identified by variations in the size and/or abundance of olivine and lapilli, and by whole-rock geochemistry. Two dominant kimberlite units in K14 include 'macrocrystic volcaniclastic kimberlite' and 'xenocrystic volcaniclastic kimberlite' (French, 2010).

3.5 Volcanogenic Observations

Physical characteristics of the Buffalo Head Hills kimberlitic intrusions have been reported by Skelton and Bursey (1998), Carlson et al. (1999), Skelton et al. (2003), Boyer et al. (2003), Eccles (2004), Eccles et al. (2004), Boyer (2005), Boyer et al. (2008), and Eccles et al. (2008a, b). Skelton and Bursey (1998) and Carlson et al. (1999) initially reported the volcaniclastic nature of the bodies in the Buffalo Head Hills kimberlite field. Subsequent studies, which focused mainly on diamondiferous ~88–81 Ma kimberlites situated in the northwestern part of the field, confirmed that these bodies are composed of pyroclastic, volcaniclastic and resedimented volcaniclastic kimberlite. A second, distinctly non-fragmental, hypabyssal-facies kimberlite (i.e., subvolcanic

intrusive material) was first recognized by Boyer et al. (2003) in the BM2 kimberlite. Lastly, Eccles et al. (2008a) suggested that the ~60 Ma bodies in the southeastern part of the field comprise assemblages that are mineralogically atypical of kimberlite, *sensu stricto*, and are better referred to as alkaline ultrabasic rocks. This section provides a synopsis of these three distinct textural or mineralogical variations, with emphasis on the ~88–81 Ma and ~60 Ma intrusions.

3.5.1 ~88–81 Ma Kimberlite

Macroscopically, the ~88–81 Ma volcaniclastic kimberlite can take on a number of guises based on the lithofacies type and subsequent changes in mineralogy and degree of alteration. However, generally, these rocks are characterized by their grey to dark bluish–grey-green colour, inequigranular texture and competent nature.

Mantle and lower crustal xenoliths can constitute as much as 30% of the total volume (e.g., K14) and are dominated by lherzolitic varieties (80%) with less abundant wehrlitic (10%) and rare harzburgitic, websteritic and eclogitic assemblages (Carlson et al., 1999). Textures of the mantle xenoliths vary from coarse-granular to coarse-tabular and porphyroclastic-sheared styles. Mantle xenocryst assemblages include predominantly olivine, peridotitic and eclogitic garnet, clinopyroxene, spinel and ilmenite. Crustal clasts consist predominantly of Cretaceous shale. Clasts of Devonian carbonate rock are also present but generally less common. Resedimented volcaniclastic kimberlite includes varying proportions of Late Cretaceous shale, siltstone and/or sandstone mixed with volcaniclastic kimberlite.

The intra- to extra-crater ~88–81 Ma volcaniclastic kimberlite can generally be described as juvenile-lapilli–bearing, olivine crystal tuff set in a fine-grained mesostasis and sometimes segregational assemblage of serpentine-, carbonate- and CaMg(Fe)-silicate–rich groundmass together with one or more of the following primary minerals: phlogopite, sulphide, perovskite, spinel, ilmenite, rutile and apatite (Figure 16a). Forsteritic olivine is the dominant mineral, forming up to 50% of the total mineral content, and occurs as ovoid, anhedral to subhedral macrocrystic olivine (up to 2 cm) and subhedral to euhedral

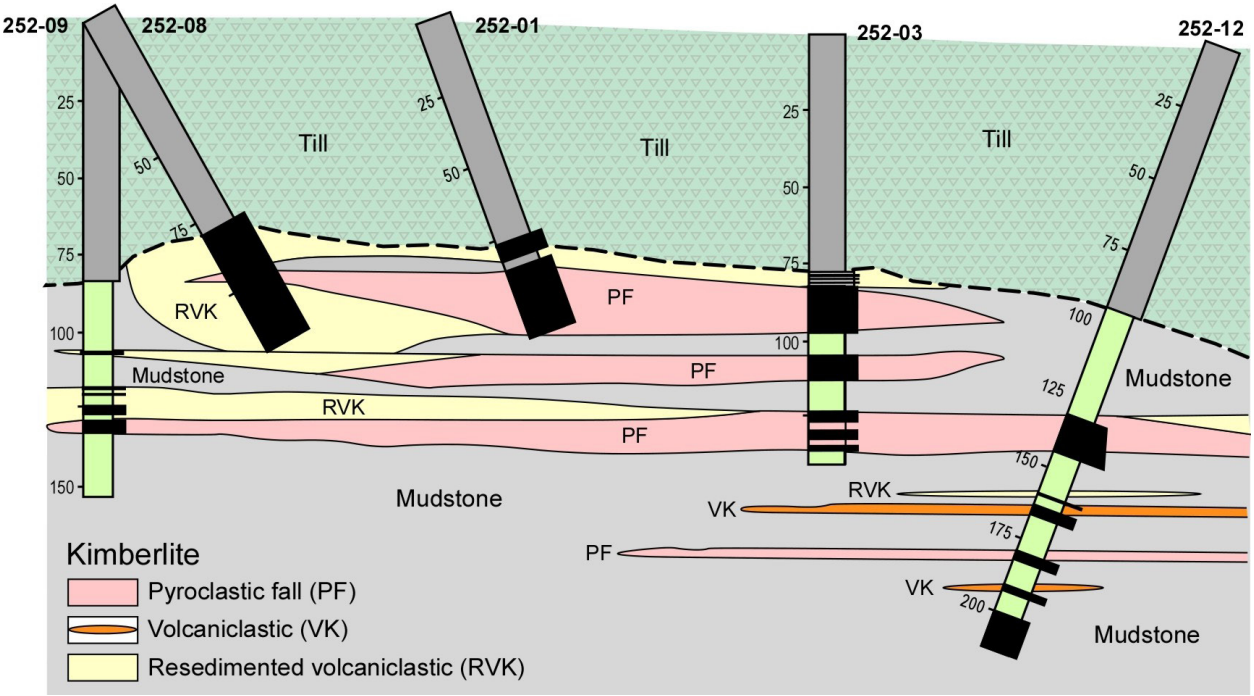

Figure 15. Drillhole cross-section of kimberlite K252 showing the complexity and tabular nature of some of the Buffalo Head Hills kimberlites (from Boyer [2005] and reproduced with L. Boyer's permission); drillhole depths in metres.

olivine phenocrysts (<2 mm). The appearance of olivine varies greatly, from unaltered crystals to those that are variably altered to completely pseudomorphed by dolomite, serpentine, calcite and, less commonly, magnetite and pyrite (Figure 16b). Dolomite alteration is represented by relict dolomite within olivine grains, and by rhombohedral dolomite crystals that appear to have been replaced by serpentine.

The next most common mineral is macrocrystalline and microphenocrystalline phlogopite, which generally forms <5% of the total mineral assemblage. Sulphide minerals are dominated by pyrite but can include chalcopyrite and sphalerite.

Ash- and lapilli-sized, juvenile and armoured pyroclasts are common in these bodies and contain an agglomeration of olivine, phlogopite, apatite, ilmenite, calcite and Ni(Fe)-sulphide minerals (Figure 16c, e, f, g). Pristine, juvenile lapilli pyroclasts, which represent fragments of the molten or semi-molten parental material ejected during volcanic eruption, have sharp, curvilinear rims, are non-nucleated and are distinguished by their contrasting mineralogy relative to the surrounding material (Figure 16b). Armoured pyroclasts represent a variety of accretionary lapilli that formed when rinds of kimberlite ash accreted to a nucleus in moisture-laden, hydroclastic eruptions. Alternatively, these pyroclasts could represent nucleation of molten material in the near-vent environment. The armoured pyroclasts are spherical to subspherical and have mineralogy similar to that of the surrounding material. They are frequently nucleated on olivine, but occasionally the ash/molten material adheres to liberated fragments of country rock.

Recognition of lithofacies changes in drillcores is critical to understanding eruptive and depositional processes. Boyer et al. (2003), Boyer (2005) and Boyer et al. (2008) completed detailed examinations of the volcanic facies present within the K6, K11, K281, K252, K296 and K300 bodies. Their findings showed that the dominant subfacies include pyroclastic-fall, pyroclastic-surge and reworked-pyroclastic deposits. Fall deposits are generally massive, poorly sorted and rich in olivine crystals, with varying amounts of juvenile and accretionary pyroclasts.

In contrast, the surge deposits are sorted to well sorted; contain laminated, bedded and crossbedded sequences; and are enriched in olivine relative to fines. Bedding and/or graded layers are observed in both facies and can range from the subcentimetre to decametre scale. Reworking of this material, either by recycling associated with multiple eruptive events or by physical reworking and resedimentation, is characterized by broken olivine grains, absence of pyroclasts (or multiphase pyroclasts in the case of multi-eruptive events) and introduction of sedimentary assemblages.

3.5.2 ~64 Ma Kimberlite

The BM2 kimberlite, located in the easternmost part of the field (Figure 12), is the only known occurrence of hypabyssal kimberlite. The volcanogenic interpretation is based on evidence of inequigranular, segregation and flow-alignment textures, as well as contact relationships with the surrounding host mudstone (Boyer et al., 2003).

Macroscopically, BM2 is dark grey to black with subrounded grains of macrocrystalline olivine set in a fine-grained matrix. In thin section,

Figure 16. (see page 29) Various micro- and macroscopic images of ~88–81 Ma kimberlite from the northwestern part of the Buffalo Head Hills field: a) highly serpentinized olivine crystals set in a groundmass of serpentine and a fine-grained CaMg(Fe)-silicate; b) olivine is replaced by dolomite that, in turn, is replaced by serpentine; c) rounded lapilli are present throughout the sample and contain a fine-grained matrix agglomeration of olivine/serpentine, calcite, phlogopite, ilmenite and perovskite; d) legend for QEMSCAN® images (parts a–c and e); e) accretionary, juvenile pyroclast nucleated on an olivine macrocryst; f) photomicrograph mosaic of an accretionary, juvenile pyroclast from K6 (surface sample; plane polars); g) curvilinear boundary of juvenile lapillus from K6 (surface sample; plane polars); h) photomicrograph of coarsely to finely bedded juvenile, pyroclast-rich kimberlite from K296 (DDH296-03 at 61 m; hand specimen). Images a–c and e are mineralogical determinations on a sample from 82.1 m in drillhole DDH252-03 using QEMSCAN® analysis at 10 μm resolution.

olivine constitutes 15%–20% of the mineral assemblage and forms subrounded to rounded grains that are altered completely to intergrowths of serpentine with minor patches of dolomite and dendritic magnetite. The groundmass consists of serpentine(?) intergrown intimately with minor to moderately abundant, irregular to poikilitic dolomite grains averaging 0.05–0.1 mm. Magnetite forms equant subhedral grains, many of which are altered along their margins to

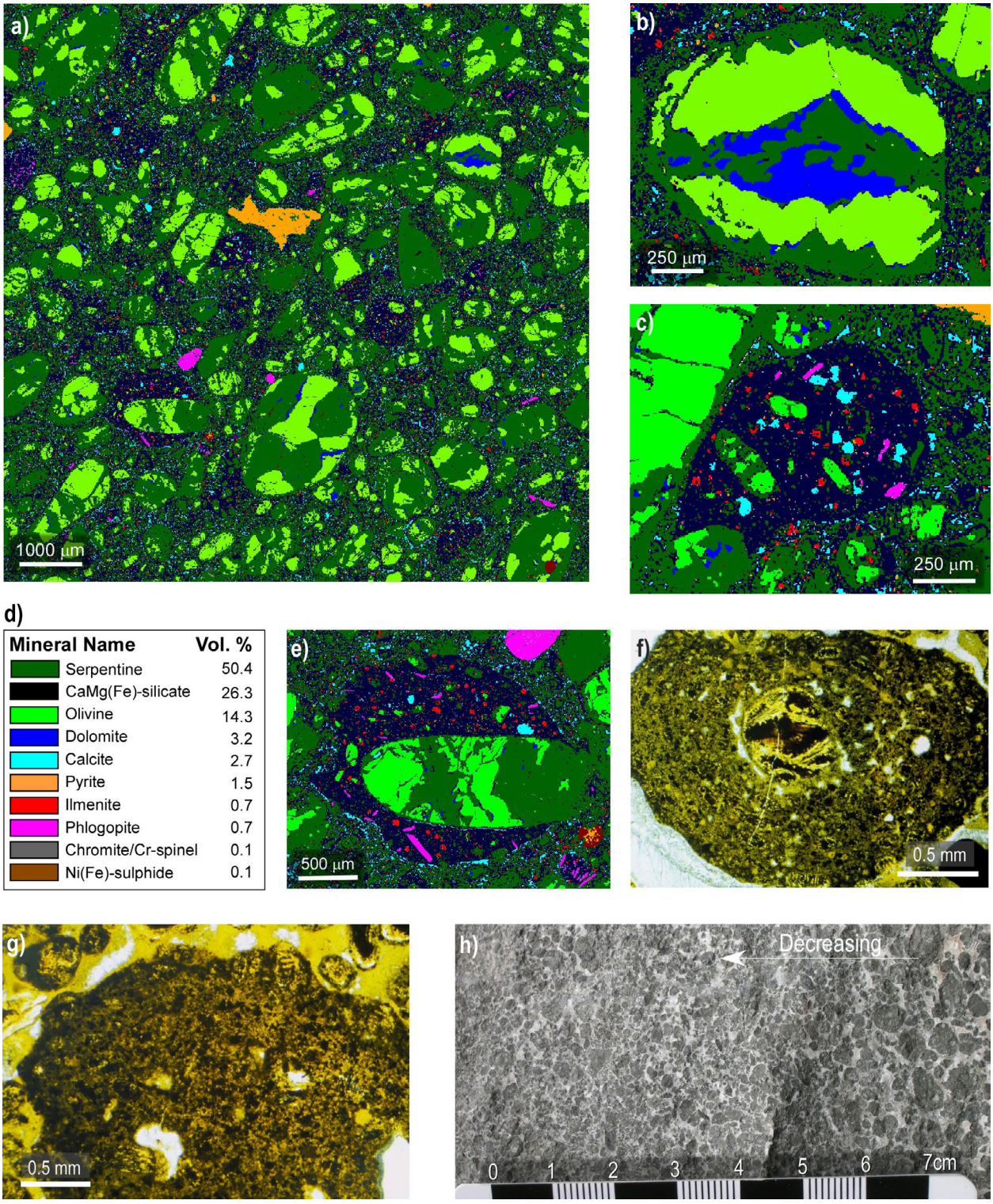

hematite and serpentine. Some magnetite has a core of dark brown chromite, suggesting that a moderate amount of the magnetite is secondary after chromite. Minor perovskite (1%–2%) forms disseminated, equant, anhedral to subhedral grains.

3.5.3 ~60 Ma Alkaline-Ultrabasic Intrusions

A cluster of six to eight intrusive bodies, best represented by the K1A and K19 bodies, occurs in the southeastern part of the Buffalo Head Hills field near Otter Lakes (Figure 12). Macroscopically, these intrusions are so extensively altered to serpentine, carbonate and secondary smectite that the original mineralogy and textures are difficult to discern. Petrographically, the samples contain fragments of pervasively altered olivine, phlogopite/muscovite, hornblende and K-feldspar set in a cryptocrystalline groundmass of uncertain composition (Figure 17). The relict olivine constitutes 10%–15% of the mineral assemblage and forms angular grains that are completely altered to a cryptocrystalline material of uncertain composition.

Serpentine and/or talc can be recognized in some of the pseudomorphed olivine grains. Phlogopite occurs in minor amounts (1%–3%) and forms equant to elongate flakes. Several flakes of colourless muscovite/talc may have been formed by alteration of phlogopite. Other accessory minerals include apatite, ilmenite, hornblende and K-feldspar. Lithic fragments include calcareous mudstone, sericite-rich fragments and cryptocrystalline fragments of uncertain origin and composition. Hornblende and K-feldspar appear to be unique to the southwestern bodies and support a different magmatic source than the northwestern kimberlite group (Eccles et al., 2008a).

3.6 Whole-Rock Geochemistry

Whole-rock geochemical data (n = 67) are available for 23, or more than half, of the intrusions in the Buffalo Head Hills field. The ~88–81 Ma and ~60 Ma bodies are represented by geochemical data from eight (BH225, K5, K7, K11, K14, K91, K252 and LL8) and two (K1A and K19) intrusions, respectively. Geochemical data are also included for the ~64 Ma BM2 intrusion, which is included with the ~88–81 Ma data because of its similar geochemical characteristics. Data from the remaining 12 intrusions have not yet undergone geochronological evaluation, or samples have not yielded datable minerals that are sufficiently unaltered for robust analysis. With the exception of the K4 cluster, which is discussed below, the undated intrusions more or less mimic the compositions of the ~88–81 Ma volcanics.

3.6.1 ~88–81 Ma and ~64 Ma Kimberlite

The majority of the Buffalo Head Hills samples, including whole-rock samples from the ~88–81 Ma K6, K14 and K281 intrusions and the ~64 Ma BM2 body, generally straddle the established contamination index (CI) of 1.0 for Group I uncontaminated kimberlite (Clement, 1982; Figure 18). High MgO (13.5–44.9 wt. %) and Mg# (93–97), and low SiO_2 (12.1–37.8 wt. %), Al_2O_3 (0.2–6.6 wt. %) and K_2O (<0.5 wt. %) characterize the ~88–81 Ma and ~64 Ma BM2 bodies (Figure 19). The ~88–81 Ma and ~64 Ma intrusions are enriched in Cr (40.7–1174.2 ppm), Nb (23.1–504 ppm) and Ni (41.6–2059.2 ppm). The chondrite-normalized REE profiles of the ~88–81 Ma bodies and the ~64 Ma BM2 body exhibit high LREE enrichment (up to 1800 times chondrite abundance for La), with steeply negative-sloping profiles (La/Yb_N ratios averaging 215; Figure 20). With respect to bulk Earth composition, the ~88–81 Ma (K6, K14, K281) and ~64 Ma (BM2) intrusions are characterized by low $^{87}Sr/^{86}Sr$ (0.70379–0.70446) and positive ε_{Nd} (+2.5 to +4.3; Figure 21).

3.6.2 ~60 Ma Alkaline-Ultrabasic Intrusions

The ~60 Ma bodies in the southeastern and southern parts of the Buffalo Head Hills field have a high CI (2.1–3.1; Figure 18). The ~60 Ma samples have MgO of 11.2–19.8 wt. % (Mg# of 87–93), SiO_2 of 38.6–46.4 wt. %, Al_2O_3 of 5.9–8.7 wt. % and K_2O of 1.5–3.9 wt. % (Figure 19). The chondrite-normalized REE profile of the ~60 Ma samples has moderate LREE (La_N of ~500 times chondrite) and a distinct flattening of the

HREE from Ho to Lu (Figure 20). The ~60 Ma K1A and K19 bodies have radiogenic $^{87}Sr/^{86}Sr$ (0.70493–0.70525) and low ε_{Nd} (–0.5 to +0.4; Figure 21).

3.6.3 *Other Whole-Rock Geochemical Observations*

A cluster of three closely spaced, undated intrusions (K4A, K4B and K4C), known as the K4 cluster, and the ~86 Ma LL8 intrusion are chemically anomalous in that they are characterized by low CI (0.75), signifying a low degree of bedrock contamination, and the lowest TiO_2 (0.2 wt. %), LREE (35–145 times chondrite abundance for La), total REE abundance ($\Sigma_{Y, La–Lu}$ of 142) and La/Yb ratios (196) of all bodies in the Buffalo Head Hills kimberlite field (Figures 18–20). In addition, K4 has higher $^{87}Sr/^{86}Sr$ (0.70621–0.70671) and lower ε_{Nd} (–7.0 to –7.3) than bulk Earth, plotting within the enriched, lower right quadrant of the Nd-Sr diagram (Figure 21). Although the whole-rock geochemistry of K4 (and LL8) may suggest a different and possibly non-kimberlite source, it is important to note that K4 has Nd-Sr isotopic compositions similar to that of the diamondiferous ~85 Ma K11 intrusion. This conundrum will be considered in Sections 3.7.3 and 3.8.

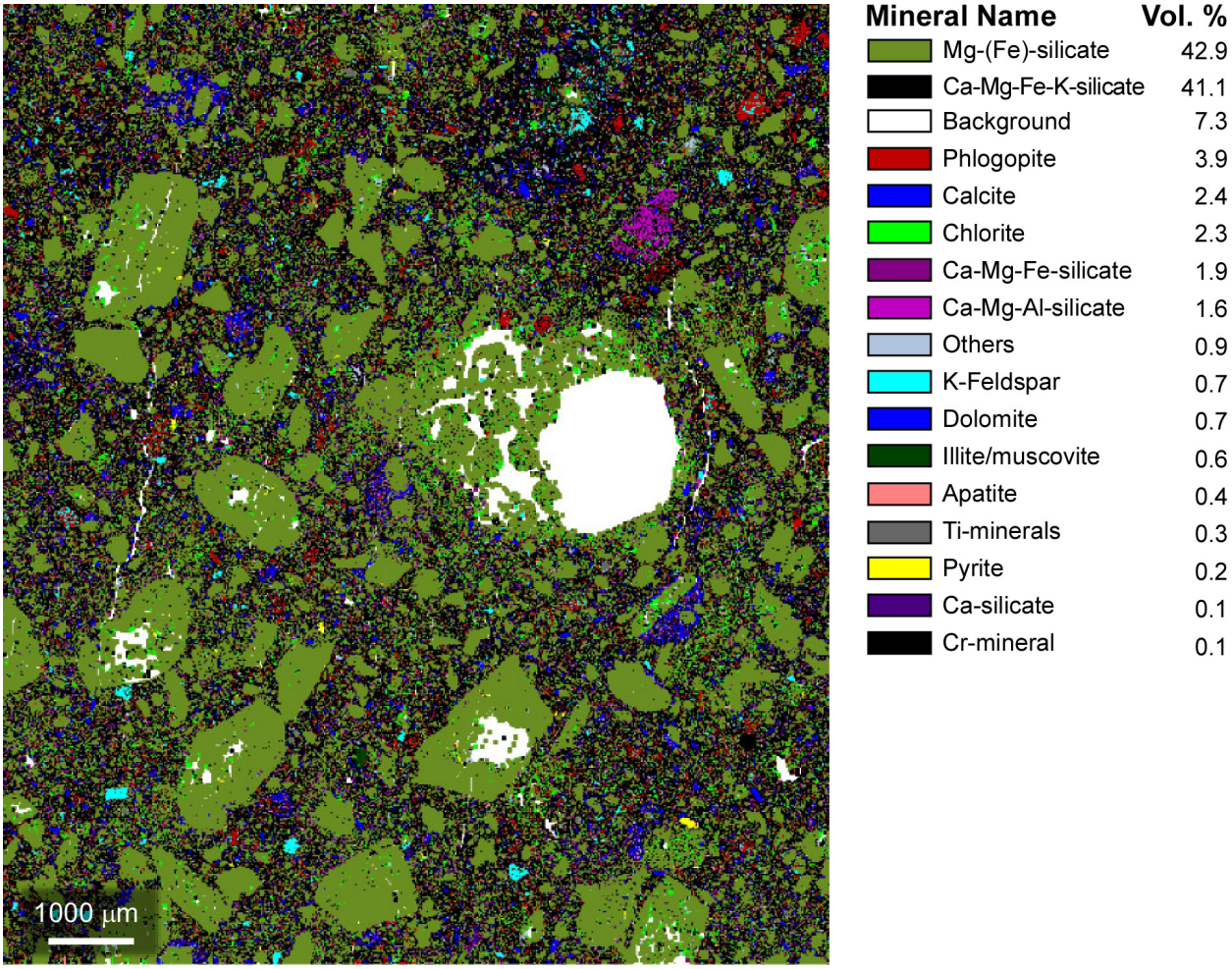

Figure 17. Mineralogical determination of the ~60 Ma Buffalo Head Hills intrusion K19 using QEMSCAN® analysis at 10 µm resolution (drillhole DDH-19-2 at 26.5 m): olivine macrocrysts are completely altered to Mg-(Fe)–silicate, which may be an intermediate alteration phase between serpentine and saponite; subhedral K-feldspar and phlogopite occur throughout a Ca-Mg-Fe-K–silicate matrix that is significantly more enriched in K than the ~88–81 Ma Buffalo Head Hills kimberlite samples.

3.7 Mantle Characteristics

The study of inclusions in xenocrystic diamonds provides information on the chemical conditions in the mantle at the time of diamond formation. Davies et al. (2004) and Banas et al. (2006) documented 47 mineral inclusions from 33 diamonds obtained from the K10, K11, K14, K91 and K252 kimberlites in the Buffalo Head Hills kimberlite field. With the exception of K10, which has yet to be tested geochronologically, four of these intrusions fall in the ~88–81 Ma group. Diamond-inclusion grains include garnet, olivine, clinopyroxene, ferropericlase, spinel and rutile, which indicate mixed eclogitic-websteritic (49%) and peridotitic (42%) sources with a minor contribution of sublithospheric diamonds (9%).

Selected peridotitic mantle xenolith/xenocryst studies include Aulbach et al. (2004), Davies et al. (2004), Hood and McCandless (2004), and Eccles and Simonetti (2008). Aulbach et al. (2004) reported that mantle xenoliths from the K6, K11 and K14 Buffalo Head Hills kimberlites include spinel lherzolite, garnet-spinel lherzolite, garnet harzburgite, sheared garnet lherzolite and pyroxenite. A modelled conductive paleogeotherm for diamondiferous Buffalo Head Hills intrusions corresponds to a heat flow of between 38 and 39 mW/m^2 (Aulbach et al., 2004), with equilibration temperatures of 1100°–1200°C ±50°C on a 40 mW/m^2 geotherm (Davies et al., 2004). Aulbach et al. (2004) recognized two metasomatic events: an older, primarily silica-melt event deep within the lithosphere; and carbonatite- and volatile-rich melts that intruded the shallow mantle.

Based on LA-ICP-MS analysis of peridotitic garnet xenocrysts from K2, K6, K11 and K14, Eccles and Simonetti (2008) inferred at least five heterogenic lithological transitions for the lower crustal–sublithospheric mantle underlying northern Alberta. From low to high temperature, these are

- fertile lherzolite, chromite-clinopyroxene-garnet equilibrium and/or wehrlite (<870°C);
- low-T lherzolite (870°–950°C);
- melt metasomatized wehrlite (950°–1000°C);
- depleted lherzolite and melt metasomatized lherzolite (1000°–1130°C); and

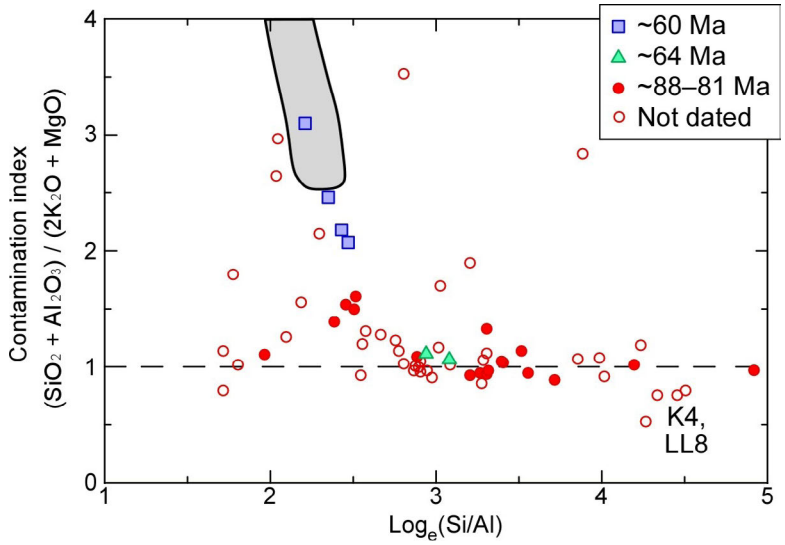

Figure 18. Plot of the contamination index (CI = [SiO_2 + Al_2O_3 + Na_2O] / [MgO + 2K_2O]) of Clement (1982) versus $\log_e$(Si/Al) for whole-rock samples from selected Buffalo Head Hills intrusions. The majority of the Buffalo Head Hills bodies have compositions that are near Clement's (1982) uncontaminated Group I kimberlite (CI near 1.0). In contrast, the ~60 Ma bodies have a higher CI (>2) that trends toward or correlates with the Mountain Lake intrusion (shaded polygon).

- moderately fertile lherzolite and high-Ti melt metasomatized lherzolite (>1130°C).

These findings support the xenolith work of Aulbach et al. (2004), who concluded that

- pyroxenite and garnet spinel lherzolite are restricted to the shallow mantle;
- fertile garnet lherzolites are concentrated at shallow depths (<140 km) and prevail at depths of <110 km;
- depleted peridotites are concentrated between depths of 120 and 160 km, with Ca-saturated garnet harzburgite concentrated in a layer between 140 and 160 km at 1000°–1200°C;
- melt metasomatized lherzolites, similar to sheared lherzolites, are concentrated between 140 and 180 km, and prevail at depths of >170 km; and
- the sheared garnet lherzolite lies on an inflection of the calculated geotherm and may constrain the lithosphere-asthenosphere boundary (LAB) to a depth of approximately 180 km.

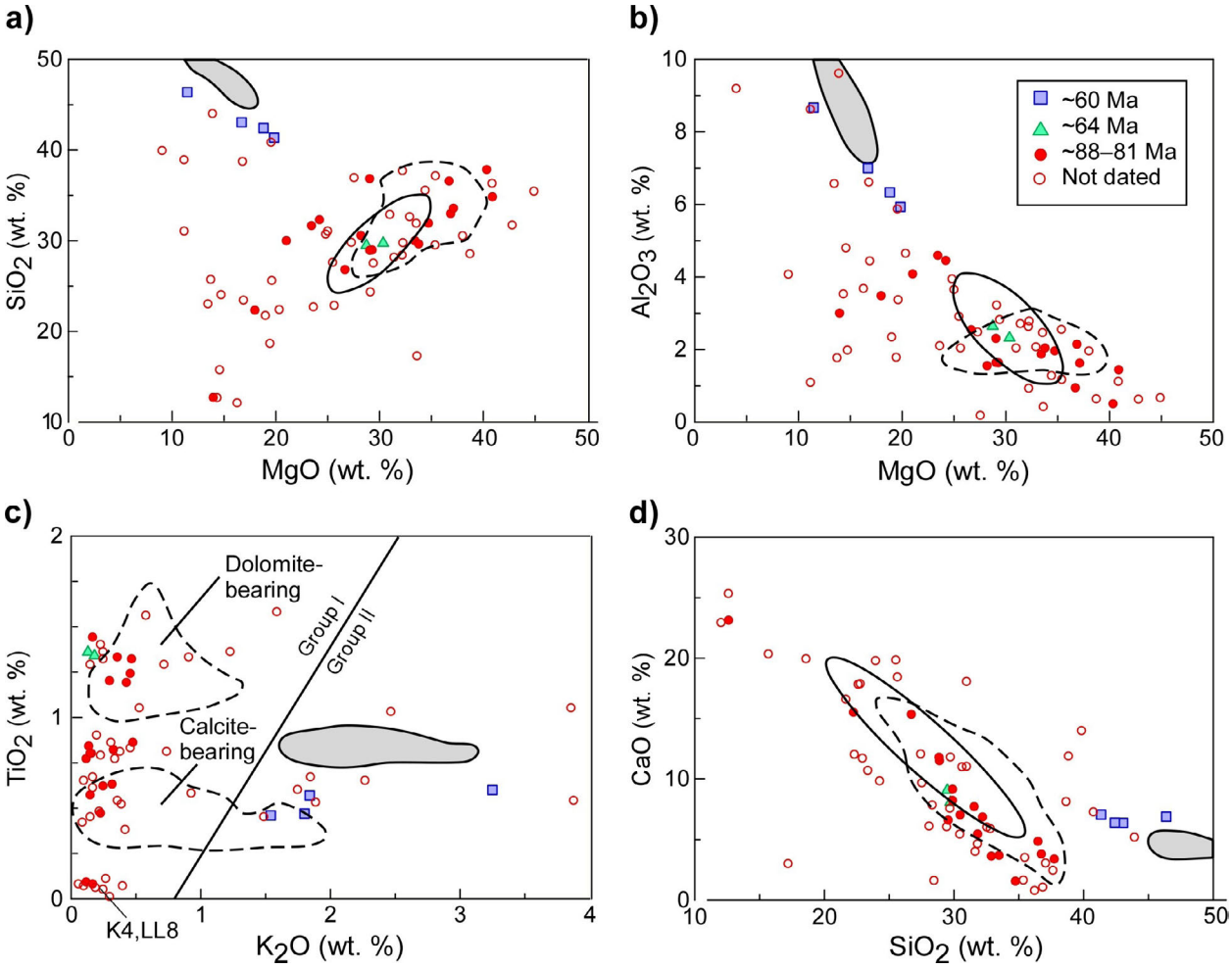

Figure 19. Whole-rock geochemical plots for selected Buffalo Head Hills intrusions: a) SiO_2 versus MgO, b) Al_2O_3 versus MgO, c) TiO_2 versus K_2O, and d) CaO versus SiO_2. Plots include, for comparison, compositions of South African kimberlites (solid polygons) from le Roex et al. (2003), Harris et al. (2004) and Becker and le Roex (2006); Ekati hypabyssal kimberlites (dashed polygons) from Kjarsgaard et al. (2009); and Mountain Lake alkaline ultrabasic intrusions (grey-filled polygon). In (c), the solid diagonal line divides low-K Group I kimberlite from high-K Group II kimberlite (Taylor et al., 1994; Kjarsgaard et al., 2009), and the dashed polygons differentiate calcite-bearing (lower TiO_2) and dolomite-bearing (higher TiO_2) uncontaminated Ekati kimberlites (Kjarsgaard et al., 2009).

Xenocryst geochemical data from AGS datasets (Eccles et al., 2002; Dufresne and Eccles, 2005; Eccles, 2007a) are discussed in Sections 3.7.1 and 3.7.2 within the context of host-emplacement ages (~88–81 Ma and ~60 Ma groups) and geochemical affinities for the various Buffalo Head Hills intrusions.

3.7.1 ~88–81 Ma Kimberlite

Peridotitic garnets from the ~88–81 Ma bodies are mainly G9 lherzolitic type (68%, n = 143 of 211), followed by G11 high-TiO_2 peridotitic (22%) and G12 wehrlitic types (10%; Figure 22a, b). End-member garnet compositions for all paragenetic assemblages are in the range of $Py_{52–75}Alm_{10–36}Sp_{0.5–1.3}Gr_{0–10}Uv_{3–21}$.

Hood and McCandless (2004) reported that kimberlites in the northwestern part of the Buffalo Head Hills cluster (i.e., ~88–81 Ma bodies) contain subcalcic (G10) garnet, but these account for a very small percentage of the total xenocryst population.

Of the 425 garnets shown on Figure 22, only two from the K14 body fall on the G9-G10 garnet boundary. These grains are characterized by 5.9–6.0 wt. % CaO, 9.9–10.1 wt. % Cr_2O_3, 14–15 mol. % knorringite, Mg# of 81 and Cr# of 29–30. The predominant lherzolitic (G9) garnet population has a wide range of Cr_2O_3 (1.2–10.2 wt. %), Mg# (76–84) and end-member compositions ($Py_{52–74}Uv_{3–18}Alm_{10–20}Gr_{0–9}$). The ~88–81 Ma peridotitic garnet has the lowest Ca-intercept distribution (3.7–4.6 with mode at 4.1; Figure 22d). A second, lower frequency Ca-intercept peak occurs at about 5.4, near the wehrlitic intercept.

Cores of lherzolitic garnet xenocrysts from the ~88–81 Ma bodies occupy a wide T_{Ni} range, but they dominate the depleted lherzolite (1000°–1130°C) and high-Ti melt metasomatized lherzolite (>1130°C) fields of Eccles and Simonetti (2008; Figures 22b and 23). A smaller subset plots as low-T (870°–950°C) fertile lherzolitic and wehrlitic garnet. In the Buffalo Head Hills kimberlite field, the depleted lherzolite is observed only in the ~88–81 Ma bodies. These grains have

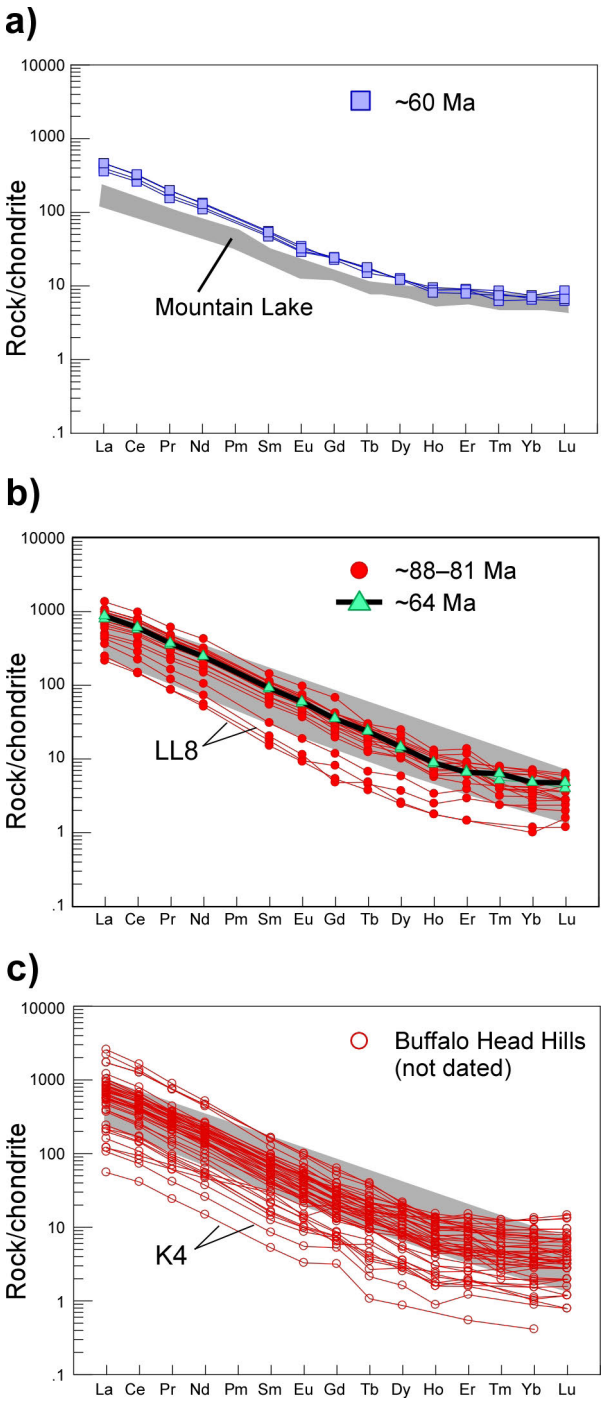

Figure 20. Chondrite-normalized REE patterns for whole-rock samples from the Buffalo Head Hills: a) the ~60 Ma Buffalo Head Hills intrusions have a similar REE profile to that of Mountain Lake; b) except for LL8, the ~64 Ma BM2 intrusion and the ~88–81 Ma intrusions correlate well with worldwide kimberlite of Mitchell (1986; shaded polygon); c) undated Buffalo Head Hills intrusions generally correlate with worldwide kimberlite, although some **bodies, such as K4, have low overall REE abundance. Normalization values from Sun and McDonough (1989).**

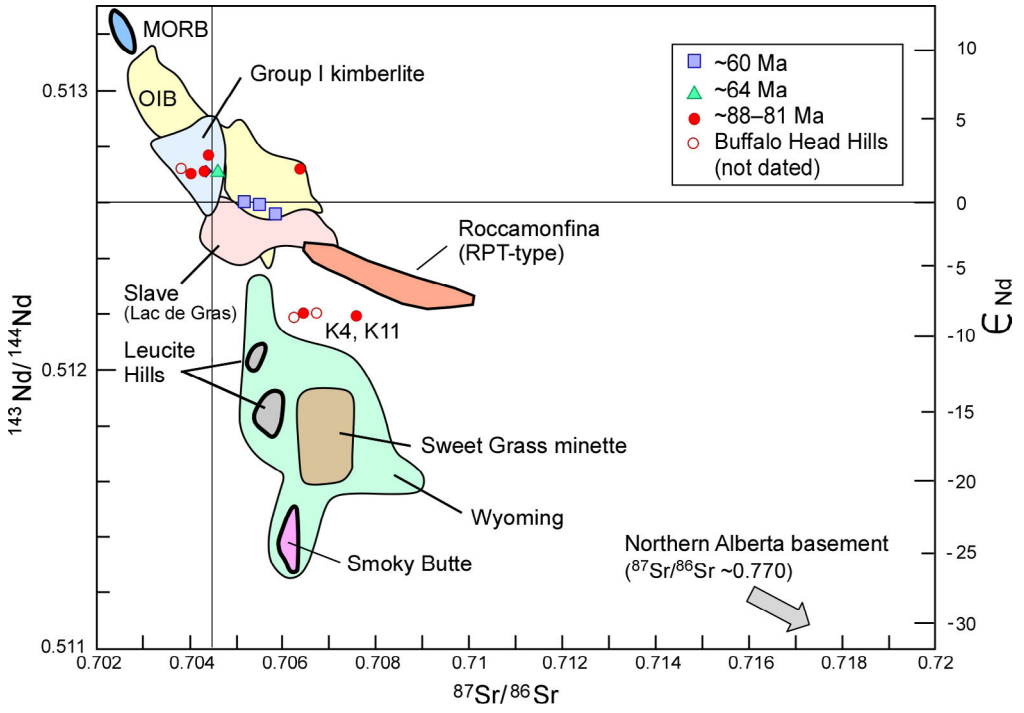

Figure 21. Nd-Sr isotope variations from selected Buffalo Head Hills intrusions; Group I kimberlite from Smith (1983), Smith et al. (1985) and Mitchell (1986); Slave (Lac de Gras) field from Dowall et al. (2000); Roccamonfina (Roman Province type) from Mitchell and Bergman (1991); Wyoming ultrapotassic fields from Vollmer et al. (1984) and O'Brien et al. (1995); Sweet Grass minette from Buhlmann (1996); and mid-ocean ridge basalt (MORB), oceanic-island basalt (OIB) and EM-II mantle reservoir from Zindler and Hart (1986).

slightly sinusoidal (Nd_N/Y_N ratio of between 1.1 and 2.4) chondrite-normalized REE profiles similar to that of the low-T depleted lherzolite (Figure 24), but are differentiated by their higher T_{Ni}, elevated Cr_2O_3 (6.6–10.1 wt. %) and lower Y (median of 2.8 ppm).

The high-Ti melt metasomatized lherzolite garnet has a high degree of re-enrichment characterized by a moderate sinusoidal pattern (Nd/Y_N of 0.5), with the highest total REE_N abundance in this dataset. Chondrite-normalized REE profiles show a sharp positive-trending slope between La and Sm, flattening of the MREE and then a slightly positive slope of the HREE. The high-Ti melt metasomatized lherzolite has a wide range of Cr_2O_3 (2.2–10.5 wt. %), high Ti (maximum of 6579 ppm and median of 3424 ppm) and high Zr (median of 63 ppm). Despite elevated Ti abundances, these garnets also have high Mg (up to 161 345 ppm) and Cr (up to 78 948 ppm).

Low-Cr garnets from the ~88–81 Ma bodies have end-member compositions in the range of $Py_{41–75}Alm_{13–43}Sp_{0.4–1.6}Gr_{0–21}Uv_{0.1–7.9}$ and include G1 megacrystic, G3/G3D eclogitic and G4/G4D pyroxenitic-websteritic-eclogitic types (Figure 25). The G3 eclogitic garnet has compositions moderately to strongly favouring pyrope ($Py_{43–63}Alm_{22–32}Gr_{16–21}$), with Mg# in the range of 54–74. Pyroxenitic-websteritic-eclogitic (G4) garnet is prominent in the ~88–81 Ma bodies (K6 and K14) and has a narrow range of Mg# (67–76) with similar average end-member compositions ($Py_{57–66}Alm_{20–28}Gr_{10–13}$). The 'D,' or diamond-facies, designation in the low-Cr G3D and G4D garnet categories of Grütter et al. (2004) constitutes a replacement for the term 'Group I eclogitic,' which originally referred to a coarse-grained eclogite texture (MacGregor and Carter, 1970) but also has a compositional connotation (i.e., Na_2O >0.7 wt. %; McCandless and Gurney, 1989). A high proportion of the K11 low-Cr garnet (74%) is classified as G3D (n = 13) and G4D (n = 1), with

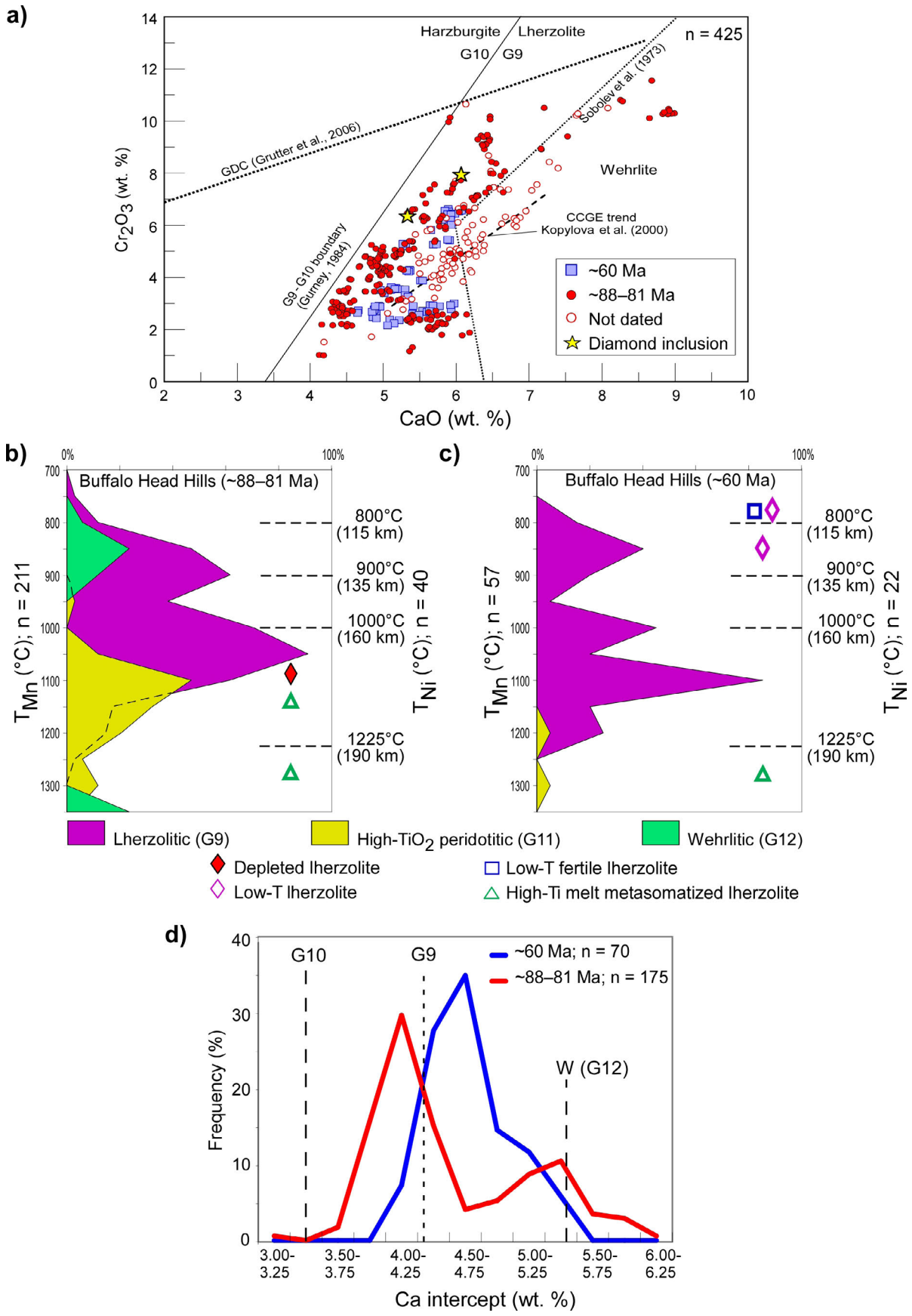
a)
Harzburgite
Lherzolite
G10
G9
n = 425
GDC (Grutter et al., 2006)
Sobolev et al. (1973)
Wehrlite
CCGE trend
Kopylova et al. (2000)
G9-G10 boundary
(Gurney, 1984)
~60 Ma
~88–81 Ma
Not dated
Diamond inclusion
Cr2O3 (wt. %)
CaO (wt. %)
b)
Buffalo Head Hills (~88–81 Ma)
800°C
(115 km)
900°C
(135 km)
1000°C
(160 km)
1225°C
(190 km)
TMn (°C); n = 211
TNi (°C); n = 40
c)
Buffalo Head Hills (~60 Ma)
TMn (°C); n = 57
TNi (°C); n = 22
Lherzolitic (G9)
High-TiO2 peridotitic (G11)
Wehrlitic (G12)
Depleted lherzolite
Low-T lherzolite
Low-T fertile lherzolite
High-Ti melt metasomatized lherzolite
d)
G10
G9
W (G12)
~60 Ma; n = 70
~88–81 Ma; n = 175
Frequency (%)
Ca intercept (wt. %)

Figure 22. (see page 36) Comparison of core compositions of peridotitic garnet xenocrysts from selected Buffalo Head Hills intrusions: a) Cr_2O_3 versus CaO, with data on peridotitic diamond inclusions from Davies et al. (2004) and Banas et al. (2006; K11, K14 and K252 kimberlites, n = 2); b) and c) relative proportion and pressure-temperature distribution of peridotitic garnet cores for selected intrusions, including Buffalo Head Hills (~88–81 Ma comprises K5, K6, K11, K14, and K252 bodies and ~60 Ma comprises K1A and K2 bodies); left Y-axis and solid polygon shading represent general peridotitic garnet paragenesis (i.e., G9, G11 and G12), together with the Grütter et al. (1999) Mn in peridotitic garnet temperature regression at 50°C intervals (T_{Mn}); right Y-axis and symbols represent a significantly smaller subset of peridotitic garnet data intended to provide a more detailed garnet nomenclature based on correlations between garnet Ni thermometry (Canil, 1999) and trace-element concentrations (Eccles and Simonetti, 2008); d) Ca-intercept method of representing garnet Cr/Ca content by a single number. Abbreviations: G9, Group 9 lherzolitic garnet; G10, Group 10 harzburgitic garnet; W, wehrlitic garnet; CCGE, chromite-clinopyroxene-garnet equilibrium; GDC, graphite-diamond constraint.

end-member compositions of $Py_{55–58}Alm_{22–23}Gr_{18–21}$ and $Py_{59}Alm_{24}Gr_{14}$, respectively. The G3D/G4D garnets plot within the high-Na_2O diamond-facies eclogitic field of Schulze (1997) but have significantly lower Na_2O than the diamond-inclusion eclogitic garnet from Davies et al. (2004) and Banas et al. (2006; Figure 25b).

Clinopyroxenes in the ~88–81 Ma bodies have a wide end-member range ($Wo_{34–49}En_{42–54}Fs_{2–6}Ae_{0.9–7}$), with high Mg# (89–94) and variable Ca# (32–54), Na_2O (0.2–2.0 wt. %) and Al_2O_3 (0.4–6.2 wt. %; n = 73). They can be classified as mainly diopside with minor Ca-Mg augite (Figure 26). Based on the Al-Cr-Na plot, the clinopyroxene data can be divided into two distinct groups: mantle-equilibrated clinopyroxene derived from kimberlite and clinopyroxene derived from non-kimberlitic sources. The two groups are also apparent on the Nimis and Taylor (2000) P-T diagram, which shows a 51–66 kbar and 1018°–1304°C group separated from a much lower P-T cluster. The high P-T clinopyroxene assimilates the 38–39 mW/m² geotherm of Aulbach et al. (2004) and the diamond-inclusion clinopyroxene data of Davies et al. (2004). Furthermore, the clinopyroxene is characterized by Mg# of 89–94, Ca# 38–46 and compositions in the range of $Wo_{33–42}En_{49–54}Fs_{4–6}Ae_{0.8–7}$.

Spinel is present in all Buffalo Head Hills bodies, in which it may form as much as 80% of the non-olivine xenocryst assemblage (Hood and McCandless, 2004). The 346 spinel xenocrysts analyzed from the ~88–81 Ma bodies appear to contain multiple chromite compositional populations (Figure 27). These include prominent low-Ti (generally <1 wt. % TiO_2)

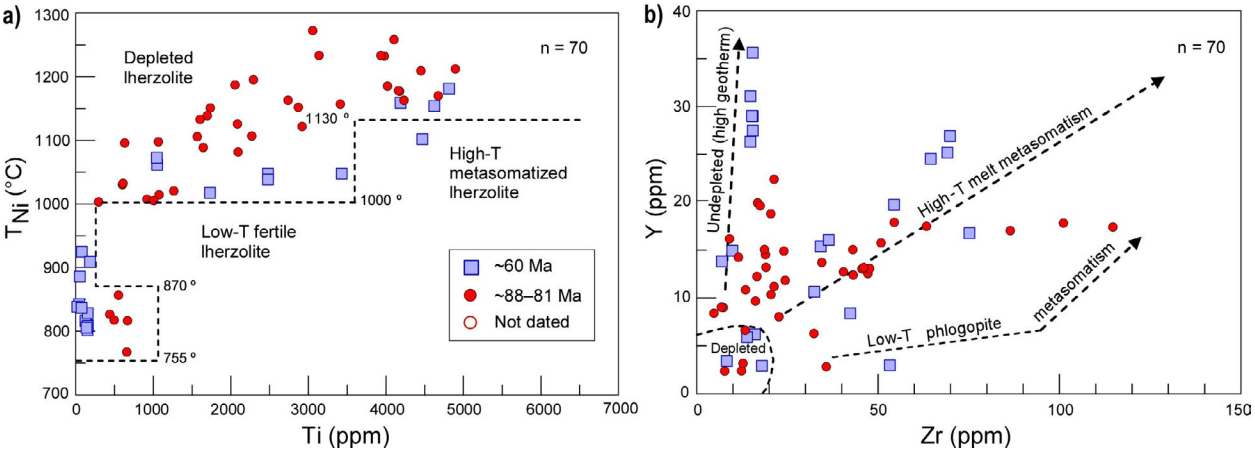

Figure 23. Variations in mantle depletion and metasomatism from trace-element compositions of the cores of peridotitic garnet xenocrysts from selected Buffalo Head Hills intrusions: a) distribution of T_{Ni} versus Ti, where T_{Ni} is calculated using the Ni-in-garnet geothermometer of Canil (1999); b) Y versus Zr on the fields and metasomatic trends of Griffin et al. (1999).

aluminomagnesian chromite (AMC); a lesser trend of magnesian ulvöspinel (magmatic trend 1), characteristic of Group I serpentine and calcite kimberlite; and a minor titanomagnetite (magmatic trend 2), thought to be initiated by extensive phlogopite crystallization (Mitchell, 1986). The magmatic trend 1 chromite characteristically plots within the kimberlite field on the MgO-TiO_2 diagram, whereas the AMC and magmatic trend 2 data plot within the ultramafic and mafic fields using the Creighton and Stachel (2008) classification scheme (Figure 27b). On the MgO-Cr_2O_3 diagram, only a few chromites plot within the diamond-inclusion field, with chromite, particularly from the K252 body, containing up to 64 wt. % Cr_2O_3. However, Hood and McCandless (2004) showed that chromite from bodies in the northernmost part of the field, analogous to the ~88–81 Ma bodies, forms high-Cr_2O_3 diamond-inclusion chromite in both the AMC and the magmatic trend 1 populations.

Other xenocryst constituents examined include olivine and ilmenite. Olivine is a dominant phase in the ~88–81 Ma bodies. Olivine diamond inclusions average a forsterite content of ~92, consistent with a lherzolitic (±wehrlitic) paragenesis for the peridotitic inclusions (Stachel et al., 2010). The compositions of ~88–81 Ma olivine cores form a tight cluster of high Mg# (89–93) and NiO (0.30–0.45 wt. %; n = 235), consistent with a mantle lherzolitic origin (Figure 28). Ilmenite is uncommon in the ~88–81 Ma bodies, and a few xenocryst cores (n = 35) from the diamondiferous K11 intrusion plot within the kimberlitic ilmenite

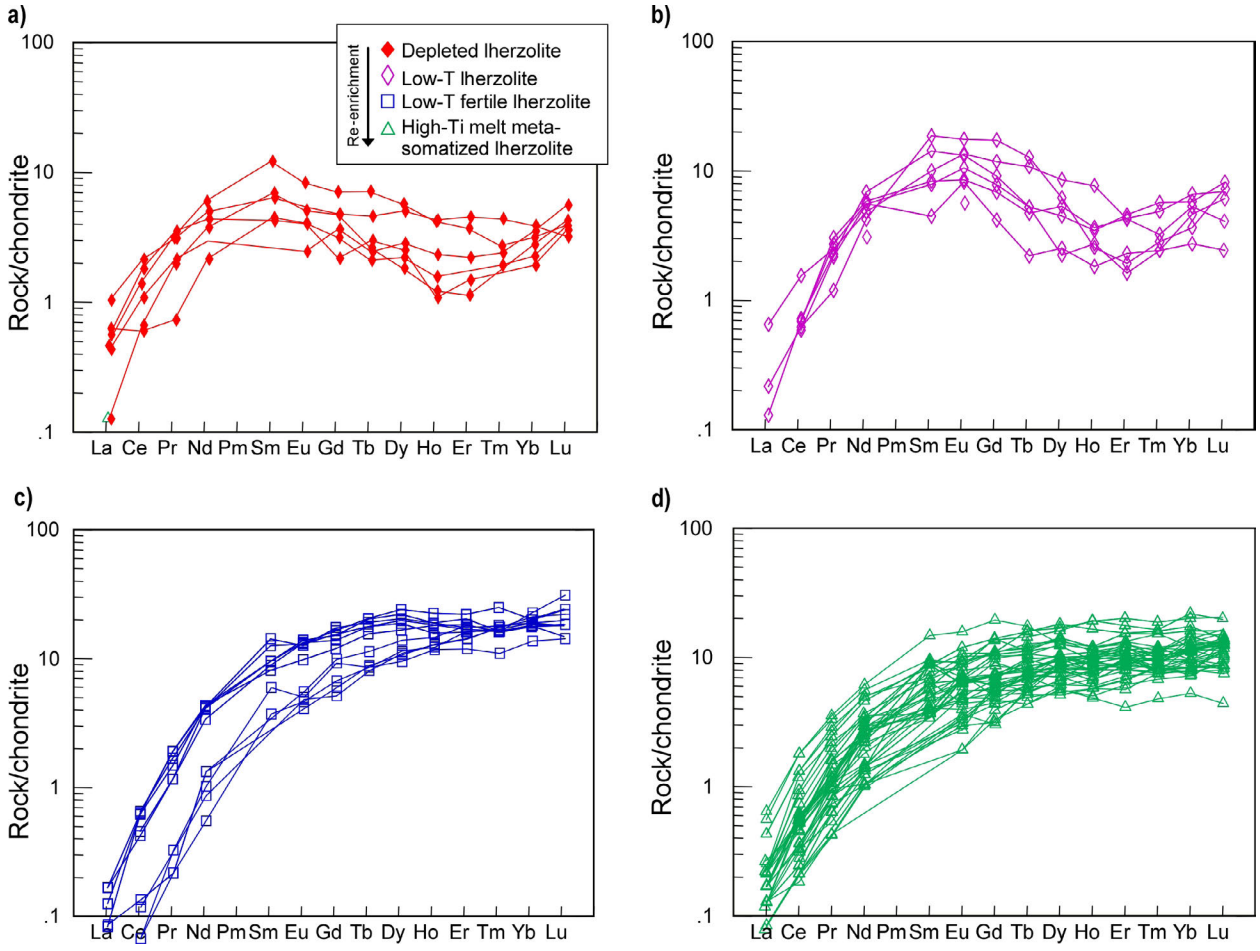

Figure 24. Chondrite-normalized REE profiles for the cores of peridotitic garnet xenocrysts from selected Buffalo Head Hills intrusions; chondrite values from Sun and McDonough (1989); nomenclature of the various lherzolitic-garnet types from Eccles and Simonetti (2008).

field (Figure 29) of Wyatt et al. (2004). A more comprehensive study of ilmenite xenocrysts from the Buffalo Head Hills kimberlites by Hood and McCandless (2004) showed that picroilmenite from the moderately diamondiferous K10 and K11 bodies (northern part of the field) has elevated MgO (>11 wt. %) and Nb_2O_5 (>1 wt. %) compared to that from the diamond-poor southern bodies. The variation in Nb composition was inferred to reflect increasing degrees of fractional crystallization in the source magma.

3.7.2 ~60 Ma Alkaline-Ultrabasic

Peridotitic garnets from the ~60 Ma bodies are dominated by G9 lherzolitic (97%, n = 55 of 57), with rare G11 high-TiO_2 peridotitic (Figure 22a, c). End-member garnet compositions are in the range of $Py_{65–74}Alm_{12–18}Sp_{0.6–1.2}Gr_{0–6.8}Uv_{6–15}$. The lherzolitic garnet is generally more calcic (4.5–6.1 wt. % CaO) and lower in Cr (2.2–6.6. wt. % Cr_2O_3) than the ~88–81 Ma peridotitic garnet. Hood and McCandless (2004) suggested that Cr composition of peridotitic garnet is an

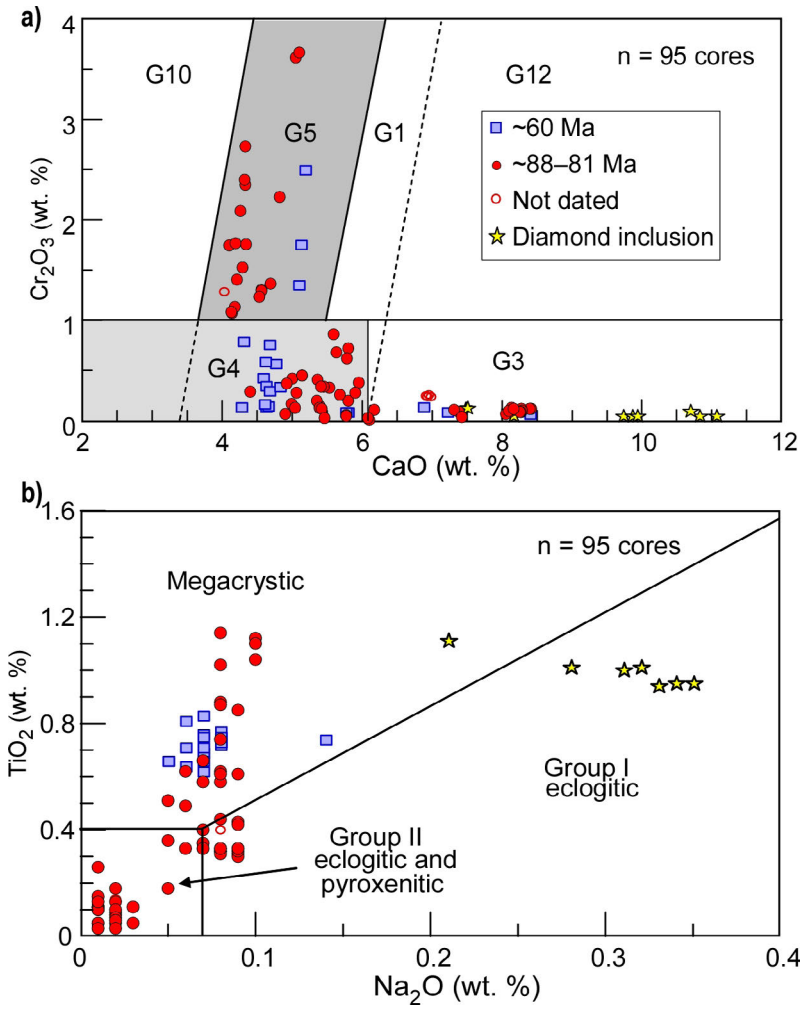

Figure 25. Classification of low-Cr garnet xenocryst cores from selected Buffalo Head Hills intrusions: a) Cr_2O_3 versus CaO, with group-number (e.g., G-1) classification nomenclature from Grütter et al. (2004); b) TiO_2 versus Na_2O in low-Cr garnet-xenocryst cores, with megacrystic and eclogitic Group I and II fields from Schulze (1997) and eclogitic diamond-inclusion data from Davies et al. (2004) and Banas et al. (2006; K14 and K252 kimberlites, n = 11); three diamond-inclusion garnets from Davies et al. (2004) with very high Na_2O (1.53–1.57 wt. %) are not shown on (b).

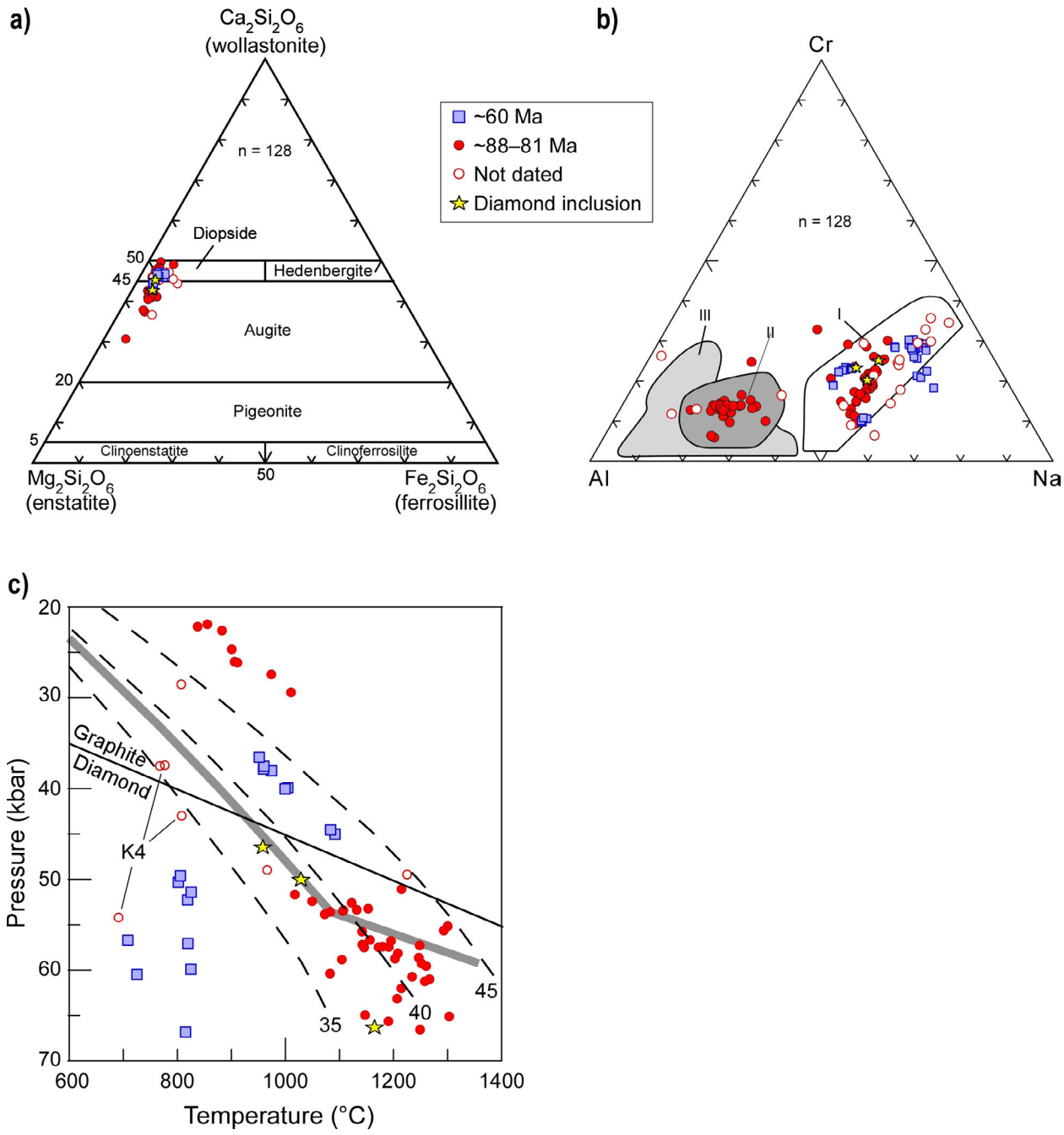

Figure 26. Variation diagrams for clinopyroxene-xenocryst cores from selected Buffalo Head Hills intrusions: a) Ca-Mg-Fe quadrilateral pyroxene classification based on the scheme of Morimoto et al. (1988); b) Al-Cr-Na diagram with classification fields modified after Morris et al. (2002), including mantle-equilibrated clinopyroxene derived from kimberlite (I), clinopyroxene from non-kimberlitic sources (II), and clinopyroxene equilibrated under crustal conditions (III); c) pressure-temperature diagram for clinopyroxene based on the thermobarometer of Nimis and Taylor (2000); garnet lherzolite–type clinopyroxene filters used cut-offs of <23 wt. % CaO and >0.5 wt. % Cr_2O_3 with <4.0 wt. % Al_2O_3 (<4.5 wt. % Al_2O_3 for Cr_2O_3 >2.25 wt. %); geotherms (in mW/m^2, dashed lines) from Pollack and Chapman (1977); diamond-graphite equilibrium (solid dark line) from Kennedy and Kennedy (1976); inferred Buffalo Head Hills geotherm (thick grey line) at 38–39 mW/m^2 from Aulbach et al. (2004), based on garnet xenocrysts, garnet lherzolite, sheared lherzolite and garnet pyroxenite; peridotitic clinopyroxene diamond-inclusion data from Davies et al. (2004; K14 kimberlite, n = 3).

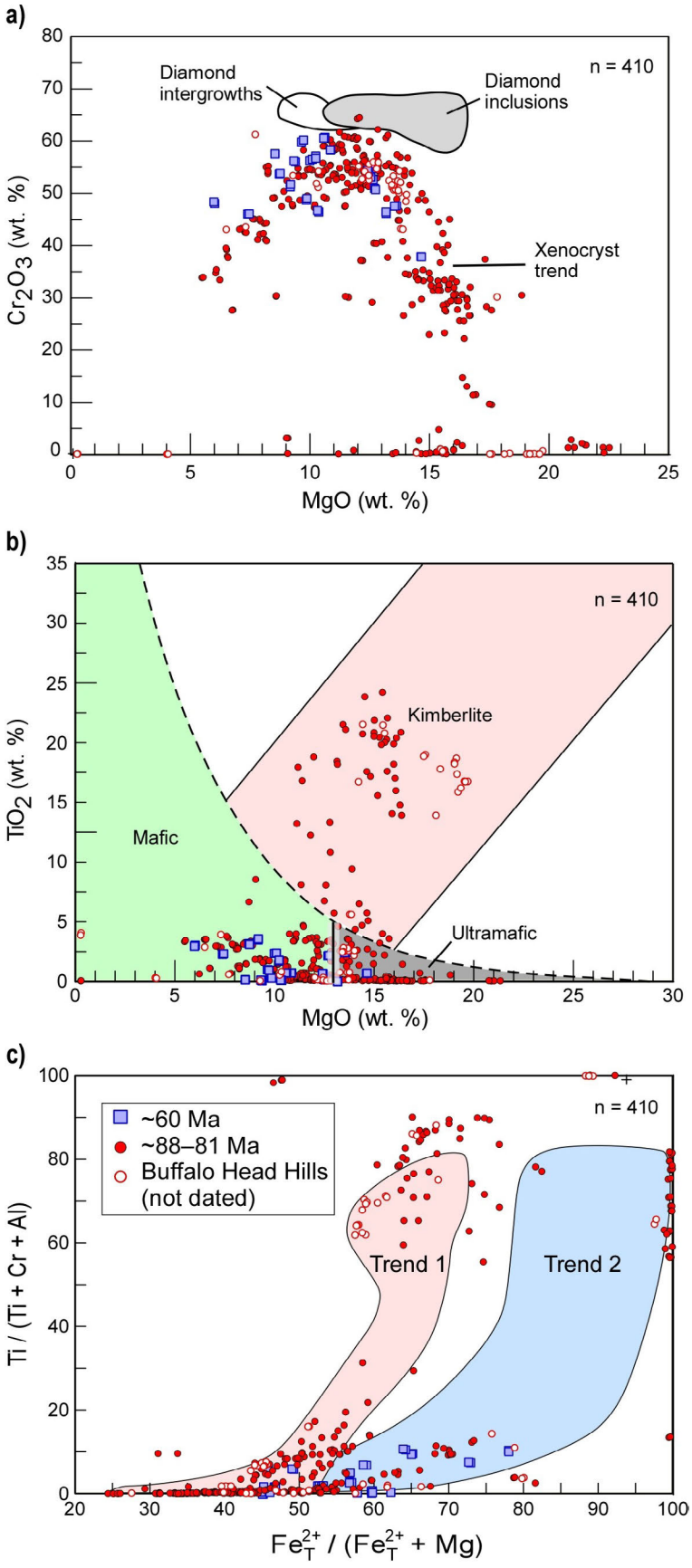

Figure 27. Variation diagrams for spinel xenocryst cores from selected Buffalo Head Hills intrusions: a) Cr_2O_3 versus MgO, with diamond-inclusion and diamond-intergrowth fields from Fipke et al. (1995); b) TiO_2 versus MgO, with fields from Creighton and Stachel (2008); c) Ti / (Ti + Cr + Al) versus Fe^{2+} / (Fe^{2+} + Mg), with magmatic trend 1 and 2 fields from Mitchell (1986).

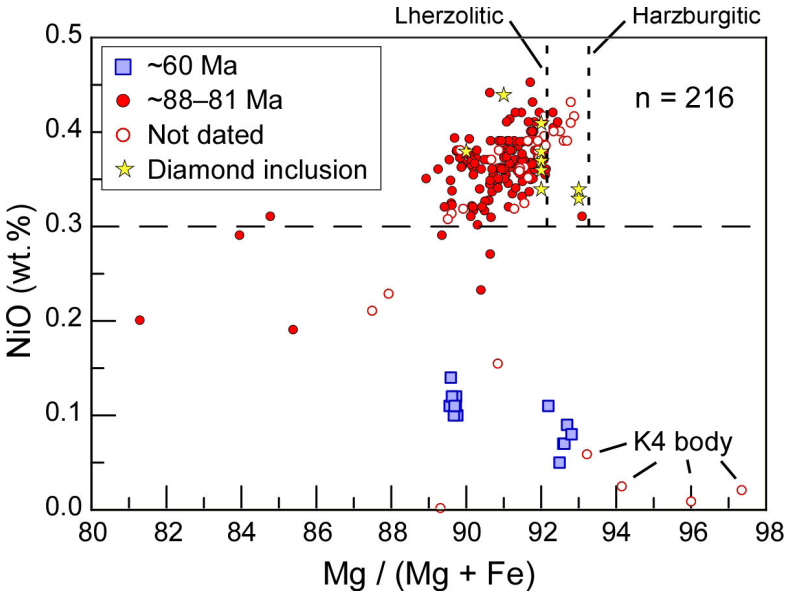

Figure 28. Plot of NiO versus Mg# (Mg / [Mg + Fe]) for olivine xenocryst cores from selected Buffalo Head Hills intrusions. Olivine with >3000 ppm Ni (long-dashed line) represents mantle olivine, based on data from mantle xenoliths and xenocrysts in kimberlite (e.g., Brett et al., 2009). Short-dashed lines represent average forsterite content of olivine inclusions in diamonds of lherzolitic (Mg# of 92.1) and harzburgitic (Mg# of 93.2) parageneses (Stachel et al., 2010). Peridotitic olivine diamond-inclusion data, from Davies et al. (2004; K14 kimberlite, n = 9), indicate an average forsterite content of 91.6.

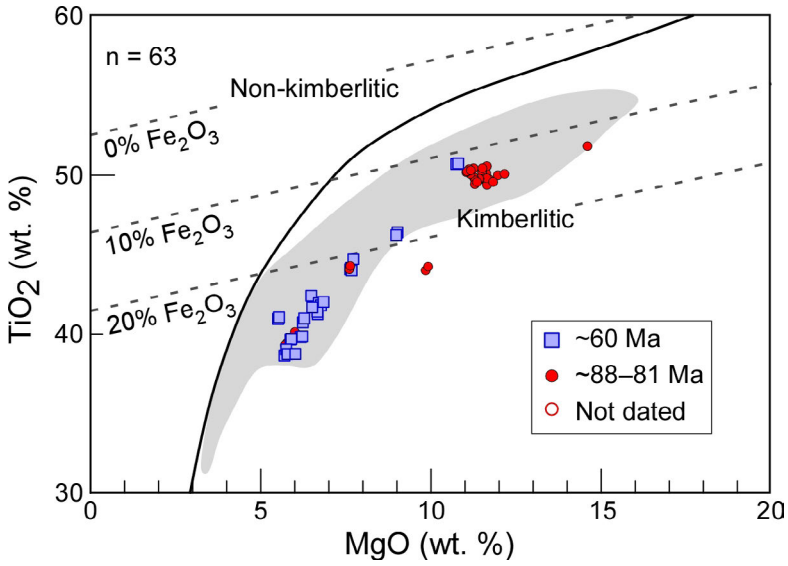

Figure 29. Plot of TiO_2 versus MgO for ilmenite xenocryst cores from selected Buffalo Head Hills intrusions. Dark grey dashed lines indicate the estimated Fe_2O_3 content of macrocrystalline ilmenite; solid line separates the fields of kimberlitic and non-kimberlitic ilmenite (Wyatt et al., 2004). Shaded polygon represents ilmenite from North American kimberlite (Schulze et al., 1995).

important discriminator of diamond content in the Buffalo Head Hills field. They noted that low-Cr garnet bodies (K2, K4A, K4B, K95 and K229) in the southern part of the field (i.e., potentially equivalent ~60 Ma intrusions) are either barren of diamonds or have low diamond content. Furthermore, the garnet bodies likely represent some contribution from shallow lherzolitic mantle. Accordingly, the Ca-intercept distribution of the ~60 Ma bodies is ~4–5.5, with its peak at ~4.6 (Figure 22d).

Based on LA-ICP-MS data, Eccles and Simonetti (2008) showed that the ~60 Ma bodies host an abundance of low-T_{Ni} (<950°C) garnet groups, such as low-T lherzolitic and low-T fertile lherzolitic. A cluster of low-T lherzolite garnet from K2 is evident in the 836°–924°C subcontinental lithospheric mantle layer. The garnet is characterized by depleted lherzolite compositions with low Ti, Y and Zr, and chondrite-normalized REE patterns that are highly sinusoidal (median Nd_N/Y_N ratio of 1.4) with hinges at Sm_N and Ho-Er_N (Figures 23 and 24). The sinusoidal REE_N patterns could be attributed to metasomatic styles that are common in the shallow lithosphere, such as interaction with an LREE-enriched metasomatic fluid, phlogopite-carbonatite-volatile–rich melt metasomatism and/or formation of garnet from residues formed at higher oxygen fugacity. In addition to the low-T lherzolite, the ~60 Ma bodies have abundant, low-T_{Ni} (<870°C) fertile lherzolite characterized by high Y (16.2–35.7 ppm) with depleted TiO_2 (0.01–0.1 wt. %) and a slightly concave-downward, increasing chondrite-normalized REE profile with a low-degree sinusoidal pattern (Nd/Y_N of 0.08; Figure 24). In addition, fertile lherzolitic garnet has high Y/Zr and low Nd/Y_N and Sc/Y_N. Collectively, these thermal and geochemical signatures suggest fertile garnet in a shallow-subcontinental lithospheric mantle setting.

The low-Cr garnet in the ~60 Ma bodies has end-member compositions in the range of $Py_{50–72}Alm_{16–27}Sp_{0.5–0.7}Gr_{3–20}Uv_{0.2–7.1}$ and is classified as predominantly megacrystic G1 garnet (n = 18 of 20), with >0.4 wt. % TiO_2 at low Cr_2O_3 and Na_2O (Figure 25). Determination of low-Cr megacrystic garnet is important because G1 garnet can occur in mantle-derived magmas other than kimberlite (e.g., alkali basalt; Schulze, 1987).

The ~60 Ma clinopyroxene has a narrow range of compositions ($Wo_{41–46}En_{46–50}Fs_{3–5}Ae_{3–7}$), Mg# (91–94) and Ca# (45–49; n=36). On the Ca-Mg-Fe quadrilateral diagram, the clinopyroxene is classified as diopside and Mg-Ca–augite (Figure 26). On the Al-Cr-Na diagram, the ~60 Ma clinopyroxene forms two distinct, albeit closely associated groups, both of which are characteristic of mantle-equilibrated clinopyroxene (Figure 26). Based on geothermobarometry, however, these two clinopyroxene groups yield either shallow depths (37–45 kbar) plotting outside the diamond-stability field, or have pressures of >48 kbar but with significantly cool (708°–836°C) clinopyroxene (Figure 26c). The latter trend of high-P, low-T clinopyroxene is likely related to clinopyroxene grains that are unsuitable for the Nimis and Taylor (2000) thermobarometer. That is, if these clinopyroxenes represent equilibrium P-T values on an ambient geotherm, then they would imply a geothermal gradient for very low heat flows (i.e., below 36 mW/m^2; based on geothermal gradients of Pollack and Chapman, 1977). This is not something one would expect for Proterozoic, or pervasively Proterozoic reworked, mantle lithosphere.

Spinel from the ~60 Ma bodies has Cr contents up to 61 wt. % Cr_2O_3, but with a low MgO (<13 wt. % and averaging 10.6 wt. %) and a prominent magmatic trend 2 characterized by low TiO_2 (0.01–3.5 wt. %) and high $Fe^{2+}_T / (Fe^{2+}_T + Mg)$ ratio (45–78; Figure 27). Olivine cores from the ~60 Ma intrusions display a narrow range of Mg# (90–93), but with extremely low Ni (0.05–0.14 wt. % NiO; Figure 28). Ilmenite from the ~60 Ma bodies classifies as kimberlitic ilmenite on the MgO-TiO_2 plot, but has low median values of TiO_2 (41.5 wt. %) and Mg# (21; Figure 29).

Electron microprobe analysis determined hornblende grains to be pargasitic-edenitic amphibole (Eccles et al., 2008a; Figure 30a). Similar grain types have been previously identified by surficial kimberlite-indicator mineral studies in the southern part of the Buffalo Head Hills field

(pargasite; Keith 2004), and as xenocrysts in some of the barren and diamond-poor bodies in the same part of the field (edenite; Hood and McCandless, 2004). Although the pargasitic-edenitic amphibole may be xenocrystic, its origin could also represent a primary phase stable at the liquidus of basic melts (Dawson and Smith, 1982), or the product of hydrous metasomatism of lherzolitic mantle (Field et al., 1989; Fialps-Guedon et al., 2000).

Potassium-feldspar occurs as untwinned subhedral grains with variable alteration. The chemical composition of these grains suggests sanidine with little variability, specifically $Or_{91–93}$, $Ab_{7–9}$ and low Ca (<0.07 wt. %; Figure 30b), although their definitive nomenclature is not known because precession photographs and crystal diffractometer analysis were not completed. If these grains are primary, this would indicate a high-pressure K-feldspar–bearing phase in the subcontinental lithosphere/upper mantle in this area.

3.7.3 Other Mantle-Characteristic Observations

The K4 cluster, albeit not dated, has mantle/lower crustal geochemical signatures consistent with those of the ~60 Ma volcanics. In particular, the geochemical compositions of certain xenocrysts, such as olivine (low NiO) and clinopyroxene (low-T), are more consistent with ~60 Ma rather than ~88–81 Ma Buffalo Head Hills magmatism (Figures 26 and 28). This seems to provide additional evidence of a shallower source for K4 compared to the ~88–81 Ma bodies. In addition, mantle xenocryst compositions provide meaningful criteria for distinguishing between the barren K4 and diamondiferous K11 intrusions.

Detailed information about kimberlites discovered in 2008, including the BE-01, -02 and -03 bodies in the eastern part of the Buffalo Head Hills field, is only just becoming publicly available. Based on xenocryst chemistry, Dufresne et al. (2010) suggested that the BE-02 and -03 bodies sampled diamond-bearing lithosphere. This conclusion is substantiated by high Cr_2O_3 Cr-spinel with a prominent xenocryst trend, peridotitic garnet with T_{Mn} estimates of >1000°C, and Cr-diopside with P-T estimates within the diamond-stability field and straddling the 40 mW/m^2 geotherm.

3.8 Summary and Classification of the ~88–81 Ma and ~60 Ma Buffalo Head Hills Intrusions

Distinct variations in the mineralogy and the whole-rock and mantle-xenocryst chemistry are evident between the ~88–81 Ma (and ~64 Ma) and the ~60 Ma intrusions (Table 3). Consequently,

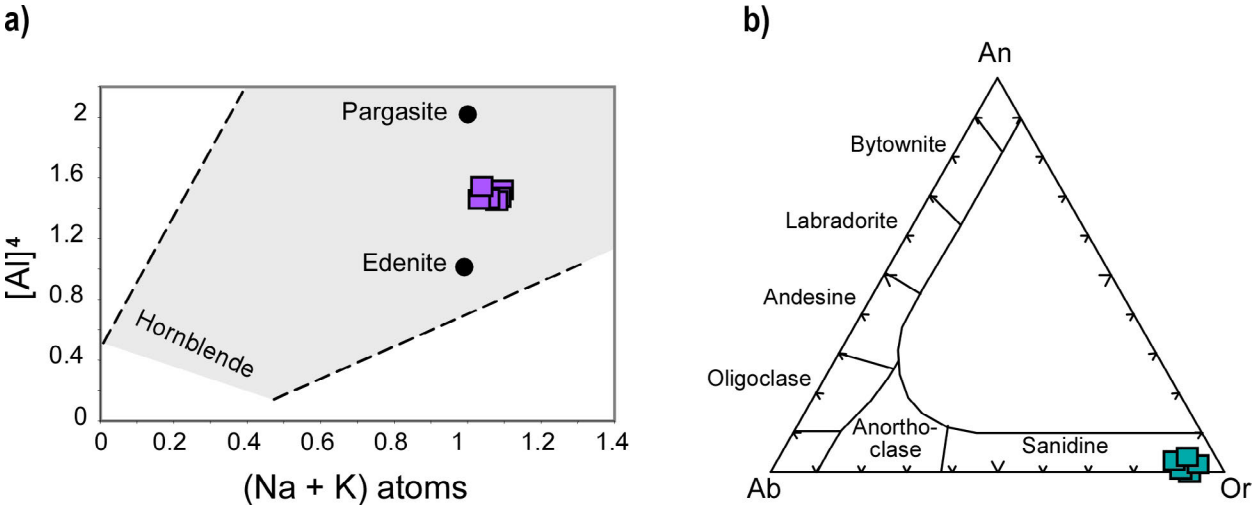

Figure 30. Electron microprobe analyses of selected minerals from the ~60 Ma K1A and K19 intrusions (solid squares): a) pargasitic-edenitic amphibole plotted on the chemical variation diagram for Ca-rich amphibole (Deer et al., 1963); b) K-feldspar (sanidine) on the ternary classification Ab-An-Or for feldspar. Abbreviation: [Al]^4, number of ions of tetrahedrally co-ordinated Al (based on 24 O).

their rock classification reflects different magmatic sources.

With low CI, the ~88–81 Ma intrusions (and the ~64 Ma BM2 intrusions) have a nearly identical major-element, trace-element and isotopic geochemical fingerprint compared to Group 1A South African kimberlite and primitive hypabyssal kimberlite at Ekati, Northwest Territories (Figures 18–21). On the plot of TiO_2 versus K_2O (Figure 19), the Buffalo Head Hills kimberlites records a continuum of TiO_2 ranges, a profile similar to serpentine- versus dolomite-bearing, uncontaminated, hypabyssal kimberlite from Ekati (Kjarsgaard et al., 2009). Mantle xenocryst compositions from the ~88–81 Ma intrusions provide additional support for a kimberlite rock classification. That is, garnet and clinopyroxene xenocrysts are representative of minerals sampled under pressures and temperatures that are consistently within the diamond-stability field, a contention reinforced by the presence of diamonds in these bodies. The conclusion is that the ~88–81 Ma intrusions represent the most primitive, depleted upper-mantle (MORB-like) intrusions in the northern Alberta kimberlite province.

In contrast, the ~60 Ma K1 and K19 intrusions in the southwestern part of the field (Figure 12) appear to be derived from a different source than the ~88–81 Ma bodies (and the ~64 Ma BM2 body). The ~60 Ma bodies are either barren or with low diamond counts (Hood and McCandless 2004) with minerals (e.g., edenite-pargasite amphibole and sanidine) atypical of kimberlite. Their CI, major-element and trace-element signatures more closely resemble those of Mountain Lake than the ~88–81 Ma bodies, suggesting a parental magma source similar to that of Mountain Lake (Figures 18–20). The ~60 Ma K1A and K19 bodies have higher $^{87}Sr/^{86}Sr$ (0.70493–0.70525) and lower ε_{Nd} (–0.5 to +0.4) than the ~88–81 Ma bodies (Figure 21). The Ca-intercept distribution in peridotitic garnet of the ~60 Ma bodies is distinctly higher than that of the ~88–81 Ma bodies (Figure 22), implying shallower sampling, a hotter geotherm and/or high metasomatism compared to the ~88–81 Ma lherzolitic garnet. Abundant Al-rich clinopyroxene with pressure estimates of between 37 and 45 kbar, low-NiO olivine and low-Ti trend 2 Cr-spinel generally support a shallow depth of sampling (Figures 26–28).

Based on these findings and the chemical similarity between the ~60 Ma intrusions and Mountain Lake, the ~60 Ma bodies in the Buffalo Head Hills, including K1 and K19, are more accurately described as alkaline-ultrabasic rocks than kimberlite. It is possible that these rocks formed in the upper mantle during a pervasive metasomatic event caused by rising temperature and the infiltration of alkali-rich fluids.

Lastly, the K4 cluster has a different whole-rock geochemical signature than many of the other bodies in the Buffalo Head Hills field. It is geochemically possible that this cluster of intrusions represents a shallow, metasomatized, sub-continental lithosphere source and is somehow related to the ~60 Ma bodies. However, it is important that K4 has similar whole-rock geochemical characteristics, including $^{87}Sr/^{86}Sr$ and ε_{Nd}, to the ~85 Ma diamondiferous K11 body (Figure 21). Eccles (2004) noted that K4 and K11 define the end-member of olivine accumulation in the Buffalo Head Hills field. It is possible, therefore, that K4 and K11 have a unique, whole-rock geochemical signature due to olivine accumulation and/or textural modification, such as crystal enrichment (olivine) in a primary pyroclastic-fall type of environment. In such instances, it is better to investigate mantle xenocryst compositions, as K11 clearly has a source compatible with the diamond-stability field and diamondiferous ~88–81 Ma kimberlite compared to the K4 intrusion.

3.9 Diamond Content

Estimated diamond contents for the Buffalo Head Hills kimberlite field are reported in Carlson et al. (1999), Skelton et al. (2003), Hood and McCandless (2004), Eccles (2007b), Eccles et al. (2008a) and various company-specific news releases, and are summarized in Appendix 1. Twenty-eight of the 41 occurrences in the Buffalo Head Hills contain diamond. Five bodies have undergone mini–bulk sampling (14–616 tonnes): K6, K11, K14, K91 and K252 (Table 4). At least

Table 3. Synopsis of the physical and chemical variations and observations for different rock-type classifications in the northern Alberta kimberlite province.

Subject	Primitive Kimberlite	Evolved Kimberlite	Alkaline Classification (Non-Kimberlite)
Area/bodies	Buffalo Head Hills kimberlite field, particularly the northwestern part (e.g., K5A, K7A, K11, K14A, K91 and K252) but also the eastern part (e.g., BM2 and possibly BE-02 and BE-03)	Birch Mountains (Legend, Phoenix and possibly Dragon, Pegasus, Roc and Valkyrie)	Mountain Lake, Buffalo Head Hills (particularly the southwestern part of the field; e.g., K1 and K19) and Birch Mountains (Xena and Kendu)
Age	~88-81 Ma (BH225, BH229, K5, K7A, K11, K14, K91, K252 and LL8); 64 Ma (BM2)	~78-70 Ma (Dragon, Legend, Phoenix, Valkyrie and Xena)	~76-68 Ma (Mountain Lake); ~60 Ma (Buffalo Head Hills K1 and K19); ~73 Ma (Xena, Birch Mountains)
Petrography	Olivine crystals and juvenile lapilli set in a fine-grained serpentine-, carbonate- and CaMg(Fe)-silicate–rich mesostasic groundmass, together with one or more of the following primary minerals: phlogopite, sulphide, perovskite, spinel, ilmenite, rutile and apatite	Coarse-grained olivine and lapilli set in an indeterminate, fine-grained, amorphous, brownish-coloured matrix of serpentine, calcite and clay minerals with disseminated and altered spinel; compared to primitive kimberlite, higher abundance of carbonate, relatively devoid of olivine macrocrysts and higher concentrations of coarse-grained opaque minerals (ilmenite, spinel and perovskite), phlogopite, apatite and sulphide	Olivine pseudomorph and juvenile-lapilli rich, set in a fine-grained matrix extensively altered to zeolitic-phase clay materials with accessory mica, feldspar, illite, Ti-minerals, pyrite, chlorite, calcite and spinel; diagnostic non-kimberlite mineral assemblages may include amphibole, sanidine, spessartine, plagioclase and analcite; zeolite-phase spectra; potassium component in the matrix mesostasis
Whole-rock major- element geochemistry	Similar to Group IA (on craton) South African kimberlite and Ekati (Northwest Territories) hypabyssal kimberlite; contamination index ~1.0, SiO_2 <38 wt. %, MgO >20 wt. %, K_2O <0.5 wt. %, TiO_2 <1.5 wt. %	Similar to Group IB (off craton) South African kimberlite; contamination index ~1.0-1.5, SiO_2 <33 wt. %, MgO >20 wt. %, K_2O <0.75 wt. %, TiO_2 2–4 wt. %	Alkaline signature, particularly similar to Roman Province–type magmas; peralkaline index <0.7, contamination index >2.0, SiO_2 45–48 wt. %, K_2O >1.5 wt. %
Whole-rock chondrite-normalized rare-earth element pattern	$LREE_N$ up to 1800; $(La/Yb)_N$ averages 215; fractionated	$LREE_N$ up to 1350; $(La/Yb)_N$ of 115–300; variable partial-melting	$LREE_N$ of 90–275; $(La/Yb)_N$ of 30–50; significantly flatter chondrite-normalized rare-earth element pattern relative to kimberlite
Whole-rock Sr-Nd isotopic signature	Low $^{87}Sr/^{86}Sr$ (0.70379–0.70446) and positive εNd (+2.5 to +4.3) similar to South African Group I kimberlite; most primitive depleted upper-mantle (MORB-like) source in northern Alberta	Radiogenic Sr (similar to Ekati, Northwest Territories)	Radiogenic Sr (similar to evolved kimberlite) to highly radiogenic Sr and depleted Nd (similar to Roman Province–type magmas)

Subject	Primitive Kimberlite	Evolved Kimberlite	Alkaline Classification (Non-Kimberlite)
Mantle (and lower crustal) characteristics	Heterogeneous; lowest peridotitic garnet Ca-intercept (mode at ~4.1); includes some Type I eclogitic garnet; clinopyroxene P-T estimates are scattered between 36 and 44 mW/m2, geotherms at 50–67 kbar; trend 1 Cr-spinel; dominant Cr-spinel xenocryst trend; olivine with >3000 ppm Ni	Heterogeneous; high periodotitic garnet Ca-intercept (mode at ~4.6–4.8); dominated by high-T melt metasomatized peridotitic garnet	Heterogeneous; high periodotitic garnet Ca-intercept (mode at ~4.6); dominated by high-T melt metasomatized peridotitic garnet; crustal (G0) garnet and low-Cr megacrystic (G1) garnet; generally abundant Al-rich, low-P and low-T clinopyroxene and low-Ti trend 2 Cr-spinel; clinopyroxene does not provide realistic P-T estimates; low-Ni olivine (<1500 ppm)
Diamond content	Diamondiferous: includes mini–bulk sampled kimberlites (K14, K91 and K252) with estimated grades of 12–55 carats per hundred tonnes	Barren to low diamond content	Barren to low diamond content

Abbreviations: MORB, mid-ocean ridge basalt

three kimberlites (K14, K91 and K252) in the northwestern part of the field have estimated grades of >12 carats per hundred tonnes (cpht).

The results of these bulk sample programs need to be viewed in the context of new geological modelling. Canterra Minerals Corporation and Shore Gold Inc. have reported that trench samples from the K14 body represent only a near-surface phase of a complex multiphase kimberlite. Previous work on K14 from a 479 tonne sample, that included both surface and drillhole material, yielded a sample grade of 12 cpht. In contrast, a surface-trench mini–bulk sample, collected at a later date, yielded 11.13 carats from 137 tonnes, providing an average sample grade of 8.1 cpht. Importantly, the geological model established for the K14 kimberlite clearly suggests that the recent bulk sampling material was sourced entirely from within the macrocrystic, volcaniclastic kimberlite facies, which may have a lower diamond-carrying capacity than the underlying, but volumetrically greater, xenocrystic volcaniclastic kimberlite facies (French, 2010).

The 35th kimberlite discovered in the Buffalo Head Hills field, kimberlite K252, provided the most encouraging results to date. A 22.8 tonne mini–bulk sample returned a total of 12.54 carats of diamonds, for an estimated diamond content of 55.0 cpht. Significantly, these results can be further broken down because the estimate combines the analytical results from two distinct kimberlite layers. Ashton reported that an upper K252 'volcaniclastic'[3] unit returned 33.7 cpht from a 13.4 tonne sample, whereas a lower K252 'breccia'[3] unit yielded 85.4 cpht from a 9.4 tonne sample (Skelton et al., 2003). These results further emphasize the importance of kimberlite-facies modelling prior to diamond testing.

During 2008, two separate drill programs by Grizzly Discoveries Inc. discovered three previously unknown kimberlite bodies (BE-01, -02 and -03). Positive diamond recovery results from the 2008 winter drill program yielded 54 diamonds greater than 0.075 mm and 26 diamonds greater than 0.106 mm from a 56.6 kg sample of BE-02. This finding encouraged a larger campaign by Grizzly. An additional 563 kg of kimberlite material collected from BE-02 and 365 kg from BE-03 yielded 316 diamonds (five diamonds >0.5 mm in one dimension) and 218 diamonds (five diamonds >0.5 mm), respectively.

Diamonds (n = 182) from the Buffalo Head Hills kimberlite field have been studied by Davies et al. (2004) and Banas et al. (2006), and summarized by Stachel et al. (2010). They are generally of high quality, with a predominance of colourless, dodecahedral crystals (Banas et al., 2006). Octahedral, irregular fragments, aggregates and macles were also observed. The largest diamond recovered, as of 2010, is a 1.3-carat stone from the K14 kimberlite, and the highest quality diamond reported is a 0.76-carat clear, yellow-coloured stone from the K6 kimberlite (cover photo). In addition, a 0.94-carat stone indicates the potential for K252 to host commercial-sized stones.

Nitrogen content and compositions imply large variations in mantle-residence conditions (Types IaA, IaB and II diamonds) and temperature (<1000°C to >1300°C) consistent with diamond formation ranging from the top of the diamond-stable lithosphere to the sublithospheric mantle. The combination of a high abundance of eclogitic diamond inclusions, sublithospheric Type II diamonds and high diamond mantle-residence temperatures suggest that diamond formation beneath the Buffalo Head Terrane involved deep subduction, possibly followed by slab break-off or formation of a megalith. Some diamonds indicate storage in conditions of normal-temperature lithosphere, such that stockworks of metasomatic channels may also present a viable model for diamondiferous mantle beneath the Buffalo Head Hills field.

3.10 Emplacement Style and Near-Surface Setting Based on Kimberlite–Host-Rock Relationships

Boyer (2005) and Boyer et al. (2008) have provided excellent reviews of potential emplacement mechanisms for the Buffalo Head Hills kimberlite field, in which they have inferred that the broadly similar geometries of these

[3] Ashton Mining of Canada Inc. logging nomenclature

Table 4. Diamond results for mini–bulk and bulk samples from the K6, K11, K14, K91 and K252 kimberlites in the Buffalo Head Hills kimberlite field (data sources: Skelton et al., 2003; Canterra Minerals Corporation, 2008): a) samples >10 tonnes; b) K252 mini–bulk sample results.

a)

	1997–2003 Results						2008–2009 Results			
	Mini-Bulk (Diamonds >0.8 mm)					Bulk (Diamonds >1.2 mm)	Mini-Bulk (Total Stones)			
	K6	K11	K14	K91	K252	K14	K6 (pit)	K14 (pit 1)	K14 (pit 2)	K14 (pit 3)
Tonnes	13.95	21.85	44.87	35.87	22.8	479	231.89	43.56	45.22	48.22
Diamonds (carats)	0.88	0.96	7.79	4.56	12.54	56.45	16.29	3.21	3.98	3.95
Content (cpht)	5.6	4.4	17	12.7	55	11.7	7.02	7.37	8.79	8.18
Largest stones (carats)	0.76	0.09; 0.1	0.6; 1.31	0.41; 0.45	0.94	0.88; 0.9	1.07	0.9	0.38	0.71

b)

Kimberlite Type	Sample Weight (kg)	Diamonds			Diamond Content (cpht)	Large Stones
		Micro (0.1–0.5 mm)	Macro (>0.5 mm)	>0.8 mm (ct)		
Volcaniclastic	124.2	118	12	4.51	33.7	Two largest stones measure 1.60 by 0.68 by 0.46 mm and 1.32 by 1.02 by 0.37 mm
Breccia	102.7	126	7	8.03	85.4	Two largest stones measure 2.35 by 2.19 by 0.63 mm and 2.45 by 1.70 by 0.45 mm
Total	**226.9**	**244**	**19**	**12.54**	**55.0**	

kimberlites indicate a similar eruption sequence. This sequence is summarized as follows and illustrated schematically in Figure 31:

1) initiation of ascent of magma
2) saturation in volatiles and fluid exsolution
3) fluid expansion by decompression
4) fragmentation of melt
5) emplacement into wet sediments and entrainment of sediment and water
6) breaching of surface, eruption column and downward propagation of depressurization front
7) decrease in upward flow, with column collapse feeding surge
8) cessation of volcanic activity and erosion of tephra ring to fill crater

Boyer (2005) proposed a combination of phreatomagmatic eruption (evidence: accretionary pyroclasts and pyroclastic surge-and-fall deposits) and exsolution-driven magmatism (evidence: intense serpentinization, carbonatization and fragmentation) to explain the eruptive mechanisms that formed the Buffalo Head Hills kimberlites. These processes worked in concert; that is, as fragmentation of the kimberlite magma through exsolution increased the ascent rate, the result was phreatic interaction between hot magma, wet sedimentary rocks and groundwater.

With respect to near-surface kimberlite–host-rock relationships, integrated geochronology and palynology provide new constraints on the nature, timing and sequence of eruptions in the Buffalo Head Hills kimberlite field. Within broadly coeval Coniacian–Campanian (~88–81 Ma) volcanism-sedimentation, and a younger Paleocene (~64 and ~60 Ma) eruptive event, three different settings are recognized that collectively define a kimberlite field characterized by stacked, often tabular kimberlite layers of varying ages (schematically illustrated in Figure 32).

3.10.1 Late Cretaceous Smoky Group–Equivalent Intra- and Extra-Crater Volcanism

The oldest volcanism in this field is recorded by a cluster of Late Cretaceous kimberlites interpreted to be emplaced coevally within the Smoky Group host strata. It is difficult to prove that these kimberlites are syndepositional because an extensive Turonian (in part or in whole) through Early Campanian hiatus, representing approximately 9 million years of missing strata, coincides with Late Cretaceous kimberlite volcanism. A stratigraphic section of the BH229 and K296 kimberlites (Figure 33) illustrates the complexity of kimberlite–host-rock relationships within the context of unconformable time gaps in this setting. In addition, the setting of syndepositional volcanism is controlled by paleotopography associated with the depositional hiatus (possibly related to tectonic uplift) and subsequently modified as part of a Late Cretaceous landscape that was transgressed by marine waters. As such, the manifestation of the bodies could include any combination of kimberlite lavas and flows, pyroclastic surge-and-fall deposits and resedimented volcaniclastic kimberlite.

3.10.2 Late Cretaceous and Paleocene Intrusive Volcanism

A second type of emplacement setting involves a complicated scenario of Late Cretaceous and Paleocene intrusive rocks penetrating significantly older sedimentary rocks. For example, the Campanian K252 kimberlite (81.3 ±2.3 Ma Rb-Sr phlogopite; Eccles et al., 2008a) is hosted in older sedimentary strata that have a bracketed (i.e., data and interpretations for below and above the intrusive kimberlite) palynological age of Cenomanian–Albian (~105–95 Ma; Figure 34). The combined geochronology suggests intrusive volcanism; however, the K252 kimberlite has previously been interpreted as having volcaniclastic textures (Boyer, 2005).

To address this inconsistency, Eccles et al. (2008b) investigated new (2008) drillcores from K252 and speculated that magmatic-sedimentary rock interaction occurs at both the lower and upper contacts of one or more kimberlite-mudstone layers. This author suggests that preliminary textural evidence supports intrusive (rather than pyroclastic) emplacement and is representative of ‘peperitic’ kimberlite, a term that has not

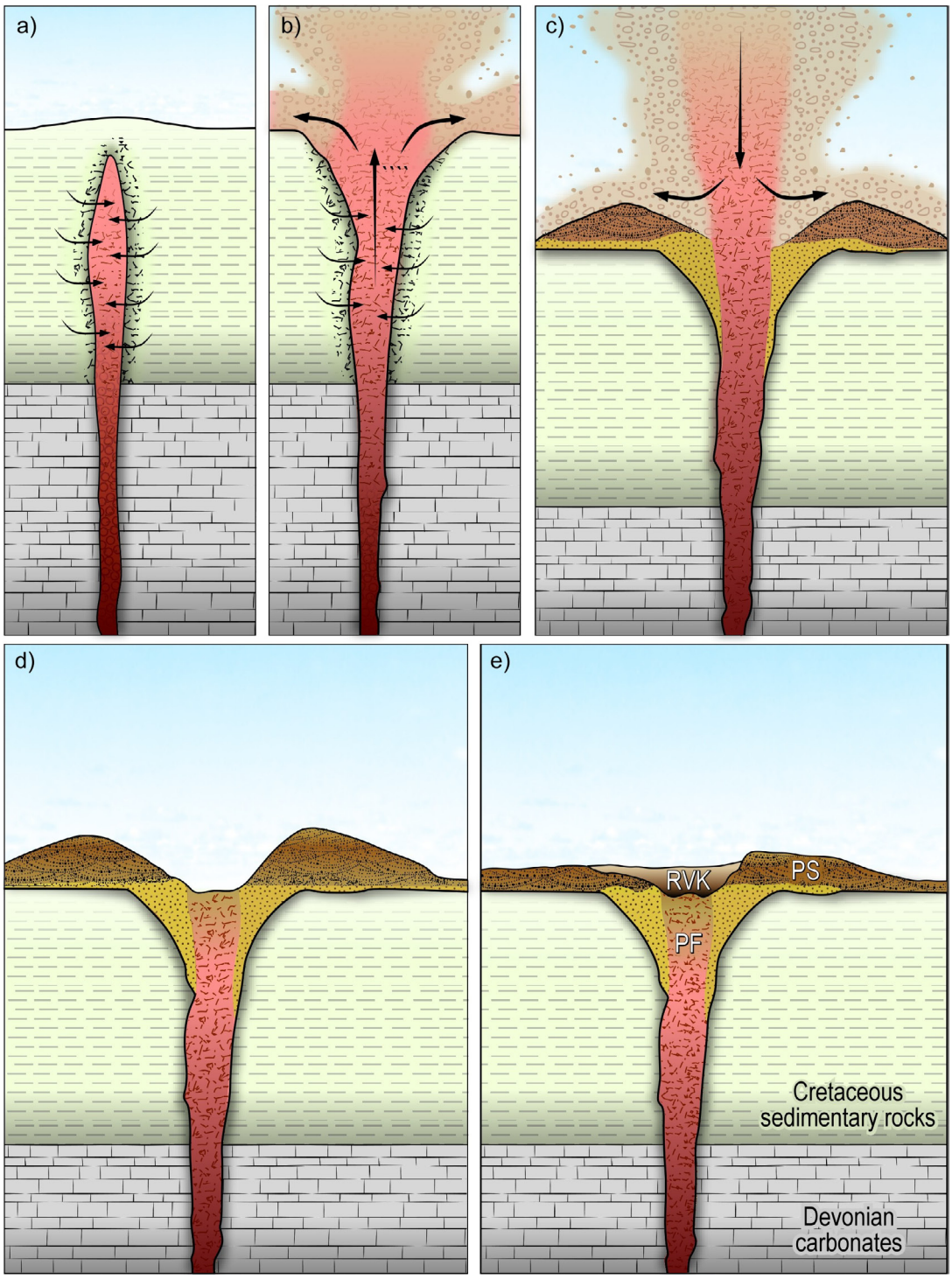

Figure 31. Schematic representation of the proposed eruptive sequence for kimberlite in the Buffalo Head Hills field (from Boyer [2005] and reproduced with L. Boyer's permission): a) penetration of the erupting magma upward into Late Cretaceous to Paleocene sedimentary strata; b) magma breaches the water table and surface, excavating a crater; c) pyroclastic surge-and-fall deposits form tephra ring(s); d) eruptive activity ceases, resulting in a tephra ring consisting of surge deposits and a crater dominated by fall deposits; e) tephra ring is subject to erosion and flattening, resulting in infilling of the crater with resedimented volcaniclastic rocks. Abbreviations: PF, pyroclastic fall; PS, pyroclastic surge; RVK, resedimented volcaniclastic kimberlite.

previously been associated with kimberlite. Peperite is defined as

> *"a genetic term applied to a rock formed essentially in situ by disintegration of magma intruding and mingling with unconsolidated or poorly consolidated, typically wet sediments. The term also refers to similar mixtures generated by the same processes operating at the contacts of lavas and hot pyroclastic flow deposits with such sediments."* (White et al., 2000)

Some of the textures used to suggest peperitic kimberlite include

- kimberlite–host-rock liquefaction and mingling (a peperitic stew intermixed with clasts of both kimberlite and mudstone);
- mechanical fluid-fluid shear, evidenced by the white-carbonate–rich veinlets orientated discordantly to host rock bedding (disruption penetrating 2–5 m from the contact); and
- thermal alteration, evidenced by scorched host rock, irregular jigsaw-fit textures and disseminated cubic pyrite, which is atypical compared to sulphide replacement of organic-rich (i.e., shells, bones) mudstone in other parts of northern Alberta.

Although these observations are preliminary, they are important and further investigation is required to determine the relationship between alternating sequences of kimberlite, mudstone and sandstone in the WCSB.

Paleocene intrusive rocks are thoroughly documented. Palynological study of the sedimentary rocks that host the Lower Paleocene (~64 Ma) BM2 kimberlite provide evidence of its multilevel intrusion into thermally enhanced, older Albian and possibly Cenomanian host rocks (Sweet et al., 2006; Figure 35). The hypabyssal-facies character and age of BM2 (Boyer et al., 2003; Eccles et al., 2008a), and the thermal enhancement of the palynomorphs adjacent to the dikes form a cohesive story of Paleocene intrusive volcanism.

3.10.3 Paleocene Paskapoo Formation–Equivalent Intra-Crater Volcanism

The youngest eruptive event is of Late Paleocene, equivalent to the Paskapoo Formation, whereas the youngest preserved host rocks capping the

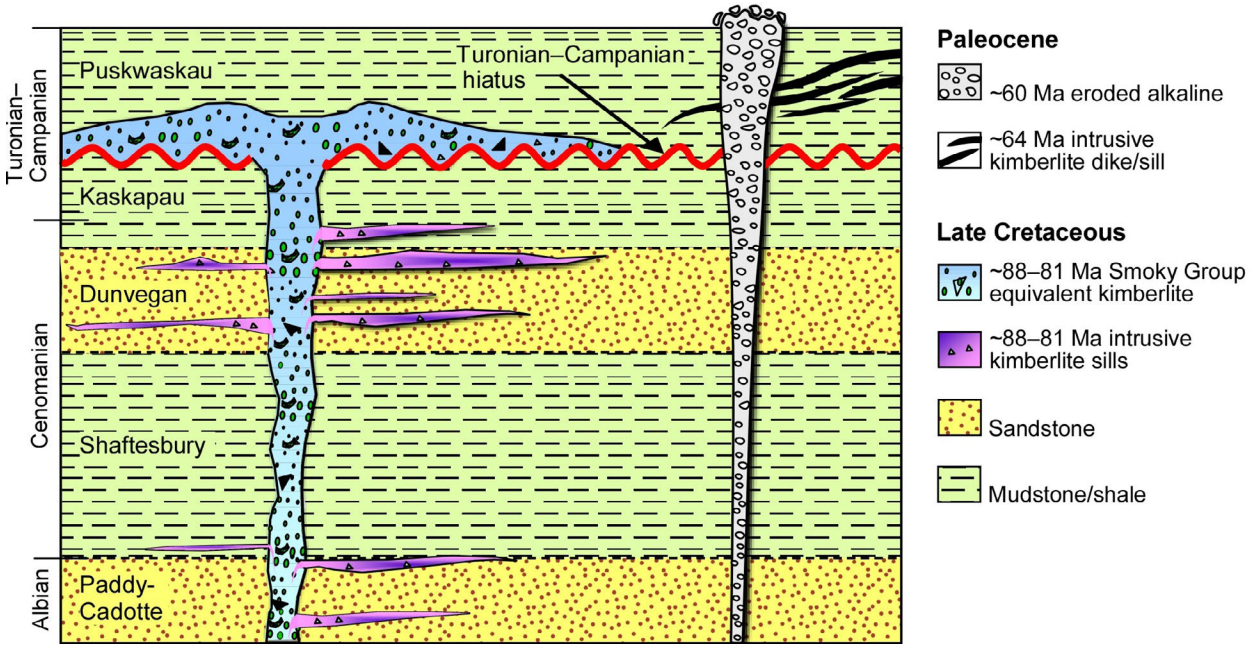

Figure 32. Schematic diagram showing potential kimberlite-hostrock relationships based on integration of palynological and geochronological data.

Buffalo Head Hills are of the Campanian Wapiti Group (ca. 78 Ma; Pawlowicz et al., 2005b; Sweet et al., 2006). Figure 36 shows that the cored portion of the ~60 Ma K1 body is bounded by early Late Campanian to Cenomanian pre-eruptive sedimentary rocks. In this instance, the only record of now-eroded latest Campanian to Paleocene host rocks is from sedimentary xenoliths in the preserved part of the truncated intra-crater facies kimberlite. All four drillholes testing K1 ended

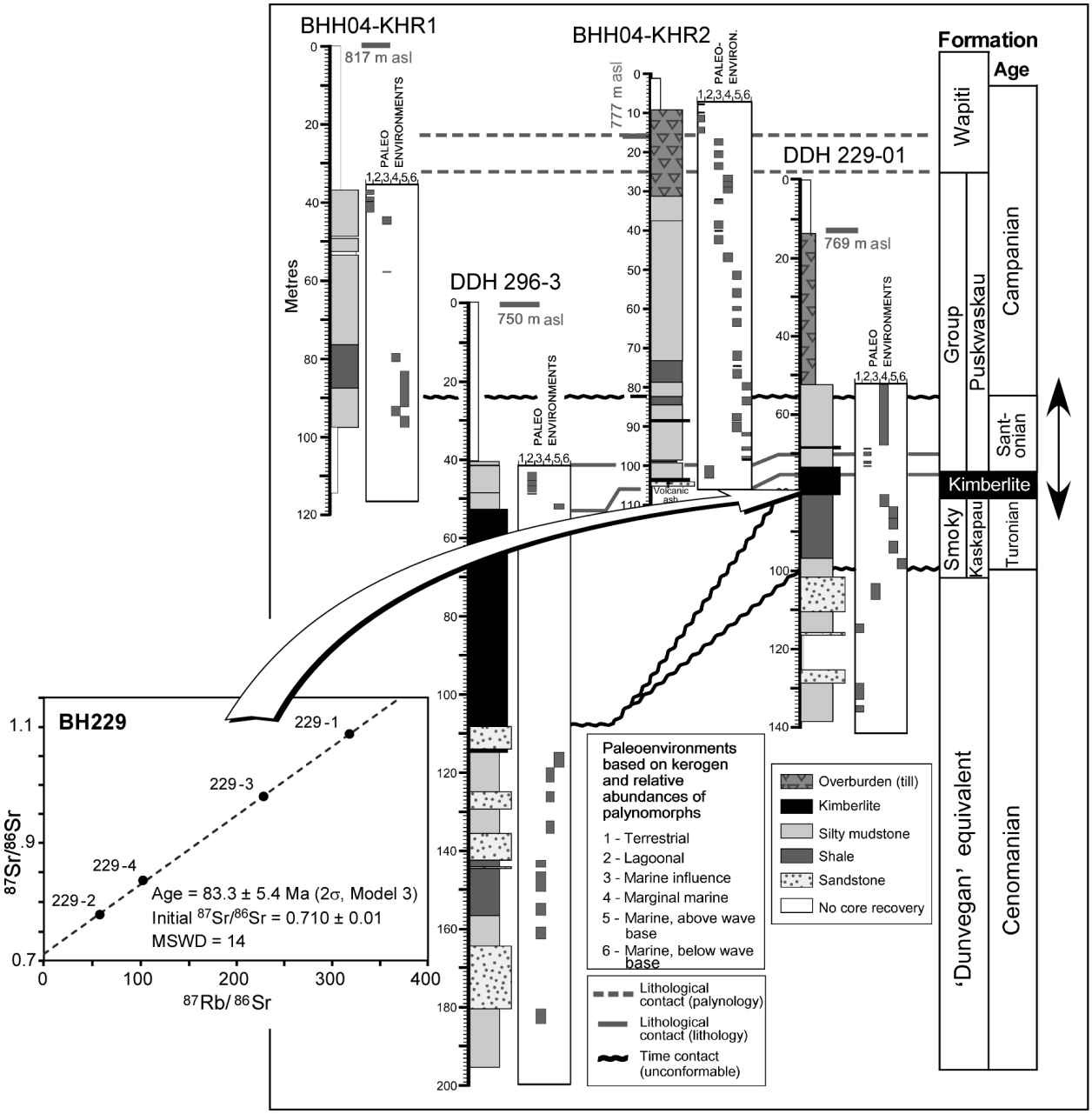

Figure 33. Stratigraphic cross-section with corresponding Rb-Sr phlogopite isochron diagram (from Eccles et al., 2008a), showing the setting of Late Cretaceous Smoky Group–equivalent 'syndepositional' volcanism for the BH229 and K296 kimberlites, Buffalo Head Hills kimberlite field. Two of the four drillholes shown (BHH04-KHR1 and BHH04-KHR2) were drilled by the Geological Survey of Canada and Alberta Geological Survey to study the uppermost Late Cretaceous and Paleocene in the Buffalo Head Hills region. The Smoky Group–equivalent volcanism is associated with an extensive Turonian to Early Campanian hiatus (double black arrow and unconformable time contact). Stratigraphic boundaries and paleoenvironments are based on palynological interpretation (Sweet et al., 2006).

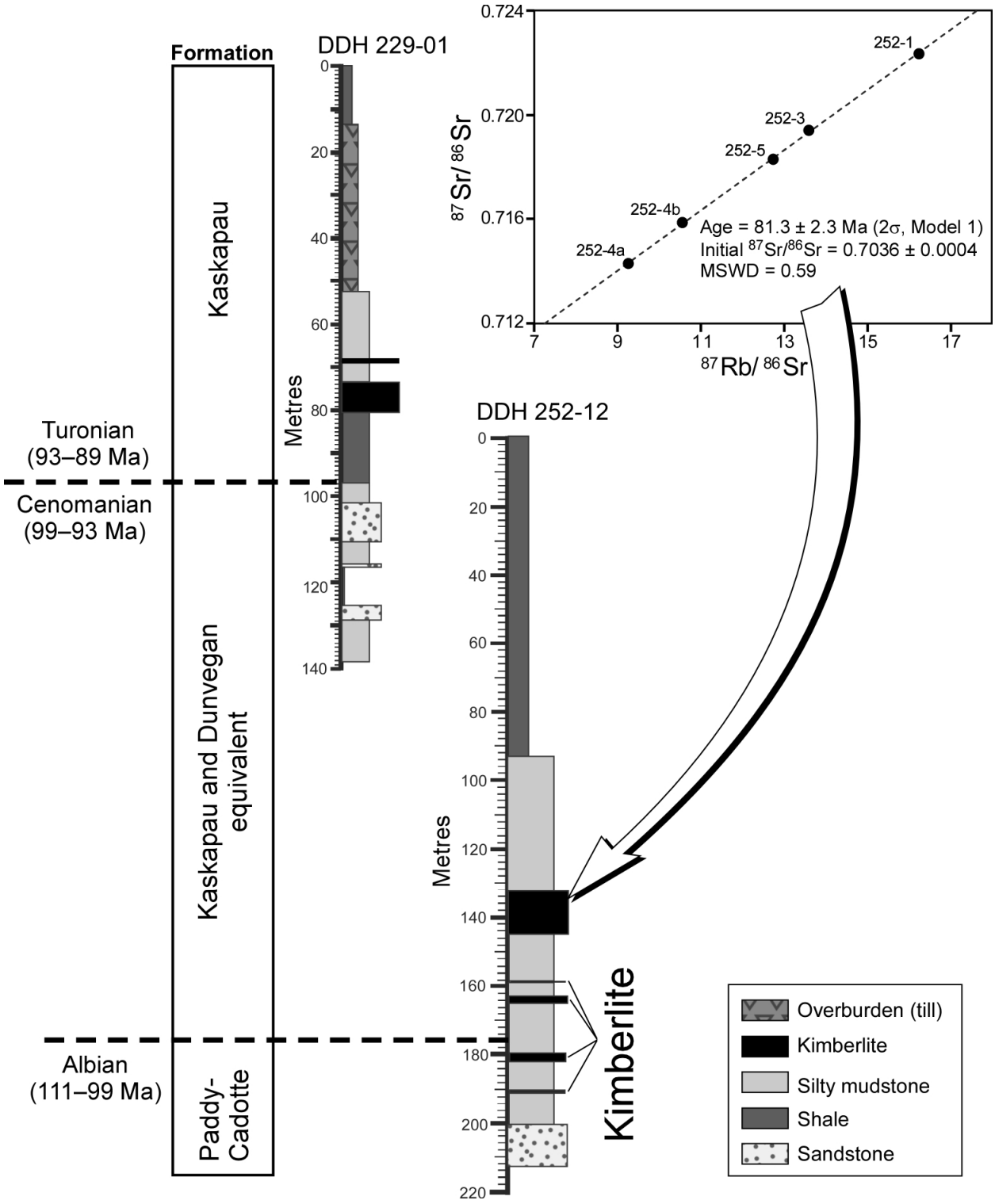

Figure 34. Stratigraphic cross-section with corresponding Rb-Sr phlogopite isochron diagram (from Eccles et al., 2008a), showing the chronological setting of the Late Cretaceous K252 kimberlite, Buffalo Head Hills kimberlite field. The Late Cretaceous Smoky Group–equivalent BH229 kimberlite (also shown in Figure 33) is included to extend the stratigraphic boundary to the Turonian. The Rb-Sr phlogopite, five-point–isochron Campanian age of 81.3 ±2.3 Ma suggests that at least part of the K252 kimberlite is intrusive into significantly older Cenomanian sedimentary rocks.

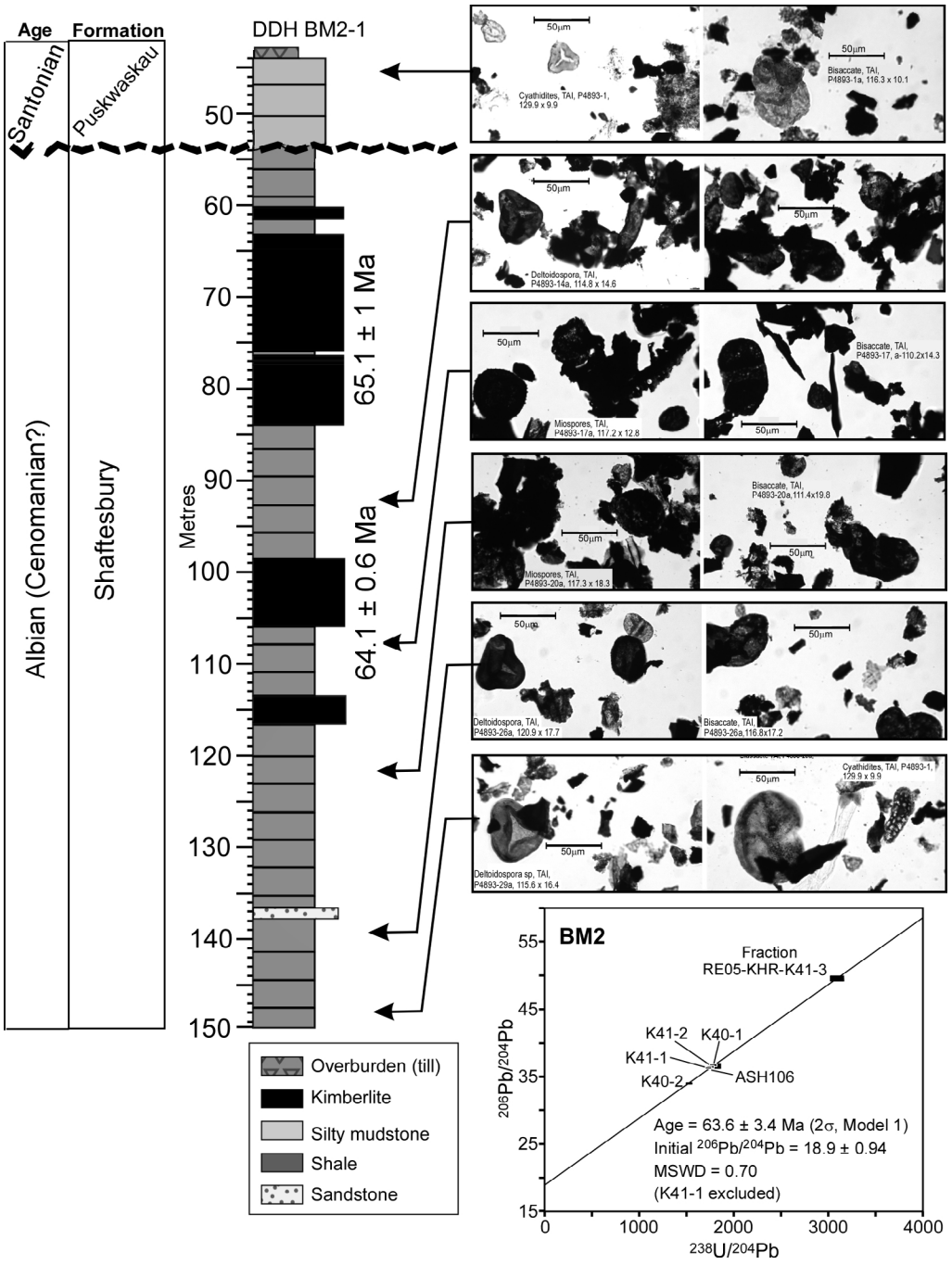

Figure 35. Stratigraphic section with corresponding palynomorphs and U-Pb perovskite isochron diagram (from Eccles et al., 2008a), showing the setting of Paleocene (~64 Ma) intrusive kimberlite BM2, Buffalo Head Hills kimberlite field. Stratigraphic boundary is based on palynological interpretation. U-Pb ages are shown both for the individual dikes and as a five-point isochron using the perovskite analysis fractions from both intrusive layers (the BM2 fraction numbers correspond to those of Eccles et al. (2008a) and are not to be confused with a 'K41' kimberlite, for which none exists). The thermal maturity of the corresponding palynomorphs is expressed by the colour of the palynomorphs as an interpreted thermal alteration index (TAI). The black, high-TAI value equals high thermal maturity. The highest thermal maturity indices occur in the 106–113.5 m interval, proximal to the kimberlite dikes (Sweet et al., 2006), thus forming a cohesive story of intrusive emplacement.

in sedimentary rocks, so the shape and extent of K1 in the near surface resembles a narrow, pipe-shaped intrusive body. Stratigraphic offset of the hiatuses in Figure 36 suggests tectonic movement possibly associated with emplacement.

The potential magnitude of post-eruptive erosional truncation to the present-day surface is based on the thickness of Campanian to Paleocene strata near the Judy Creek coalfield, 300 km south-southwest. Here, the composite thickness of Late Campanian to Paskapoo strata is about 450 m (Baofang and Dawson, 1988; Jerzykiewicz, 1997). This is probably a maximum thickness, given the positions of the Judy Creek coalfield (closer) and Buffalo Head Hills (farther) relative to the orogen.

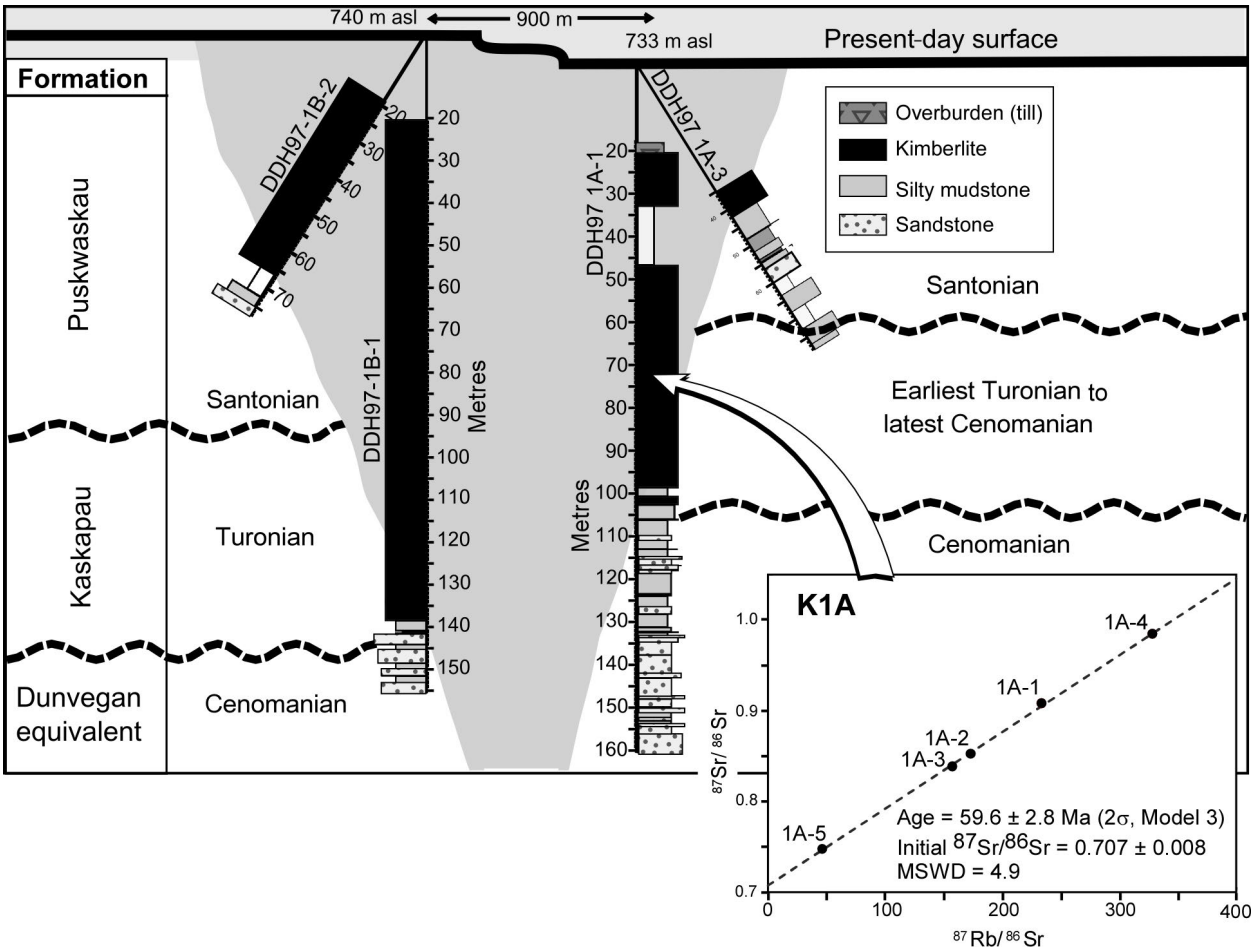

Figure 36. Stratigraphic cross-section with corresponding Rb-Sr phlogopite isochron diagram (from Eccles et al., 2008a), showing the setting of eroded Paleocene volcanism, K1 kimberlite, Buffalo Head Hills kimberlite field. Stratigraphic boundaries are based on palynological interpretation. The ultramafic body has been eroded to the present-day surface (ca. 78 Ma). The shaded polygon represents the proposed outline of the ultramafic body. Heavy dashed lines indicate the two possible hiatuses determined by palynological investigation (Sweet et al., 2006).

4 Birch Mountains

4.1 Discovery and Exploration History

The Legend property, hereafter referred to as the Birch Mountains kimberlite field, is in the Birch Mountains of northeastern Alberta, approximately 430 km north of Edmonton and 135 km northwest of Fort McMurray (Figure 1). The property was acquired in 1997 by a joint venture between Montello Resources Ltd. and Redwood Resources Ltd. From March to June 1998, a 42 770 line-km fixed-wing aeromagnetic survey was flown and the results were processed to identify possible kimberlite target anomalies.

In August 1998, Kennecott Canada Exploration Inc. became the operator, with Montello and Redwood remaining as joint-venture participants. Based on the aeromagnetic survey, 35 targets were selected. Between late 1998 and early 1999, ground and helicopter geophysical surveys were completed on 27 of the 35 targets, 14 of which were tested with 19 drillholes totalling 2713 m.

Between September and November 1998, 11 holes were drilled on 8 targets, intersecting 7 intrusive bodies: Phoenix, Roc, Dragon, Valkyrie, Pegasus, Xena and Legend (Figure 37). All of the ultramafic occurrences discovered to date in the Birch Mountains have positive magnetic responses except for the Dragon body, which has a negative response. The intrusions were encountered at depths of between 12 m (Legend) and 136 m (Dragon) beneath overburden and Late Cretaceous bedrock. Kennecott postulated that one other target, Gryphon, may be a kimberlite due to the circular nature and negative profile of the magnetic response and anomalous indicator minerals from material sampled at the bottom of the drillhole at 147.4 m. Aravanis (1999) suggested that, in addition to the discovered intrusions, the Legend property contains at least another six intrusions, as defined by magnetic data. These targets include Shedu, Lammasu, Kendu, Dutchman, Hippogriff and Gemini. In 2000, due to the reported poor diamond content, Kennecott, Montello and Redwood allowed the exploration permits to lapse.

New Blue Ribbon Resources Ltd., in a joint venture with Montello Resources Ltd., re-staked the property and, in 2000, drilled one of the geophysical targets previously identified by Kennecott. As a result, New Blue Ribbon discovered an eighth body in the Birch Mountains field, Kendu, which was intersected at a depth of 91.4 m beneath overburden. Despite an abundance of xenolith and xenocryst material, caustic fusion on a split of the Kendu core did not return diamond.

During January and February 2007, Grizzly Discoveries Inc. collected a 10.2 tonne mini–bulk sample from the Legend kimberlite via 13 drillholes. The sample was processed at the DeBeers Canada dense media separation (DMS) facility in Grande Prairie, Alberta. One macrodiamond was recovered from an amalgamated sample from Legend 001, 002 and 003 that formed a DMS concentrate weighing 64.45 kg. This diamond was described as a colourless, included, twinned octahedron measuring 2.1 mm by 1.58 mm by 1.46 mm. A second amalgamated sample from Legend 004, 005 and 006 yielded three microdiamonds from 168.35 kg of drillcore.

4.2 Geological Setting

The basement rocks underlying the Birch Mountains kimberlite field belong to the southern subsurface extension of the Early Proterozoic Taltson-Thelon orogenic belt, which is known as the Taltson magmatic arc in northeastern Alberta. The Taltson magmatic zone is defined by a 150–200 km wide, north-trending belt of positive aeromagnetic anomalies contained within broader aeromagnetic lows similar to those identified on mapped portions of the exposed shield. The Taltson magmatic zone is dominated by 1.99–1.93 Ga granitoid rocks, which can be separated into two distinct age groups. The ‘early’ magmatic suite comprises 1.99–1.96 Ga, metaluminous to moderately peraluminous granitoids (Deskenatlata, Colin Lake and Wylie Lake granitoids; Bostock et al., 1987; McDonough et al., 1995). The

'late' magmatic suite comprises 1.95–1.93 Ga, moderate to strongly peraluminous granitoids (Slave, Konth and Arch Lake granitoids; Bostock et al., 1987, 1991; McNicoll et al., 1994). These granitoids intrude complex, lithologically diverse metaplutonic rocks and paragneisses that range from 2.4 to 2.1 Ga (Bostock et al., 1991; McNicoll et al., 2000).

The plate-margin accretionary model (e.g., Hoffman, 1988, 1989; Ross et al., 1991; Thériault and Ross, 1991; Ross and Eaton, 2002) assumes that the northern Alberta part of the Canadian Shield comprises a series of distinct continental slivers, formed between 2.32 and 1.99 Ga, that were accreted to the margin of the Archean Rae hinterland at ca. 2.0–1.9 Ga. In the case of the Taltson magmatic zone, this hypothesis proposes that an early 1.99–1.96 Ga granitoid suite was formed by subduction of oceanic crust beneath a continental margin. The Taltson magmatic zone was then deformed by direct collision between formerly separate crustal blocks, which also generated the late, 1.95–1.93 Ga, largely anatectic plutons.

An alternative hypothesis, the plate-interior model (Bostock and van Breemen, 1994; Burwash et al., 2000; Chacko et al., 2000; De et al., 2000; Ranger, 2004), acknowledges similarities in both

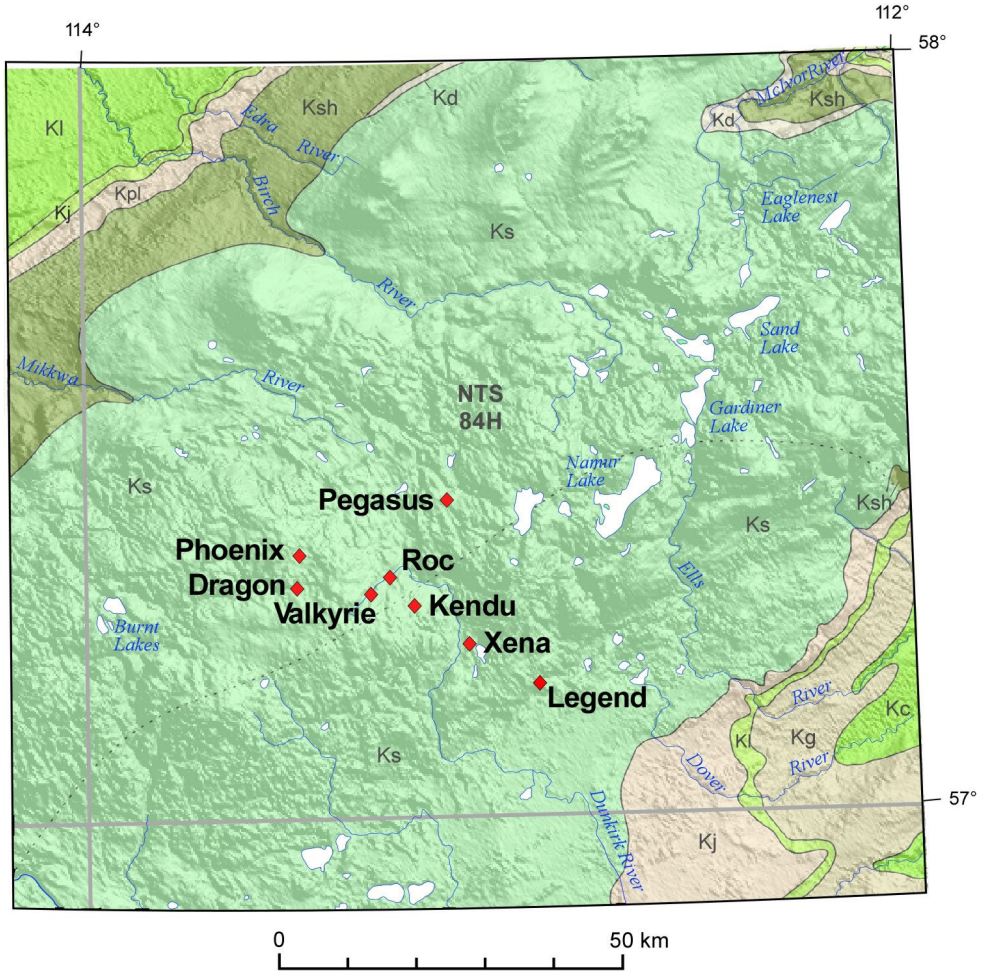

Figure 37. Location of the kimberlite and related rock occurrences in the Birch Mountains field of north-central Alberta, superimposed on the bedrock geology and hill-shaded digital elevation model of Hamilton et al. (1999). Late Cretaceous bedrock abbreviations: Kc, Clearwater Formation; Kl, Loon River Formation; Kg, Grand Rapids Formation; Kj, Joli Fou Formation; Kpl, Pelican Formation; Ksh, Shaftesbury Formation (shale and silty shale); Kd, Dunvegan Formation (sandstone); and Ks, Smoky Group (shale and silty shale).

the pre- and post-2.0 Ga history of the Buffalo Head Terrane and Taltson magmatic zone, and the general lack of a mantle component associated with Phanerozoic subduction-related granitoid rocks. This hypothesis implies that a single block of largely coherent crust, composed of the Buffalo Head Terrane, the Taltson magmatic zone and likely the western Rae Province, has existed since at least 2.3 Ga. Thus, the actual plate boundary of western Laurentia at ca. 2.0 Ga is farther to the west, such that the Taltson magmatic zone granitoid rocks in northeastern Alberta have an intracrustal origin. Lastly, Card and Ashton (2010) proposed that the Taltson magmatic zone is not an extension of the Thelon magmatic arc in the Northwest Territories but a separate entity, and that the orogeny included an element of northeast-directed accretion along the southern margin of the Rae Province.

Near the Birch Mountains kimberlite field, basement rocks are overlain by approximately 200–600 m of lithologically diverse Devonian carbonate, evaporite and clastic sedimentary sequences that are unconformably overlain by Cretaceous, marine to deltaic, clastic sedimentary rocks (Mossop and Shetsen, 1994). The uppermost bedrock is composed predominantly of dark grey marine shale and silty shale of the middle to Late Cretaceous LaBiche Formation and Late Cretaceous Smoky Group (Hamilton et al., 1999). Exposures of the Late Cretaceous Smoky Group are limited to topographic highs and stream cuts, with most of the upper portions of the Smoky Group having been eroded. The Smoky Group's lowermost marine shale unit, the Kaskapau Formation, is most prominent. The Kaskapau includes the Second White Speckled Shale Formation marker unit, which is unconformably overlain by the light grey marine shale of the Late Cretaceous Lea Park Formation (Dufresne et al., 2001). This time gap is estimated to be 4–8 million years, and may be coincident with kimberlite emplacement in the Birch Mountains.

Quaternary sediment thickness in the area varies from 45 m to more than 150 m (Pawlowicz and Fenton, 1995). Kennecott drill logs from 1998 showed drift thicknesses of between 12 and 122 m, with five of the seven intrusive bodies having between 85 and 97 m of overburden (Aravanis, 1999).

Structurally, the Birch Mountains kimberlite field lies along the projected axis of the Devonian Peace River Arch and near the eastern (erosional) edge of the Grosmont reef complex. A major, north-trending structural feature, known as the 'Rimbey-Leduc-Meadowbrook reef chain,' extends through the Birch Mountains kimberlite field (Figure 1). The linear position and length (018° for approximately 180 km) of this reef trend suggests both structural and inherited topographic controls (Sikabonyi and Rodgers, 1959; Keith, 1970; Switzer et al., 1994). In addition, several potential lineaments occur in the area, such as Devonian lineaments inferred from facies changes within the Woodbend basin, and Cretaceous topographic lineaments inferred from isopachs of the Viking and Mannville strata (Pană et al., 2001).

4.3 Palynology and Geochronology

A detailed palynological study has not been completed on the cores from the Birch Mountains kimberlite field, but nine shale samples from the Roc, Dragon, Pegasus and Legend intrusions were selected for palynological analysis. Four of the samples contained abundant palynomorph assemblages that yielded Late Cretaceous ages ranging from Late Albian to Maastrichtian (ca. 100–70 Ma; G. Dolby *in* Aravanis, 1999). Depositional environments vary from open marine to nearshore marine.

Age determinations by the Rb-Sr phlogopite and U-Pb perovskite isotopic methods were carried out on five of the eight known ultramafic bodies in the Birch Mountains (Phoenix, Dragon, Xena, Legend and Valkyrie; Aravanis 1999; Eccles 2004; Appendix 1). Recommended results yield a tight assemblage of emplacement ages between 77.6 ±0.8 and 70.3 ±1.6 Ma (Figure 38).

A robust, five-fraction, weighted-average $^{206}Pb/^{238}U$ date of 77.6 ±1.1 Ma (Eccles, 2004) for the Phoenix body is significantly older than the previously reported three-point isochron ages of 70.3 ±1.6 and 70.9 ±0.4 Ma by U-Pb perovskite

and Rb-Sr phlogopite, respectively (Aravanis, 1999). This could be the result of separate eruption events, although the sample that provided the ~78 Ma result was collected from the same drillcore, same lithology and on either side of the sample that yielded the ~71 Ma age. Further examination and analyses are therefore needed to resolve the disparity in these age determinations.

A reliable geochronological age for emplacement of the Kendu body has proven difficult to obtain. Isotopic U-Pb (rutile) and Rb-Sr (phlogopite) results are roughly constrained between 79.4 ±1.6 and 64.3 ±0.1 Ma. An estimate for the emplacement age of the Kendu body is from the light brown-orange rutile fraction that yielded a $^{206}Pb/^{238}U$ date of 79.4 ±1.6 Ma. Two-point whole-rock and phlogopite Rb-Sr isochrons from Kendu also yielded ages of 64.3 ±0.1 and 72.7 ±0.1 Ma, respectively. The ~79 Ma U-Pb age is not recommended as a robust emplacement age and should only be considered as an upper limit on the emplacement age. Other Kendu rutile fractions yielded older U-Pb isotope ages (up to 93.0 ±0.3 Ma), suggesting an older rutile component. Xenoliths from the Kendu body include garnet pyroxenite, mafic granulite and granulite (Eccles et al., 2010), so it is likely that the rutile fractions analyzed have multiple origins and may include both mantle and lower-crustal components.

4.4 Inferred Morphology

The approximate dimensions of the Birch Mountains bodies, as inferred from ground total-field magnetic anomalies, are between 200 by 200 m (4 ha) and 1400 by 150 m (21 ha; Aravanis, 1999). Keeping in mind that no drillholes have penetrated deeper than 250 m, the Birch Mountains bodies have complex emplacement settings and morphologies similar to those of the Buffalo Head Hills field. Of the eight Birch Mountains intrusions, drillhole log descriptions cite three intrusions (Dragon, Pegasus and Xena) with interlayered ultramafic material and mudstone, two intrusions (Pegasus and Roc) that bottom out in mudstone, and three intrusions

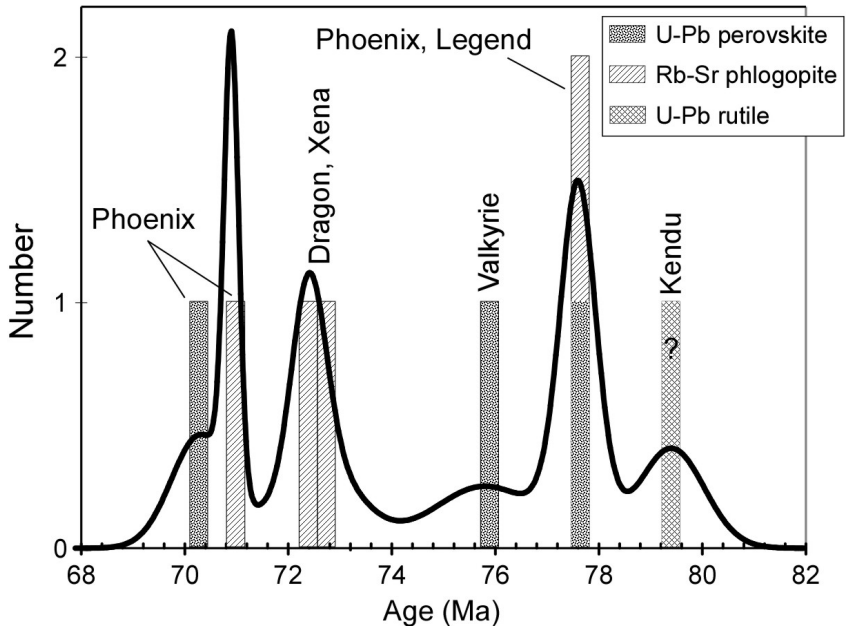

Figure 38. Cumulative probability diagram of Rb-Sr phlogopite isochron ages (diagonal pattern) and U-Pb perovskite model ages (stipple) for selected Birch Mountains intrusions (Aravanis, 1999; Eccles, 2004). Included is a U-Pb rutile (crosshatch) estimate for the Kendu intrusion, which should only be considered a maximum emplacement age and not a robust age of emplacement for this body.

(Legend, Phoenix and Kendu) with continuous intersections of intrusive material.

The majority of the exploration activity has been completed on the Legend intrusion, which was drill tested with a total of 14 holes (Aravanis, 1999; Dufresne et al., 2007). Three distinct phases of kimberlite were intersected at depths of approximately 12–206 m, including a massive section of dark grey, competent pyroclastic kimberlite, light grey tuff, and/or resedimented volcaniclastic kimberlite and grey-green, lapilli-dominated pyroclastic kimberlite. Figure 39 is a schematic representation of the Legend body. Legend's morphology appears similar to that of the classic pipe model often associated with kimberlites. Accretionary lapilli-rich kimberlite dominates the central portion of the body, with the dark grey pyroclastic kimberlite forming the main intrusion and giving way to dark grey, resedimented, pyroclastic kimberlite to kimberlitic mudstone at the edges of the body.

4.5 Volcanogenic Observations

Aravanis (1999), Eccles (2004) and Dufresne et al. (2007) completed macroscopic and microscopic observations on cores from the Birch Mountains kimberlite field. Crater-facies pyroclastic kimberlite and resedimented volcaniclastic kimberlite characterize the Birch Mountains intrusions. The volcanic rocks are characterized by massive layers and bedded and graded layers comprising alternating coarse lapilli (2–64 mm) and laminae of finer ash-tuff (<2 mm; Aravanis, 1999). Macroscopically, the Birch Mountains rocks are generally inequigranular and competent, containing juvenile lapilli and olivine macrocrysts set in a fine-grained, grey-green matrix.

The cores contain clasts of country rock but are generally devoid of basement and upper-mantle material. The country-rock fragments are typically black angular clasts of shale, green subangular to rounded clasts of argillite, and rare carbonate.

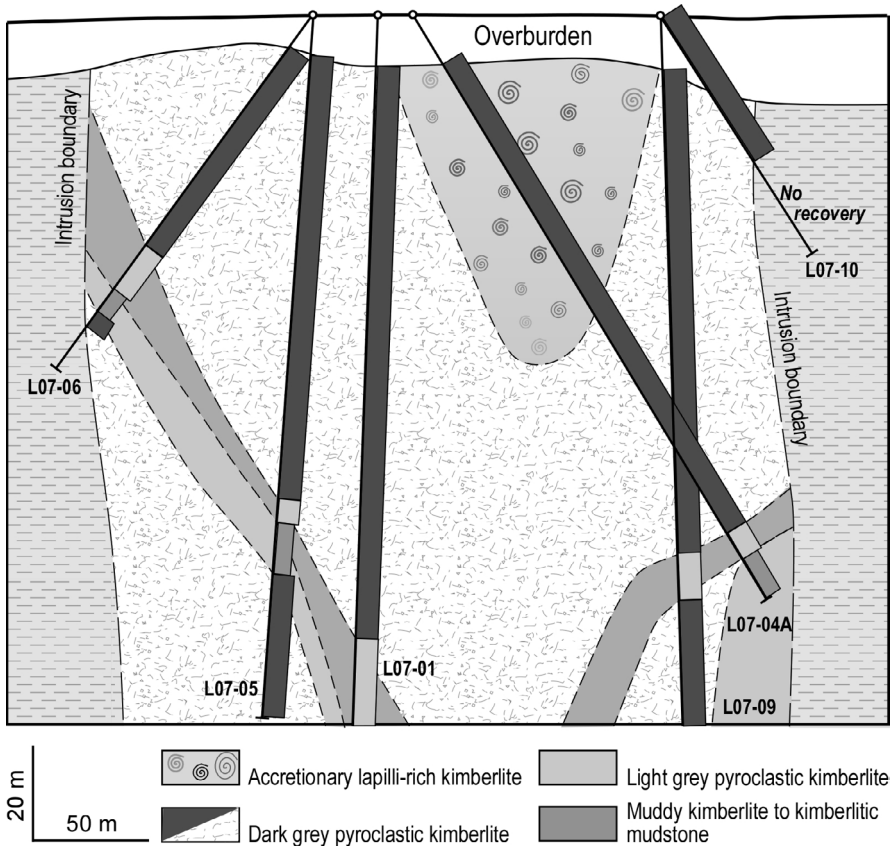

Figure 39. Schematic lithological cross-section of the Legend body, based on **drillhole information from Dufresne and Banas (2009).**

Macroscopic examination of the drillcore from the seven intrusions discovered in 1998 and 1999 revealed few to no mantle xenoliths or xenocrysts in these samples. In contrast, the Kendu intrusion, which was the last body discovered in this field (in 2000), is characterized by an abundance of mantle and/or lower-crustal xenolithic and xenocrystic material.

Petrographically, these rocks contain variable amounts of lapilli and exhibit a macrocrystic-porphyritic texture. Coarse-grained olivine and other silicate/aluminosilicate minerals reside in a brownish-coloured, indeterminate matrix of serpentine, calcite, clay minerals and oxide minerals (Figure 40). Olivine is fresh to variably altered, but commonly is totally pseudomorphed by calcite, dolomite and magnesite. Opaque minerals include corroded and atoll-textured spinel, anhedral to subhedral perovskite, and disseminated macrocrystalline and microcrystalline ilmenite. Macrocrystalline phlogopite is colourless to bronze and, in most instances, highly altered. Accessory minerals include anhedral pyrite, Ni-(Fe)–sulphide and apatite.

Several physical features suggest that the Birch Mountains bodies are derived from relatively evolved magmas. The rocks have a serpentine- and carbonate-rich (including magnesite) matrix. They are relatively devoid of olivine macrocrysts, and they have higher concentrations of coarse-grained opaque minerals (ilmenite, spinel and perovskite), phlogopite, apatite and sulphide compared to primitive kimberlite from the Buffalo Head Hills (e.g., Figure 41).

Lapilli are diverse in shape, texture and mineralogy. They generally have rounded to elliptical shapes with curvilinear margins, range from about 0.5 to 3 mm in diameter and have variable proportions of relict olivine, spinel, perovskite and phlogopite. They are composed primarily of pseudomorphed, subhedral to anhedral microphenocrystalline olivine with less common macrocrystalline olivine, spinel and perovskite set in a grey-green matrix. Some lapilli are rimmed by spinel and/or perovskite necklaces. The diversity of the juvenile lapilli implies derivation from several distinct pyroclastic units.

The Kendu and Xena bodies are petrographically dissimilar from the other bodies in the Birch Mountains field. In contrast to the other bodies, Kendu's crystals and matrix are almost completely altered to serpentine and contain an abundant assemblage of garnet pyroxenite and granulite xenoliths (Eccles et al., 2010). Kendu uniquely comprises 'pelletal-textured' lapilli with haloes of tangentially aligned, fine-grained (<0.01 mm long) phlogopite-rich and vermiform-serpentine–rich (lizardite) microlitic material that surrounds olivine pseudomorphs and other pre-existing constituents (Figure 42).

Xena is strongly altered and entirely lacking in juvenile lapilli. The matrix contains, in addition to serpentinized olivine, anhedral spinel and clay minerals, and atypical kimberlite fragments including quartz, feldspar and biotite. Lastly, Aravanis (1999) observed that juvenile material from Xena atypically resembles a strongly altered welded ash.

4.6 Whole-Rock Geochemistry

Six of the Birch Mountains bodies have whole-rock chemistry similar to that of kimberlite. These include the Dragon, Legend, Pegasus, Phoenix, Roc and Valkyrie intrusives, hereafter referred to collectively as the Birch Mountains kimberlites. The Birch Mountains kimberlite samples generally have CI values of >0.8 and <1.5 (average 1.2, n = 32; Figure 43). They have Group IB (off-craton) South African kimberlite signatures characterized by high average MgO (24 wt. %, n = 32) and TiO_2 (3.1 wt. %), with low average SiO_2 (26 wt. %), Al_2O_3 (3.5 wt. %) and K_2O (0.6 wt. %; Figure 44).

With respect to high-field-strength incompatible elements, the Birch Mountains kimberlites have moderately enriched Nb (215–509 ppm), Zr (112–324 ppm), Hf (3.1–9.1 ppm), Y (12–22 ppm) and Ni (468–670 ppm). The chondrite-normalized REE patterns for the Birch Mountain kimberlite samples coincide with, or are slightly more abundant than, the REE pattern for average

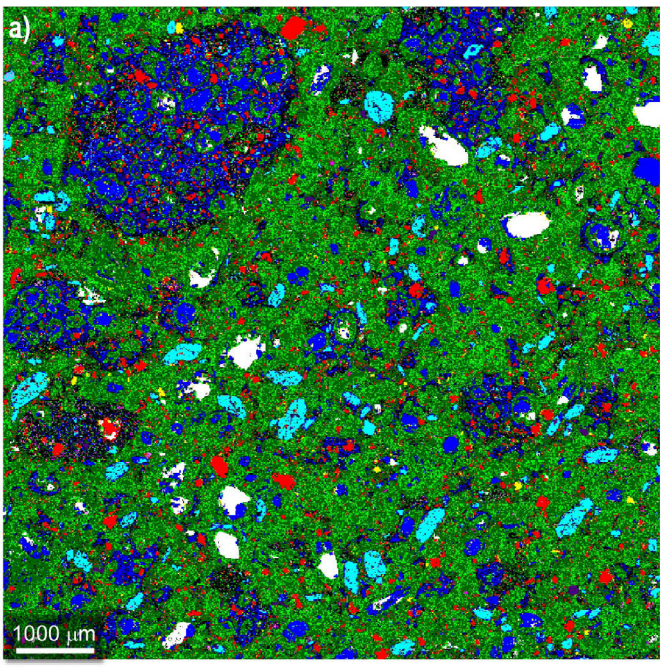

Mineral Name	Vol. %
Serpentine	48.0
Ca-Mg-(Fe)-silicate	15.0
Olivine	14.7
Dolomite	10.9
Ti-minerals	5.9
Calcite	3.7
Pyrite	0.8
Other	0.5
Apatite	0.3
Phlogopite	0.2
Ni(Fe)-sulphide	0.1
Cr-spinel	0.1
Background	0.1

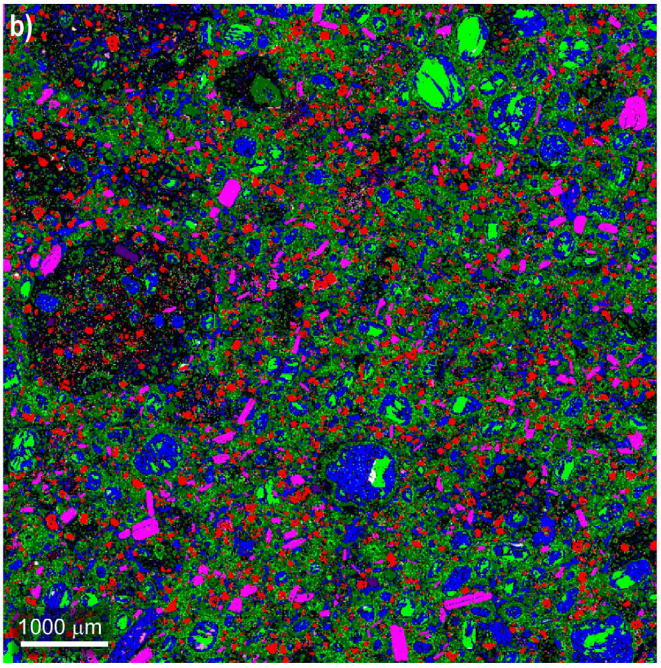

Mineral Name	Vol. %
Serpentine	32.7
Ca-Mg-(Fe)-silicate	27.9
Dolomite	14.7
Olivine	10.2
Ti-minerals	8.8
Phlogopite	3.7
Others	1.1
Apatite	0.4
Cr-spinel	0.2
Calcite	0.2
Pyrite	0.1
Ni-(Fe)-sulphide	0.1
Background	0.1

Figure 40. Mineralogical determinations of the Legend (drillhole 98DH-LE-01 at 44 m) and Phoenix (drillhole 98DH-PH-01 at 130 m) bodies, Birch Mountains field, using QEMSCAN® analysis at 10 µm resolution: a) Legend is a highly altered kimberlite sample in which primary olivine crystals, lapilli and the matrix are almost completely replaced by dolomite, calcite, serpentine and a Ca-Mg-(Fe)–silicate; ilmenite is the main Ti-bearing mineral in this sample; b) Phoenix contains subhedral olivine crystals that are completely pseudomorphed by dolomite, with abundant phlogopite, set in a matrix that is completely serpentinized; round kimberlitic lapilli are present and contain a variety of minerals, including altered olivine, phlogopite, perovskite, apatite and possibly ulvöspinel; this sample has a high percentage of Ti-bearing minerals, including perovskite, ilmenite, ulvöspinel(?), titanomagnetite and others too fine grained to identify.

kimberlite (Figure 45). Generally, the majority of the Birch Mountains kimberlite samples are LREE enriched (up to 1340 times chondrite abundance for La), with La/Yb ratios of 114–294. Not all of the bodies in the Birch Mountains kimberlite group were analyzed isotopically, but the Legend and Phoenix $^{87}Sr/^{86}Sr$ ratios have radiogenic values that are generally atypical of isotopic compositions for Group I kimberlite (Figure 46). However, these radiogenic values are comparable in isotopic Sr-Nd space to the diamondiferous kimberlites of the Slave Province, Northwest Territories.

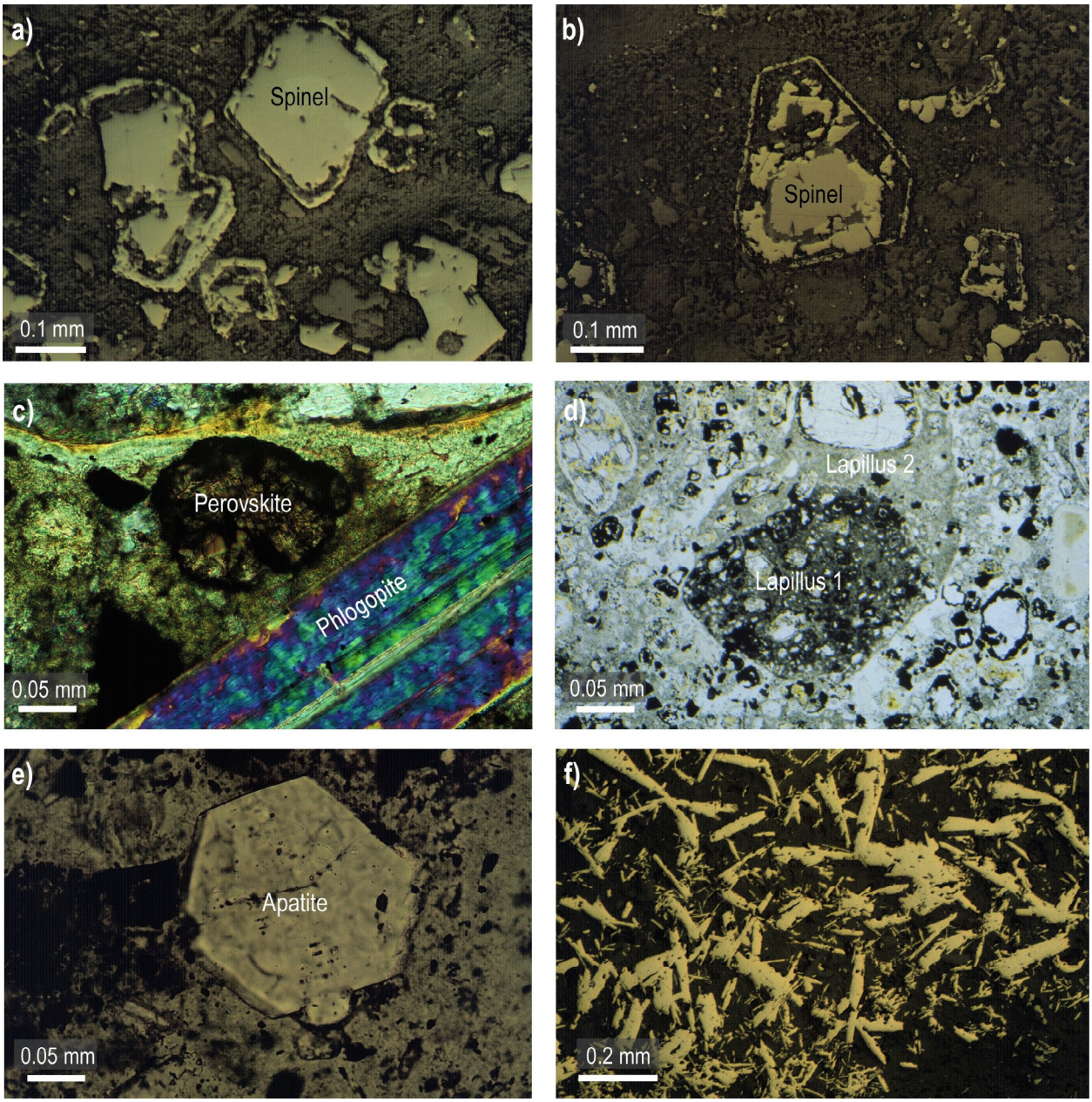

Figure 41. Photomicrographs of selected minerals and lapilli from the Legend (drillhole 98DH-LE-01 at 44 m) and Phoenix (drillhole 98DH-PH-01 at 130 m) intrusions, Birch Mountains field: a) and b) corroded and atoll-textured spinel (Phoenix, plane polars); c) matrix perovskite and phlogopite (Phoenix, crossed polars); d) multilayered or multigeneration lapilli showing one type of lapillus amalgamating with another (Phoenix, plane polars); e) hexagonal apatite (Legend, plane polars); and f) needle-textured sulphide (Legend, crossed polars).

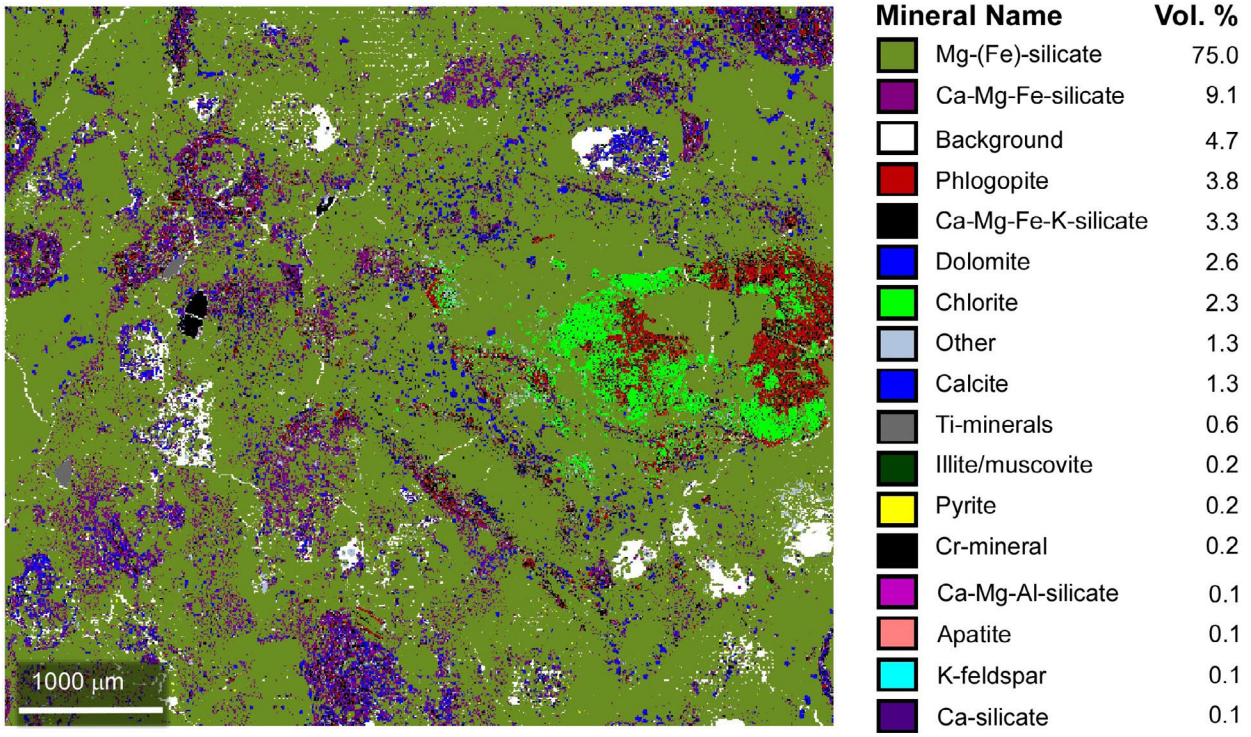

Figure 42. QEMSCAN® **mineralogical determination of the Kendu body, Birch Mountains field. Kendu is almost completely altered to a Mg-(Fe)–silicate (serpentine?), which destroyed the original mineral textures. The main carbonate minerals include dolomite and calcite. Chlorite is more abundant in Kendu than in any other Birch Mountains body. In many instances, fine-grained phlogopite crystals tangentially surround serpentine-altered primary minerals.**

In contrast to the Birch Mountains kimberlites, whole-rock compositions of Xena and Kendu correlate well with petrographic observations that these bodies are atypical of kimberlite. Xena has a significantly higher CI of between 2.4 and 3.4, compared to the Birch Mountains kimberlites (Figure 43). In addition, in contrast to the Birch Mountains kimberlites, Xena has significantly higher SiO_2 (49 wt. %) and Al_2O_3 (9.3 wt. %), and higher K_2O (2.5 wt. %; Figure 44). The Xena and Kendu bodies have atypical chondrite-normalized REE profiles compared to the Birch Mountains kimberlite group (Figure 45). In general, they have a lower overall abundance of REE, lower LREE and higher HREE (the last is particularly evident for Xena). The Xena body has La/Yb ratios of 31–53 and displays a flattening HREE signature. Kendu also has a lower LREE (220 to 275 times chondrite abundance for La) and a profile that is similar to that of Xena but with a noticeably steeper, negatively sloping HREE (La/Yb of 88–97). Kendu has more radiogenic

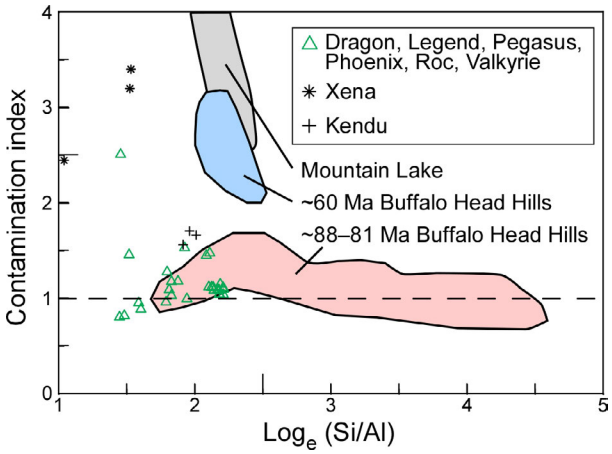

Figure 43. Plot of the contamination index ([SiO_2 + Al_2O_3 + Na_2O] / [MgO + 2K_2O]) of Clement (1982) versus $\log_e$(Si/Al) for whole-rock samples from the Birch Mountains kimberlite field. Compositions of the Mountain Lake and the ~88–81 Ma and ~60 Ma Buffalo Head Hills bodies from this study are included for comparison.

$^{87}Sr/^{86}Sr$ (0.70778–0.70879) and lower ε_{Nd} (–4.0 to –6.3) than bulk Earth composition and plots within the enriched, bottom right quadrant of the Nd-Sr diagram (Figure 46). High initial $^{87}Sr/^{86}Sr$ in Kendu is similar to that of Roman Province volcanism.

4.7 Mantle Characteristics

The Birch Mountains kimberlite group (Dragon, Legend, Pegasus, Phoenix, Roc and possibly Valkyrie) contain abundant olivine, ilmenite and chromite, with lesser peridotitic garnet and clinopyroxene, and rare orthopyroxene and low-Cr garnet (Aravanis, 1999). The Kendu intrusion contains lherzolitic garnet, low-Cr garnet, high-Mg picroilmenite, Cr-rich clinopyroxene and spinel.

Garnet xenocrysts are more or less restricted to Kendu, Legend and Xena (Figure 47). Kendu garnet includes lherzolitic (G9, 84%, total n = 189), followed by wehrlitic (G12, 8%), pyroxenitic, websteritic and eclogitic (G4, 6%), and high-TiO_2 peridotitic (G11, 2%) types. Legend garnet includes low-Cr megacrysts (G1, 55%, total n = 486), high-TiO_2 peridotitic (G11, 31%) and lherzolitic (G9, 14%) types. Xena garnet includes high TiO_2 peridotitic (G11, 67%, total n = 12) and lherzolitic (G9, 33%) garnet. As such, the Birch Mountains garnet has high Ca, as indicated by the

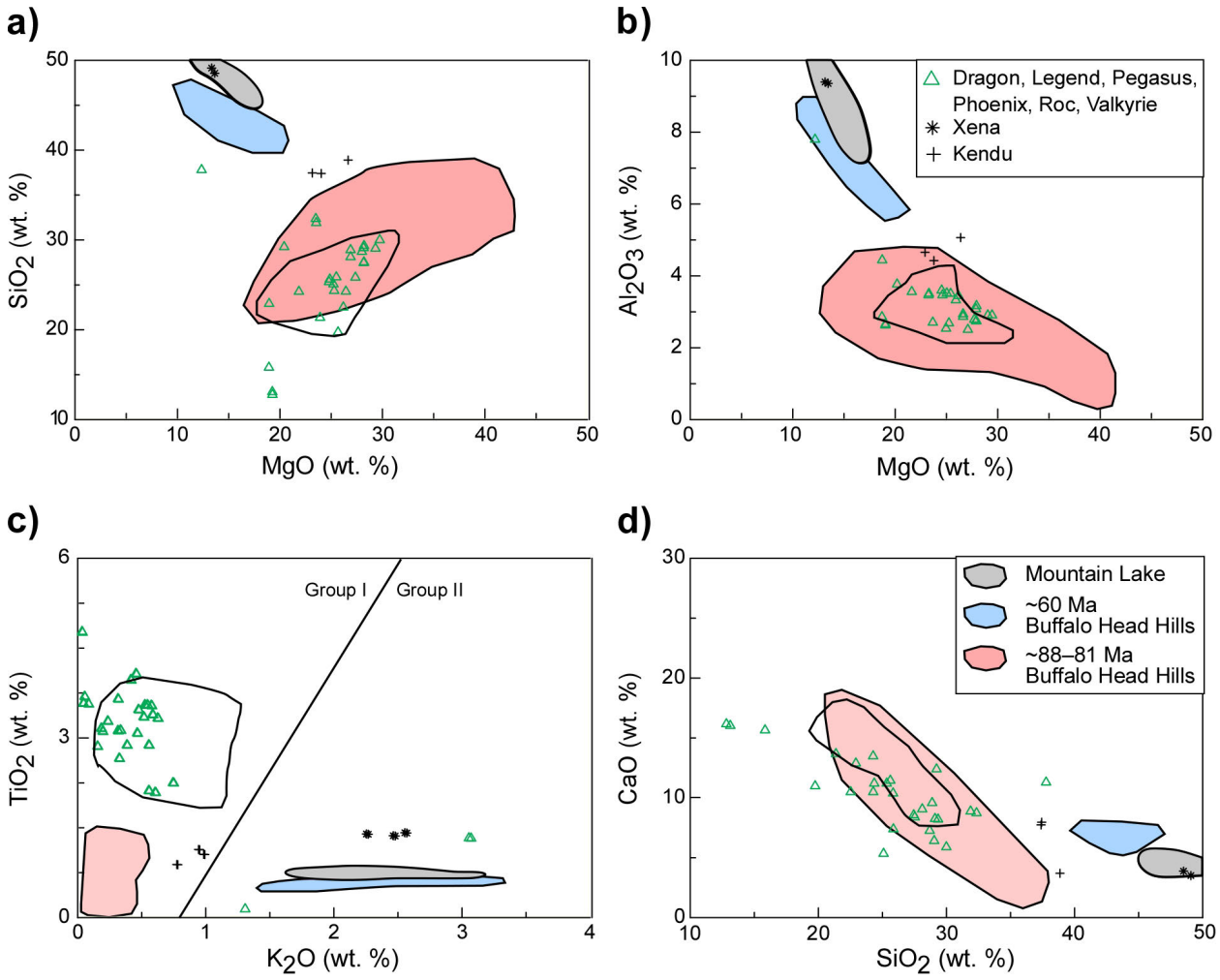

Figure 44. Plots of SiO_2 versus MgO (a), Al_2O_3 versus MgO (b), TiO_2 versus K_2O (c) and CaO versus SiO_2 (d) for whole-rock samples from the Birch Mountains kimberlite field. Compositions of Group IB (off-craton) South African kimberlites (solid polygon) from Smith et al. (1985) and Becker and le Roex (2006), and Mountain Lake and Buffalo Head Hills bodies from this study are included for comparison.

Cr_2O_3-CaO diagram and Ca-intercept distributions (Figure 47a, b). The Ca-intercept of Legend is bimodal, with a high-frequency node at 4.6 and a lesser frequency node at 5.9. Kendu has a high-frequency Ca-intercept node of 4.6–4.9, with a generally high Ca-intercept trending toward wehrlite paragenesis.

Kendu lherzolitic garnet is restricted to low T_{Mn} and low T_{Ni} (between 830° and 1000°C), and includes wehrlitic and melt metasomatized wehrlitic garnet (Figures 47c and 48). The low-T (T_{Ni} of 830°–942°C) wehrlitic garnet generally follows the chromite-clinopyroxene-garnet equilibrium (CCGE) trend of Kopylova et al. (2000) in CaO-Cr_2O_3 space. It has low chondrite-normalized REE, a highly sinusoidal pattern (median Nd_N/Y_N ratio of 2.4), low Y (0.7–13.2 ppm) and Zr (2.9–10.4 ppm), and depleted Ti (median of 129 ppm; Figure 48a, b). Kendu also contains melt metasomatized wehrlite that is characterized by moderate temperature (T_{Ni} of 961°–1000°C), high median values of Y (31 ppm) and Zr (111 ppm), a high overall abundance of REE and a unique chondrite-normalized REE signature with distinctly enriched La_N-Ce_N.

High-Ti (>1120°C) melt metasomatized lherzolitic garnet dominates the Legend and Xena bodies (Figures 47d, e and 48). Their chondrite-normalized REE plot has a moderately sinusoidal pattern (Nd/Y_N of 0.5) characterized by a sharp, positive-trending slope between La and Sm, flattening of the MREE and slightly positive HREE (Figure 48). Melt metasomatized lherzolitic garnet from Legend and Xena can contain high Cr_2O_3 (up to 13.7 wt. % in Xena), Ti (up to 6579 ppm in Legend) and Zr (up to 142 ppm in Legend).

Megacrystic garnet (G1, 80%, total n = 30) dominates Legend's low-Cr garnet population, followed by minor populations of pyroxenitic, websteritic and eclogitic (G4), and eclogitic (G3) types (Figure 49). Eclogitic (G3) garnet is most dominant in the Kendu body, as it accounts for 91% of the total garnet (total n = 33), followed by minor amounts of pyroxenitic, websteritic and eclogitic types (G4). Eclogitic (G3) garnet from the Kendu body has significantly low Mg# (36–49) and high Ca# (38–45) and FeO (Kendu averages 19 wt. % FeO, n = 29). Eclogitic garnet from Kendu and Legend has low pyrope and high almandine and grossular end-member compositions ($Py_{27–34}Alm_{39–49}Gr_{21–22}$), and is likely

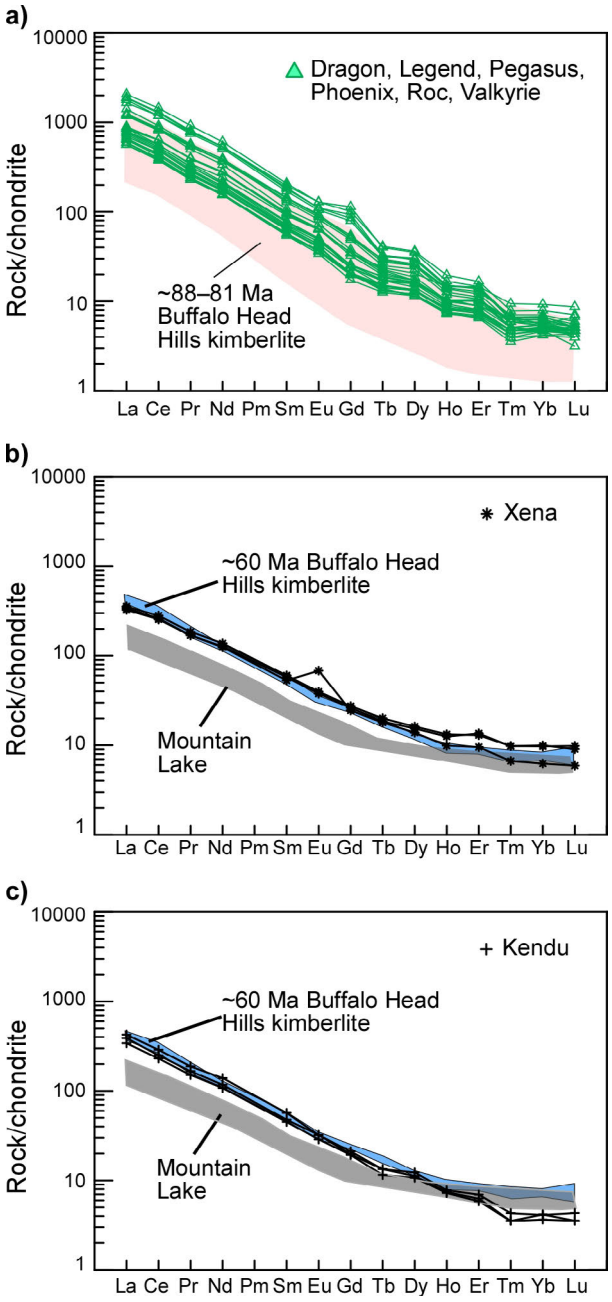

Figure 45. Chondrite-normalized REE patterns for whole-rock samples from the Birch Mountains kimberlite field. Compositions of the Mountain Lake and the ~88–81 Ma and ~60 Ma Buffalo Head Hills bodies from this study are included for comparison. Normalization values from Sun and McDonough (1989).

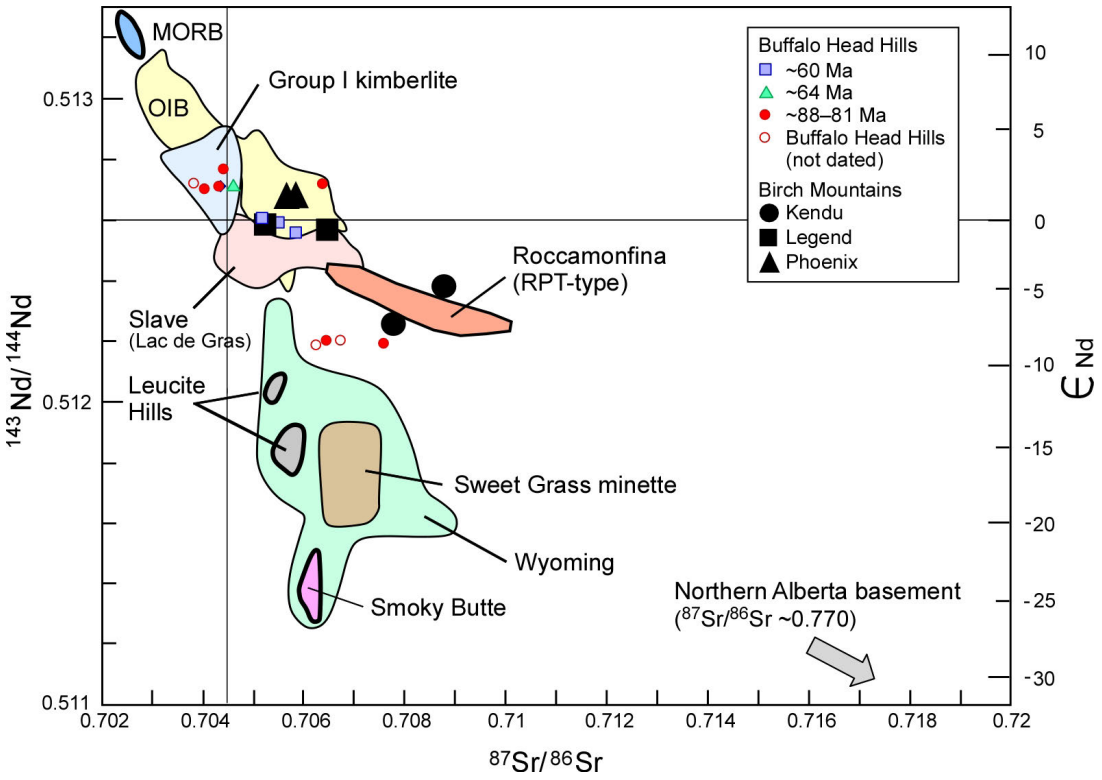

Figure 46. Nd-Sr isotope variations from selected kimberlitic rocks in northern Alberta, with emphasis on selected Birch Mountains intrusions (solid black symbols). Included for comparison are Group I kimberlite from Smith (1983), Smith et al. (1985) and Mitchell (1986); Slave Province Lac de Gras field from Dowall et al. (2000); Roccamonfina (Roman Province type) from Mitchell and Bergman (1991); Wyoming ultrapotassic fields from Vollmer et al. (1984) and O'Brien et al. (1995); Sweet Grass minette from Buhlmann (1996); mid-oceanic ridge basalt (MORB), oceanic-island basalt (OIB) and EM-II mantle reservoir from Zindler and Hart (1986); and Buffalo Head Hills isotopic compositions from this study.

better characterized as lower-crustal eclogitic garnet. One grain from Kendu's G3 population has >0.7 wt. % Na_2O, classifying it as diamond-facies eclogitic G3D based on the elevated Na compositions in eclogitic diamond inclusions (0.11 wt. % Na_2O; Figure 49). However, the significance of this G3D garnet in Kendu is downgraded because physical and chemical observations suggest that the intrusion has a shallow source and is therefore not a product of deep-sourced kimberlite magmatism.

Clinopyroxene from the Dragon, Kendu, Legend and Xena bodies generally classifies as diopside but has, at minimum, a bimodal distribution (Figure 50). Xena and, to a lesser extent, Kendu

Figure 47. (see page 69) Compositional overview of peridotitic garnet from selected Birch Mountains intrusions: a) plot of Cr_2O_3 versus CaO for cores of peridotitic garnet xenocrysts; b) Ca-intercept method of representing garnet Cr/Ca content by a single number; c) to e) relative proportion and pressure-temperature distribution of peridotitic garnet cores for Kendu, Legend, and Xena; left Y-axis and solid polygon shading represent general peridotitic garnet paragenesis (i.e., G9, G11 and G12), together with the Grütter et al. (1999) Mn in peridotitic garnet temperature regression at 50°C temperature (T_{Mn}) intervals; right Y-axis and symbols represent a significantly smaller subset of peridotitic garnet data intended to provide a more detailed garnet nomenclature based on correlations between garnet Ni thermometry (Canil, 1999) and trace-element concentrations (Eccles and Simonetti, 2008). Abbreviations: G9, Group 9 lherzolitic garnet; G10, Group 10 harzburgitic garnet; W, wehrlitic garnet; CCGE, chromite-clinopyroxene-garnet equilibrium; GDC, graphite-diamond constraint.

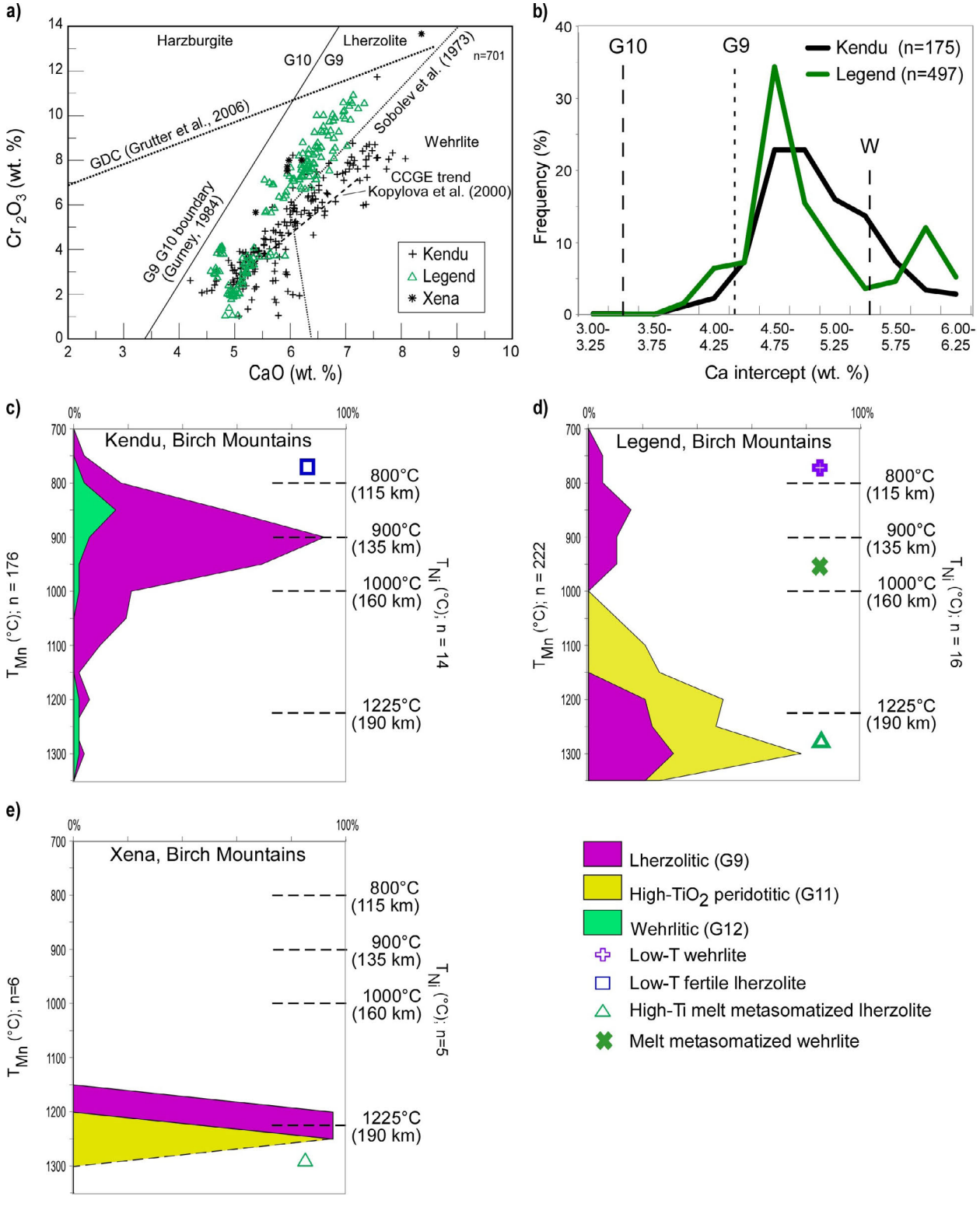
a)
Harzburgite
Lherzolite
G10
G9
n=701
GDC (Grutter et al., 2006)
Sobolev et al. (1973)
Wehrlite
CCGE trend
Kopylova et al. (2000)
G9 G10 boundary (Gurney, 1984)
Kendu
Legend
Xena
Cr2O3 (wt. %)
CaO (wt. %)
b)
G10
G9
W
Kendu (n=175)
Legend (n=497)
Frequency (%)
3.00-3.25
3.50-3.75
4.00-4.25
4.50-4.75
5.00-5.25
5.50-5.75
6.00-6.25
Ca intercept (wt. %)
c)
Kendu, Birch Mountains
800°C (115 km)
900°C (135 km)
1000°C (160 km)
1225°C (190 km)
TMn (°C); n = 176
TNi (°C); n = 14
d)
Legend, Birch Mountains
TMn (°C); n = 222
TNi (°C); n = 16
e)
Xena, Birch Mountains
TMn (°C); n=6
TNi (°C); n=5
Lherzolitic (G9)
High-TiO2 peridotitic (G11)
Wehrlitic (G12)
Low-T wehrlite
Low-T fertile lherzolite
High-Ti melt metasomatized lherzolite
Melt metasomatized wehrlite

are dominated by high Al, which is characteristic of clinopyroxene from non-kimberlite sources or clinopyroxene that equilibrated under crustal conditions.

Legend has a significant low-Cr clinopyroxene population, which likely correlates with its significant megacrystic garnet population. One population of Legend clinopyroxene is equivalent to mantle-equilibrated clinopyroxene, with inferred P-T estimates of 50–66 kbar and 1000°–1250°C that are variably distributed around the 40 mW/m^2 geotherm and possibly trending toward higher geotherms (Figure 50c). It should be noted, however, that the majority of the Legend clinopyroxene does not satisfy the Ramsay and Tompkins (1994) criteria for garnet lherzolite (>0.5 wt. % Cr_2O_3 with <4.0 wt. % Al_2O_3). These include a large number of analyses that would have plotted in this high-P and -T group. Thus, it is possible that the Legend clinopyroxene is influenced by the precision of the analysis. Until this discrepancy is rectified, it is difficult to conclude that this clinopyroxene is indicative of diamond-bearing mantle.

Low-T and low-P clinopyroxene characterizes Kendu and Xena, likely a function of either its non-mantle source or the absence of garnet, in which case it is spinel facies. Dragon clinopyroxene has unrealistic P-T estimates of 45–55 kbar at ~800°C. To reiterate from Section 3.7.2,

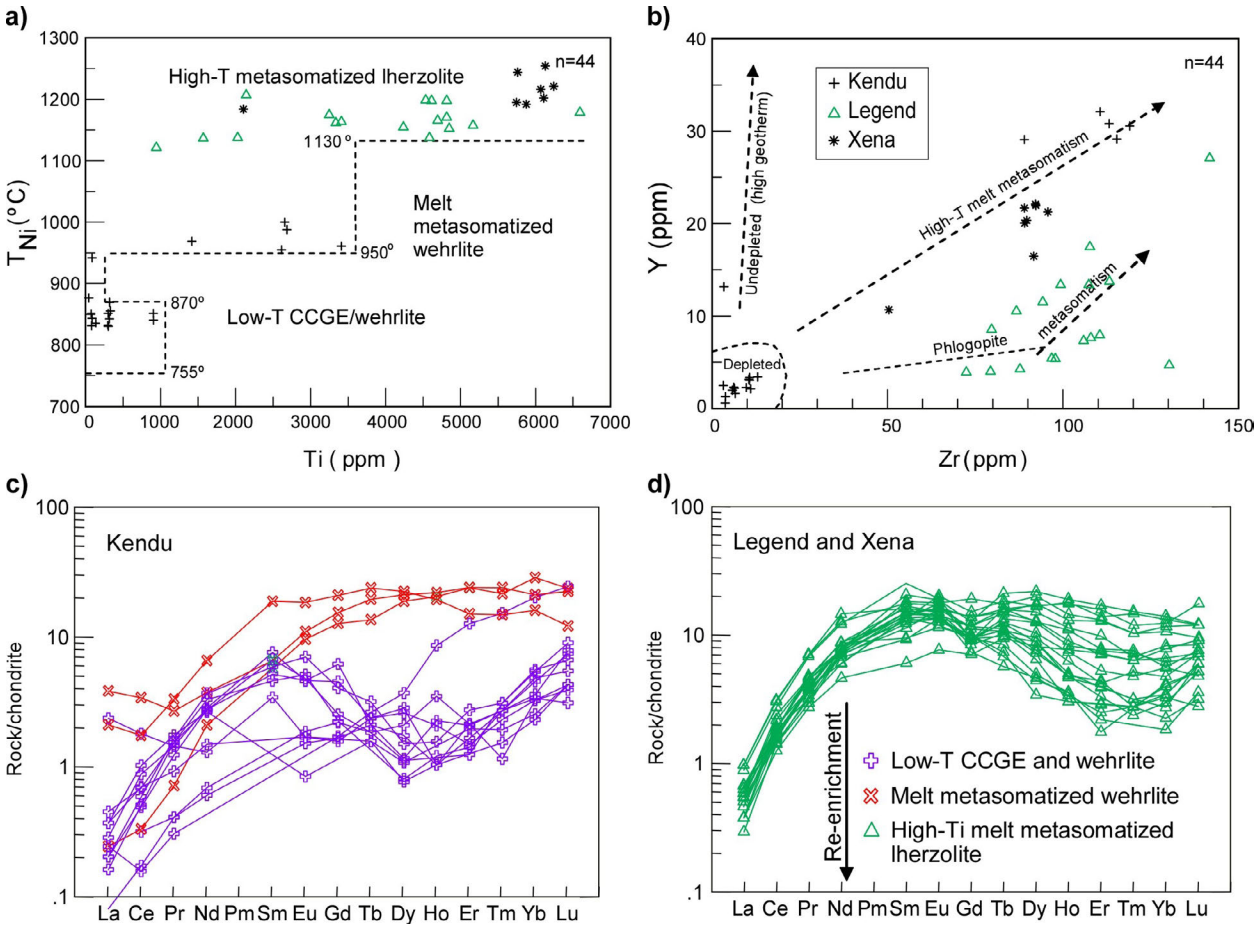

Figure 48. Variations in mantle depletion and metasomatism from trace-element compositions of the cores of peridotitic garnet xenocrysts for selected Birch Mountains intrusions: a) distribution of T_{Ni} versus Ti, where T_{Ni} is calculated using the Ni-in-garnet geothermometer of Canil (1999); b) plot of Y versus Zr on the fields and metasomatic trends of Griffin et al. (1999); c) and d) chondrite-normalized REE profiles for the cores of peridotitic garnet xenocrysts; chondrite values from Sun and McDonough (1989). Nomenclature for the various lherzolitic and wehrlitic garnet types from Eccles and Simonetti (2008). Abbreviation: CCGE, chromite-clinopyroxene-garnet equilibrium trend of Kopylova et al. (2000).

if Dragon clinopyroxene represents equilibrium P-T values on an ambient geotherm, then the implied geothermal gradient would be well below 36 mW/m^2, the opposite of what one would expect for thin or reworked Proterozoic lithosphere.

Olivine dominates the xenocryst assemblage from the Birch Mountains bodies. Olivine core compositions for the Dragon, Legend, Pegasus, Phoenix, Roc, Valkyrie and Xena bodies generally have >3000 ppm Ni, typical of mantle peridotite and kimberlite, but with low $Fo_{88–92}$ (Figure 51). Legend has the highest Fo content and Pegasus the lowest. Phoenix and possibly Valkyrie have several populations of olivine, including a prolific positive-sloping trend of Phoenix core compositions toward higher Fo and Ni. The general linear nature of these olivine compositions may represent differing magmatic fractionation trends (Kjarsgaard et al., 2010). All of the Birch Mountains intrusions contain some low Ni concentrations (<1000 ppm), but this is most apparent in Phoenix and Kendu, with the latter characterized by high Fo (>91) with distinctly low Ni (<1000 ppm).

Phlogopite from the Phoenix body follows a trend of increasing Al with decreasing Ti,

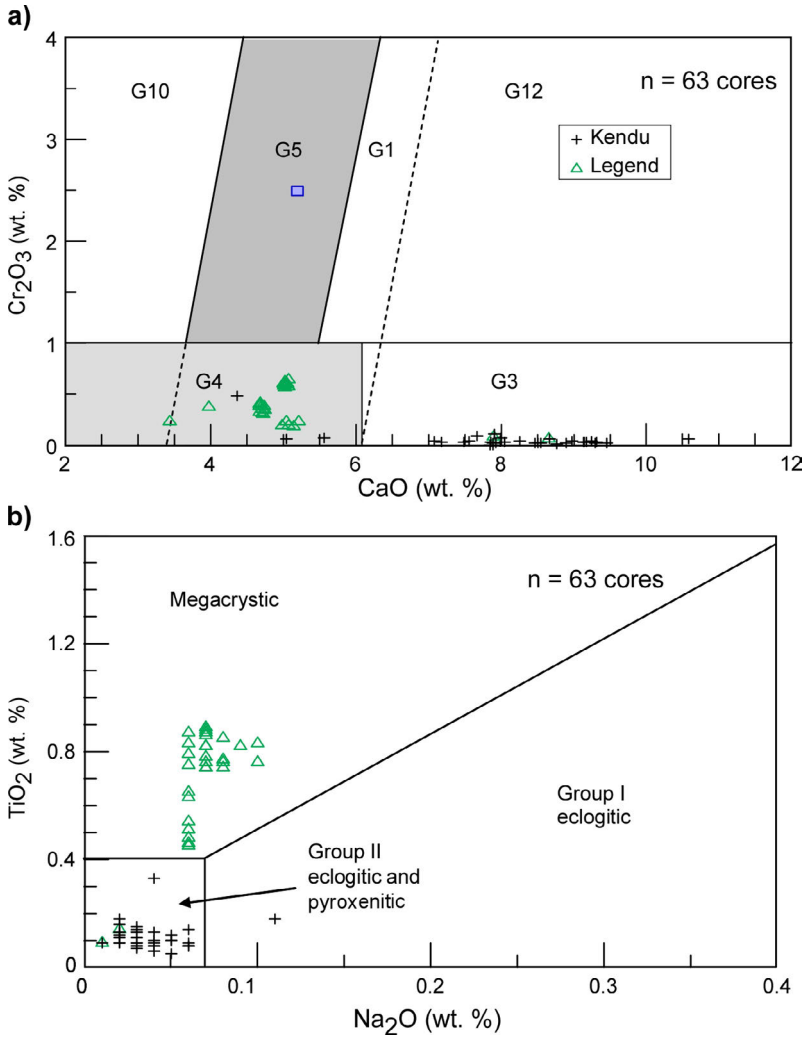

Figure 49. Classification of low-Cr garnet xenocryst cores from selected Birch Mountains intrusions: a) plot of Cr_2O_3 versus CaO, with group-number (e.g., G-1) classification nomenclature from Grütter et al. (2004); b) plot of TiO_2 versus Na_2O, with megacrystic and eclogitic Group I and II fields from Schulze (1997).

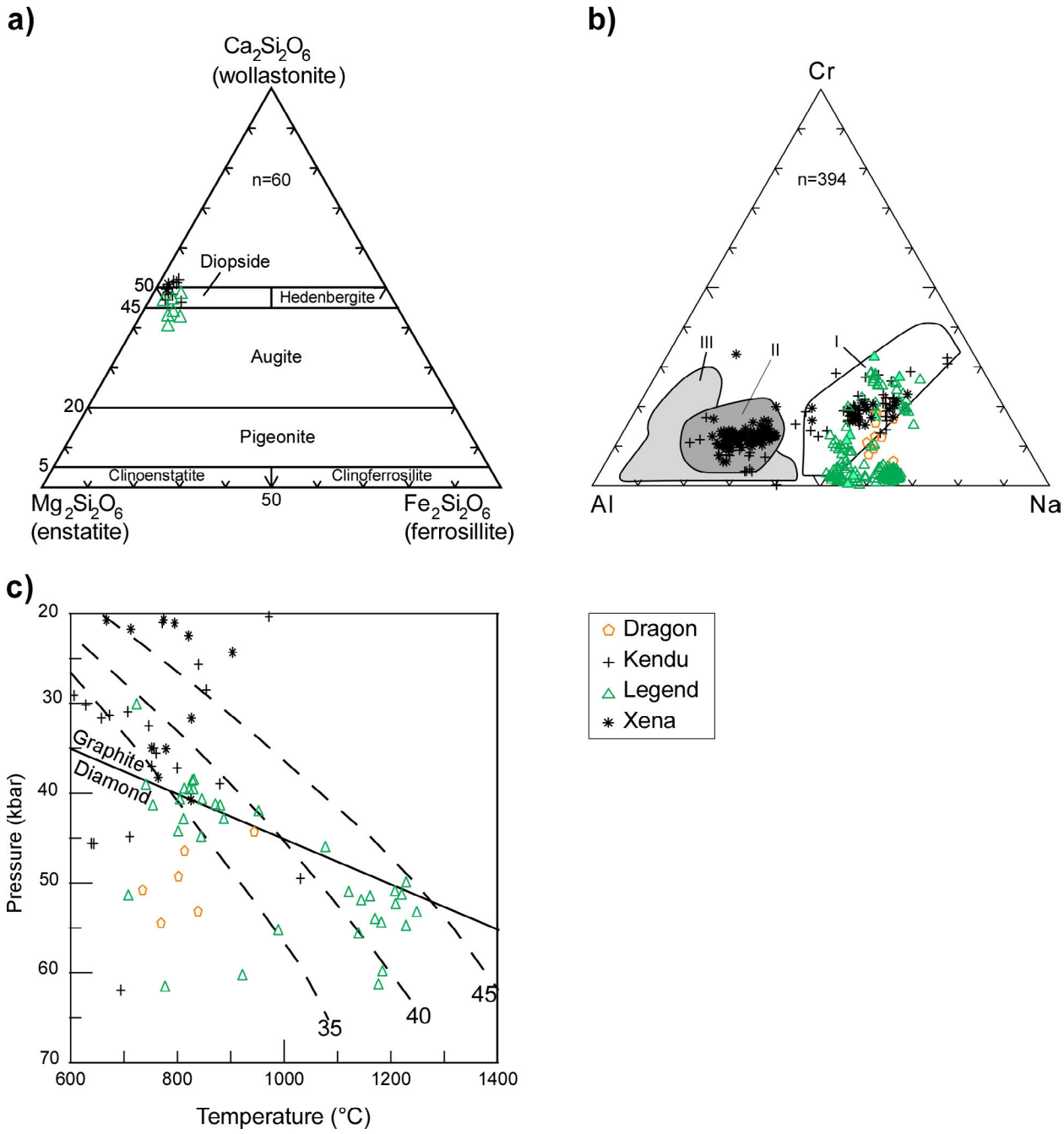

Figure 50. Variation diagrams for clinopyroxene xenocryst cores from selected Birch Mountains intrusions: a) Ca-Mg-Fe quadrilateral pyroxene classification based on the scheme of Morimoto et al. (1988); b) Al-Cr-Na diagram with classification fields modified after Morris et al. (2002), including mantle-equilibrated clinopyroxene derived from kimberlite (I), clinopyroxene from non-kimberlitic sources (II), and clinopyroxene equilibrated under crustal conditions (III); c) pressure-temperature diagram for clinopyroxene based on the thermobarometer of Nimis and Taylor (2000); garnet-lherzolite–type clinopyroxene filters used cut-offs of <23 wt. % CaO, and >0.5 wt. % Cr_2O_3 with <4.0 wt. % Al_2O_3 (<4.5 Al_2O_3 for Cr_2O_3 >2.25 wt. %); geotherms (in mW/m^2, dashed lines) from Pollack and Chapman (1977); diamond-graphite equilibrium (solid dark line) from Kennedy and Kennedy (1976).

previously described by Mitchell (1986) for Group I kimberlite (Figure 52). In contrast, Kendu phlogopite has high TiO_2 (generally >2.3 wt. % and up to 5 wt. %; Creighton and Eccles, 2003) and plots along a non-kimberlite minette or alnoite trend, as shown by Mitchell (1986).

Chrome-spinel occurs in all Birch Mountains bodies, in which it is typically disseminated, altered and corroded. Spinel, in conjunction with perovskite and ilmenite, may form necklaces around discrete crystals of olivine and lapilli. Atoll-textured spinel is common in the Phoenix

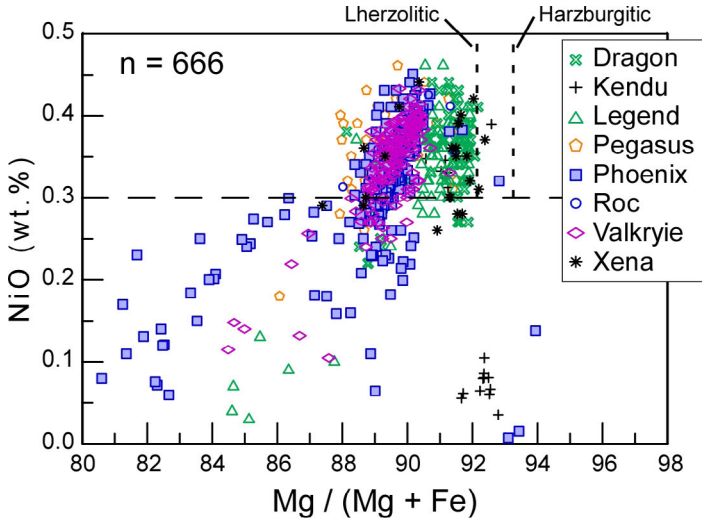

Figure 51. Plot of NiO versus Mg# (Mg / Mg + Fe) for olivine xenocryst cores from selected Birch Mountains intrusions; olivine with >3000 ppm Ni (long-dashed line) represents mantle olivine, based on olivine data from mantle xenoliths and xenocrysts in kimberlite (e.g., Brett et al., 2009); short-dashed lines represent average forsterite content of olivine diamond inclusions in **lherzolitic (Mg# 92.1) and harzburgitic (Mg# 93.2) parageneses (Stachel et al., 2010).**

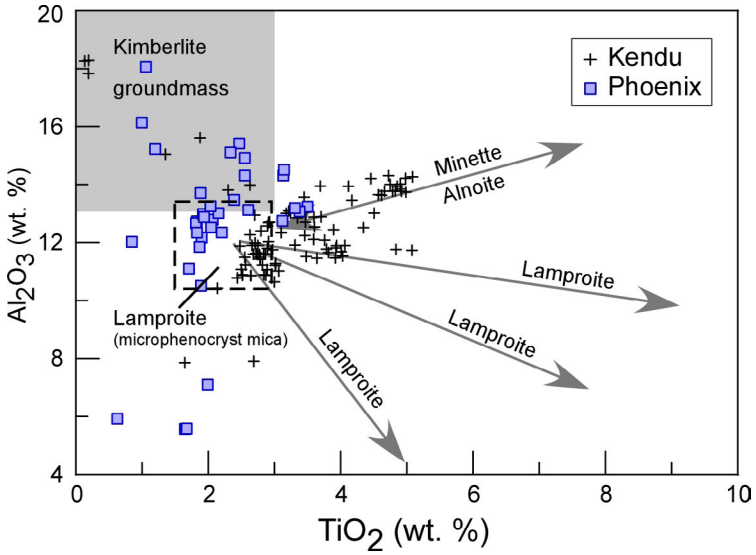

Figure 52. Al_2O_3 versus TiO_2 compositional variation of mica from selected Birch Mountains intrusions; composition trends for micas in minette, lamproite and kimberlite from Mitchell (1995).

body, with chromite cores surrounded by multiple atolls of resorbed spinel (dominantly magnetite). The spinel rarely has sufficiently high Cr compositions to be classified as diamond-inclusion chromite. Only two spinel grains, one each from Legend and Pegasus, have 60–61 wt. % Cr_2O_3 (Figure 53). Chrome-spinel from Phoenix and Legend has Fe_T^{2+} / (Fe_T^{2+} + Mg) ratios between 0.2 and 0.65, and roughly defines end-member compositions of magmatic trend 1 kimberlite (Mitchell, 1986; Figure 53). Kendu contains some spinel grains that plot in the magmatic trend 1 field, but the majority follows magmatic trend 2, progressing from aluminous magnesiochromite to ulvöspinel-magnetite and titanomagnetite with increasing degree of differentiation. Magmatic trend 2–type spinel is also present in the Dragon, Pegasus and Xena bodies. This is in general agreement with the MgO-TiO_2 classification scheme of Creighton and Stachel (2008), in which aluminous magnesiochromite and magmatic trend 2 data plot within the ultramafic and mafic fields.

Ilmenite is present in all of the Birch Mountains bodies, particularly Legend, in which Mg-ilmenite macrocrysts constitute up to 5 vol. % and are up to 9 mm in diameter. Ilmenite occurs as intergrowths with groundmass spinel and perovskite, or as disseminated single-crystal and polycrystalline macrocrysts. With the exception of ilmenite from Valkyrie and Xena, the majority of the Birch Mountains ilmenite has a wide range of compositions (e.g., 38–55 wt. % TiO_2, 0.1–21 wt. % MgO and 1–50 wt. % FeO) and plots within the Wyatt et al. (2004) field for kimberlite (Figure 54). In contrast, ilmenite from Valkyrie and Xena has high TiO_2 (48–56 wt. %) and FeO (28–49 wt. %), and low MgO (majority <11 wt. %, average 6.3 wt. %), so these grains unequivocally plot in the non-kimberlite field of Wyatt et al. (2004).

4.8 Comparative Summary and Classification of the Birch Mountains Intrusions

The major-element geochemistry of the Birch Mountains kimberlites (Dragon, Legend, Pegasus, Phoenix and Roc) differs slightly from that of the Buffalo Head Hills ~88–81 Ma primitive kimberlite, but correlates well with Group IB (off-craton) South African kimberlite (Figures 43 and 44). Compared to the ~88–81 Ma Buffalo Head Hills kimberlites, the Birch Mountains kimberlites have appreciably lower Ni, MgO and SiO_2, and higher high-field-strength incompatible elements (Nb, Zr, Hf and Y), $Fe_2O_3^T$, MnO, CaO, P_2O_5 and TiO_2. The Legend and Phoenix $^{87}Sr/^{86}Sr$ ratios are more radiogenic than those from the majority of the ~88–81 Ma Buffalo Head Hills bodies, but correlate well with those of the ~60 Ma Buffalo Head Hills alkaline bodies (Figure 46). The Birch Mountains kimberlites have a higher Ca-intercept for peridotitic garnet, eclogitic garnet with low pyrope end-member composition and lower Fo and Ni olivine compositions relative to the ~88–81 Ma Buffalo Head Hills kimberlites. The Birch Mountains Dragon, Legend, Pegasus, Phoenix and Roc intrusions are therefore classified as Group IB-type evolved kimberlite magma. The accumulation of carbonate and late-stage minerals, abundance and large size of opaque minerals, similar whole-rock chemistry to Group IB (off-craton) South African kimberlite, variable partial-melting REE patterns, radiogenic Sr-isotope signatures and complex mantle signatures all attest to this evolved magma contention and imply shallower sampling, mantle metasomatism or a combination of these factors in the Birch Mountains field

The Xena intrusion is not kimberlite, but rather has affinities to a potassic alkaline classification. In contrast to the Birch Mountains kimberlite samples, Xena has significantly higher SiO_2 and Al_2O_3, higher K_2O, lower overall abundance of REE, lower LREE and higher HREE, so it is closer in whole-rock composition to the Mountain Lake intrusions (Figures 43–45). There are also geochemical indications, such as similar La/Yb ratios and a flattening HREE profile, suggesting that Xena and the ~60 Ma Buffalo Head Hills intrusions are related. Xena has whole-rock and mantle compositions that suggest a metasomatized mantle with extremely high temperatures of last equilibration. Based on its chemical similarity to Mountain Lake, Xena should be classified

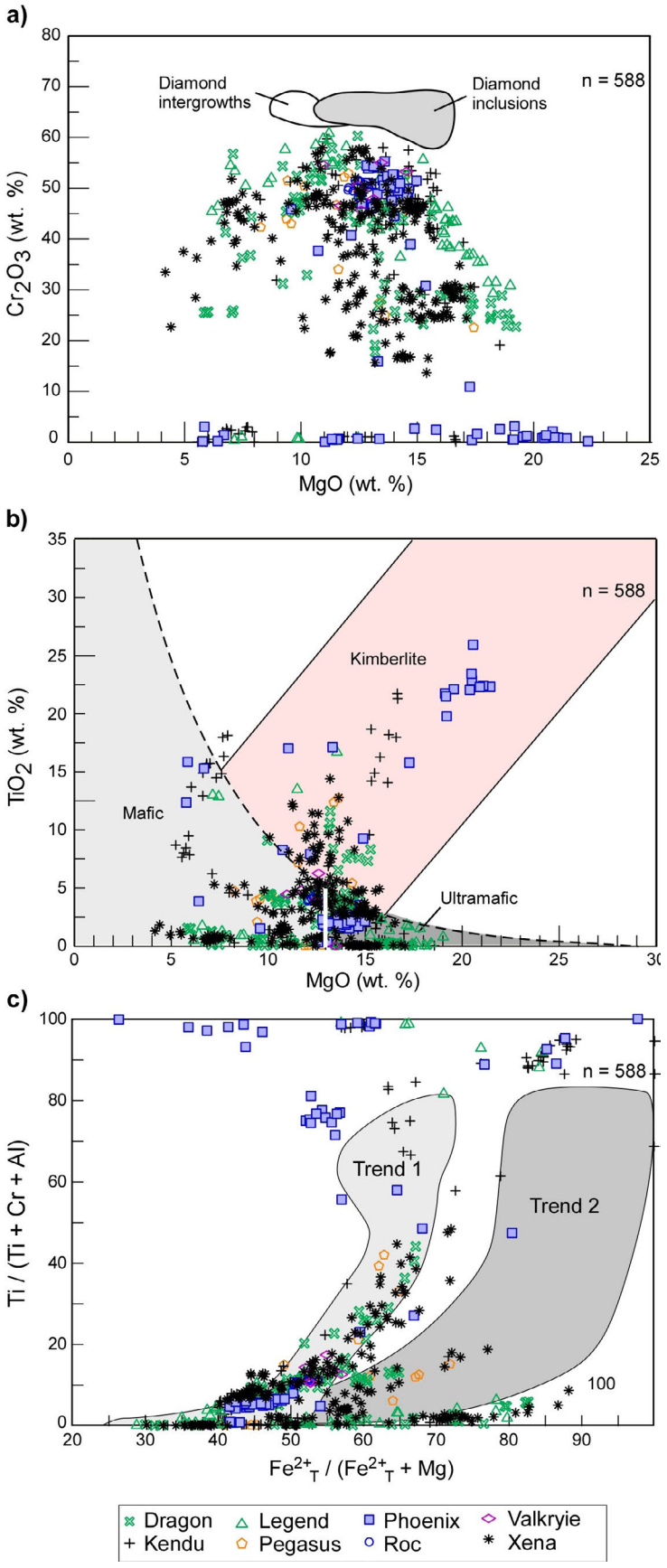

Figure 53. Variation diagrams for spinel xenocryst cores from selected Birch Mountains intrusions: a) Cr_2O_3 versus MgO, with diamond-inclusion and intergrowth fields from Fipke et al. (1995); b) TiO_2 versus MgO, with fields from Creighton and Stachel (2008); c) Ti / (Ti + Cr + Al) versus Fe^{2+} / (Fe^{2+} + Mg), with fields from Mitchell (1986).

as Roman Province–type magmatism or, more specifically, alkali-olivine basalt or basanite.

Kendu's mantle signature suggests derivation from significantly shallower depths (in the lower crust or upper mantle) than all other northern Alberta intrusions. Kendu's whole-rock composition typically plots between those of Xena (and Mountain Lake) and the Birch Mountains kimberlites (Figures 43–45). It has low LREE (220 to 275 times chondrite abundance for La) and an REE profile that is similar to the ~60 Ma and Xena bodies, but it has a noticeably steeper negatively sloping HREE (La/Yb of 88–97) than Xena. Kendu has higher $^{87}Sr/^{86}Sr$ (0.70778–0.70879) and lower ε_{Nd} (–4.0 to –6.3) than bulk Earth composition and plots within the enriched, bottom right quadrant of the Nd-Sr diagram. The high initial $^{87}Sr/^{86}Sr$ indicates a source composition similar to that of Roman Province volcanism. This Nd-Sr isotopic composition could also be attributed to recycling of continental crust, sediments and delaminated lithosphere into the mantle, and/or mantle metasomatism (e.g., Menzies, 1983; White, 1985; Zindler and Hart, 1986). The Kendu body contains olivine with high Fo (>91) but distinctly low Ni (<1000 ppm). This olivine composition is similar to those of the ~60 Ma Buffalo Head Hills bodies. Despite several similarities to the ~60 Ma Buffalo Head Hills bodies, Kendu's physical and chemical attributes necessitate a shallower source. It is not representative of kimberlite *sensu stricto* and therefore deserves a unique classification that has yet to be unequivocally determined.

4.9 Diamond Content

All eight Birch Mountains intrusions have been sampled for diamond. During the initial discovery by Kennecott, three samples totalling ~771 kg were taken from the Phoenix and Legend bodies (Aravanis, 1999). Two samples totalling 364.7 kg from Phoenix returned three microdiamonds and two macrodiamonds. A 406.5 kg sample from Legend yielded four microdiamonds (Appendix 1). In 2001, New Blue Ribbon Resources Ltd. submitted 170 kg of split core from the Kendu ultramafic body for caustic fusion. The test did not yield any macro- or microdiamonds.

During 2007, Grizzly Discoveries Inc. collected a 10.2 tonne mini–bulk sample from the Legend

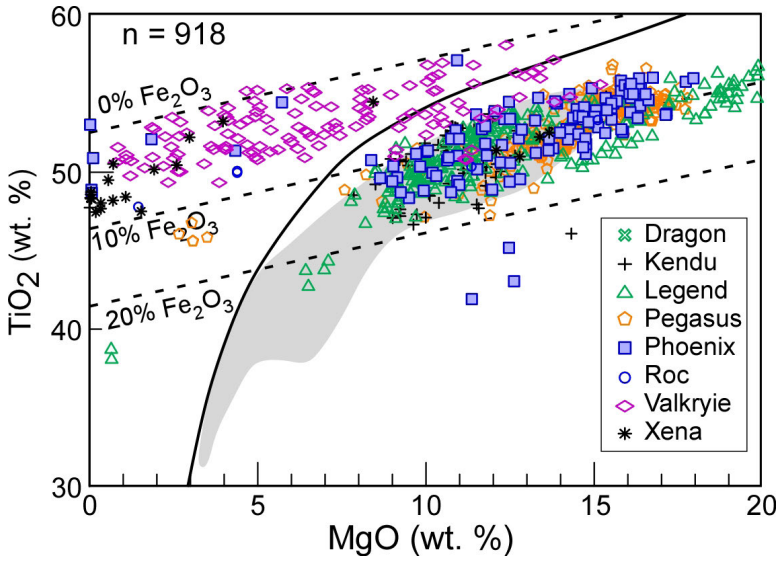

Figure 54. Plots of TiO_2 versus MgO for ilmenite xenocryst cores from selected Birch Mountains bodies; dark grey dashed lines indicate estimated Fe_2O_3 content of macrocrystalline ilmenite; solid line separates fields of kimberlitic and non-kimberlitic ilmenite from Wyatt et al. (2004); shaded polygon represents ilmenite from North American kimberlite (Schulze et al., 1995).

body via 13 drillholes. The sample was split into three subsamples, based on mineralogical and textural differences within the kimberlite, and processed at the DeBeers Canada dense media separation facility in Grande Prairie, Alberta. Standard caustic fusion on a heavy-mineral concentrate sample totalling 64.45 kg yielded one colourless, included, twinned octahedron with dimensions of 2.1 mm by 1.58 mm by 1.46 mm. In addition, three microdiamonds were recovered from 168.35 kg of drillcore selected for mineral chemistry and microdiamond recovery (Appendix 1).

5 Summary and Observations

The summary and observations are presented under the following headings: discovery; geochronology and setting; rock classification; mantle considerations; diamond considerations; and Alberta's future diamond prospectivity. Due to the breadth of data in the report, the summary and discussion are presented in point form to emphasize succinctly a number of important points of interest. Key references are provided so the reader can further investigate specific topics.

5.1 Discovery, Geochronology and Setting

- During the last 20 years, 51 kimberlite, alkaline and related ultramafic intrusions have been discovered in northern Alberta: two at Mountain Lake in northwestern Alberta, 41 at Buffalo Head Hills in north-central Alberta and eight at Birch Mountains in northeastern Alberta.

- The majority of the bodies were discovered in a six-year period from 1997 to 2003. The most recent documented kimberlite discovery in northern Alberta occurred during 2008 with the discovery of the BE-01 to -03 intrusions in the eastern part of the Buffalo Head Hills field.

- Collectively, kimberlites and related rocks in northern Alberta were emplaced during a 28 million-year period spanning the Late Cretaceous to Paleocene (~88–60 Ma).

- Volcanism consisted of short intervals of violent eruption separated by longer, volcanically quiescent intervals. Combined palynological and geochronological determinations, summarized in Eccles et al. (2008a), document episodes of kimberlitic magmatism during the Late Cretaceous (~88–81 Ma, Buffalo Head Hills; ~78–70 Ma, Birch Mountains; ~76–75 Ma, Mountain Lake) and the Paleocene (~64 and ~60 Ma, Buffalo Head Hills). The northern Alberta kimberlite province is therefore classified as a Type 2 province, defined by Mitchell (1986) as a province consisting of several kimberlitic fields of similar age.

- An extensive Turonian to Early Campanian hiatus, representing approximately 9 million years of missing strata, coincides with Late Cretaceous kimberlite volcanism in the Buffalo Head Hills area of north-central Alberta (Sweet et al., 2006). A similar Cenomanian/Turonian to Santonian time gap of approximately 4–8 million years was postulated to occur in the Birch Mountains area of northeastern Alberta and may be contemporaneous with Birch Mountains volcanism (Dufresne et al., 2001).

- Three different volcanic settings are recognized in the Buffalo Head Hills kimberlite field: Late Cretaceous Smoky Group–equivalent intra- and extra-crater facies, Late Cretaceous and Paleocene intrusive sills and/or dikes, and Paskapoo Formation–equivalent Paleocene intra-crater facies. Collectively, these volcanic episodes define a complex kimberlite field characterized in the near surface by tabular kimberlite layers and more classical kimberlite pipe-like bodies of varying ages.

- The majority of the intrusions discovered to date have large, near-surface dimensions characterized by tabular volcaniclastic layers that, upon drilling, have no apparent feeder. This profile essentially defines the Skinner and Marsh (2004) Class 2 kimberlite morphological description of pyroclastic-enriched bodies with shallow saucer-shaped craters <500 m in depth.

- The dominance of pyroclastic surge-and-fall deposits (i.e., phreatomagmatic volcanism; Boyer, 2005) and mudstone-dominated host rocks suggests that large volumes of the northern Alberta intrusions erupted in a marine environment and some could have erupted subaqueously. Kimberlites hosted in sandstone and/or sandstone-dominated resedimented volcaniclastic deposits may represent Late Cretaceous magmatism that is penecontemporaneous with major depositional hiatuses.

- The integration of palynological and geochronological data provides evidence of Late Cretaceous and Paleocene intrusive volcanism. Intrusive kimberlite sills and/or dikes may occur in the Buffalo Head Hills if
    - material from an earlier eruption forms a caprock at the top of the emplacement pathway and forces subsequent younger eruptions to either break through the now-solid cap or penetrate outward, between strata, into preferential zones of weakness; and/or
    - the eruption(s) is/are forceful enough to erupt both vertically and horizontally as the magma nears and breaches the surface. This scenario may be particularly applicable if Class 2 kimberlites are indeed CO_2-rich, water-poor hot magmas that are able to rise to shallow levels, encounter groundwater and undergo phreatomagmatism (e.g., Skinner and Marsh, 2004), or if Buffalo Head Hills kimberlite is generated by some combination of exsolution-driven magmatism (e.g., exsolution of volatiles to instigate magma ascent) and phreatomagmatism, as suggested by Boyer (2005).

- Relative to Cretaceous to Paleocene ultramafic magmatism elsewhere in North America, the northern Alberta kimberlite province is temporally closest to the Lac de Gras kimberlite field in the Northwest Territories (~74–45 Ma; Creaser et al., 2004; Heaman et al., 2004;), despite being separated by more than 900 km. Either the overlap in age of volcanism for the northern Alberta and Lac de Gras kimberlite fields is coincidental or tectonic controls associated with Paleocene to Late Cretaceous volcanism are similar. If the latter, then it is difficult to fit their temporally similar magmatism into a plume model. Rather, a more regionally encompassing model, such as Farallon Plate subduction with magmatism migrating up the subducted oceanic lithosphere subsequent to changes in plate convergence velocities (McCandless, 1999; Currie and Beaumont, 2011), seems to be more consistent with a Cretaceous to Eocene corridor of ultramafic magmatism that crudely parallels the western margin of North America (Heaman et al., 2004; Eccles et al., 2008a).

- Current evidence suggests that some correlation between ultramafic magmatism and local tectonic features acted in concert with larger scale orogenic events (e.g., subduction) to control the generation and emplacement of northern Alberta kimberlite province magmas. Regional features resulting in magma generation could have been influenced by some combination of mantle hot cells, subduction and deep-seated structure. On a more local scale, it is postulated that deep-seated structures associated with the initial development of the Peace River Arch and possible subsequent reactivation (e.g., Laramide Orogeny and foreland-bulge migration) provided pathways for the emplacement of kimberlitic magma in northern Alberta (Eccles et al., 2001; Paganelli et al., 2002; Pană and Eccles, 2003).

5.2 Rock Classification

- Pyroclastic kimberlitic rocks, or juvenile lapilli-bearing olivine tuff, are by far the dominant textural rock type in the northern Alberta kimberlite province, followed by resedimented volcaniclastic kimberlitic rocks and less common hypabyssal (intrusive) kimberlitic rocks.

- The integration of petrography and geochemistry of minimally contaminated volcaniclastic rocks has been used to compare, and aid in the classification of ultramafic rocks in the three separate areas of the northern Alberta kimberlite province. These areas are generally distinguished from one another by their non-archetypal kimberlite alkaline rock signatures or, in the case of bona-fide kimberlites, by their primitive to evolved magmatic signatures. Table 3 provides a synopsis of the physical and chemical variations of primitive kimberlite, evolved

kimberlite and alkaline rock classifications from the northern Alberta kimberlite province.

- The Mountain Lake intrusion is not archetypal kimberlite. Proposed classifications are somewhat equivocal because of pervasive clay alteration, but the integration of petrographic, geochemical and mantle compositions favours a potassic alkaline classification, such as alkali olivine basalt or basanite.

- A group of ~88–81 Ma diamondiferous kimberlites in, but not necessarily restricted to, the northwestern part of the Buffalo Head Hills bodies is physically and chemically similar to Group 1A (on-craton) South African kimberlite and uncontaminated hypabyssal kimberlite from Ekati, Northwest Territories. In Nd-Sr isotopic space, the ~88–81 Ma Buffalo Head Hills bodies have the most primitive depleted-upper-mantle (MORB-like) source in the northern Alberta kimberlite province.

- The ~60 Ma intrusions in the southeastern part of the Buffalo Head Hills have nonexistent to low diamond counts, and minerals and compositions that differ from archetypal kimberlite. Based on their mineralogical and chemical similarity to non-kimberlite bodies in other parts of northern Alberta (Mountain Lake and Xena, Birch Mountains), the Paleocene Buffalo Head Hills bodies are more appropriately referred to as alkaline rocks.

- The Birch Mountains field contains an eclectic mixture of alkaline to evolved kimberlite compositions. The evolved kimberlites (e.g., Legend, Phoenix) are differentiated from the Buffalo Head Hills bodies by their higher abundance of carbonate and late-stage minerals (phlogopite and ilmenite), lower abundance of coarse macrocrystalline olivine, and geochemical compositions that correlate with Group IB (off-craton) South African kimberlite. The Xena body has an alkaline classification that compositionally mimics Mountain Lake. Kendu is also designated as non-kimberlite based on a shallower source and a more alkaline signature than bona fide northern Alberta kimberlite.

- Kimberlites in the Buffalo Head Hills and Birch Mountains fields are indicative of magma with very low degrees of partial melting. The dominant process of magmatic differentiation in these fields is crystal fractionation and accumulation of olivine, which acts as the main differentiation process between primitive and evolved Group I–type kimberlites. The Birch Mountains bodies represent an evolved magmatic field that is further differentiated by varying degrees of partial melting and source enrichment (i.e., mantle metasomatism), and/or less efficient carbonate loss during ascent than the ~88–81 Ma Buffalo Head Hills bodies (Eccles, 2004; Eccles et al., 2004).

5.3 Mantle Considerations

- A comprehensive set of garnet xenocryst compositions for selected bodies from Mountain Lake, Buffalo Head Hills and Birch Mountains provides a unique opportunity to study the chemical nature of a cross-section of lower crustal–subcontinental lithospheric mantle beneath northern Alberta.

- Peridotitic garnet xenocryst datasets created by the Alberta Geological Survey, together with mineral assessment report data (e.g., Aravanis, 1999), show that selected bodies from the northern Alberta kimberlite province are dominated by lherzolitic (G9) garnet, followed by high-TiO_2 peridotitic (G11) and lesser amounts of wehrlitic (G12) garnet.

- Distinct changes in the Ti, chondrite-normalized REE, Y and Zr contents of peridotitic garnet xenocrysts provide evidence for varying degrees of depletion or re-enrichment of the protolith (Eccles and Simonetti, 2008). Based on peridotitic garnet compositions—and using T_{Ni} (Ni thermometer of Canil, 1999) as a proxy of depth—at least five heterogenic variations or subgroups of sublithospheric mantle underlie northern Alberta. From low to

high temperature, these are fertile lherzolite and wehrlite (<870°C), low-T lherzolite (870°–950°C), melt metasomatized wehrlite (950°–1000°C), depleted lherzolite and melt metasomatized lherzolite (1000°–1130°C), and moderately fertile lherzolite and high-Ti melt metasomatized lherzolite (>1130°C).

- Variations in these mantle subgroups are evident, not only at the intra- and inter-field scale but even with intrusions that are in proximity to one another. This implies selective mantle sampling by the bodies, and/or significant local variability in the mantle due to depletion or re-enrichment of the protolith (Eccles and Nowicki, 2010).

- The permissive window for diamond preservation is best represented by depleted lherzolitic garnet compositions observed within a T_{Ni} zone of between 1000° and 1130°C that is restricted to the Buffalo Head Hills kimberlite field (Eccles and Simonetti, 2008). The depleted lherzolitic garnet is characterized by depleted Ti, Zr and Y; a flattened middle and heavy REE profile; and a good correlation with peridotitic garnet-clinopyroxene inclusion pairs from Buffalo Head Hills diamonds that yielded equilibration temperatures of 1100°–1200°C ±50°C on a 40 mW/m^2 geotherm (Davies et al., 2004).

- The rarity of G10 garnet, a lherzolite trend shifted to slightly higher Ca content and 38 mW/m^2 conductive geotherm values that do not exceed 43 kbar all imply that the northern Alberta kimberlite province displays features more typical of Proterozoic lithosphere (Eccles and Nowicki, 2010; Nowicki and Harvey, 2010). However, it is worth considering that the relatively high degree of depletion in a peridotitic diamond window underlying the Buffalo Head Hills at 160–180 km, 1000°–1130°C and low Ti, Y and Zr may be consistent with an Archean subcontinental lithospheric mantle that has been strongly modified in Proterozoic time.

- A high proportion of high-Ti metasomatized mantle is apparent across northern Alberta. Despite some of the high-Ti melt metasomatized lherzolitic garnet recording T_{Ni} similar to that of the depleted lherzolite, the high-Ti melt metasomatized lherzolitic garnet has abundant Ti, Zr and Y, suggestive of melt metasomatism.

- Based on the abrupt chemical changes (e.g., Ti, Y and Zr) at the lower boundary (1130°C) of the high-T_{Ni} layer, the approximate depth of the lithosphere-asthenosphere boundary (LAB) is 180 km. This matches the LAB depth prediction of Aulbach et al. (2004), based on their P-T correlation of sheared garnet lherzolite. The 180 km LAB depth also agrees with the results of a recent magnetotelluric study in the Buffalo Head Hills by Türkoğlu et al. (2007), who modelled a decrease in electrical resistivity at a depth of approximately 200 km.

- In contrast to the Buffalo Head Hills, the Mountain Lake and Birch Mountains areas seem to be characterized by a geothermal gradient associated with thin lithosphere or a hot, extensively re-enriched asthenospheric-type mantle. The Legend and Xena bodies sampled garnet only from high-T_{Ni} mantle layers (>1130°C) with high Y and Zr, and low Zr/Y ratios, which correspond to re-enriched high-T melt metasomatism. The Legend body also sampled garnet with high Zr/Y ratios and sinusoidal REE profiles, attesting to a complicated metasomatic history that possibly involved significant melt metasomatic processes. Conversely, a low-T_{Ni} (<1000°C and predominantly <870°C) garnet signature from the Birch Mountains Kendu body suggests that this body sampled, or even originated in, mantle that is much shallower than the mantle sampled by other bodies in the northern Alberta kimberlite province. Clinopyroxene data from Mountain Lake, Kendu and Xena (alkaline rock types) may have sampled a source characterized by spinel stability.

- The composition of low-Cr garnet from selected Buffalo Head Hills and Birch Mountains bodies is highly variable (Eccles,

2009). Despite processing more than 30 kg of material from the Mountain Lake body, no low-Cr garnet was observed. Megacrystic (G1) garnet is dominant in the K1A, K14 and Legend bodies. Eclogitic (G3), group I eclogitic (G3D) and pyroxenitic-websteritic-eclogitic (G4) garnet dominate the Kendu, K11 and K6 bodies, respectively. Kendu eclogitic (G3) garnet compositions correlate well with those from a previous study of mafic granulite xenoliths in the same body, in which pressure estimates are quite shallow (~19 kbar) compared to those from the diamond-stability field (Eccles et al., 2010). The diamondiferous K11 body has the highest number of G3D and G4D diamond-facies eclogitic garnets (14 of 16 grains), with Na_2O contents of 0.07–0.09 wt. %.

- Fertile lherzolitic garnet in the upper part of Buffalo Head Hills mantle (<115 km depth and <800°C) could in some way reflect mafic melts, observed as prominent horizontal reflections in LITHOPROBE surveys, that may have been produced during the terrane-accretion process (e.g., Winagami reflection sequence; Ross and Eaton, 2002).

5.4 Diamond Considerations

- The best diamond test results to date are from the Buffalo Head Hills field, where at least 28 of the 41 bodies contain diamond. At least three bodies in the Buffalo Head Hills field contain estimated diamond grades of >11 cpht, with the best results coming from kimberlite K252, from which a 22.8 tonne mini–bulk sample returned a total of 12.54 carats of diamonds for an estimated grade of 55.0 cpht (Skelton et al., 2003; Table 4). The K252 diamond results were further broken down by Ashton into an upper 'volcaniclastic'[4] unit that returned 33.7 cpht from a 13.4 tonne sample and a lower 'breccia'[4] unit that yielded 85.4 cpht from a 9.4 tonne sample.

- At present, the ~88–81 Ma kimberlites of the Buffalo Head Hills field correspond to a northwestern cluster of diamondiferous bodies (e.g., K5, K6, K11, K14 and K252) and define a 'diamond window' in the Buffalo Head Hills kimberlite field at ~88–81 Ma; this diamond window seems particularly prevalent at ~81 Ma.

- The northern Alberta diamond play is still in its early exploration stages. New discoveries in the eastern part of the Buffalo Head Hills field (BE-02 and BE-03) may indicate that diamondiferous bodies are not restricted to a cluster of kimberlites in the northwestern part of the field. Hence, when considering the spatial location of diamondiferous bodies, perhaps it is more realistic to consider a complex multi-episode field, such as the Buffalo Head Hills, in three-dimensions, rather than limiting our thinking to a two-dimensional view of the field.

- The presence of a dominant lherzolitic (±wehrlitic) garnet xenocryst assemblage, and lherzolitic and wehrlitic diamond inclusions, suggests that the diamond populations recovered from the Buffalo Head Hills include a significant population from peridotitic subgroups that are generally only a minor component of the peridotitic diamond budget in worldwide economic kimberlite deposits.

- There is little or no evidence for a harzburgitic association, suggesting that either a Proterozoic or a Proterozoic-altered lithosphere underlies northern Alberta.

- The presence of Group 1 eclogitic garnet in Buffalo Head Hills diamond inclusions and as xenocrysts in the diamondiferous K11 body suggests that the underlying mantle includes some component of eclogite/websterite with type 1 compositional characteristics. This is significant because eclogitic (or E-type) diamond represents one of the most dominant diamond sources worldwide.

- Xenocrysts from the Mountain Lake and Birch Mountains fields exhibit diamond-poor scenarios in which individual bodies appear to have sampled metasomatized mantle

[4] Ashton Mining of Canada Inc. logging nomenclature

with extremely high temperatures of last equilibration (e.g., Mountain Lake, Legend and Xena) or significantly shallower depths in the lower crust–upper mantle (e.g., Kendu). These circumstances would lead to destruction of diamond (if present) or the presence of material from the lower crust or mantle that originated at a depth with significantly lower P-T conditions than those in the field of diamond stability.

- The combination of eclogitic diamond inclusions, sublithospheric Type II diamonds and high diamond-mantle-residence temperatures suggests that diamond formation beneath the Buffalo Head Terrane involved deep subduction (Banas et al., 2006; Stachel et al., 2010). Conversely, some diamonds indicate storage in conditions of normal-temperature lithosphere, so stockworks of metasomatism channels may also present a viable model for diamond formation beneath the Buffalo Head Hills field.

5.5 Alberta's Future Diamond Prospectivity

- Discoveries and exploration activities during the last 20 years indicate that Alberta has the potential to host an economic diamond deposit. For example,
  - the Buffalo Head Hills group of kimberlites is the third largest district of significantly diamond-bearing kimberlites in Canada after Lac de Gras in the Northwest Territories and Fort à la Corne in Saskatchewan;
  - about 60% of the bodies are diamondiferous, with at least three kimberlites containing estimated grades of between 11 and 55 cpht;
  - diamonds from the Buffalo Head Hills kimberlites are generally colourless crystals of high quality; and
  - Buffalo Head Hills diamond-inclusion garnet compositions indicate both peridotitic- and eclogitic-type diamond parageneses.
- Exploration may be drawn out longer in Alberta than, for example, the Northwest Territories because of
  - complex Quaternary history and the thickness of overburden (surficial deposits related to glacial movement and/or erosion);
  - lack of kimberlite-indicator mineral sampling; and
  - mantle-mineral chemistry of diamondiferous bodies in Alberta not being consistent with those of known economic kimberlites found elsewhere (i.e., the general lack of evidence for Archean [harzburgitic] lithosphere causes debate about whether Alberta is underlain by Proterozoic lithosphere or Archean lithosphere that was strongly modified in Proterozoic time).
- Alberta will have an important economic diamond deposit in its future if explorers can discover
  - a 'near-surface' deposit with diamond grades similar to, or better than, the estimated 55 cpht in K252;
  - an economic deposit, or marginal-grade deposit, with stones of quality similar to that of some of the high-quality diamonds (clear to yellow, inclusion free) found to date;
  - a marginal-grade deposit, but with areally extensive surface dimensions, similar to many of the bodies discovered to date (up to 48 ha in surface area); or
  - a new cluster of diamondiferous bodies associated with unexplained kimberlite-indicator mineral anomalies with favourable chemistry in areas of northern Alberta not currently associated with known diamondiferous kimberlite fields.

6 References

Aravanis, T. (1999): Legend property assessment report, Birch Mountains area, Alberta; Alberta Energy, Mineral Assessment Report 20000003, 1208 p.

Atkinson, E. and Pryde, R. (2006): Seismic investigation of selected kimberlite pipes in the Buffalo Head Hills kimberlite field, north-central Alberta; Alberta Energy and Utilities Board, EUB/AGS Special Report 79, poster, URL <http://www.ags.gov.ab.ca/publications/abstracts/SPE_079.html> [February 2011].

Aulbach, S., Griffin, W.L., O'Reilly, S.Y. and McCandless, T.E. (2004): Genesis and evolution of the lithospheric mantle beneath the Buffalo Head Terrane, Alberta (Canada); Lithos, v. 77, no. 1-4, p. 413–451.

Balzer, S.A. (2000): Quaternary geology and dispersal patterns, Winagami region, Alberta; Ph.D. thesis, University of Alberta, 358 p. (*also* Alberta Energy and Utilities Board, EUB/AGS Special Report 14, 343 p., URL <http://www.ags.gov.ab.ca/publications/abstracts/SPE_014.html> [February 2011].

Banas, A., Stachel, T., Muehlenbachs, K. and McCandless, T.E. (2007): Diamonds from the Buffalo Head Hills, Alberta: formation in a non-conventional setting; Lithos, v. 93, no. 1-2, p. 199–213.

Baofang, L. and Dawson, F.M. (1988): Stratigraphic framework and depositional setting, Judy Creek coalfield, northern Alberta; *in* Current research, part D, Geological Survey of Canada, Paper 88-1D, p. 121–128.

Barnes, S.J. and Roeder, P.L. (2001): The range of spinel compositions in terrestrial mafic and ultramafic rocks; Journal of Petrology, v. 42, no. 12, p. 2279–2302 [and Access 2000 database].

Barton, M. (1979): A comparative study of some minerals occurring in the potassium-rich alkaline rocks of the Leucite Hills, Wyoming, the Vico Volcano, western Italy, and the Toro-Ankole region, Uganda; Neues Jahrbuch für Mineralogie (Abhandlungen), v. 137, no. 2, p. 113–134.

Becker, M. and le Roex, A.P. (2006): Geochemistry of South African on- and off-craton, Group I and Group II kimberlites: petrogenesis and source region evolution; Journal of Petrology, v. 47, no. 4, p. 673–703.

Bostock, H.H. and van Breeman, O. (1994): Ages of detrital and metamorphic zircons and monazites from a pre-TMZ basin at the western margin of the Rae Province; Canadian Journal of Earth Sciences, v. 31, no. 8, p. 1353–1364.

Bostock, H.H., van Breeman, O. and Loveridge, W.D. (1987): Proterozoic geochronology in the Taltson Magmatic Zone, NWT; *in* Radiogenic age and isotopic studies: report 1, Geological Survey of Canada, Paper 87-2, p. 73–80.

Bostock, H.H., van Breeman, O. and Loveridge, W.D. (1991): Further geochronology of plutonic rocks in northern TMZ, District of Mackenzie, NWT; *in* Radiogenic age and isotopic studies: report 4, Geological Survey of Canada, Paper 90-2, p. 67–78.

Boyer, L.P. (2005): Kimberlite volcanic facies and eruption in the Buffalo Head Hills, Alberta; M.Sc. thesis, University of British Columbia, 156 p.

Boyer, L.P., Hood, C.T.S., McCandless, T.E., Skelton, D. and Tosdal, R. (2003): Volcanology of the Buffalo Hills kimberlites, Alberta, Canada: some preliminary observations; 8th International Kimberlite Conference, Extended Abstracts, FLA 0253, 4 p.

Boyer, L.P., McCandless, T.E., Tosdal, R. and Russell, K. (2008): Volcanic facies and eruption styles in the Cretaceous Buffalo Head Hills kimberlites, Alberta, Canada; 9th International Kimberlite Conference, Frankfurt, Germany, Extended Abstracts, 9IKC-A-00367, 3 p.

Brett, R.C., Russell, J.K. and Moss, S. (2009): Origin of olivine in kimberlite: phenocryst or impostor? Lithos, v. 112S, p. 201–212.

Buhlmann, A.L. (1996): Eocene minettes and their mica-clinopyroxenite inclusions in the Milk River area, southern Alberta: nature and origin; M.Sc. thesis, University of Alberta, 139 p.

Buhlmann, A.L., Cavell, P., Burwash, R.A., Creaser, R.A. and Luth, R.W. (2000): Minette bodies and cognate mica-clinopyroxenite xenoliths from the Milk River area, southern Alberta: records of a complex history of the northernmost part of the Archean Wyoming craton; Canadian Journal of Earth Sciences, v. 37, no. 11, p. 1629–1650.

Burwash, R.A., Chacko, R. and Muehlenbachs, K. (1993): Tectonic interpretation of Kimiwan Isotopic Anomaly, northwestern Alberta; *in* LITHOPROBE Alberta basement transects: report of transect workshop, G.M. Ross (ed.), LITHOPROBE Secretariat, University of British Columbia, LITHOPROBE Report 47, p. 340–349.

Burwash, R.A., Krupička, J. and Wijbrans, J.R. (2000): Metamorphic evolution of the Precambrian basement of Alberta; The Canadian Mineralogist, v. 38, no. 2, p. 423–434.

Calgary Herald (1998): Forget oil: diamonds new lure; Calgary Herald, January 3, 1998, p. A1.

Canil, D. (1999): The Ni-in-garnet geothermometer: calibration at natural abundances; Contributions to Mineralogy and Petrology, v. 136, no. 3, p. 240–246.

Canterra Minerals Corporation (2008): Buffalo Hills property drilling update; Canterra Minerals Corporation (formerly Diamondex Resources Ltd.), news release, October 15, 2008.

Card, C.D. and Ashton, K.E. (2010): The case for separate Taltson and Thelon orogenies: evidence from the shield in western Saskatchewan; GeoCanada 2010, Calgary, Alberta, Abstract, 4 p.

Carlson, S.M., Hillier, W.D., Hood, C.T., Pryde, R.P. and Skelton, D.N. (1999): The Buffalo Hills kimberlites: a newly-discovered diamondiferous kimberlite province in north-central Alberta, Canada; *in* Proceedings of the Seventh International Kimberlite Conference, J.J. Gurney, J.L. Gurney, M.D. Pascoe, and S.H. Richardson (ed.), v. 1, p. 109–116.

Chacko, T., De, S.K., Creaser, R.A. and Muehlenbachs, K. (2000): Tectonic setting of the TMZ at 1.9–2.0 Ga: a granitoid-based perspective; Canadian Journal of Earth Sciences, v. 37, no. 11, p. 1597–1609.

Civetta, L., Innocenti, F., Manetti, P., Peccerillo, A. and Poli, G. (1981): Geochemical characteristics of potassic volcanics from Mt. Ernici (southern Latium, Italy); Contributions to Mineralogy and Petrology, v. 78, no. 1, p. 37–47.

Clement, C.R. (1982): A comparative geological study of some major kimberlite pipes in the Northern Cape and Orange Free State, Ph.D. thesis, University of Cape Town, 432 p. plus figures, tables and appendices.

Creaser, R.A., Grütter, H., Carlson, J. and Crawford, B. (2004): Macrocrystal phlogopite Rb-Sr dates for the Ekati property kimberlites, Slave Province, Canada: evidence for multiple intrusive episodes in the Paleocene and Eocene; Lithos, v. 76, no. 1-4, p. 399–414.

Creighton, S. and Eccles, D.R. (2003): A preliminary study of the mineral chemistry of selected Alberta kimberlites; 8th International Kimberlite Conference, Extended Abstracts (CD-ROM).

Creighton, S. and Stachel, T. (2008): An empirical chromite classification for positive identification of kimberlite in diamond exploration; 9th International Kimberlite Conference, Extended Abstracts, 9IKC-A-00402, 3 p.

Currie, C.A. and Beaumont, C. (2011): Are diamond-bearing Cretaceous kimberlites related to low-angle subduction beneath western North America?; Earth and Planetary

Science Letters, v. 303, no. 1-2, p. 59–70, doi:10.1016/j.epsl.2010.12.036.

Davies, R.M., Griffin, W.L., O' Reilly, S.Y. and McCandless, T.E. (2004): Inclusions in diamonds from the K14 and K10 kimberlites, Buffalo Head Hills, Alberta, Canada: diamond growth in a plume?; Lithos, v. 77, no. 1-4, p. 99–111.

Dawson, F.M., Jerzykiewicz, T. and Sweet, A.R. (1989): A preliminary analysis of the stratigraphy and sedimentology of the coal bearing Wapiti Group, northwestern Alberta; *in* Advances in western Canadian coal geoscience, forum proceedings, W. Langenberg (comp.), Alberta Research Council, Alberta Geological Survey, Information Series 103, p. 1–11, URL <http://www.ags.gov.ab.ca/publications/abstracts/INF_103.html> [December 2010].

Dawson, J.B. and Smith, J.V. (1982): Upper mantle amphiboles: a review; Mineralogical Magazine, v. 45, no. 337, p. 35–46.

Dawson, J.B. and Stephens, W.E. (1975): Statistical classification of garnets from kimberlite and associated xenoliths; Journal of Geology, v. 83, no. 5, p. 589–607.

De, S.K., Chacko, T., Creaser, R.A. and Muehlenbachs, K. (2000): Geochemical and Nd-Pb-O isotope systematics of granites from the Taltson magmatic zone, northeastern Alberta: implications for early Proterozoic tectonics in western Laurentia; Precambrian Research, v. 102, no. 3-4, p. 221–249.

Deer, W.A., Howie, R.A. and Zussman, J. (1963): Rock forming minerals, volume 2; Longman Publishing, London, United Kingdom.

Dobrzhinetskaya, L., Green, H.W., II and Wang, S. (1996): Alpe Arami: a peridotite massif from depths of more than 300 kilometres; Science, v. 271, no. 5257, p. 1841–1845.

Dowall, D., Nowell, G., Pearson, D.G. and Kjarsgaard, B. (2000): The nature of kimberlite source regions: a Hf-Nd isotopic study of Slave craton kimberlites; Goldschmidt 2000 (Tenth Annual Goldschmidt Conference, September 3–8, 2000), Journal of Conference Abstracts, v. 5, no. 2, p. 357, URL <http://www.the-conference.com/JConfAbs/5/357.pdf> [January 2011].

Droop, G.T.R. (1987): A general equation for estimating Fe^{3+} concentrations in ferromagnesian silicates and oxides from microprobe analyses, using stoichiometric criteria; Mineralogical Magazine, v. 51, no. 361, p. 431–435.

Dufresne, M.B. and Banas, A. (2009): Assessment report for the Legend Property, Birch Mountains, northern Alberta; Alberta Energy, Mineral Assessment Report 20090010, 40 p.

Dufresne, M.B. and Eccles, D.R. (2005): A guide to kimberlite-indicator mineral trends in Alberta, including observations from recently compiled indicator mineral data; Alberta Energy and Utilities Board, EUB/AGS Special Report 20, 277 p., URL <http://www.ags.gov.ab.ca/publications/abstracts/SPE_020.html> [December 2010].

Dufresne, M.B., Banas, A. and Testo, B. (2010): The Western Canada Sedimentary Basin exploration experience—a look at the new kimberlite discoveries in the Buffalo Head Hills; *in* Kimberlites and related rocks in the Western Canada Sedimentary Basin, GeoCanada 2010 Short Course, Calgary, Alberta, 4 p.

Dufresne, M.B., Carey, H. and Raffle, K. (2007): Assessment report for the Legend property, Birch Mountains, northern Alberta; Alberta Energy, Mineral Assessment Report 20070016, 38 p.

Dufresne, M.B., Eccles, D.R. and Leckie, D.A. (2001): The geological and geochemical setting of the mid-Cretaceous Shaftesbury formation and other Colorado Group sedimentary units in northern Alberta; Alberta Energy and Utilities Board, EUB/AGS Special Report 9, 108 p., URL <http://www.ags.gov.ab.ca/publications/abstracts/SPE_009.html> [December 2010].

Dufresne, M.B., Eccles, D.R., McKinstry, B., Schmitt, D.R., Fenton, M.M., Pawlowicz, J.G. and Edwards, W.A.D. (1996): The diamond potential of Alberta; Alberta Energy, Alberta Geological Survey, Bulletin 63, 158 p., URL <http://www.ags.gov.ab.ca/publications/abstracts/BUL_063.html> [December 2010].

Dyke, A.S., Andrews, J.T., Clark, P.U., England, J.H., Miller, G.H., Shaw, J. and Veillette, J.J. (2002): The Laurentide and Innutian ice sheets during the last glacial maximum; Quaternary Science Reviews, v. 21, no. 1-3, p. 9–31.

Eccles, D.R. (2004): Petrogenesis of the northern Alberta kimberlite province; M.Sc. thesis, University of Alberta, 191 p.

Eccles, D.R. (2007a): Alberta kimberlite xenocryst dataset; Alberta Energy and Utilities Board, EUB/AGS Digital Dataset 2007-0008, URL <http://www.ags.gov.ab.ca/publications/abstracts/DIG_2007_0008.html> [December 2010].

Eccles, D.R. (2007b): Alberta diamond occurrences dataset; Alberta Energy and Utilities Board, EUB/AGS Digital Dataset 2007-0009, URL <http://www.ags.gov.ab.ca/publications/abstracts/DIG_2007_0009.html> [December 2010].

Eccles, D.R. (2009): Compositions of low-chromium garnet xenocrysts from selected ultramafic bodies in the northern Alberta kimberlite province; Energy Resources Conservation Board, ERCB/AGS Open File Report 2009-21, 20 p., URL <http://www.ags.gov.ab.ca/publications/abstracts/OFR_2009_21.html> [December 2010].

Eccles, D.R. and Luth, R.W. (2001): Major- and trace-element geochemistry of ultramafic diatremes in Alberta; Alberta Energy and Utilities Board, EUB/AGS Earth Sciences Report 2001-05, 56 p., URL <http://www.ags.gov.ab.ca/publications/abstracts/ESR_2001_05.html> [December 2010].

Eccles, D.R. and Nowicki, T. (2010): Northern Alberta mantle cross-section; *in* Kimberlites and related rocks in the Western Canada Sedimentary Basin, GeoCanada 2010 Short Course, Calgary, Alberta, 5 p.

Eccles, D.R. and Simonetti, A. (2008): A study of peridotitic garnet xenocryst compositions from selected ultramafic bodies in the northern Alberta kimberlite province: implications for mantle stratigraphy and garnet classification; Energy Resources Conservation Board, ERCB/AGS Earth Sciences Report 2008-01, 40 p., URL <http://www.ags.gov.ab.ca/publications/abstracts/ESR_2008_01.html> [December 2010].

Eccles, D.R., Creaser, R.A., Heaman, L.M. and Ward, J. (2008a): Rb-Sr and U-Pb geochronology and setting of the Buffalo Head Hills kimberlite field, northern Alberta; Canadian Journal of Earth Sciences, v. 45, no. 5, p. 513–529.

Eccles, D.R., Dufresne, M.B., Copeland, D.A., Csanyi, W. and Creighton, S. (2002): Alberta kimberlite-indicator mineral geochemical compilation; Alberta Energy and Utilities Board, EUB/AGS Earth Sciences Report 2001-20, 4 p. plus data, URL <http://www.ags.gov.ab.ca/publications/abstracts/ESR_2001_20.html> [December 2010].

Eccles, D.R., Grunsky, E.C., Grobe, M. and Weiss, J. (2001): Structural emplacement model for kimberlitic diatremes in northern Alberta; Alberta Energy and Utilities Board, EUB/AGS Earth Sciences Report 2000-01, 106 p., URL <http://www.ags.gov.ab.ca/publications/abstracts/ESR_2000_01.html> [December 2010].

Eccles, D.R., Haynes, M. and Csanyi, W. (2000): Diamond and metallic-mineral potential of the Peerless Lake map area, north-central Alberta; Alberta Energy and Utilities Board, EUB/AGS Earth Sciences Report 2000-08, 88 p., URL <http://www.ags.gov.ab.ca/publications/abstracts/ESR_2000_08.html> [December 2010].

Eccles, D.R., Heaman, L.M., Luth, R.W. and Creaser, R.A. (2004): Petrogenesis of the Late Cretaceous northern Alberta kimberlite province; Lithos, v. 76, no. 1-4, p. 435–459.

Eccles, D.R., Schmidberger, S.S. and Cox, R. (2010): Garnet pyroxenite and granulite xenoliths from northeastern Alberta: evidence of a 1.5 Ga lower crust and mantle in western Laurentia; Precambrian Research, v. 177, no. 3-4, p. 339–354.

Eccles, D.R., Sweet, A.R., Creaser, R.A., Heaman, L.M. and Boyce, K. (2008b): Emplacement characteristics of Late Cretaceous and Paleocene volcaniclastic and coherent kimberlite in northern Alberta, Canada; oral presentation at Saskatchewan Geological Survey, Open House, December 2008.

Edmonton Journal (1998): Alberta has "tremendous potential" for diamonds; Edmonton Journal, January 3, 1998, p. D1.

Fenton, M.M. and Pawlowicz, J.G. (1997): Diamond indicator mineral anomaly from till sample site NAT95-134; Alberta Energy and Utilities Board, EUB/AGS Geo-Note 1997-01, 6 p., URL <http://www.ags.gov.ab.ca/publications/abstracts/GEO_1997_01.html> [December 2010].

Fialps-Guedon, C.I., Robert, J.L. and Delbove, F. (2000): Experimental study of Cr-incorporation in pargasite; American Mineralogist, v. 85, no. 5-6, p. 687–693.

Field, M. and Scott Smith, B.H. (1999): Contrasting geology and near-surface emplacement of kimberlite pipes in southern Africa and Canada; *in* Proceedings of the Seventh International Kimberlite Conference, Cape Town, South Africa, J.J. Gurney, J.L. Gurney, M.D. Pascoe and S.H. Richardson (ed.), Red Roof Design cc, South Africa, v. 1, p. 214–237.

Field, S.W., Haggerty, S.E. and Erlank, A.J. (1989): Subcontinental metasomatism in the region of Jagersfontein, South Africa; *in* Kimberlites and related rocks, volume 2: their mantle/crust setting, diamonds and diamond exploration, J. Ross (ed.), Geological Society of Australia, Special Publication 14, p. 771–783.

Fipke, C.E., Gurney, J.J. and Moore, R.O. (1995): Diamond exploration techniques emphasising indicator mineral chemistry and Canadian examples; Geological Survey of Canada, Bulletin 423, 86 p.

French, A.C. (2010): Update and summary of the geology of the K14 kimberlite, Buffalo Hills, Alberta; *in* Kimberlites and related rocks in the Western Canada Sedimentary Basin, GeoCanada 2010, Short Course, 3 p.

Griffin, W.L., O'Reilly, S.Y., Doyle, B.J., Pearson, N.J., Coopersmith, H., Kivi, K., Malkovets, V. and Pokhilenko, N. (2004): Lithosphere mapping beneath the North America plate; Lithos, v. 77, no. 1-4, p. 873–922.

Griffin, W.L., Shee, S.R., Ryan, C., Win, R.R. and Wyatt, B.A. (1999): Harzburgite to lherzolite and back again: metasomatic processes in ultramafic xenoliths from the Wesselton kimberlite, Kimberley, South Africa; Contributions to Mineralogy and Petrology, v. 134, no. 2-3, p. 232–250.

Grütter, H.S. and Apter, D.B. (1998): Kimberlite-and lamproite-borne chromite phenocrysts with "diamond-inclusion"-type chemistries; *in* Seventh International Kimberlite Conference, J.J. Gurney, J.L. Gurney, M.D. Pascoe and S.H. Richardson (ed.); Red Roof Design cc, South Africa, Extended Abstracts, p. 280–282.

Grütter, H.S., Apter, D.B. and Kong, J. (1999): Crust-mantle coupling: evidence from mantle-derived xenocrystic garnets; *in* Proceedings of the Seventh International Kimberlite Conference, J.J. Gurney, J.L. Gurney, M.D. Pascoe and S.H. Richardson (ed.), Red Roof Design cc, South Africa, p. 307–313.

Grütter, H.S., Gurney, J.J., Menzies, A.H. and Winter, F. (2004): An updated classification scheme for mantle-derived garnet, for use by diamond explorers; Lithos, v. 77, no. 1-4, p. 841–857.

Gurney, J.J. (1984): A correlation between garnets and diamonds in kimberlite; *in* Kimberlite occurrence and origin: a basis for conceptual models in exploration, J.E. Glover and P.G.

Harris, (ed.), University of Western Australia, Publication 8, p. 143–166.

Gurney, J.J., Helmstaedt, H. and Moore, R.O. (1993): A review of the use and application of mantle mineral geochemistry in diamond exploration; Pure and Applied Chemistry, v. 65, no. 12, p. 2423–2442.

Hamilton, W.N., Langenberg, W.C., Price, M.C. and Chao, D.K. (1999): Geological map of Alberta; Alberta Energy and Utilities Board, EUB/AGS Map 236, scale 1: 1 000 000, URL http://www.ags.gov.ab.ca/publications/abstracts/MAP_236.html [January 2011].

Harris, M., le Roex, A.P. and Class, C. (2004): Geochemistry of the Uintjiesberg kimberlite, South Africa: petrogenesis of an off-craton Group I kimberlite; Lithos, v. 74, no. 3-4, p. 149–165.

Hauff, P.L., Eccles, D.R. and Grunsky, E. (2001): Alteration mineralogy of Alberta kimberlites: PIMA™ infrared spectroscopic analysis; Alberta Energy and Utilities Board, EUB/AGS Special Report 12, 74 p., URL <http://www.ags.gov.ab.ca/publications/abstracts/SPE_012.html> [December 2010].

Heaman, L.M., Kjarsgaard, B.A. and Creaser, R.A. (2004): The temporal evolution of North American kimberlites; Lithos, v. 76, no. 1-4, 377–397.

Hearn, B.C., Jr. (1986): Alkalic ultramafic magmas in north-central Montana, USA: genetic connections of alnöite, kimberlite, and carbonatite; *in* Proceedings of the Fourth International Kimberlite Conference, J. Ross et al. (ed.), Geological Society of Australia Special Publication 14, Blackwell Scientific Publications, p. 109–119.

Hein, F.J. and Eccles, D.R. (2008): Preliminary stratigraphic framework for selected kimberlites in the Buffalo Head Hills region, north-central Alberta; Energy Resources Conservation Board, ERCB/AGS Geo-Note 2008-02, 66 p., URL <http://www.ags.gov.ab.ca/publications/abstracts/GEO_2008_02.html> [December 2010].

Hoffman, P.F. (1988): United plates of America: the birth of a craton; Annual Review of Earth and Planetary Sciences, v. 16, p. 543–604.

Hoffman, P.F. (1989): Precambrian geology and tectonic history of North America; *in* The geology of North America—an overview; Geological Society of America, v. A, p. 447–512.

Hood, C.T.S. and McCandless, T.E. (2004): Systematic variations in xenocryst mineral composition at the province scale, Buffalo Hills kimberlites, Alberta, Canada; Lithos, v. 77, no. 1-4, p. 733–747.

Hope, J. and Eaton, D. (2002): Crustal structure beneath the Western Canada Sedimentary Basin: constraints from gravity and magnetic modelling; *in* Special issue: the LITHOPROBE Alberta basement transect, G. Ross (ed.), Canadian Journal of Earth Sciences, v. 39, p. 291–312.

Jerzykiewicz, T. (1997): Stratigraphic framework of the uppermost Cretaceous to Paleocene strata of the Alberta Basin; Geological Survey of Canada, Bulletin 510, 121 p.

Keith, J.W. (1970): Tectonic control of Devonian reef sedimentation, Alberta; American Association of Petroleum Geologists Bulletin, v. 54, p. 854.

Keith, T. (2004): Cr-rich amphiboles within till as potential kimberlite indicator minerals, southern Buffalo Head Hills, Alberta; B.Sc. thesis, University of Alberta, 61 p.

Kellett, R.L., Steensma, G.J. and Zahynacz, R.M. (2005): Geophysical signature of the Mountain Lake intrusion: a study to support future kimberlite exploration in Alberta; Alberta Energy and Utilities Board, EUB/AGS Special Report 64, 37 p., URL <http://www.ags.gov.ab.ca/publications/abstracts/SPE_064.html> [December 2010].

Kennedy, C.S. and Kennedy, G.C. (1976): The equilibrium boundary between graphite and diamond; Journal of Geophysical Research, v. 81, no. 14, p. 2467–2470.

Kjarsgaard, B.A. (1994): Potassic magmatism in the Milk River area, southern Alberta: petrology and economic potential; *in* Current research 1994-B, Geological Survey of Canada, p. 59–68.

Kjarsgaard, B.A. (1997): Diamond in Alberta: studies of potential host rocks of deep-seated origin and applications of indicator mineral exploration techniques; *in* Exploring for minerals in Alberta: Geological Survey of Canada geoscience contributions, Canada-Alberta Agreement on Mineral Development (1992–1995), R.W. Macqueen (ed.), Geological Survey of Canada, Bulletin 500, p. 185–208.

Kjarsgaard, B.A., Pearson, D.G. and Malarkey, J. (2010): The kimberlite olivine phenocryst/ macrocryst/ xenocryst problem, re-visited; GeoCanada 2010, Cratons, Kimberlites and Diamonds plenary session, abstract, 2 p.

Kjarsgaard, B.A., Pearson, D.G., Tappe, S., Nowell, G.M. and Dowall, D.P. (2009): Geochemistry of hypabyssal kimberlites from Lac de Gras, Canada: comparisons to a global database and applications to the parent magma problem; Lithos, v. 112S, p. 236–248.

Kopylova, M.G., Price, S.E. and Russell, J.K. (2000): Primitive magma from the Jericho pipe, N.W.T., Canada: constraints on primary kimberlite melt chemistry; Journal of Petrology, v. 41, no. 6, p. 789–808.

Le Bas, M.J. (1989): Nephelinitic and basanitic rocks; Journal of Petrology, v. 30, no. 5, p. 1299–1312.

Leckie, D.A., Kjarsgaard, B.A., Peirce, J.W., Grist, A.M., Collins, M., Sweet, A., Stasiuk, L., Tomica, M.A., Eccles, D.R., Dufresne, M.B., Fenton, M.M., Pawlowicz, J.G., Balzer, S.A., McIntyre, D.J. and McNeil, D.H. (1997): Geology of a Late Cretaceous possible kimberlite at Mountain Lake, Alberta—chemistry, petrology, indicator minerals, aeromagnetic signature, age, stratigraphic position and setting; Geological Survey of Canada, Open File 3441, 202 p.

Le Maitre, R.W. (1976): The chemical variability of some common igneous rocks; Journal of Petrology, v. 17, no. 4, p. 589–598.

Le Maitre, R.W. (1989): A classification of igneous rocks and glossary of terms: recommendations of the IUGS Commission on the Systematics of Igneous Rocks; Blackwell Scientific Publishers, Oxford, United Kingdom, 193 p.

le Roex, A.P., Bell, D.R. and Davis, P. (2003): Petrogenesis of Group I kimberlites from Kimberley, South Africa: evidence from bulk-rock geochemistry; Journal of Petrology, v. 44, no. 12, p. 2261–2286.

MacGregor, I.D. and Carter, J.L. (1970): The chemistry of clinopyroxenes and garnets of eclogite and peridotite xenoliths from the Roberts Victor mine, South Africa; Physics of the Earth and Planetary Interiors, v. 3, p. 391–397.

McCandless, T.E. (1999): Kimberlite: mantle expressions of deep-seated subduction; *in* Proceedings of the 7th International Kimberlite Conference, J.J. Gurney, J.L. Gurney, M.D. Pascoe and S.H. Richardson (ed.), v. 2, p. 545–549.

McCandless, T.E. and Gurney, J.J. (1989): Sodium in garnet and potassium in clinopyroxene: criteria for classifying mantle eclogites; *in* Kimberlites and related rocks, J. Ross (ed.), Geological Society of Australia, Special Publication 14, v. 2, p. 827–832.

McDonough, M.R., McNicoll, V.J. and Schetselaar, E.M. (1995): Age and kinematics of crustal shortening and escape in a two-sided oblique-slip collisional and slip orogen, Paleoproterozoic TMZ, northeastern Alberta; *in* 1995 Alberta basement transects workshop, G.M. Ross (ed.), LITHOPROBE Secretariat, University of British Columbia, LITHOPROBE Report 47, p. 264–308.

McNicoll, V.J., McDonough, M.R. and Grover, T. (1994): U-Pb geochronological studies in the southern TMZ, northeastern Alberta; *in* Report of LITHOPROBE Alberta basement transects workshop, G.M. Ross (ed.),

LITHOPROBE Secretariat, University of British Columbia, LITHOPROBE Report 37, p. 270–273.

McNicoll, V.J., Theriault, R.J. and McDonough, M.R. (2000): Taltson Basement Gneisses: U-Pb and Nd isotopic constraints of the basement to the Paleoproterozoic TMZ, northeastern Alberta; Canadian Journal of Earth Sciences, v. 37, no. 11, p. 1575–1596.

Menzies, M. (1983): Mantle ultramafic xenoliths in alkaline magmas: evidence for mantle heterogeneity modified by magmatic activity; *in* Continental basalts and mantle xenoliths, C.J. Hawkesworth and M.J. Norry (ed.), Shiva Publishers, Nantwich, United Kingdom, Geology Series, p. 92–110.

Mitchell, R.H. (1986): Kimberlites: mineralogy, geochemistry, and petrology; Plenum Press, New York, 442 p.

Mitchell, R.H. (1995): Kimberlites, orangeites, and related rocks; Plenum Press, New York, New York, 410 p.

Mitchell, R.H. and Bergman, S.C. (1991): Petrology of lamproites; Plenum Press, New York, New York, 447 p.

Moore, R.O., Gurney, J.J., Griffin, W.L. and Shimzu, N. (1991): Ultra-high pressure garnet inclusions in Monastery diamonds: trace element abundance patterns and conditions of origin; European Journal of Mineralogy, v. 3, no. 2, p. 213–230.

Morimoto, N., Fabries, J., Ferguson, A.K., Ginzburg, I., V., Ross, M., Seifert, F.A., Zussman, J., Aoki, K. and Gottardi, G. (1988): Nomenclature of pyroxenes; American Mineralogist, v. 73, no. 9-10, p. 1123–1133.

Morris, T.F., Sage, R.P., Ayer, J.A. and Crabtree, D.C. (2002): A study in clinopyroxene composition: implications for kimberlite exploration; Geochemistry, Exploration and Environment Analysis, v. 2, no. 4, p. 321-331.

Mossop, G.D. and Shetsen, I. (1994): Introduction; *in* Geological atlas of the Western Canadian Sedimentary Basin, G.D. Mossop and I. Shetsen (comp.), Canadian Society of Petroleum Geologists and Alberta Research Council, p. 1–12, URL <http://www.ags.gov.ab.ca/publications/wcsb_atlas/atlas.html> [December 2010].

Muehlenbachs, K., Burwash, R.A. and Chacko, T. (1993): A major oxygen isotope anomaly in the basement rocks of Alberta; *in* Alberta basement transects workshop, G.M. Ross (ed.), LITHOPROBE Secretariat, University of British Columbia, LITHOPROBE Report 31, p. 120–124.

Nimis, P. and Taylor, W.R. (2000): Single clinopyroxene thermobarometry for garnets peridotites, part I: calibration and testing of a Cr-in-Cpx barometer and an enstatite-in-Cpx thermometer; Contributions to Mineralogy and Petrology, v. 139, no. 5, p. 541–554.

Northern Miner (1997a): Ashton pulls diamonds from property in Alberta; Northern Miner, May 26, 1997, p. 6.

Northern Miner (1997b): Ashton, Pure Gold find more diamonds in Alberta; Northern Miner, September 29, 1997, p. D2.

Nowicki, T.E. and Harvey, S.E. (2010): Composition of garnet xenocrysts from kimberlite of Saskatchewan; *in* Kimberlites and related rocks in the Western Canada Sedimentary Basin, GeoCanada 2010, Short Course, 5 p.

O'Brien, H.E., Irving, A.J., McCallum, I.S. and Thirwall, M.F. (1995): Strontium, neodymium and lead isotopic evidence for the interaction of post-subduction asthenospheric potassic mafic magmas of the Highwood Mountains, Montana, USA, with ancient Wyoming craton lithospheric mantle; Geochimica et Cosmochimica Acta, v. 59, p. 4539–4556.

O'Connell, S.C., Dix, G.R. and Barclay, J.E. (1990): The origin, history and regional structural development of the Peace River Arch, Western Canada; Bulletin of Canadian Petroleum Geology, v. 38A, p. 4–24.

Okulitch, A.V. (2002): Geological time chart, 2002; Geological Survey of Canada, Open File 3040, chart.

Paganelli, F., Grunsky, E.C. and Richards, J.P. (2002): Structural interpretation of RADARSAT-1 principal components imagery and its potential application to kimberlite exploration in the Buffalo Head Hills area, north-central Alberta; Alberta Energy and Utilities Board, EUB/AGS Special Report 21, 52 p., URL <http://www.ags.gov.ab.ca/publications/abstracts/SPE_021.html> [December 2010].

Pană, D.I. and Eccles, D.R. (2003): Structural control of kimberlite pipes in the Buffalo Head Hills–Loon River Lowlands area: evidence versus conventional wisdom; 12th Annual Calgary Mining Forum, Abstracts, p. 45.

Pană, D.I., Waters, E.J. and Grobe, M. (2001): GIS compilation of structural elements in northern Alberta, release 1.0; Alberta Energy and Utilities Board, EUB/AGS Earth Sciences Report 2001-01, 53 p., URL <http://www.ags.gov.ab.ca/publications/abstracts/ESR_2001_01.html> [December 2010].

Pawlowicz, J.J. and Fenton, M.M. (1995): Drift thickness of Alberta; Alberta Energy and Utilities Board, EUB/AGS Map 227, scale 1:2 000 000, URL <http://www.ags.gov.ab.ca/publications/abstracts/MAP_227.html> [December 2010].

Pawlowicz, J.G., Fenton, M.M. and Weiss, J.A. (2005a): Auger core lithologs, Swan Lake area, southern Buffalo Head Hills, Alberta; Alberta Energy and Utilities Board, EUB/AGS Geo-Note 2005-07, 43 p., URL <http://www.ags.gov.ab.ca/publications/abstracts/GEO_2005_07.html> [December 2010].

Pawlowicz, J.G., Jean, G.M. and Fenton, M.M. (1995): Preliminary stratigraphic tests to support mineral exploration, northern Alberta: report for the end fiscal year 1994–95; Alberta Department of Energy, Alberta Geological Survey, Open File Report 1995-11, 34 p., URL <http://www.ags.gov.ab.ca/publications/abstracts/OFR_1995_11.html> [December 2010].

Pawlowicz, J.G., Prior, G.J., Dolby, G., Eccles, D.R. and Fenton, M.M. (2005b): Early to Late Campanian palynological ages of mudstone and siltstone in the Sawn Lake area, southern Buffalo Head Hills, Alberta; Alberta Energy and Utilities Board, EUB/AGS Geo-Note 2005-01, 19 p., URL <http://www.ags.gov.ab.ca/publications/abstracts/GEO_2005_01.html> [December 2010].

Pollack, H.N. and Chapman, D.S. (1977): On the regional variation of heat flow, geotherms and lithospheric thickness; Tectonophysics, v. 38, no. 3-4, p. 279–296.

Ramsay, R.R. and Tompkins, L.A. (1994): The geology, heavy mineral concentrate mineralogy, and diamond prospectivity of the Boa Esperanca and Cana Verde pipes, Corrego D'anta, Minas Gerais, Brazil; *in* Proceedings of the Fifth International Kimberlite Conference: kimberlites, related rocks and mantle xenoliths, H.O.A. Meyer and O.H. Leonardos (ed.), CPRM Special Publication, Brasil, p. 329–345.

Ranger, I.M. (2004): Petrology and geochronology from basement core of the Paleoproterozoic Red Earth Granulite domain, north-central Alberta; M.Sc. thesis, University of Alberta, 175 p.

Rich, A. (2003): Assessment report on the Mountain Lake permits; Alberta Energy, Mineral Assessment Report 20030007, 13 p.

Ross, G.M. and Eaton, D.W. (1997): Winagami reflection sequence: seismic evidence for post-collisional magmatism in the Proterozoic of Western Canada; Geology, v. 25, no. 3, p. 199–202.

Ross, G.M. and Eaton, D.W. (2002): Proterozoic tectonic accretion and growth of western Laurentia: results from LITHOPROBE studies in northern Alberta; Canadian Journal of Earth Sciences, v. 39, no. 3, p. 313–329.

Ross, G.M., Broome, J. and Miles, W. (1994): Potential fields and basement structure—

Western Canada Sedimentary Basin; *in* Geological atlas of the Western Canadian Sedimentary Basin, G.D. Mossop and I. Shetson (comp.), Canadian Society of Petroleum Geologists and Alberta Research Council, p. 41–48.

Ross, G.M., Parrish, R.R., Villeneuve, M.E. and Bowring, S.A. (1991): Geophysics and geochronology of the crystalline basement of the Alberta Basin, Western Canada; Canadian Journal of Earth Sciences, v. 28, no. 4, p. 512–522.

Schulze, D.J. (1987): Megacrysts from alkaline volcanic rocks; *in* Mantle xenoliths, P.H. Nixon (ed.), John Wiley & Sons Ltd., New York, New York, p. 433–452.

Schulze, D.J. (1997): The significance of eclogite and Cr-poor megacryst garnets in diamond exploration; Exploration and Mining Geology, v. 6, no. 4, p. 349–366.

Schulze, D.J., Anderson, P.F.N., Hearn, B.C. and Hetman, C.M. (1995): Origin and significance of ilmenite megacrysts and macrocrysts from kimberlite; International Geology Review, v. 37, no. 9, p. 780–812.

Sikabonyi, L.A. and Rodgers, W.J. (1959): Paleozoic tectonics and sedimentation in the northern half of the west Canadian Basin; Journal of the Alberta Society of Petroleum Geologists, v. 7, no. 9, p. 193–216.

Skelton, D. and Bursey, T. (1998): Assessment report: Buffalo Head Hills property (AL01), Ashton Mining of Canada Inc.; Alberta Energy, Mineral Assessment Report 19980015, 155 p.

Skelton, D. and Bursey, T. (1999): Assessment report: Buffalo Head Hills (AL01), Loon Lake (AL02), Birch Mountain (AL03), Rabbit Lake (AL04), and Muddy River (AL05) properties, Ashton Mining of Canada Inc.; Alberta Energy, Mineral Assessment Report 19990011, 1126 p.

Skelton, D. and Willis, D. (2002): Assessment report for the Buffalo Hills property, 2002, Ashton Mining of Canada Inc.; Alberta Energy, Mineral Assessment Report 20020010, 279 p.

Skelton, D., Clements, B., McCandless, T.E., Hood, C., Aulbach, S., Davies, R. and Boyer, L.P. (2003): The Buffalo Head Hills kimberlite province, Alberta; Proceedings of the 8th International Kimberlite Conference, Northern Alberta–Slave Kimberlite Field Trip Guide Book, p. 11–20.

Skinner, E.M.W. and Marsh, J.S. (2004): Distinct kimberlite pipe classes with contrasting eruption processes; Lithos, v. 76, no. 1-4, p. 183–200.

Skupinski, A. and Langenberg, C.W. (2002): Petrography of the Mountain Lake pipe, Grande Prairie area, Alberta, Canada; Alberta Energy and Utilities Board, EUB/AGS Special Report 15, 38 p., URL <http://www.ags.gov.ab.ca/publications/abstracts/SPE_015.html> [December 2010].

Smith, C.B. (1983): Pb, Sr and Nd isotopic evidence for sources of southern African Cretaceous kimberlites; Nature, v. 304, p. 51–54.

Smith, C.B., Gurney, J.J., Skinner, E.M.W., Clement, C.R. and Ebrahim, N. (1985): Geochemical character of southern African kimberlites: a new approach based on isotopic constraints; South African Journal of Geology, v. 88, no. 2, p. 267–280.

Sobolev, N.V., Lavrent'ev, Y.G., Pokhilenko, N.P. and Usova, L.V. (1973): Chrome-rich garnets from the kimberlites of Yakutia and their paragenesis; Contributions to Mineralogy and Petrology, v. 40, no. 1, p. 39–52.

Stacey, J.S. and Kramers, J.D. (1975): Approximation of terrestrial lead isotope evolution by a two-stage model; Earth and Planetary Science Letters, v. 26, no. 2, p. 207-221.

Stachel, T., Banas, A. and McCandless, T.E. (2010): Diamonds in the Western Canada Sedimentary Basin; *in* Kimberlites and related rocks in the Western Canada Sedimentary Basin, GeoCanada 2010 Short Course, 3 p.

Stachel, R., Brey, G.P. and Harris, J.W. (2000): Kankan diamonds (Guinea) I: from the lithosphere down to the transition zone; Contributions to Mineralogy and Petrology, v. 140, no. 1, p. 1–15.

Sturm, R. (2002): PX-NOM—an interactive spreadsheet program for the computation of pyroxene analyses derived from the electron microprobe; Computers and Geosciences, v. 28, no. 4, p. 473–483.

Sun S-s. and McDonough, W.F. (1989): Chemical and isotopic systematics of oceanic basalts: implications for mantle compositions and processes; *in* Magmatism in the ocean basins, A.D. Saunders and M.J. Norry (ed.), Geological Society, London, Special Publication 42, p. 313–345.

Sweet, A.R., Eccles, R. and Boyce, K. (2006): Kimberlite, host rocks, hiatuses and palynology; north-central Alberta kimberlite fields (abstract); Geological Society of America, Annual Meeting, October 22–25, Philadelphia, Pennsylvania.

Switzer, S.B., Holland, W.G., Christie, D.S., Graf, G.C., Hedinger, A.D., McAuley, R.J., Wierzbicki, R.A. and Packard, J.J. (1994): Devonian Woodbend-Winterburn strata of the Western Canada Sedimentary Basin; *in* Geological atlas of the Western Canada Sedimentary Basin, G.D. Mossop and I. Shetsen (comp.), Canadian Society of Petroleum Geologists and Alberta Research Council, p. 165–202.

Taylor, W.R., Tompkins, L.A. and Haggerty, S.E. (1994) Comparative geochemistry of West African kimberlites: evidence for a micaceous kimberlite end-member of sublithospheric origin; Geochimica et Cosmochimica Acta, v. 58, no. 19, p. 4017–4037.

Thériault, R.J. and Ross, G.M. (1991): Nd isotopic evidence for crustal recycling in the ca. 2.0 Ga subsurface of Western Canada; Canadian Journal of Earth Sciences, v. 28, no. 8, p. 1140–1147.

Trommelen, M.S., Paulen, R.C. and Weiss, J.A. (2006): Surficial geology of the Sawn Lake area (NTS 84B/13); Alberta Energy and Utilities Board, EUB/AGS Map 314, scale 1:50 000, URL <http://www.ags.gov.ab.ca/publications/abstracts/MAP_314.html> [December 2010].

Türkoğlu, E., Unsworth, M.J. and Pană, D.I. (2007): Deep electrical structure of Buffalo Head Hills, northern Alberta: implications for diamond exploration; Alberta Energy and Utilities Board, EUB/AGS Special Report 88, 27 p., URL <http://www.ags.gov.ab.ca/publications/abstracts/SPE_088.html> [December 2010].

Villeneuve, M.E., Ross, G.M., Theriault, R.J., Miles, W., Parrish, R.R. and Broome, J. (1993): Tectonic subdivision and U-Pb geochronology of the crystalline basement of the Alberta Basin, Western Canada; Geological Survey of Canada, Bulletin 447, 86 p.

Vollmer, R., Ogden, P., Schilling, J.G., Kingsley, R.H. and Waggoner, D.G. (1984): Nd and Sr isotopes in ultrapotassic volcanic rocks from the Leucite Hills, Wyoming; Contributions to Mineralogy and Petrology, v. 87, no. 4, p. 359–368.

Ward, J. and Willis, D. (2004): Assessment report for the Buffalo Head Hills Property 2004, Ashton Mining of Canada Inc.; Alberta Energy, Mineral Assessment Report 20040018, 84 p.

White, W.M. (1985): Sources of oceanic basalts: radiogenic isotopic evidence; Geology, v. 13, p. 115–118.

White, J.D.L., McPhie, J. and Skilling, I.P. (2000): Peperite: a useful genetic term; Bulletin of Volcanology, v. 62, p. 65–66.

Wood, B.D. and Williams, A.C. (1994): Mountain Lake prospect, Alberta, Monopros Ltd. metallic and industrial permits 9390080014, 9390080019 and 9390080020; Alberta Energy, Mineral Assessment Report 19940001, 5 p.

Wood, B.D., Scott Smith, B.H. and de Gasparis, S. (1998): The Mountain Lake kimberlitic

pipes of northwest Alberta: exploration, geology and emplacement model; *in* Seventh International Kimberlite Conference, J.J. Gurney, J.L. Gurney, M.D. Pascoe and S.H. Richardson (ed.), Red Roof Design cc, South Africa, Extended Abstracts, p. 960–962.

Wyatt, B.A., Baumgartner, M., Anckar, E. and Grütter, H. (2004): Compositional classification of 'kimberlitic' and 'non-kimberlitic' ilmenite; Lithos, v. 77, no. 1-4, p. 819–840.

Zindler, A. and Hart, S. (1986): Chemical geodynamics; Annual Review of Earth and Planetary Science, v. 14, p. 493–571.

Appendix 1 – Location, Geochronology and Diamond Estimates of Kimberlite and Related Rock Types in the Northern Alberta Kimberlite Province

Number	Kimberlite	NTS	UTM Location (NAD 27)[1]			Overburden Depth (m)[2]	Age (Ma)[3]	Error (±Ma)	Dating Technique	Initial Exploration Diamond Results			Mini-Bulk DMS Diamond Results		Location Reference	Age Reference	Diamond Reference
			Easting	Northing	Zone					Weight (kg)	Micro (<0.5 mm)	Macro (>0.5 mm)	Weight (tonnes)	Diamond (cpht)			
1	K1A	84B	569562	6284754	11	20–34	59.6	2.8	5-point Model 3 Rb-Sr phlogopite isochron (MSWD = 4.9)	184.3	2	0			Skelton and Bursey (1998)	Eccles et al. (2008)	Skelton and Bursey (1998)
1	K1B	84B	568989	6284585	11	15–19				182.1	2	2			Skelton and Bursey (1998)		Skelton and Bursey (1998)
2	K2	84B	571566	6287827	11	2–3				180.9	3	0			Skelton and Bursey (1998)		Skelton and Bursey (1998)
3	K3	84B	564460	6288865	11	26									Skelton and Bursey (1999)		
4	K4A	84B	578380	6301519	11	25–26				194.7	2	1			Skelton and Bursey (1998)		Skelton and Bursey (1998)
5	K4B	84B	578464	6300991	11	8-9				197.30	4	0			Skelton and Bursey (1998)		Skelton and Bursey (1998)
6	K4C	84B	578821	6301274	11	44–51									Skelton and Bursey (1998)		
7	K5A	84B	582488	6306214	11	3–57	87.6	4.6	U-Pb perovskite individual fraction	300.80	74	1			Skelton and Bursey (1998)	Carlson et al. (1999); Eccles et al. (2008)	Skelton and Bursey (1998)
7	K5B	84B	582812	6306408	11	50–56									Skelton and Bursey (1998)		
8	K6	84B	585263	6308732	11	0–variable				682.8	194	5	13.95 231.89	5.6 7.0	Skelton and Bursey (1998)		Skelton and Bursey (1998); Skelton and Willis (2002); Skelton et al. (2003): Ward and Willis (2004)
9	K7A	84B	583262	6311236	11	69	85.6	2.4	U-Pb perovskite weighted average (2 fractions)						Skelton and Bursey (1998)	Carlson et al. (1999); Eccles et al. (2008)	
10	K7B	84B	583131	6312089	11	35				101.40	1	0			Skelton and Bursey (1998)		Skelton and Bursey (1998)
11	K7C	84B	583053	6312455	11	37									Skelton and Bursey (1998)		
12	K8	84B	567934	6314643	11	41				274.20	4	1			Skelton and Willis (2002)		Skelton and Bursey (1999); Skelton and Willis (2002)
13	K10	84G	611098	6319234	11	127				99.10	4	1			Skelton and Bursey (1999)		Skelton and Bursey (1999)
14	K11	84G	619673	6320124	11	13–19	84.8	0.9	4-point Model 1 Rb-Sr phlogopite isochron (MSWD = <0.01)	189.50	106	14	21.85	4.4	Skelton and Bursey (1999)	Eccles et al. (2008)	Skelton and Bursey (1999); Skelton et al. (2003)
15	K14A	84B	582900	6315141	11	3–57	86.8 & 82.8	2.1 & 9.2	U-Pb perovskite weighted average (2 fractions), and 5-point Model 1 Rb-Sr phlogopite isochron (MSWD =	516.20	455	28	44.87 479 137	17 11.7 8	Skelton and Bursey (1998) Skelton and Bursey (1998) Skelton and Bursey (1998)	Carlson et al. (1999); Eccles et al. (2008); this report	Skelton and Bursey (1998); Skelton et al. (2003)
15	K14B	84B	582821	6315278	11	13–22											
15	K14C	84B	583030	6315357	11	0–32											
16	K15	84B	616150	6297113	11	43									Skelton and Bursey (1999)		
17	K19	84B	575033	6289103	11	4–5	60.3	0.8	4-point Model 1 Rb-Sr phlogopite isochron (MSWD = 1.7)						Skelton and Bursey (1998)	Eccles et al. (2008)	
18	K32	84B	602244	6295791	11	84				101.60	1	0			Skelton and Bursey (1999)		Skelton and Bursey (1999)
19	K91	84B	581820	6317052	11	10–15	86.1	3	U-Pb perovskite weighted average (2 fractions)	117.00	180	12	35.87	12.7	Skelton and Bursey (1999)	Carlson et al. (1999); Eccles et al. (2008)	Skelton and Bursey (1999); Skelton et al. (2003)
20	K92	84B	614124	6315852	11	81				89.90	2	1			Skelton and Bursey (1999)		Skelton and Bursey (1999)
21	K93	84B	613605	6316976	11	21									Skelton and Bursey (1999)		

Number	Kimberlite	NTS	UTM Location (NAD 27)[1]			Overburden Depth (m)[2]	Age (Ma)[3]	Error (±Ma)	Dating Technique	Initial Exploration Diamond Results			Mini-Bulk DMS Diamond Results		Location Reference	Age Reference	Diamond Reference
			Easting	Northing	Zone					Weight (kg)	Micro (<0.5 mm)	Macro (>0.5 mm)	Weight (tonnes)	Diamond (cpht)			
22	K95	84B	576317	6293011	11	24				189.60	2	0			Skelton and Bursey (1999)		Skelton and Bursey (1999)
23	K252	84B	584255	6309195	11	68–94	81.3	2.3	5-point Model 1 Rb-Sr phlogopite isochron (MSWD = 0.59)	226.90	244	19	22.8	55	Skelton and Willis (2002)	Eccles et al. (2008)	Skelton and Willis (2002)
24	BH225	84B	582702	6315670	11	24–32	68.4 & 81.5	5.2 & 5.1	U-Pb perovskite linear regression (4 fractions), and 2-point Rb-Sr phlogopite errorchron	96.00	67	5	1	3.5	Skelton and Willis (2002)	Carlson et al. (1999); Eccles et al. (2008); this report	Skelton and Willis (2002); Skelton et al. (2003)
25	BH229	84B	578790	6301843	11	53	83.3	5.4	4-point Model 2 Rb-Sr phlogopite isochron (MSWD = 14)						Skelton and Willis (2002)	Eccles et al. (2008)	
26	BH230	84B	564509	6289109	11	41				313.00	2	0			Skelton and Willis (2002)		Skelton and Willis (2002)
27	BH251	84B	577802	6301661	11	101									Skelton and Willis (2002)		
28	BH281	84B	595805	6301208	11	38				268.60	11	0			Skelton and Willis (2002)		Skelton and Willis (2002)
29	K296	84B	568757	6302291	11	30–47				324.00	173	2			Ward and Willis (2004)		Ward and Willis (2004)
30	K300	84B	569198	6298803	11	24–43				208.20	121	0			Ward and Willis (2004)		Ward and Willis (2004)
31	BE-01	84B	624796	6306797	11	125				265.35	2	0			M. Dufresne (pers. comm., 2010)		Grizzly Discoveries Ltd. news releases
32	BE-02	84B	627626	6303486	11	109				518.55	314	2			M. Dufresne (pers. comm., 2010)		Grizzly Discoveries Ltd. news releases
33	BE-03	84B	627252	6303753	11	66				365.35	218	0			M. Dufresne (pers. comm., 2010)		Grizzly Discoveries Ltd. news releases
34	BM2	84B	632349	6309823	11	44	63.5	0.7	U-Pb perovskite weighted average (6 fractions)						Skelton and Bursey (1999)	Carlson et al. (1999); Boyer et al. (2003); Eccles et al. (2008)	
35	BM3	84B	631219	6314208	11	88									Skelton and Bursey (1999)		
36	BM16	84B	631777	6314519	11	101									Skelton and Willis (2002)		
37	LL7	84B	622800	6245550	11	111									Skelton and Willis (2002)		
38	LL8	84B	629936	6301692	11	75	86	1.2	4-point Model 1 Rb-Sr phlogopite isochron (MSWD = 1.2)	270.00	2	0			Skelton and Bursey (1999)	Eccles et al. (2008)	Skelton and Bursey (1999)
39	WP	84B	583117	6315594	11	27				89.00	2	2			Skelton and Bursey (1999)		Skelton and Bursey (1999)
40	TQ155	84B	581750	6293950	11	34				509.10	71	0			Skelton and Willis (2002)		Skelton and Bursey (1999); Willis and Skelton (2002)
41	TQ160	84B	591150	6279919	11	39				45.90	2	0			Skelton and Willis (2002)		Skelton and Bursey (1999); Willis and Skelton (2002)
42	Dragon	84H	350875	6357480	12	122	72.4	0.91	5-point Rb-Sr phlogopite isochron (MSWD = 1.4)						Aravanis (1999)	Aravanis (1999)	
43	Kendu	84H	368561	6353407	12	99									L. Kryska (pers. comm., 2000)		
44	Legend	84H	386200	6340600	12	12	77.6	0.84	5-point Rb-Sr phlogopite isochron (MSWD = 1.2)	406.5	4	0	10.2	n/a	Aravanis (1999)	Aravanis (1999)	Aravanis (1999)
45	Pegasus	84H	374692	6368251	12	87									Aravanis (1999)		

Number	Kimberlite	NTS	UTM Location (NAD 27)[1]			Overburden Depth (m)[2]	Age (Ma)[3]	Error (±Ma)	Dating Technique	Initial Exploration Diamond Results			Mini-Bulk DMS Diamond Results		Location Reference	Age Reference	Diamond Reference
			Easting	Northing	Zone					Weight (kg)	Micro (<0.5 mm)	Macro (>0.5 mm)	Weight (tonnes)	Diamond (cpht)			
46	Phoenix	84H	351500	6330580	12	103	77.6, 70.9 & 70.3	1.1, 0.43 & 1.6	U-Pb perovskite weighted average (5 fractions), and 3-point Rb-Sr phlogopite isochron (MSWD = 1.2), and U-Pb perovskite weighted average (3 fractions)	384.7	3	2			Aravanis (1999)	Aravanis (1999); Eccles et al. (2008)	Aravanis (1999)
47	Roc	84H	365051	6357585	12	86									Aravanis (1999)		
48	Valkyrie	84H	362350	6355490	12	129–132	75.8	2.7	U-Pb perovskite weighted average (3 fractions)						Aravanis (1999)	Aravanis (1999)	
49	Xena	84H	376850	6347300	12	86	72.6	2.1	6-point Rb-Sr phlogopite isochron (MSWD = 0.98)						Aravanis (1999)	Aravanis (1999)	
50	Mountain Lake North	83N	454635	6145915	11	5.8	68, 76–75 & 78–72	n/a	Palynology on shale clasts, palynology on interbedded sediments and clasts, and apatite fission-track dating on sandstone	Insignificant quantities of diamonds					Leckie et al. (1997)	Leckie et al. (1997); Wood et al. (1998)	Wood et al. (1998)
51	Mountain Lake South	83N	454780	6145325	11	5.5									Leckie et al. (1997)		

[1] Location based on Universal Transverse Mercator (UTM) co-ordinate system; co-ordinates are based on a combination of selecting the centre of ground magnetic targets and drilling results

[2] When multiple drillholes tested the body, the range of overburden depths is provided.

[3] Rb-Sr model ages calculated assuming initial $^{87}Sr/^{86}Sr$ value of 0.705; isotopic data in Appendices 3a (U-Pb perovskite) and 3b (Rb-Sr phlogopite)

Abbreviations: DMS, dense-media separation; n/a, not available.

Appendix 2 – Government Reports and Datasets Considered during this Documentation of the Physical and Chemical Nature of the Northern Alberta Kimberlite Province

Author(s)	Year	Title	Source	Publication	Abstract and PDF Download Site or Journal Homepage
Eccles, D.R., Simonetti, S.S. and Cox, R.	2010	Garnet pyroxenite and granulite xenoliths from northeastern Alberta: evidence of ~1.5 Ga lower crust and mantle in western Laurentia	Precambrian Research	Volume 177, p. 339–354	Journal homepage: http://www.elsevier.com/locate/precamres
Eccles, D.R.	2009	Geochemical and petrographic evaluation of downhole gamma-ray anomalies in the Buffalo Head Hills kimberlite field, north-central Alberta (NTS 84B/13)	Alberta Geological Survey	Open File Report 2009-03	http://www.ags.gov.ab.ca/publications/abstracts/OFR_2009_03.html
Eccles, D.R.	2009	Compositions of low-chromium garnet xenocrysts from selected ultramafic bodies in the northern Alberta kimberlite province	Alberta Geological Survey	Open File Report 2009-21	http://www.ags.gov.ab.ca/publications/abstracts/OFR_2009_21.html
Eccles, D.R. and Simonetti, A.	2008	A study of peridotitic garnet xenocryst compositions from selected ultramafic bodies in the northern Alberta kimberlite province: implications for mantle stratigraphy and garnet classification	Alberta Geological Survey	Earth Sciences Report 2008-01	http://www.ags.gov.ab.ca/publications/abstracts/ESR_2008_01.html
Eccles, D.R., Creaser, R.A., Heaman, L.M. and Ward, J.	2008	Rb-Sr and U-Pg geochronology and setting of the Buffalo Head Hills kimberlite field, northern Alberta	Canadian Journal of Earth Science	Volume 45, p. 513–529	Journal homepage: http://pubs.nrc-cnrc.gc.ca/rp-ps/journalDetail.jsp?jcode=cjes
Eccles, D.R.	2007	Alberta diamond inclusion dataset	Alberta Geological Survey	Digital Dataset 2007-0006	http://www.ags.gov.ab.ca/publications/abstracts/DIG_2007_0006.html
Eccles, D.R.	2007	Alberta kimberlite xenocryst dataset	Alberta Geological Survey	Digital Dataset 2007-0008	http://www.ags.gov.ab.ca/publications/abstracts/DIG_2007_0008.html
Eccles, D.R.	2007	Alberta diamond occurrences dataset	Alberta Geological Survey	Digital Dataset 2007-0009	http://www.ags.gov.ab.ca/publications/abstracts/DIG_2007_0009.html
Türkoğlu, E., Unsworth, M. and Pană, D.I.	2007	Deep electrical structure of Buffalo Head Hills, northern Alberta: implications for diamond exploration	Alberta Geological Survey	Special Report 88	http://www.ags.gov.ab.ca/publications/abstracts/SPE_088.html
Atkinson, E., Pryde, R.	2006	Seismic investigation of selected kimberlite pipes in the Buffalo Head Hills kimberlite field, north-central Alberta	Alberta Geological Survey	Special Report 79	http://www.ags.gov.ab.ca/publications/abstracts/SPE_079.html
Dufresne, M.B. and Eccles, D.R.	2005	A guide to kimberlite-indicator mineral trends in Alberta including observations from recently compiled indicator mineral data	Alberta Geological Survey	Special Report 20	http://www.ags.gov.ab.ca/publications/abstracts/SPE_020.html
Kellett, R.L., Steensma, G.J. and Zahynacz, R.M.	2005	Geophysical signature of the Mountain Lake intrusion: a study to support future kimberlite exploration in Alberta	Alberta Geological Survey	Special Report 64	http://www.ags.gov.ab.ca/publications/abstracts/SPE_064.html
Eccles, D.R.	2004	Alberta kimberlite (GIS data, point features)	Alberta Geological Survey	Digital Dataset 2004-0035	http://www.ags.gov.ab.ca/publications/abstracts/DIG_2004_0035.html
Eccles, D.R. and Sutton, R.	2004	Magnetic susceptibility measurements on kimberlite and sedimentary rocks in Alberta	Alberta Geological Survey	Geo-Note 2003-41	http://www.ags.gov.ab.ca/publications/abstracts/GEO_2003_41.html
Eccles, D.R., Heaman, L.M., Luth, R.W. and Creaser, R.A.	2004	Petrogenesis of the Late Cretaceous northern Alberta kimberlite province	Lithos	Volume 76, p. 435–459	Journal homepage: www.elsevier.com/locate/lithos
Eccles, D.R. and Luth, R.W.	2003	Major- and trace- element geochemistry of kimberlitic rocks in northern Alberta	Alberta Geological Survey	Earth Sciences Report 2001-05	http://www.ags.gov.ab.ca/publications/abstracts/ESR_2001_05.html
Eccles, D.R., Heaman, L.M. and Creaser, R.A.	2003	Radiogenic isotope geochemistry of kimberlitic rocks in northern Alberta: constraints for source of magmatism and emplacement age	Alberta Geological Survey	Geo-Note 2003-37	http://www.ags.gov.ab.ca/publications/abstracts/GEO_2003_37.html
Paganelli, F., Grunsky, E. and Richards, J.P.	2003	Structural interpretation of RADARSAT-1 Principal Components Imagery and its potential application to kimberlite exploration in the Buffalo Head Hills area, north-central Alberta	Alberta Geological Survey	Special Report 21	http://www.ags.gov.ab.ca/publications/abstracts/SPE_021.html
Eccles, D.R., Dufresne, M.B., Copeland, D.A., Csanyi, W. and Creighton, S.	2002	Alberta kimberlite-indicator mineral geochemical compilation	Alberta Geological Survey	Earth Sciences Report 2001-20	http://www.ags.gov.ab.ca/publications/abstracts/ESR_2001_20.html
Eccles, D.R.	2002	Petrographic characteristics of selected kimberlitic rocks in northern Alberta	Alberta Geological Survey	Earth Sciences Report 2002-07	http://www.ags.gov.ab.ca/publications/abstracts/ESR_2002_07.html
Skupinski, A. and Langenberg, C.W.	2002	Petrography of the Mountain Lake pipe, Grande Prairie area, Alberta	Alberta Geological Survey	Special Report 15	http://www.ags.gov.ab.ca/publications/abstracts/SPE_015.html
Hauff, P.L., Eccles, D.R. and Grunsky, E.	2001	Alteration mineralogy of Alberta kimberlites: PIMA infrared spectroscopic analysis	Alberta Geological Survey	Special Report 12	http://www.ags.gov.ab.ca/publications/abstracts/SPE_012.html

Author(s)	Year	Title	Source	Publication	Abstract and PDF Download Site or Journal Homepage
Leckie, D.A., Kjarsgaard, B., Peirce, J.W., Grist, A.M., Collins, M., Sweet, A., Stasiuk, L., Tomica, M.A., Eccles, R., Dufresne, M., Fenton, M.M., Pawlowicz, J.G., Balzer, S.A., McIntyre, D.J. and McNeil, D.H.	1997	Geology of a late Cretaceous possible kimberlite at Mountain Lake, Alberta—chemistry, petrology, indicator minerals, aeromagnetic signature, age, stratigraphic position and setting	Natural Resources Canada, Geological Survey of Canada	Open File 3441	http://geopub.nrcan.gc.ca/moreinfo_e.php?id=208916&_h=OFR%203441
Dufresne, M.B., Eccles, D.R., McKinstry, B., Schmitt, D.R., Fenton, M.M., Pawlowicz, J.G. and Edwards, W.A.D.	1996	The diamond potential of Alberta	Alberta Geological Survey	Bulletin 63	http://www.ags.gov.ab.ca/publications/abstracts/BUL_063.html
LeCheminant, A.N., Richardson, D.G., Dilabio, R.N.W., and Richardson, K.A.	1996	Searching for diamonds in Canada	Natural Resources Canada, Geological Survey of Canada	Open File 3228	http://geopub.nrcan.gc.ca/moreinfo_e.php?id=208202&_h=OFR%203228

Appendix 3 – Isotopic Results for Selected Kimberlite and Related Rock Bodies of the Northern Alberta Kimberlite Province

a) U-Pb-Th Perovskite and Rutile (pages 105–106)

b) Rb-Sr Phlogopite (pages 107–108)

a) U-Pb-Th Perovskite and Rutile

Body and Sample Number[1]	Drillhole	Sample Depth (m)	Description (Approximate Number of Grains)	Weight (µg)	U (ppm)	Th (ppm)	Pb (ppm)	Th/U	TCPb (pg)	Isotopic Ratios					$^{206}Pb/^{238}U$ Age (Ma)	Recommended Age (Ma)[4]	MSWD (n)	Reference
										$^{206}Pb/^{204}Pb$	$^{238}U/^{204}Pb$	$^{206}Pb/^{238}U$	$^{207}Pb/^{235}U$	$^{207}Pb/^{206}Pb$				
BM2																		
ASH106-1[2]	DDH-BM2-01	102	Cubes	235	94	1960	10	20.81	913	33.98±0.10	1529.4±30.2	0.01005±32	0.0557±164	0.0402±118	63.2±2.0	63.5 ±0.7[5]	0.57 (6)	Carlson et al. 1999; Boyer et al. 2003; Eccles et al. 2008
BM2 - Upper dike																		
RE05-KHR-K40-1[2]	DDH-BM2-01	69.5-71.8	Small black-brown cubes (150)	72	134	3365	16	25.06	350	36.39±0.22	1756.6±36.8	0.01013±28	0.0622±144	0.0446±102	63.9±1.8			
RE05-KHR-K40-2[2]	DDH-BM2-01	69.5-71.8	Large black-brown cubes (60)	89	120	3423	15	28.62	390	36.25±0.16	1733.9±35.2	0.01018±28	0.0656±138	0.0467±98	64.2±1.8			
BM2 - Lower dike																		
RE05-KHR-K41-1[2]	DDH-BM2-01	98.8-102	Small brown cubes (200)	50	90	1828	9	20.30	161	36.83±0.36	1816.4±49.4	0.00987±28	0.0533±138	0.0392±42	62.3±1.8			
RE05-KHR-K41-2[2]	DDH-BM2-01	98.8-102	Small medium brown cubes (150)	73	106	2481	12	23.36	278	36.66±0.22	1784.4±39.0	0.01012±28	0.0596±136	0.0427±98	63.8±1.8			
RE05-KHR-K41-3[2]	DDH-BM2-01	98.8-102	Small brown irregular fragments (200)	65	194	1953	11	10.08	258	49.49±0.38	3093.9±69.0	0.00998±22	0.0769±74	0.0559±54	63.4±1.4			
BH225																		
ASH128-1[3]	DDH 225-01	75.3	Brown to dark brown fragments (70)	112	247	5828	45	23.59	1774	31.53±0.10	977.4±6.4	0.01328±38	0.0730±232	0.0399±126	72.4±2.4	68.4 ±5.2[6]	(2)	Carlson et al. 1999; Eccles et al. 2008
RE05-KHR-K19-1[3]	BH225-01	50.7-52.2	Medium-small brown cubes (230)	57	97	2787	17	28.73	342	31.31±0.06	1014.8±3.8	0.01254±36	0.0599±214	0.0347±124	68.6±2.4			
RE05-KHR-K19-2[3]	BH225-01	50.7-52.2	Medium brown cubes (175)	123	110	3343	20	30.37	764	34.18±0.38	1121.9±14.0	0.01390±38	0.0761±276	0.0397±142	78.2±2.4			
RE05-KHR-K19-3[3]	BH225-01	50.7-52.2	Large brown black cubes (80)	196	129	3066	18	23.77	1168	34.95±0.24	1356.2±12.4	0.01207±30	0.0658±192	0.0395±114	68.4±2.0			
K7A																		
ASH028-1	DDH7A-01	162.3	Euhedral brown cubes (110)	67	74	3555	26	48.02	724	24.22±0.30	435.4±11.0	0.01299±104	0.0796±782	0.0444±420	83.2±6.6	85.6 ±2.4[5]	0.60 (2)	Carlson et al. 1999; Eccles et al. 2008
ASH028-2	DDH7A-01	162.3	Irregular brown fragments (14)	75	80	4733	43	59.34	359	32.70±0.30	1052.8±14.2	0.01342±40	0.0842±264	0.0455±140	86.0±2.6			
K91																		
ASH066-1	DDH91-05/06	<45	Large dark brown cubes (13)	14	142	3193	29	22.55	178	28.07±0.50	710.4±34.8	0.01340±54	0.0467±348	0.0253±188	85.8±3.4	86.1 ±3.0[5]	0.11 (2)	Carlson et al. 1999; Eccles et al. 2008
ASH066-2	DDH91-05/06	<45	Tiny brown euhedral cubes (179)	33	104	4502	24	43.34	307	28.34±0.30	717.1±19.8	0.01359±104	0.0561±322	0.0299±174	87.0±6.6			
K14A																		
ASH017-1	DDH14-01	196.3	Dark brown cubes (175)	33	114	318	24	2.79	281	30.02±0.26	841.4±13.6	0.01362±50	0.1319±322	0.0703±168	87.2±3.2	86.8 ±2.1[5]	0.11 (2)	Carlson et al. 1999; Eccles et al. 2008
ASH017-2	DDH14-02	196.3	Large dark brown parts of cubes (20)	19	113	227	20	2.01	141	31.89±0.28	986.3±25.8	0.01350±44	0.1402±334	0.0753±172	86.5±2.8			
K5A																		
ASH016-1	DDH-5A-02	114	Red-orange cubes (37)	22	68	175	17	2.56	112	30.55±0.68	875.9±39.2	0.01369±72	0.1659±514	0.0879±250	87.6±4.6	87.6 ±4.6[7]	(1)	Carlson et al. 1999; Eccles et al. 2008
Phoenix																		
ABK-75-1	98DH-PH-01	105	Large, brown, broken (25)	432	123	8305	37	67.80	3405	19.3±0.4	974.9±2.6	0.01242±1.9	0.0660±115	0.0385±67	79.6±1.2	77.6 ±1.1	(1)	Eccles (2004)
ABK-75-2	98DH-PH-01	105	Small, altered, cubic (5)	235	112	2988	19	26.56	1823	18.6±0.4	911.2±8.8	0.01170±2.6	0.0556±195	0.0344±119	75.0±1.6			
ABK-76-1	98DH-PH-01	130	Large, black, cubic (40)	80	122	2301	16	18.86	586	18.9±0.4	1043.8±2.7	0.01203±1.8	0.0627±104	0.0378±63	77.1±1.1			
ABK-76-2	98DH-PH-01	130	Small, brownish black (200)	325	120	2078	15	17.37	2435	19.8±0.4	1002.79±6.5	0.01213±2.1	0.0702±142	0.0420±83	77.7±1.3			
ABK-76-3	98DH-PH-01	130	Large, brown, cubic (50)	128	131	3018	18	23.04	974	19.9±0.4	1087.8±5.2	0.01211±1.7	0.0724±104	0.0433±62	77.6±1.1			
Kendu - rutile																		
ABK-82-1[2]	K-00-01	127.25	Brown, semi-transparent, angular (27)	334	9	n/a	0	n/a	55	17.3±2.1	3900.8±366	0.01453±5	0.1019±39	0.0509±19	93.0±0.3	None recommended (see text)		Eccles (2004)
ABK-82-2[3]	K-00-01	127.25	Amber, semi-transparent, angular (30)	530	9	n/a	0	n/a	104	8.9±1.7	2999.9±78.3	0.01240±12	0.0822±39	0.4819±23	79.4±0.8			
ABK-82-3[3]	K-00-01	127.25	Amber, semi-transparent, angular (50)	441	8	n/a	0	n/a	35	31.1±3.8	7803.4±726.5	0.01440±6	0.1057±25	0.0532±12	92.2±0.4			
ABK-82-4[2]	K-00-01	127.25	Brown, semi-transparent, angular (50)	945	9	n/a	0	n/a	166	20.5±1.3	3150.8±50.7	0.01354±12	0.0986±37	0.0528±20	86.7±0.8			

[1] Ashton samples designated by the sample number prefix ASH; Kennecott samples designated by the sample number prefix VR

[2] $^{206}Pb/^{238}U$ age calculated using an initial $^{206}Pb/^{204}Pb$ ratio of 18.9

[3] $^{206}Pb/^{238}U$ age calculated using an initial $^{206}Pb/^{204}Pb$ ratio of 20.9

[4] Age calculation method: [5] weighted average $^{206}Pb/^{238}U$; [6] linear regression; [7] individual $^{206}Pb/^{238}U$

Atomic ratios corrected for blank (5 pg Pb, 1 pg U), spike and initial common Pb (Stacey and Kramers, 1975)

All errors reported at 2σ

Abbreviations: MSWD, mean square of weighted deviates; n, number of samples; n/a, not available

b) Rb-Sr Phlogopite

Body and Sample Number[1]	Drillhole	Sample Depth (m)	Description (Approximate Number of Grains)	Weight (µg)	U (ppm)	Th (ppm)	Pb (ppm)	Th/U	TCPb (pg)	Isotopic Ratios							$^{206}Pb/^{238}U$ Age (Ma)	$^{208}Pb/^{232}Th$ Age (Ma)
										$^{238}U/^{204}Pb$	$^{235}U/^{204}Pb$	$^{206}Pb/^{204}Pb$	$^{207}Pb/^{204}Pb$	$^{208}Pb/^{204}Pb$	$^{232}Th/^{204}Pb$	$^{208}Pb/^{232}Th$		
Valkyrie																		
VR-1	98DH-VA-02	158.2	Opaque, large, smooth (4)	115	7	197	1	26.95	n/a	715±2.5	5.19±2.5	27.54±0.81	16.01±0.47	112.19±1.38	19910±2.5	0.003699±1.96	79.9±2.2	74.64±1.46
VR-2	98DH-VA-02	158.2	Opaque, small, euhedarl (na)	41	4	71	1	20.20	n/a	403±8.8	2.92±8.8	22.79±1.5	15.83±0.65	68.91±2.88	8408±8.8	0.003612±6.25	66.2±8.9	72.88±4.56
VR-3	98DH-VA-02	158.2	Brown, suhedral (na)	63	115	1671	12	14.54	n/a	1405±1	10.19±0.98	35.76±0.66	16.32±0.64	116.68±0.7	21110±.9	0.003701±1.42	78.1±2.4	74.67±1.06
Phoenix																		
VR-1	98DH-PH-01	113.9	Brown	85	192	317	11	1.65	n/a	1614±1.3	11.71±1.3	37.64±0.76	16.66±0.8	49.79±0.76	2.75±1.27	0.004085±9.3	75.5±2.2	82.39±7.66
VR-2	98DH-PH-01	113.9	Dark brown	129	172	3601	22	20.94	n/a	1311±0.55	9.51±0.55	34.18±0.3	16.26±0.29	140.37±0.38	28.37±0.5	0.003589±1.06	76.0±2.5	72.42±0.77
VR-3	98DH-PH-01	113.9	Black	76	146	13538	60	92.60	n/a	642±0.88	4.66±0.88	26.87±0.43	15.98±0.48	258.25±0.52	61.44±0.9	0.003576±0.86	82.2±5.1	72.15±0.62

Body and Sample Number[1]	Drillhole	Recommended Age (Ma)[4]	MSWD (n)	Reference
Valkyrie				
VR-1	98DH-VA-02	75.8 ±2.7	$^{208}Pb/^{232}Th$; 0.005 (3)	Aravanis (1999)
VR-2	98DH-VA-02			
VR-3	98DH-VA-02			
Phoenix				
VR-1	98DH-PH-01	70.3 ±1.6 Ma	$^{206}Pb/^{238}U$; 0.58 (3)	Aravanis (1999)
VR-2	98DH-PH-01			
VR-3	98DH-PH-01			

[1] Ashton samples designated by the sample number prefix ASH; Kennecott samples designated by the sample number prefix VR

[2] $^{206}Pb/^{238}U$ age calculated using an initial $^{206}Pb/^{204}Pb$ ratio of 18.9

[3] $^{206}Pb/^{238}U$ age calculated using an initial $^{206}Pb/^{204}Pb$ ratio of 20.9

[4] Age calculation method: [5] weighted average $^{206}Pb/^{238}U$; [6] linear regression; [7] individual $^{206}Pb/^{238}U$

Atomic ratios corrected for blank (5 pg Pb, 1 pg U), spike and initial common Pb (Stacey and Kramers, 1975)

All errors reported at 2σ

Abbreviations: MSWD, mean square of weighted deviates; n, number of samples; n/a, not available

b) Rb-Sr Phlogopite

Body and Sample ID	Drillhole	Sample Depth (m)	Weight (g)	Rb (ppm)	Sr (ppm)	$^{87}Rb/^{86}Sr$	$^{87}Sr/^{86}Sr$	$^{87}Sr/^{86}Sr$ 2σ	Model Age (Ma)[1]	Recommended Age (Ma)	Points, Model, Probability of Fit and MSWD	Reference
K1A												
1A-1	DDH-1A-01	55-58	0.00341	343.1	4.326	234.0	0.90837	0.00004	61.2			
1A-2	DDH-1A-01	55-58	0.00409	304.0	5.145	173.4	0.85207	0.00003	59.7			
1A-3	DDH-1A-01	55-58	0.00739	374.3	6.947	157.9	0.83873	0.00005	59.6	59.6 ±2.8	5-point, Model 3, Fit = 0.0021, MSWD = 4.9	Eccles et al. (2008)
1A-4	DDH-1A-01	55-58	0.00443	409.3	3.704	328.3	0.98481	0.00004	60.0			
1A-5	DDH-1A-01	55-58	0.00242	320.9	20.15	46.27	0.74756	0.00012	64.8			
K14												
K14A-A	Surface trench	0	0.00239	242.4	22.36	31.49	0.74005	0.00004	78.3			
K14A-B	Surface trench	0	0.00503	266.3	25.58	30.21	0.73835	0.00011	77.7		5-point, model 1,	
K14A-C	Surface trench	0	0.00711	257.8	24.80	30.17	0.73851	0.00003	78.2	82.8 ±9.2	fit = 0.93,	This report
K14A-D	Surface trench	0	0.00722	299.8	24.96	34.88	0.74400	0.00003	78.7		MSWD = 0.15	
K14A-E	Surface trench	0	0.00816	298.8	29.60	29.30	0.73749	0.00003	78.0			
K14B-A	Surface trench	0	0.00427	263.0	34.31	22.23	0.72931	0.00002	77.0			
~~K14B-B~~[2]	~~Surface trench~~	~~0~~	~~0.00549~~	~~230.8~~	~~30.14~~	~~22.22~~	~~0.73015~~	~~0.00005~~	~~79.7~~	86 ±11	2-point	This report
K14B-C	Surface trench	0	0.00381	155.4	17.22	26.19	0.73414	0.00003	78.3			
K19												
19-1	DDH-19-2	27-29	0.00774	259.6	7.920	95.58	0.78695	0.00005	60.4			
19-2	DDH-19-2	27-29	0.00509	303.7	2.237	406.0	1.05094	0.00013	60.0	60.3 ±0.8	4-point, Model 1, Fit = 0.19, MSWD = 1.7	Eccles et al. (2008)
19-3	DDH-19-2	27-29	0.00536	394.4	2.668	443.3	1.08384	0.00043	60.2			
19-4	DDH-19-2	27-29	0.00136	312.8	12.27	74.22	0.76728	0.00003	59.1			
BH225												
BH225-A	BH225-07-01	76.8	0.00485	313.8	37.10	24.54	0.73204	0.00003	77.6	81.5 ±5.1	2-point	This report
BH225-B	BH225-07-01	76.8	0.00433	319.0	53.22	17.38	0.72375	0.00002	76.0			
K252												
252-1	DDH-252-08	118-119	0.00089	270.1	48.19	16.25	0.72234	0.00003	75.1			
252-3	DDH-252-08	118-119	0.00122	374.2	79.70	13.61	0.71941	0.00004	74.5		5-point, Model 1,	
252-4a	DDH-252-08	118-119	0.00119	382.0	119.4	9.269	0.71429	0.00003	70.6	81.3 ±2.3	Fit = 0.76,	Eccles et al. (2008)
252-4	DDH-252-08	118-119	0.00273	332.9	91.22	10.57	0.71587	0.00003	72.4		MSWD = 0.59	
252-5	DDH-252-08	118-119	0.00363	351.3	79.81	12.75	0.71829	0.00002	73.4			
BH229												
229-1	DDH-229-01	74.0	0.00152	358.7	3.379	318.3	1.08723	0.00011	84.5			
229-2	DDH-229-01	74.0	0.00167	681.1	34.07	58.25	0.77723	0.00003	87.3	83.3 ±5.4	4-point, Model 3, Fit = 0, MSWD = 14	Eccles et al. (2008)
229-3	DDH-229-01	74.0	0.00071	437.7	5.669	229.2	0.98087	0.00005	84.7			
229-4	DDH-229-01	74.0	0.00062	529.5	15.03	103.3	0.83655	0.00003	89.7			
K11												
11-1	DDH-11-01	32-35	0.00259	562.3	3.148	549.8	1.37197	0.00022	85.4			
11-2	DDH-11-01	32-35	0.00222	549.1	5.543	296.6	1.06724	0.00011	85.9		4-point, Model 1,	
11-3	DDH-11-01	32-35	0.00257	621.4	4.269	442.9	1.24335	0.00038	85.5	84.8 ±0.9	Fit = 0.999,	Eccles et al. (2008)
~~11-4~~[2]	~~DDH-11-01~~	~~32-35~~	~~0.00318~~	~~510.6~~	~~3.538~~	~~440.0~~	~~1.26096~~	~~0.00011~~	~~88.9~~		MSWD = <0.01	
11-5	DDH-11-01	32-35	0.00314	516.8	18.52	81.53	0.80804	0.00003	88.9			
LL8												
LL8-1	DDH-LL8-01	133-135	0.00871	596.8	9.936	177.5	0.92481	0.00002	87.2			
LL8-4	DDH-LL8-01	148-149	0.01012	650.2	3.951	505.0	1.32598	0.00004	86.5		4-point, Model 1,	
LL8-6	DDH-LL8-01	148-149	0.00558	611.1	3.520	534.6	1.36702	0.00010	87.2	86.0 ±1.2	Fit = 0.29,	Eccles et al. (2008)
LL8-7	DDH-LL8-01	148-149	0.00405	631.1	2.415	829.2	1.71346	0.00007	85.6		MSWD = 1.2	
K300												
300-1	DDH-300-01	85-88	0.00218	277.1	97.11	8.268	0.72039	0.00002	131.0			
300-2	DDH-300-01	85-88	0.00241	567.7	104.3	15.79	0.73190	0.00003	119.9	None recommended		Eccles et al. (2008)
300-3	DDH-300-01	85-88	0.00302	551.8	101.1	15.83	0.73212	0.00004	120.5			
300-4	DDH-300-01	85-88	0.00356	462.5	57.56	23.33	0.74000	0.00003	105.6			
Dragon												
VR-1	98DH-DR-01	142.5	0.0144	475.0	73.70	18.69	0.72369	0.00006	70.4			
VR-2	98DH-DR-01	142.5	0.0084	456.0	80.00	16.51	0.72154	0.00007	70.5			
VR-3	98DH-DR-01	142.5	0.007	448.0	50.60	25.68	0.73083	0.00012	70.8	72.42 ±0.91	5-point, MSWD = 1.4	Aravanis (1999)
VR-4	98DH-DR-01	142.5	0.0074	474.0	123.30	11.14	0.71594	0.00009	69.2			
VR-5	98DH-DR-01	142.5	0.0023	592.0	74.40	23.06	0.72839	0.00017	71.4			
Kendu												
ABK 81 phl-1	K-00-01	127.25	n/a	170.1	27.56	17.8834	0.705826	0.000016	74.27	None recommended		Eccles (2004)
ABK 82 phl-1	K-00-01	127.25	n/a	310.3	93.86	9.5778	0.708776	0.000096	98.75			
Legend												
VR-6	98DH-LE-01	29.9	0.008	858.0	5.09	514.43	1.27026	0.00086	77.3			
VR-7	98DH-LE-01	29.9	0.0051	888.0	4.43	618.82	1.38249	0.00125	77.1			
VR-8	98DH-LE-01	29.9	0.0167	850.0	7.37	346.22	1.08179	0.00031	76.6	77.63 ±0.84	5-point, MSWD = 0.91	Aravanis (1999)
VR-9	98DH-LE-01	29.9	0.0039	799.0	7.42	322.03	1.05609	0.00072	76.7			
VR-10	98DH-LE-01	29.9	0.0035	730.0	3.80	590.80	1.35048	0.00127	76.9			
Phoenix												
VR-1	98DH-PH-01	113.9	0.0047	591.8	27.24	63.24	0.76803	0.00004	64.6			
VR-2	98DH-PH-01	113.9	0.00341	434.3	42.59	29.58	0.73398	0.00003	57.1	70.89 ±0.43	3-point, MSWD = 1.2	Aravanis (1999)
VR-3	98DH-PH-01	113.9	0.02265	81.9	2.25	106.18	0.81097	0.00003	66.9			
Phoenix												
VR-11	98DH-PH-01	113.9	0.248	726.0	1.66	1459.60	2.31236	0.00020	77.5			
VR-12	98DH-PH-01	113.9	0.147	715.0	1.63	1471.10	2.32239	0.00023	77.4			
VR-13	98DH-PH-01	113.9	0.116	863.0	1.99	1450.10	2.29963	0.00062	77.4	88 ±12; 6-point, MSWD = 1.3; not recommended given 70.89 ±0.43 value above		Aravanis (1999)
VR-14	98DH-PH-01	113.9	0.0161	830.0	1.91	1453.20	2.29181	0.00236	76.9			
VR-15	98DH-PH-01	113.9	0.013	850.0	1.99	1424.00	2.24525	0.00388	76.1			
VR-16	98DH-PH-01	113.9	0.0259	837.0	2.09	1319.50	2.14209	0.00629	76.7			

Body and Sample ID	Drillhole	Sample Depth (m)	Weight (g)	Rb (ppm)	Sr (ppm)	$^{87}Rb/^{86}Sr$	$^{87}Sr/^{86}Sr$	$^{87}Sr/^{86}Sr$ 2σ	Model Age (Ma)[1]	Recommended Age (Ma)	Points, Model, Probability of Fit and MSWD	Reference
Phoenix												
ABK-75-PHL3	98DH-PH-01	105	0.01055	383.2	80.10	13.8603	0.705446	0.000040	73.29	None recommended		Eccles (2004)
ABK 75 re-run	98DH-PH-01	105	n/a	381.1	230.14	4.7932	0.705658	0.000019	80.68			
ABK76-PH1-1	98DH-PH-01	130	0.00500	378.2	67.51	16.2325	0.701813	0.000036	57.21			
ABK 76 re-run	98DH-PH-01	130	n/a	367.8	61.30	17.3882	0.701522	0.000016	56.95			
Xena												
VR-17	98DH-XE-01	157.4	0.0118	566.0	68.43	23.97	0.72974	0.00021	72.7	72.6 ±2.1	6-point, MSWD = 0.98	Aravanis (1999)
VR-18	98DH-XE-01	157.4	0.0172	457.0	46.91	28.26	0.73389	0.00029	72.0			
VR-19	98DH-XE-01	157.4	0.0461	528.0	57.92	26.42	0.73207	0.00012	72.1			
VR-20	98DH-XE-01	157.4	0.023	479.0	65.46	21.20	0.72670	0.00012	72.0			
VR-21	98DH-XE-01	157.4	0.0213	359.0	75.71	13.74	0.71883	0.00047	70.8			
VR-22	98DH-XE-01	157.4	0.0891	551.0	62.70	25.47	0.73103	0.00005	71.9			

[1] Model age calculated assuming initial $^{87}Sr/^{86}Sr$ value of 0.705

[2] Discarded (strikethrough) analyses: phlogopite slightly chloritized

Abbreviation: MSWD, mean square of weighted deviates